



MPHIL

Development of Stimuli Responsive Azulene-Containing Molecules for Sensing

Williams, Georgia

Award date:
2021

Awarding institution:
University of Bath

[Link to publication](#)

Alternative formats

If you require this document in an alternative format, please contact:
openaccess@bath.ac.uk

General rights

Copyright and moral rights for the publications made accessible in the public portal are retained by the authors and/or other copyright owners and it is a condition of accessing publications that users recognise and abide by the legal requirements associated with these rights.

- Users may download and print one copy of any publication from the public portal for the purpose of private study or research.
- You may not further distribute the material or use it for any profit-making activity or commercial gain
- You may freely distribute the URL identifying the publication in the public portal ?

Take down policy

If you believe that this document breaches copyright please contact us providing details, and we will remove access to the work immediately and investigate your claim.

Development of Stimuli Responsive Azulene-Containing Molecules for Sensing

Georgia Williams

Supervisor:

Dr Simon Lewis

Co-supervisors:

Prof Tony James
Dr Andrew Johnson

Examiners:

Dr Dan Pantos
Prof Robert Stockman

MPhil Thesis

Acknowledgements

I would like to thank my supervisor Dr Simon Lewis for his advice and guidance during my time on this project and for allowing me to research and expand my knowledge within organic chemistry.

I would also like to thank the past and present group members in the Lewis group as well as other colleagues in the Chemistry department for their support. Sincere thanks to an exceptional friend and colleague Susana Estopiñá Durán, whose passion and enthusiasm has helped to inspire me to become a great scientist.

Finally, thank you to my family and friends for their constant support behind the scenes.

Abstract

This report investigates the synthesis of stimuli responsive molecules and their response towards thiols for use as possible chemodosimeters in azulene/guaiazulene based systems. These constructs were chosen due to their striking colour changes in response to external stimuli thereby making excellent molecules to be used in colorimetric tests and sensor applications.

A wide range of reactions were carried out starting from the synthesis of electron-withdrawing groups located on the 5-membered ring of the azulene/guaiazulene construct followed by the synthesis of electron-withdrawing groups on the 7-membered ring of guaiazulene. All the compounds were synthesised in good yields and full characterization data was collected for each novel compound. The response of the molecules to thiol analytes was tested *via* any visual colour changes, NMR, MS and UV-Vis analysis. This was then followed by selectivity tests with a wide range of amino acids and other thiol containing compounds as followed by the literature. The halochromic properties of selected azulenes were also investigated, as well as their NMR responses to protonation.

Abbreviations

Å	Angstroms
CE	Capillary Electrophoresis
Cys	Cysteine
DCM	Dichloromethane
DMF	Dimethylformamide
DMSO	Dimethylsulfoxide
DNA	Deoxyribonucleic acid
DNBS	2,4-dinitrophenyl sulfonyl
EtOH	Ethanol
eq.	Equivalents
GSH	Glutathione
Hcy	Homocysteine
HIV	Human immunodeficiency virus
HPLC	High Performance Liquid Chromatography
Hz	Hertz
IC	Internal conversion
ICT	Intramolecular charge transfer
ISC	Intersystem crossing
IR	Infrared
MDR	Multidrug resistance
MeCN	Acetonitrile
MeOH	Methanol
M	Molar
mM	Millimolar
MS	Mass Spectrometry

NAC	<i>N</i> -Acetyl-L-cysteine
NMR	Nuclear magnetic resonance
PET	Photo-induced electron transfer
ROS	Reactive oxygen species
t	Time
TBA	Tetrabutylammonium
TBAF	Tetra- <i>n</i> -butylammonium fluoride
TFA	Trifluoroacetic acid
THF	Tetrahydrofuran
TLC	Thin Layer Chromatography
UV	Ultraviolet
Vis	Visible
WHO	World Health Organisation
ppm	Parts per million

Table of Contents

Acknowledgements	2
Abstract	3
Abbreviations	4
Table of Contents	6
Chapter 1: Introduction	7
1.1. <i>Biothiols</i>	7
1.2. <i>Concept of a Chemical Sensor</i>	8
1.2.1 <i>Stimuli Responsive Molecules</i>	9
1.2.2 <i>Detection Analysis for Sensors</i>	9
1.3. <i>Azulene and Guaiazulene Compounds as Chemical Sensors</i>	12
1.3.1 <i>Azulene upon protonation</i>	12
1.3.2 <i>Guaiazulene and Azulene for Heavy Metal Sensing</i>	14
1.3.3 <i>Azulene and Guaiazulene for Fluoride Sensing</i>	15
1.3.4 <i>Azulene for Nitrite Detection</i>	17
1.3.5 <i>Azulene for Phosphate Detection</i>	19
1.3.6 <i>Azulene for Mercury Detection</i>	20
1.3.7 <i>Azulene for Silver Cation Detection</i>	22
1.4. <i>Thiol Reactive Probes and Chemosensors</i>	24
1.4.1 <i>Nucleophilic Substitution for Thiol Labelling</i>	24
1.4.2 <i>Michael Addition for Thiol Labelling</i>	26
1.4.3 <i>Disulphide Cleavage for Thiol Labelling</i>	27
1.4.4 <i>Selectivity amongst thiols</i>	28
Chapter 2: Results and Discussion	33
2.1. <i>Sulfide Sensors</i>	33
2.1.1 <i>Guaiazulene and Azulene functionalised barbituric acid motifs (5-membered ring)</i>	34
2.1.2 <i>Guaiazulene and Azulene functionalised cyanoacetic acid (5-membered ring)</i>	39
2.1.3 <i>Guaiazulene as a thiol receptor motif on 7-membered ring</i>	47
2.1.3.1 <i>Michael Acceptors on 7-membered ring</i>	47
2.1.3.2 <i>Cyclic Adducts on 7-membered ring</i>	51
2.1.3.3 <i>Nosyl Group on 7-membered ring</i>	53
Chapter 3: Conclusions and future work	54
3.1. <i>Conclusion</i>	54
3.2. <i>Future Work</i>	55
Chapter 4: Experimental	57
Chapter 5: References	73
Chapter 6: Appendix 1 – Spectra and Charts	75

Chapter 1: Introduction

1.1. Biothiols

Within the last decade, the use of proteins in therapeutic applications has gained increasing attention. Since the approval of the recombinant insulin in 1982, there has been a large increase in the number of approved drugs which are derived from recombinant proteins.¹

Within proteins there consists hundreds of smaller units called amino acids, and these are the essential chemicals needed for the body to function. These are classed as the basic building blocks of life and take on a variety of different roles in the body from being able to support the metabolism and protecting your heart. Thiols are predominantly located within these amino acids and constitute a major proportion of the total body antioxidants where they have a significant role in cellular defence against reactive oxygen species (ROS). In recent years, the detection of biothiols *i.e.* thiol containing amino acids and peptides as well as Glutathione (GSH), Homocysteine (HCy) and Cysteine (Cys) has received growing interest due to the effect these compounds exhibit in physiological systems.²

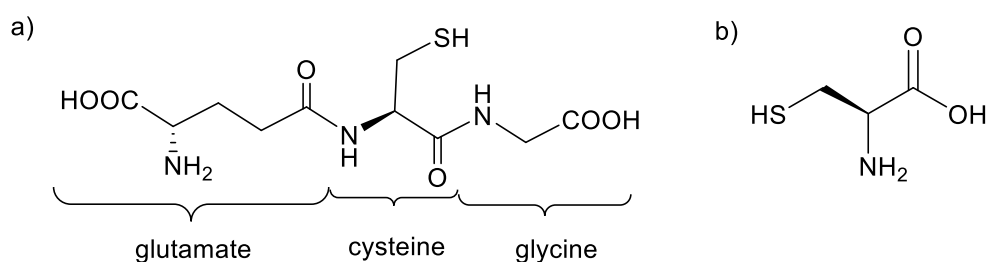


Figure 1: Structures of GSH (a) consisting of 3 amino acids as labelled and Cys (b)

GSH plays a vital role in several biological processes and is the most abundant intracellular non-protein thiol.³ It has a pivotal role in maintaining a reduced environment *via* acting as a redox regulator inside cells as well as having a role in toxin defence mechanisms, neutralization of free radicals and peroxides and acting as a signal transport and gene regulator.⁴ GSH exerts a profound protective effect on cells and when there is an abnormal level of GSH in the body, this can be a hallmark of various physiological conditions such as Alzheimer's, liver damage, human immunodeficiency viruses (HIV) and various cancer types.

Of the three amino acids in the GSH structure (glutamate, glycine, and Cys), Cys has the lowest intracellular concentration. Cys acts as an antioxidant and deficiency of this thiol results in various syndromes such as liver damage, Parkinson's disease, loss of muscle fat and tissue, skin lesions and weakness.⁵ In addition, it also acts as a critical extracellular reducing agent *via* the formation of disulfide bonds in the cytoplasm. Disulfide bonds are important for stabilising the tertiary structure of a protein.

In addition to Cys, *N*-Acetyl-L-cysteine (NAC) is an acetylated Cys residue (figure 3) which is a membrane-permeable Cys precursor that does not require active transport or delivery. Once NAC enters a cell it rapidly hydrolyses to release Cys. As such, NAC is an antioxidant and a free-radical scavenger that can increase intracellular GSH therefore it is able to increase cell protection towards oxidative stress⁶ and can help to reduce the oxidative effect of ROS through correcting or preventing GSH depletion.⁷

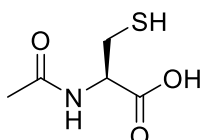


Figure 2: Structure of NAC

The ability to maintain an intracellular reduced state in the body is helped by certain proteins and is essential in reducing the harmful effects associated with oxidative stress.⁸ The term oxidative stress refers to an imbalance of production and accumulation of ROS in cells and tissues which subsequently causes damage to lipids, proteins and deoxyribonucleic acid (DNA). ROS are produced as a by-product of oxygen metabolism and are also used to serve several physiological roles such as cell signalling. There are many types of reactive oxygen species such as superoxide radicals, hydrogen peroxide, hydroxyl radicals and singlet oxygen which are all responsible for maintaining processes in the bodies defence mechanism towards the onset and/or progression of several diseases which include cancer, diabetes and cardiovascular diseases *etc.*⁹

Due to the harmful effects which are caused by elevated levels of oxidative stress and the important role which biothiols have in reducing these, the development of a rapid, facile and sensitive method for the detection of biothiols within biological systems is significant for monitoring of disease states in clinical diagnosis and is the focus of numerous research efforts.¹⁰ Particularly, simple methods for detection that involve using stable, non-toxic reagents that have sensitivity as well as selectivity are highly desirable.

1.2. Concept of a Chemical Sensor

Chemical information is essential to the survival and progression of all forms of life and chemical analysis is critical to life support, having many substantial applications in monitoring the quality of air, water, food, biodegradation and disease diagnosis to monitor the health of patients. In addition, obtaining chemical information to protect life *i.e.* to detect explosives, biological warfare agents *etc.* is as equally important. Therefore, chemical analysis is currently a very active research domain which can be shown by the increase in the number of publications produced in the last six decades.¹¹

Many traditional methods of chemical analysis relied on human and animal odour perception however there are many drawbacks to these methods such as biased approaches as a result of age, health, fatigue, mood *etc.* Other methods are currently now being investigated to replace many of these traditional based approaches. One example which is being researched extensively over the last few years includes the subject of chemical sensors.

A chemical sensor is defined as a self-contained device that can provide real-time analytical information from a test sample. In general, a chemical sensor comprises of two basic functional parts, a receptor and transducer.¹² The receptor can sense chemicals (often termed as an analyte or determinand) which results in an energy change that is able to be detected by the transducer into a measurable readout *i.e.* as an electrochemical, colorimetric, fluorescence response *etc.* From this signal, the chemical sensor can provide both qualitative and quantitative information about chemical compounds *via* an appropriate detection scheme.

As well as chemical species, there are also many physical values such as pressure, temperature, concentration *etc.* which can be determined, and sensors used to detect these are known as physical sensors. Recognition systems which are based on biochemical or biological mechanisms are known as biosensors.

There are many applications of chemical sensors in environmental, healthcare, agriculture and biotechnology.¹³ As such, the global industry demand and the rise in demand for testing and monitoring solutions from the healthcare sectors using chemical sensors is expected to grow worldwide. **Figure 3** displays the percentage market share for chemical sensors by region, where the demand for chemical sensors in North American regions is greatest followed by the Asia-Pacific.¹⁴

Chemical Sensors Market Share(%), By-Region, (2016)

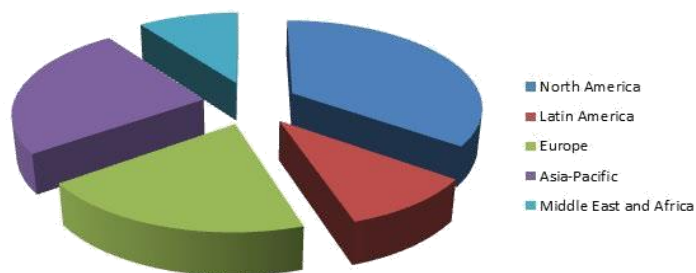


Figure 3: Chemical Sensors Market Share (%), By Region, 2016. Figure reproduced from reference Research Nester.¹⁴

This growth has been fuelled partly due to the low-cost materials and advances in nano and micro fabrications research. The future of the healthcare industry is looking towards quick and reliable detection processes to provide analytical and qualitative information in treatments and in diagnosis, and chemical sensors can help meet these goals.

Unlike chemosensors whose general principles operate based on coordination events and reversible signal changes, a chemodosimeter functions through a highly selective and irreversible chemical reaction with the target analyte. Deciding on which sensor to develop will largely depend on the type of analyte being tested however for the purposes of acting as a thiol sensor a chemodosimeter is favourable due to the ability of recording and measuring the changes that occur following a chemical reaction over an extended time period suitable for long term analysis and without the possibility of being affected by slight changes in the environment. Such irreversible reactions that can take place on the sensor molecules with thiols include Michael additions or addition to an aldehyde to form a thiazolidine (discussed later in the report).

1.2.1 Stimuli Responsive Molecules

Within the medical sector, there is an increasing demand for producing new agents that are sensitive, efficient and will improve the responses to pathology. As an example, the development of stimuli responsive molecules that could act as chemical sensors to target antimicrobial resistance or multidrug resistance (MDR) agents would allow for the simultaneous detection of concentration levels of such agents within the body ultimately leading to enhanced prognosis of pathological conditions in complex diseases such as cancer or other degenerative diseases.¹⁵

There are many challenges that are associated with developing such molecules once they are administered inside the body in order to produce the desired results due to other environmental conditions. Ideally, the stimuli responsive molecules must have a successful and simple route of administration, an effective delivery to the biological area of interest, have an appropriate response suitably adapted to the biological event (*via* an external or internal stimuli) and should be non-toxic, biocompatible and biodegradable.

There are several reported stimuli responsive molecules in the literature which can be used to release a drug payload though their ability to be either pH-responsive,¹⁶ redox-responsive,¹⁷ temperature-responsive light,¹⁸ ROS¹⁹ and hypoxia sensitive.²⁰ All the aforementioned stimuli have been explored resulting in established novel aspects although few have reached clinical studies, due to the absence of a standardized manufacturing methods particularly for nanocarriers which have received no regulatory or ethical approval to date.

1.2.2 Detection Analysis for Sensors

As discussed previously, chemical sensors can be classified into many different types which link directly to the method of analysis used to detect them which include optical absorption, electrical, electrochemical and physical.

Optical analysis focuses on the study of the energy exchange between electromagnetic radiation (receiver) and matter (analyte). There are several types of electromagnetic radiation that exist, which all differ in wavelength, frequency and energy. **Figure 4** shows the regions of the

electromagnetic spectrum.²¹ Optical imaging is highlighted between the regions of Infrared (IR) and Ultraviolet (UV) radiation (around 10^{-7} meter (m)).

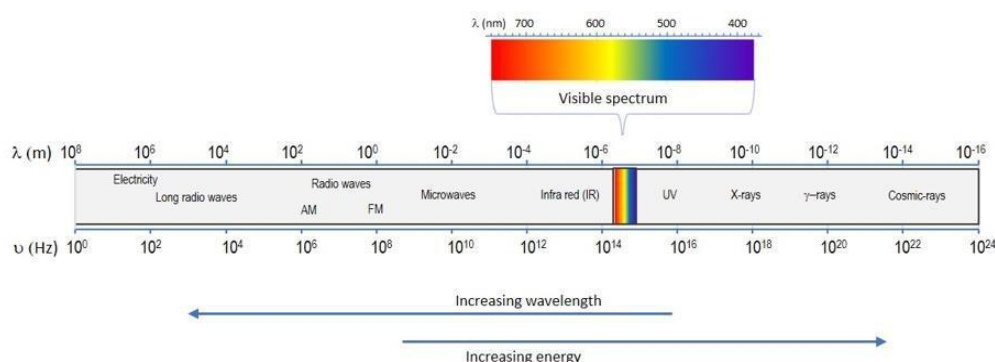


Figure 4: The Electromagnetic Spectrum and the visible light region which is the region studied within optical imaging. Figure reproduced from reference G. Butcher.²¹

Ultraviolet-visible (UV-Vis) spectroscopy refers to the absorption spectroscopy of the ultraviolet and the full visible spectral regions. In this region of the electromagnetic spectrum (wavelengths between 800-200 nanometre (nm)) atoms and molecules can undergo electronic transitions due to the energy gained from light (photons) that cause electrons to become excited from a bonding or a non-bonding orbital into an empty anti-bonding orbital. The Beer Lambert Law is the principle behind absorbance spectroscopy, **equation 1**.

$$A = \epsilon cl$$

Equation 1: Beer- Lambert Law equation, where absorbance (A , arb units), molar absorptivity ($M^{-1}cm^{-1}$) of the compound, concentration of solution (c , M) and path length of the cuvette (l , cm)

The components of a UV-Vis instrument consist of a light source (usually a deuterium or tungsten lamp), a sample holder, detector (or a diode array detector) and often a monochromator to analyse one wavelength at a time.

Absorption spectroscopy is a complementary analysis to fluorescence spectroscopy which deals with transitions from the excited state to the ground state (opposite to absorption spectroscopy).

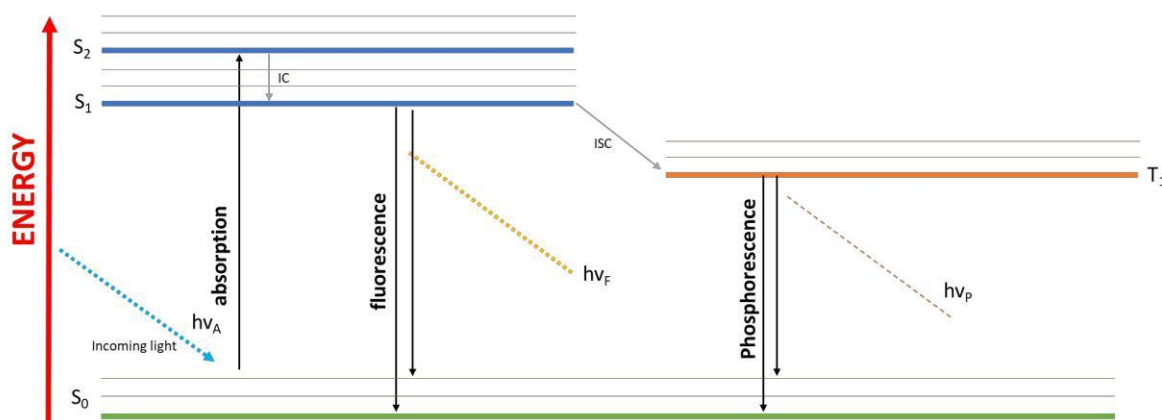


Figure 5: Jablonski diagram to illustrate the process of absorption, fluorescence and phosphorescence with singlet energy levels (S_0 , S_1 and S_2) and the triplet level (T_1). Proceeding internal conversion (IC) and intersystem crossing (ISC) lead to both fluorescence and phosphorescence.

In fluorescence spectroscopy, an excited photon ($h\nu_A$) which is produced from an external source (*i.e.* a light source) is absorbed by a fluorophore that elevates its energy to a higher electronic energy

level (S_1 or S_2 or potentially even higher singlet levels). During the fluorescence lifetime, this elevated energy (S_2) will decay back down to the lower energy state (S_1) through internal conversion (IC) producing a photon emission of a lower energy ($h\nu_F$) and longer wavelength. When de-exciting from S_2 to S_1 both states are singlets where all the electron spins are paired (opposite spins) thus the spin of the excited electron is still paired to the ground state electron. The difference in energy between the $h\nu_A$ - $h\nu_F$ is called the Stokes shift which has an energy that is specific for each compound. In this way, many compounds exhibit fluorescence properties which can be used as a reliable tool for semi-quantitative analysis and detection of such compounds. Furthermore, the emergence of fluorescent detection is vast, and applications extend across a wide range of fields in chemical sensing, dyes, biological detectors and fluorescence labelling *etc.*

In contrast, during the process of phosphorescence, intersystem crossing causes a spin conversion of the electron from S_1 to T_1 . In this way, the excited electron in the triplet state is no longer paired with the ground state electron *i.e.* they are parallel to each other (same spin). Since this intersystem crossing involves an additional 'forbidden' spin transition, this process is less likely to take place and the process undergoing a phosphorescent relaxation from the T_1 state takes a longer time compared to fluorescence relaxation.

Physical analysis of a sensor involves measuring the variations in physical properties of samples which include temperature, density, thermal diffusivity, thickness and strength amongst others. The two main types of physical sensors include temperature and distance sensors. Differences in the temperature between a temperature sensor and a temperature measurement device are often used in this technique and can be split into two groups; contact and non-contact. Such chemical sensors are often used within industry in control systems *i.e.* bimetallic sensors. Distance sensor analysis is often based on the optical, acoustic, inductive, capacitive and photoelectric physics and therefore have numerous associated analytical methods used to analyse these processes into a detectable read-out.

1.3. Azulene and Guaiazulene Compounds as Chemical Sensors

Azulene and its alkyl derivative guaiazulene have ignited keen interest for chemists due to their unusually bright blue colour. In contrast to naphthalene which is a non-polar structural isomer, azulene has a large permanent dipole moment and a polar asymmetric structure.²² Both aromatic compounds have unique structures in that they consist of an electronically positive seven-membered ring, polarity of which contributes towards a tropylium cation and an electrically negative five-membered ring which constitutes to a cyclopentadienide anion both fused together to produce an unsaturated bicyclic system. These characteristics of the molecules allows for the tropylium cation to act as an electron acceptor, while the cyclopentadienyl anion to act as an electron donor. These properties allow the compounds to display interesting electroactive properties and absorption spectra sensitive to the nature of the substituents on the rings.²³

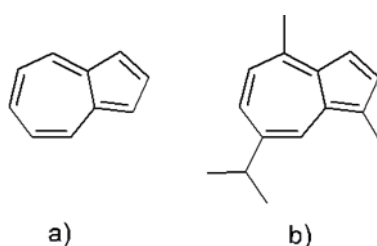


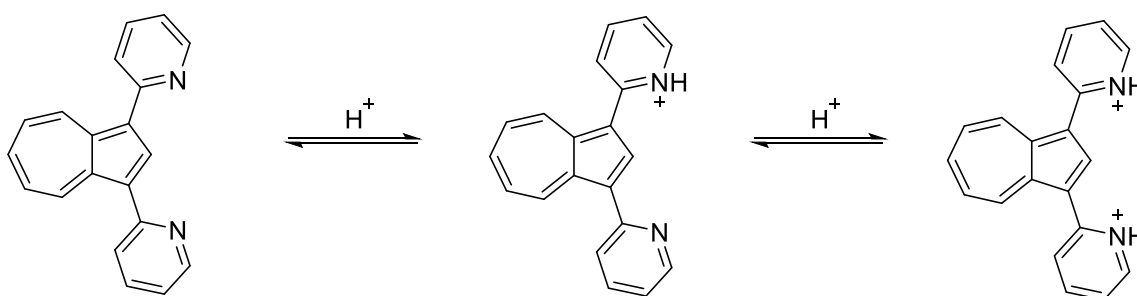
Figure 6: Structures of azulene (a) and guaiazulene (b)

Azulene is a strong chromophore and has stimulated significant research as an attractive building block towards the development of new multi-responsive and functional materials due to its unusual photophysical properties and subsequent effects on the absorption spectra. Colour changing reactions are important for identification and quantitative analysis of substances and can be used as important indicators in acid-base titrations, chelatometry, etc.

1.3.1 Azulene upon protonation

It is well known that the addition of protic acid or metal ions to azulene results in a noticeable colour change.²⁴ For this reason, several derivatives of azulene have been developed in the attempts of understanding such azulenichromophores as multi-responsive molecules and their potential to become commercialized as analytical reagents.

As part of these efforts, in 2007 Shimizu *et al.* synthesised a range of 1- and 2-pyridylazulenes and 1,3-dipyridylazulenes for their use as colorimetric reaction indicators.²⁵ For these compounds, a blue to red colour was reported upon addition of a strong organic acid, trifluoroacetic acid (pK_a 0.3) and at a maximum of 20 equivalents (eq.) of acid a blue shifting of absorbance peaks was observed.



Scheme 1: Successive protonation of synthesized 1,3-Di(2-pyridyl) azulene in acidic solution. Scheme reproduced from reference Shimizu *et al.*²⁵

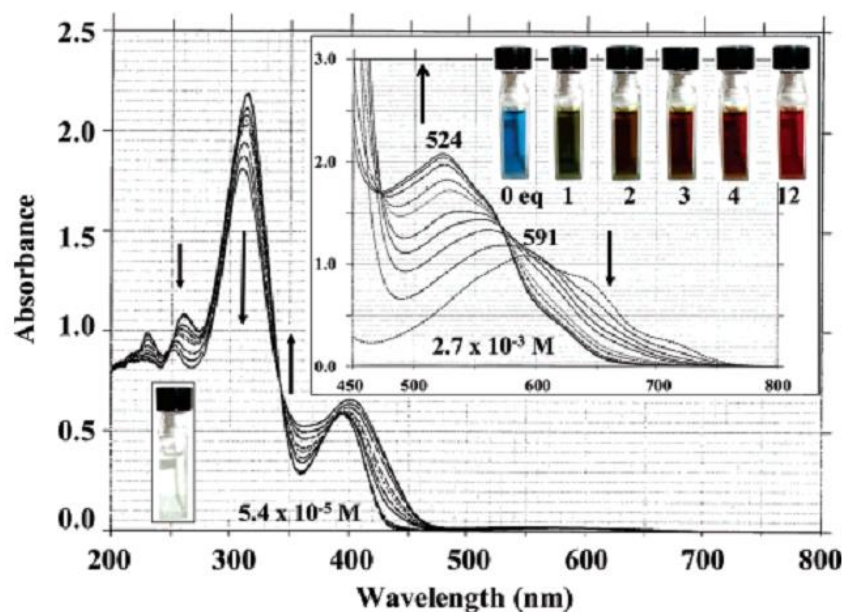


Figure 7: Spectrum and colour change of 1,3-di(2-pyridyl)azulene at $5.4 \times 10^{-5} \text{ M}$ and $2.7 \times 10^{-3} \text{ M}$ concentration and the addition of trifluoroacetic acid (TFA) in dichloromethane (DCM) at 1 to 20 eq. variation. Figure reproduced from reference Shimizu *et al.*²⁵

Following this, it was found that the protonation was reversible as upon neutralization of the acidic solutions with triethylamine reverted the colour back to blue from red. This reversible reaction was investigated further to determine the transition intervals over which these colour changes occurred thus allowing for the compounds to be used as possible pH indicators. For the 1,3-di(2-pyridyl)azulene compound studied, it was found that the transition interval was between pH 4.0-5.8. As the compound formed two species upon protonation, it was found that the species both had pKa's of 5.7 (first protonation) and 5.5 (second protonation) suggesting that the ease of protonation of both species is similar producing an equal equilibrium.

Acidic titrations of azulenic derivatives have also been carried in the group of Lewis *et al.* in 2019 through which a series of azulenes containing pentafluorosulfanylphenyl substituents were synthesised.²⁶ The inclusion of SF₅ groups posed several advantages including chemical and thermal stability, strong electron-withdrawing capabilities, large steric demand and an increase in lipophilicity to name a few. The compounds were produced through a Suzuki-Miyaura cross coupling between commercially available SF₅-aryl bromides and the product of an Ir-catalysed C-H borylation of azulene. This allowed for several products to be synthesised that contained the SF₅ located around the phenyl ring.

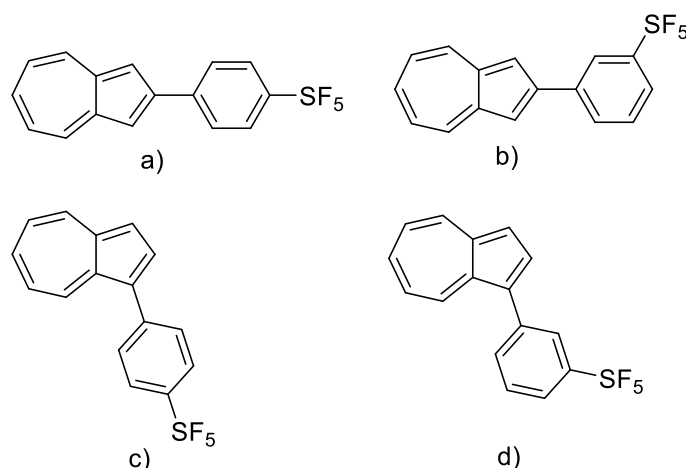


Figure 8: Synthesis of azulenes containing SF₅ containing substituents. Figure reproduced from reference Lewis *et al.*²⁶

Upon reaction of SF₅-aryl bromides and the catalysed products of azulene borylation, several products are produced whereby the SF₅ substituent can be located at the 2-and 3- positions of the phenyl ring (a or b and c or d) and at two different sites on the five-membered ring of the azulene (1 and 2 position).

Analysis of the compound through UV-Vis in DCM indicated that all the isomers had strong absorbance in the green-to-red region and were blue before protonation. Upon addition of the trifluoroacetic acid to the solutions, interestingly it was found that the compounds a) and b) underwent prominent colour changes to yellow-brown and red respectively i.e. when the substituent SF₅ is aligned with the dipole of the azulene core. The results from this test are shown below.

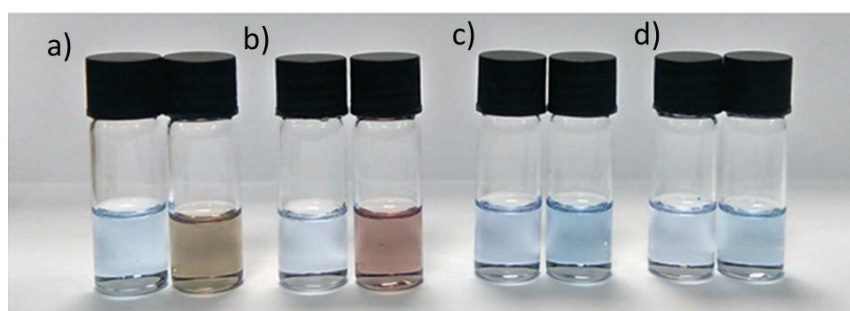


Figure 9: SF₅ containing compounds (a-d) in DCM solutions with (right) and without (left) TFA. Figure reproduced from reference Lewis et al.²⁶

Although the spectroscopic response in the visible region was similar for each molecule before protonation, there was a variation in absorbances in the blue region upon protonation most noticeably for compounds a) and b) which is reconfirmed through a visual colour change and thus potential use as chemical sensors.

1.3.2 Guiazulene and Azulene for Heavy Metal Sensing

Upon the discovery of the potential of azulene to act as a chemical sensor, chemists started to investigate this compound further and its detection of other types of analytes. In 2017, Birzan et al., studies a derivative of azulene in its ability to functionalise electrodes as a result of its high polarizability and spontaneous electron drift from the five membered ring to the seven membered ring.²⁷ Electrochemical analysis via cyclic voltammetry, differential pulse-voltammetry and rotation disk voltammetry were deployed to show that the azulene monomer (L) could be used to obtain modified electrodes through electrochemical polarisation. The chemically modified electrodes contained films formed on the surface of the electrode coated with the polyazulene (polyL) and were used for the recognition of heavy metal cations.

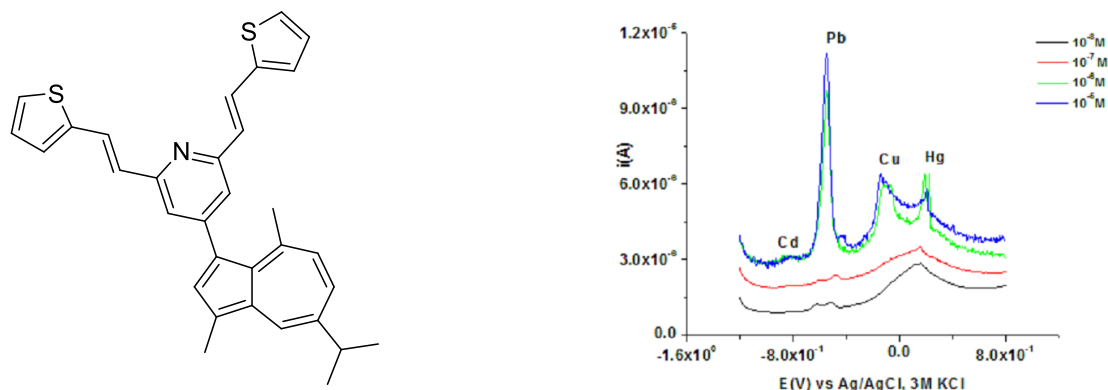


Figure 10: 4- (5-isopropyl-3,8-dimethylazulen-1-yl)-2,6-bis ((E)-2-(thiophen-2-yl)vinyl)pyridine (L) and Anodic stripping curve. Figure reproduced from reference Birzan et al.²⁷

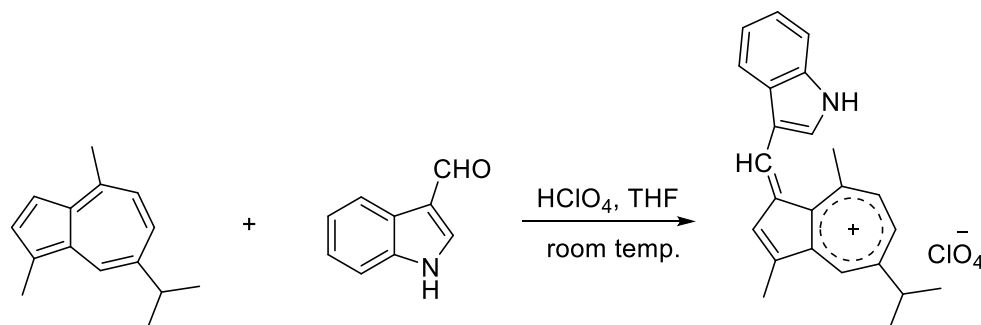
An anodic stripping curve was produced when the polyL modified electrodes were immersed in acetate buffer at pH 5.5 containing different concentrations of Cd (II), Pb(II), Cu (II) and Hg (II) ions.

The group later went on to synthesise another modified azulene construct which involved substituting the nitrogen atom on the pyridine ring with an oxygen.²⁷ This was then analysed using similar electrochemical methods for the presence of metal ions and was found to have a detection limit of 10^{-7} M for all the metal ions tested (Cu (II), Cd (II), Hg (II) and Pb (II)) in aqueous media. The concentration ranges detected would be suitable for the category of waters with the content of the previously mentioned ions between 10^{-7} M and 10^{-5} M.

1.3.3 Azulene and Guaiazulene for Fluoride Sensing

The potential of using azulene and guaiazulene based compounds for the detection of fluoride ions has become increasingly attractive for chemists over recent years. The control of drinking -water quality is essential for the prevention of dental and skeletal fluorosis, conditions of which can occur when the exposure to fluoride concentrations exceed 1.5 mg L^{-1} . As such, being able to detect fluoride concentrations is critical particularly in areas where there is high ground -water fluoride content such as in Brazil, China, India and in parts of Africa.

In 2014, the first research into developing sensors for fluoride using guaiazulene based systems were explored by S.H Gwon *et al.*²⁸ where they were able to synthesise a chemosensor design which incorporated an electron “push” donor and “pull” acceptor based on conjugated linkers, incorporating guaiazulene and indole moieties. This chemosensor was synthesised through a one-step condensation reaction showing selective sensing properties towards CN^- and F^- anions.



Scheme 2: Synthetic scheme of chemosensor. Scheme reproduced from reference S.H Gwon et al.²⁸

The spectral changes of the chemosensor was recorded upon the addition of fluoride anions, where initially the absorbance value for the molecule was at 585 nm. When fluoride was added, this absorbance value decreased accompanied with new absorbance values at 509 nm leading to a gradual colour change from purple to pink suggesting that there is an intermolecular charge transfer that is caused through the coordination of between the -NH of the indole and anions through the hydrogen donating-accepting effect of the chemosensor.

Following this, the Lewis group began investigating fluoride detection further using other azulene derivatives based on the incorporation of a pinacolborane as the receptor motif. In the first instance, several isomeric azulene-pinacolboranes were developed and tested with tetra-*n*-butylammonium (TBAF) fluoride in tetrahydrofuran (THF).²³ In each solution, the TBAF corresponds to 3.4 mg L⁻¹ of fluoride anion.

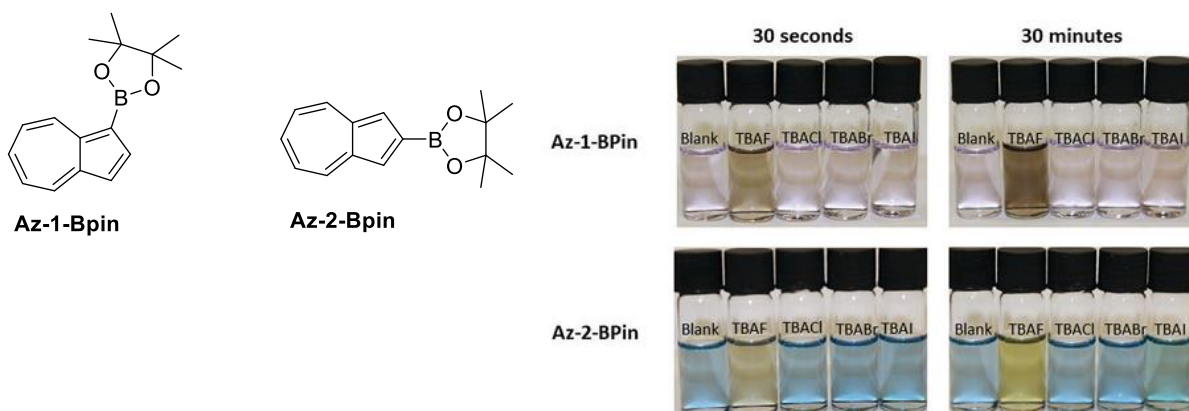


Figure 11: Test solutions of Az-1-Bpin and Az-2-Bpin with TBAF after 30 seconds and 30 minutes. Figure reproduced from reference Lewis et al.²³

The pictures in **figure 11** show that the azulene-pinacolborane conjugates produced are viable as colorimetric fluoride indicators that are selective and provide high-speed responsive colour changes. Unfortunately, however the colorimetric sensor was not able to detect fluoride in water itself or any water/organic solvent mix which would be useful for practical purposes and in drinking water applications.

This research was then explored again by the same group which were able to synthesise very similar azulene-pinacolboranes, but which now incorporated chlorine and ester side chains on the azulene backbone to improve the water solubility of these compounds. Similarly to the Az-1-Bpin molecule, the new sensor developed (NAz-6-Bpin) would bind to the fluoride anion through the boron atom thus disrupting the conjugation between the azulene ring and the vacant *p*-orbital on the *sp*²-hybridised boron as it reconfigures to *sp*³ hybridisation.²⁹ This change to the π -system would therefore, in theory, lead to a colorimetric response.

Tests were then carried out to determine the response of the NAz-6-Bpin in THF (0.5 mM) towards a series of halide analytes and it was found that there was an immediate colour change in response to the TBAF analyte from a pink to a yellow colour change along with a hypsochromic shift. The limit of detection for the TBAF in THF was 1.68 mg and a 1:1 stoichiometry of fluoride binding. With all other analytes tested, there was found to be no change of colour (remained pink).

The ability of the NAz-6-Bpin to detect fluoride in water/organic solvent mixtures was then evaluated using a 1:1, v/v aqueous/organic mixtures of the compound at 0.5 mM and NaF (10 eq.) using a THF, acetonitrile (MeCN), ethanol (EtOH) and methanol (MeOH) solvents. The optimised conditions were found with a 3:7 EtOH/H₂O mixture which was used in titration experiments with increasing concentrations of fluoride to which a red/pink to yellow/orange colour change was observed.

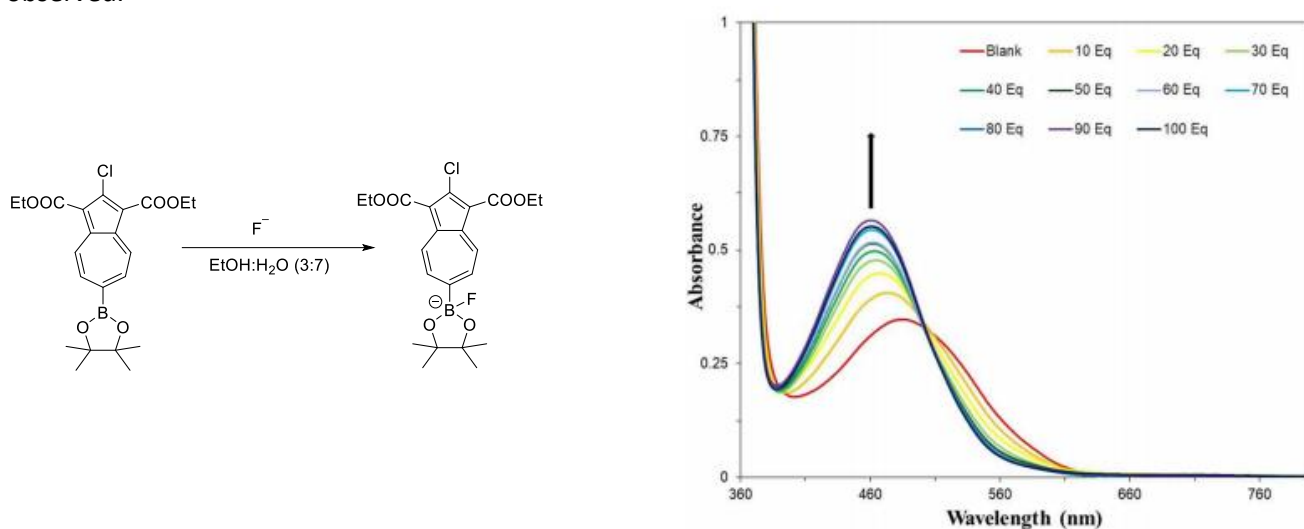


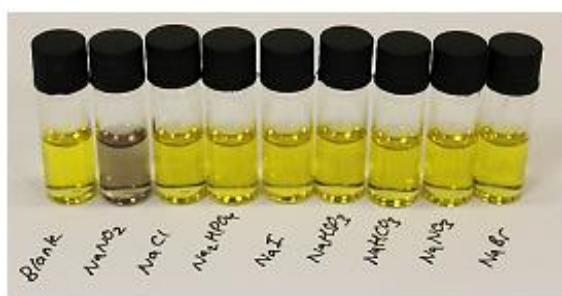
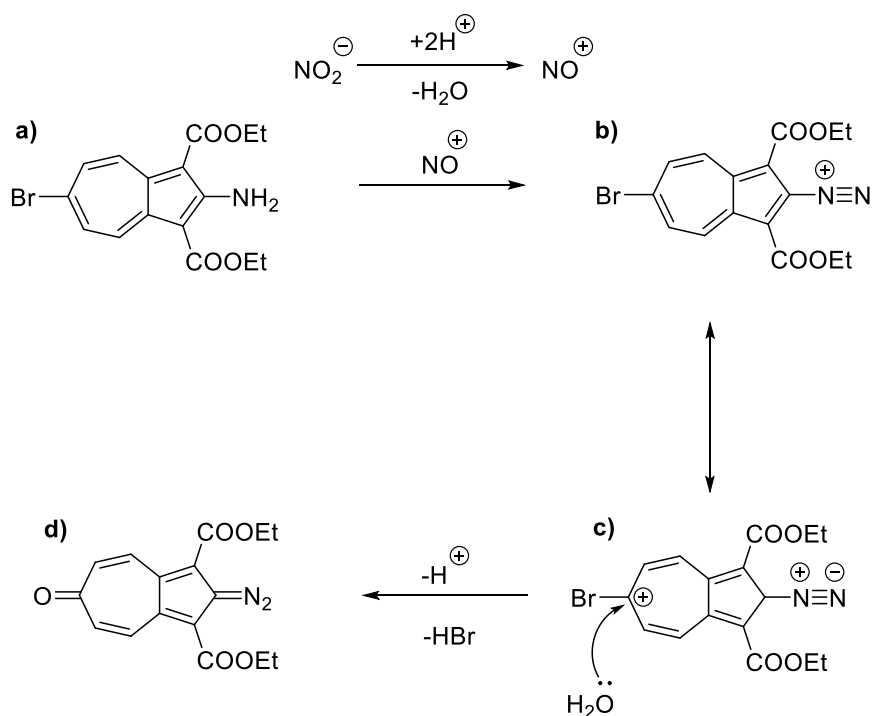
Figure 12: UV-Vis titration of NAz-6-Bpin in EtOH/H₂O 3:7, v/v (0.5 mM) with NaF. Figure reproduced from reference Lewis *et al.*²⁹

A noticeable colour change was observed after 10-20 eq. of NaF were added to produce a hypsochromic shift from a peak maximum of 486 nm to 462 nm. The limit of detection for the UV-Vis was found to be 5.75 mg L⁻¹ and the visual limit of detection was 10 mg L⁻¹.

1.3.4 Azulene for Nitrite Detection

Nitrites salts are used in many food preservatives particularly within cured meat products which to increase shelf life and produce a positive effect on the organoleptic properties of the product. However, the World Health Organisation (WHO) has specified that an acceptable range of nitrite ion per day is between 0-0.06 mg/kg of body weight, where an intake greater than these values poses potential carcinogenic risks. As such, being able to detect and quantify the nitrite content of a given sample provides early warning detection signals which could be used alongside the current British Standard testing procedure (Griess test) for the detection of nitrites.

The group of Lewis *et al.* were able to synthesise and evaluate an azulene-based chemodosimeter for the detection of nitrite.³⁰ The probe was found to be selective towards nitrite over other anions to which an instantaneous colour change from yellow to grey resulted until an eventual deep yellow/orange colour was produced as an endpoint from which quantitative analysis data was obtained. The analysis data was collected in a mixture of MeCN, deionised water, 35 % HCl_(aq), the sensor (5 mmol/L) and the analyte (5 mmol/L).



Scheme 3 and Figure 13: Reaction of the azulene chemodosimeter (a) with nitrosonium ion and selectivity of (d) with various anions in solution after 1 minute (left) and 10 minutes (right). Scheme and figure reproduced from reference Lewis et al.³⁰

The changes associated with the dose-response characteristics of the sensor with the addition of NaNO_2 analyte was also assessed through UV-Vis titrations. From this, it was found that increasing equivalents of nitrite produced an increase in absorbance at $\lambda = 318 \text{ nm}$ and a proportional increase in the absorbance for the diazoquinone, alongside a decrease in absorbance of the probe itself (at $\lambda = 320 \text{ nm}$ and 332 nm). The absorbance dose values suggested a 1:1 dose-response relationship between the sensor and the formation of diazoquinone.

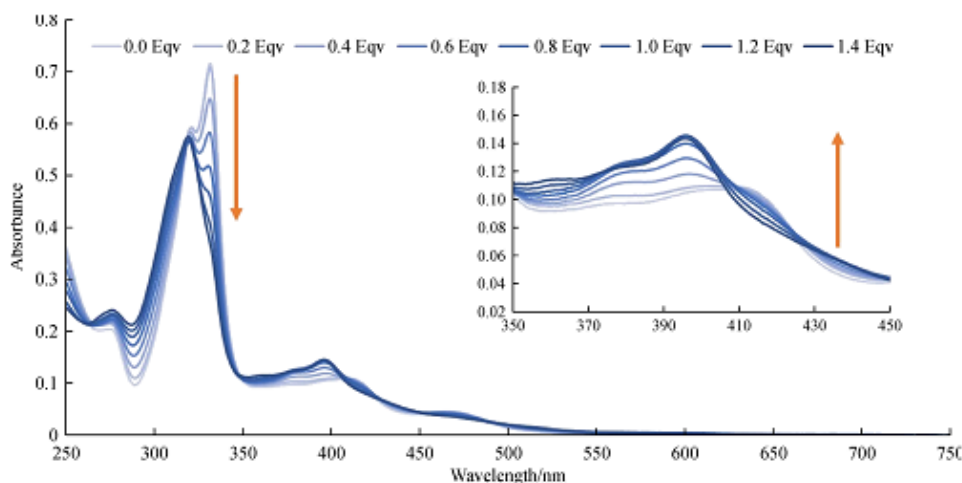


Figure 14: Dose response of the probe with increasing equivalents of NaNO_2 analyte. Figure reproduced from reference Lewis et al.³⁰

1.3.5 Azulene for Phosphate Detection

Azulene based probes have also found uses for acting as receptors for the recognition and sensing of phosphate anions. Phosphate anions are particularly one of the most important anions within biological systems, serving as key intermediates in many biological functions and processes such that being able to bind or detect these phosphate targets would serve to help with drug investigation analysis and other practical applications.

One such design of an anion receptor that has been researched by Jurczak *et al.* research group in Poland³¹ is that of a macrocyclic host molecule where the macrocyclic topology of the receptor is used to help with controlling the geometry of the binding site. They were able to develop a two 20-membered macrocyclic tetramide receptors based on azulene.

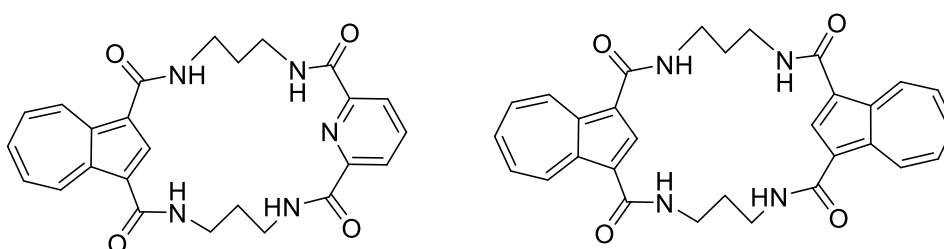


Figure 15: Synthesised macrocyclic tetramide receptors, receptor 1 (left) and receptor 2 (right). Figure reproduced from reference Jurczak *et al.*³¹

The conformational properties of the free receptors and their anion binding capabilities were investigated in solid state via X-ray crystallography and it was found that in both macrocycles all of the amide -NH hydrogen-bond donors point convergently towards the inner cavity creating a well-organised binding site for anionic guests.

As both macrocycles contain a chromophoric azulene moiety it is expected that such molecules will serve as anion sensors through naked-eye detection. The molecules were dissolved in DMSO and phosphate anions were introduced as tetrabutylammonium salts (TBA) salts and a moderate colour change of the sample in the presence of phosphate anions was visually observed whereas the macrocycles appeared to be insensitive to the presence of other anions. Particularly, the sensitivity towards both H_2PO_4^- and $\text{HP}_2\text{O}_7^{3-}$ triggered a visually apparent colour change.



Figure 16: Colour changes of receptors in dimethyl sulfoxide (DMSO) in the absence and presence of anions (3 eq. of TBA salts). Figure reproduced from reference Jurczak *et al.*³¹

Further optical studies were then carried out through UV-Vis spectroscopy and it was found that there was a red-shift in the absorption bands upon the addition of both H_2PO_4^- and $\text{HP}_2\text{O}_7^{3-}$ coupled

with a decrease in the intensity. Furthermore, receptor **1** appeared to be most sensitive to the presence of the phosphate anions as shown through the change of absorbance triggered by the anion addition.

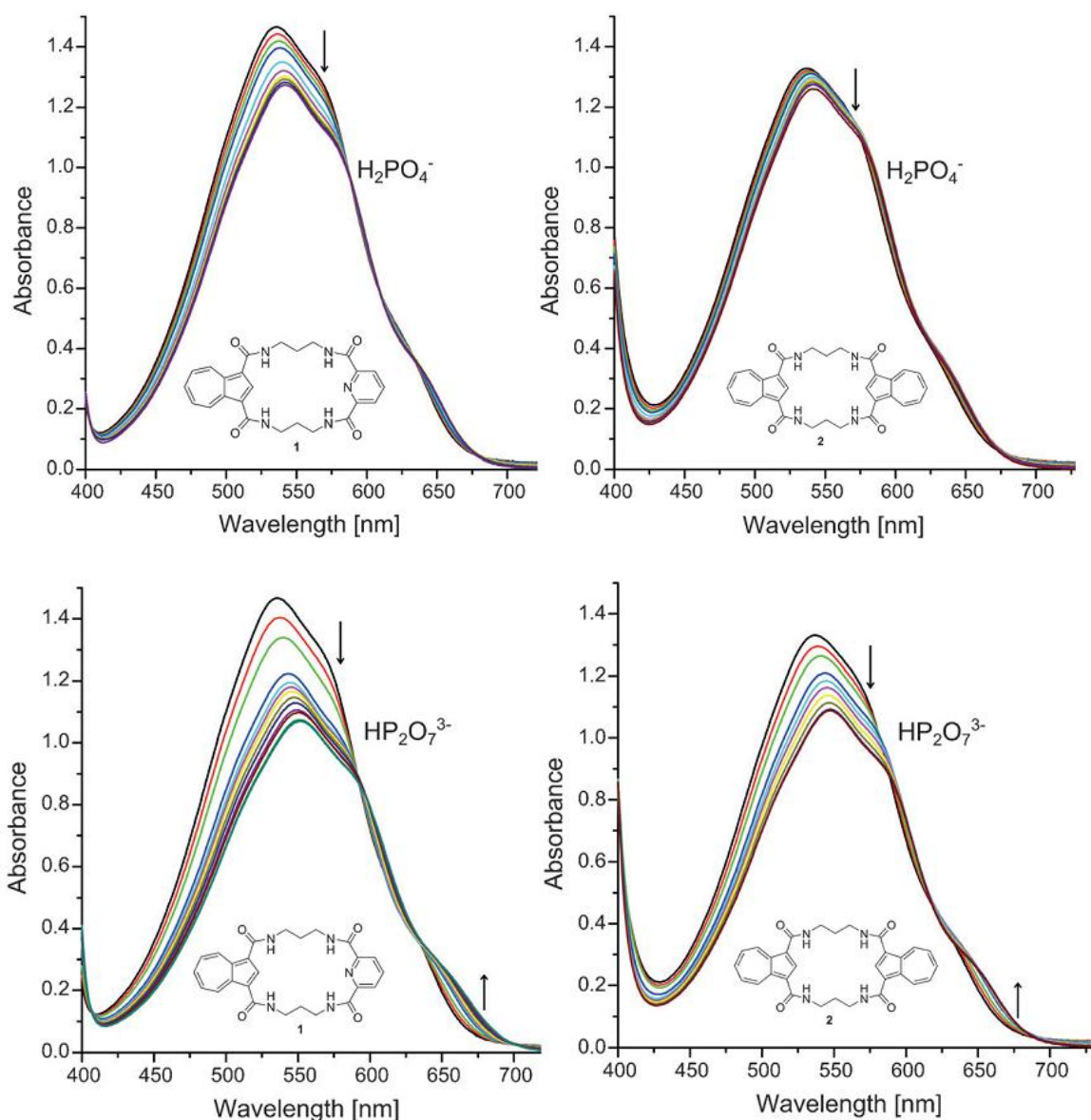


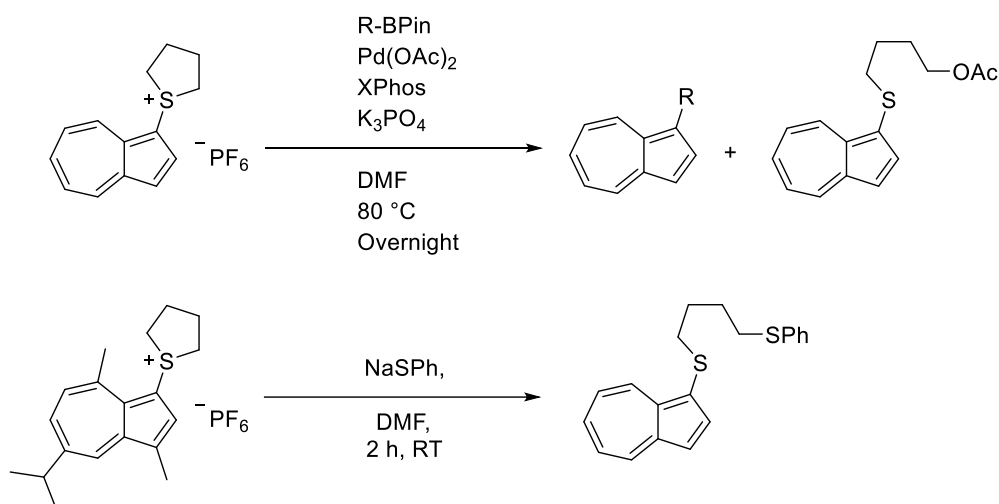
Figure 17: Spectral changes of macrocycles **1-2** upon addition of TBA salts of phosphate anions, where a) **1** with H₂PO₄⁻ (0-4 eq.); b) **2** with H₂PO₄⁻ (0-5 eq.); c) **1** with HP₂O₇³⁻ (0-3 equivalents) and d) **2** with HP₂O₇³⁻ (0-3 eq.). Figure reproduced from reference Jurczak et al.³¹

Further binding studies showed that these receptors bind strongly to a series of anions even in highly demanding media such as DMSO and water or with methanol. In particular, the affinity of symmetrical macrocycle **2** with two azulene-based subunits towards H₂PO₄⁻ is much higher compared to macrocycle **1** with one azulene-based subunit.

1.3.6 Azulene for Mercury Detection

The most common sources of mercury contamination in water comes from the salts of mercury (inorganic mercury) the compounds of which are water-soluble and cause poisoning when dissolved in water or in food and are ingested. Mercury intake has the potential to cause impairment of any organ in the body or any subcellular structure.

All forms of mercury have the potential to bind with sulfhydryl groups and selenohydryl groups of proteins and this has led many groups to use this property in order to develop colorimetric and fluorescent probes for the detection of mercury. One such example of this is from the work of a PhD student in the Lewis group in Bath, UK in which they were able to use an azulene sulfonium salt as a pseudohalide in a cross-coupling reaction.³² This reaction produced a by-product which resulted from a ring opening after the attack of a nucleophilic anion (the counter anion of the palladium complex used). This by-product was then used as a potential mercury sensor since it contained a sulphur group that has a strong affinity towards mercury and is attached directly to a chromophore, **scheme 4**.



Scheme 4: Two-step synthesis of the mercury sensor. Scheme reproduced from reference Lewis et al.³²

The potential mercury sensor candidate at 500 μM was then tested in an MeCN/H₂O (1:9) based system with various metal salts at 500 μM and a naked-eye selectivity test was carried out in which it was found that the colour of the solution changed from an initial blue to a green colour upon addition of Hg(NO₃)₂ salt (all other salts tested that were non-mercury based remained blue). Interestingly, the colour difference was more noticeable at lower concentrations of sensor and analyte (both at 50 μM) which resulted in a colourless to yellow colour change. This change in colour also corresponded to a new absorbance maximum of the bound mercury to the compound at 450 nm. As this work is not yet published to date, work to determine if the compound responds to real water contaminated with mercury is due to be carried out to determine if decomposition of the compound is likely to occur with differences in temperature, air and moisture.

The group went on further to synthesise a dithiane based azulene sensor. The resulting chemodosimeter was able to exhibit good chemoselectivity over other metal cations which were also tested as well as a vivid colour change visible to the naked eye changing from a light blue to a red colour when tested at a 500 μM concentration with 500 μM analyte Hg(NO₃)₂ (1:1) and NaOH. UV-Vis absorption spectra indicated a shift in the absorption maxima to longer wavelengths upon addition of Hg²⁺ ions.³³

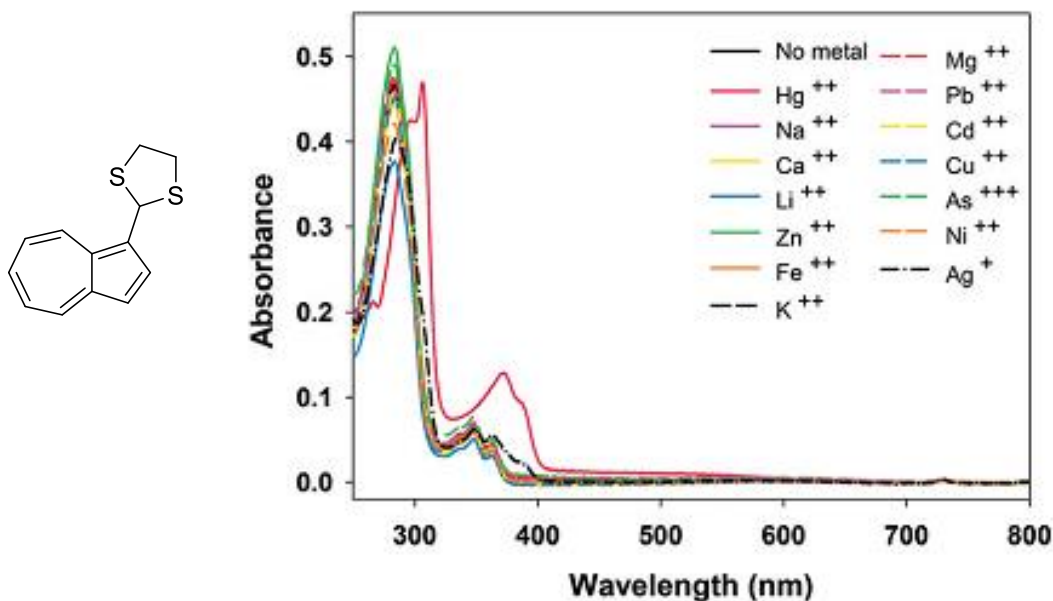


Figure 18: Colorimetric azulene mercury (II) chemodosimeter and UV-Vis absorption spectrum titration data at 500 μM concentration with 500 μM analytes in MeCN/H₂O. Figure reproduced from Lewis *et al.*³³

Such vivid colour changes are particularly useful for test applications in developing countries as visible indicators to help determine drinking water safety analysis.

1.3.7 Azulene for Silver Cation Detection

In 2013, Shimizu *et al.* synthesised two azulene derivatised azathiocrown ether moieties that were shown to be highly selective for detecting Ag⁺ ions shown by a colour change from orange to violet.³⁴

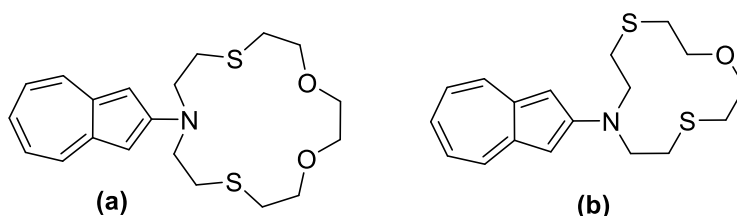


Figure 19: Developed silver detection azathiocrown ether moieties. Figure reproduced from reference Shimizu *et al.*³⁴

Changes to the spectral properties of the crown ethers were studied upon the addition of metal ions as the π -conjugated systems of azulene was expected to change. When one equivalent of Ag⁺ ions was added to azathiocrown ether (a) the violet colour changed to a yellowish orange suspension which when analysed showed a substantial red shift (75 nm) with an isosbestic point at 545 nm upon the addition of one equivalent of AgClO₄.

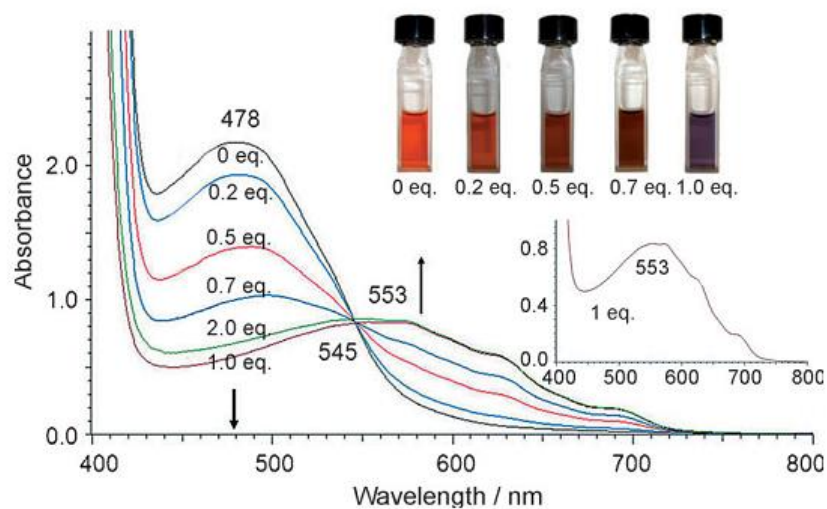


Figure 20: Spectral and colour changes of azulene derivatised azathiocrown ether (a) ($3.4 \times 10^{-3} M$) upon the addition of $AgClO_4$ in acetone. Amounts of $AgClO_4$ added varied from 0.2-2.0 eq. Figure reproduced from reference Shimizu et al.³⁴

Such behaviours occurred for both azathiocrown ethers. The shifts in the spectrum correspond to ion-dipole interactions such that as the dipole moment in azulene is reduced upon electronic excitation, the complexed Ag^+ ions will be destabilised to the ground state and stabilised in the excited state thus causing a bathochromic shift. The rapid formation of these complexes in these solutions were verified through nuclear magnetic resonance (NMR) and mass spectrometry (MS) analysis. In further studies, it was shown that other metal ions do not interfere with the Ag^+ colour change attributed to the relatively strong binding of the azathiocrown ether moiety to the Ag^+ ions.

1.4. Thiol Reactive Probes and Chemosensors

Thiols are important molecules in the environment and in biological processes therefore the selective detection of thiols using reaction-based probes and sensors is very important to research and in disease diagnosis.³⁵

Sulfhydryl containing compounds have unique chemical reactivity and can be specifically utilised in chemical reactions and in biological processes. The sulfhydryl group of Cys is an ideal nucleophile in enzyme catalysis and can readily undergo reversible redox reactions under physiological conditions thus maintaining tertiary and quaternary structures through disulfide formation.³⁶

Many of the detection methods used for thiol recognition, includes probes and labelling agents that are based on nucleophilic addition and substitution, Michael addition, metal-sulfur interactions, disulfide bond or Selenium- Nitrogen (Se-N) bond cleavage amongst others. Due to the strong nucleophilicity of the sulfhydryl group, it can readily react with electrophiles leading to some thiol probes behaving as Michael acceptors or alkylating agents which are able to be conjugated to a chromophore or fluorophore thus producing a detectable readout.³⁷

1.4.1 Nucleophilic Substitution for Thiol Labelling

Some halogenated alkylating/labelling agents which have been explored to date are monobromobimane (mBrB or mBB), 4-fluoro-7-sulfamoylbenzofurazan (ABD-F), 7-fluorobenzo-2-oxa-1,3-diazole-4-sulfonic ammonium salt (SBD-F), 5-iodoacetamidofluorescein (5-IAF), 2-chloro-1-methylpyridinium (CMPI) and 2-chloro-1-methylquinolinium tetrafluoroborate (CMQT). The halogen group on each of these compounds allows them to readily undergo nucleophilic substitution with other thiols. Some of the compounds listed namely mBrB, ABD-F, SBD-F and 5-IAF can form fluorescent conjugates with thiols whereas CMPI and CMQT yield UV absorbing conjugates.³⁸

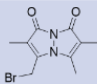
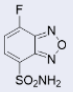
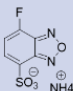
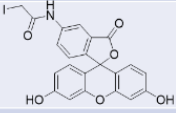
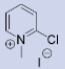
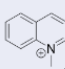
Alkylating/Labeling Agent	Abbreviation	Fluorescent Conjugates	UV Absorbing Conjugates	Thiol Reaction Times (min)
	mBrB	✓		2-20
	ABD-F	✓		5-60
	SBD-F	✓		60
	5-IAF	✓		15-120
	CMPI		✓	15-30
	CMQT		✓	1-4

Table 1: Common alkylating/ labelling agents for nucleophilic substitution with thiols.

All the agents listed in **table 1** have broad ranges in their reaction times, values of which are shown at the optimum pH and reaction temperature.

These agents have been used for quantitative analysis of thiols in urine and in plasma however a drawback of these agents is that they lack selectivity among various thiols as they rely only upon simple nucleophilic addition or substitution for chromogenic or fluorescent labelling and therefore separations though use of High performance Liquid Chromatography (HPLC) or Capillary Electrophoresis (CE) is needed to differentiate between the various thiol derivatives.

There are several other examples in the literature which use a 2,4-dinitrophenyl sulfonyl (DNBS) moiety which can act as an electron sink when attached to the fluorophore thus having the potential to incur a photo-induced electron transfer (PET) quenching the fluorescence, examples of which are shown in **figure 21**. Furthermore, the compounds below can also undergo de-sulfonylation in the

presence of thiols, thus releasing SO₂ gas and the attached fluorophore resulting in a fluorescence increase.

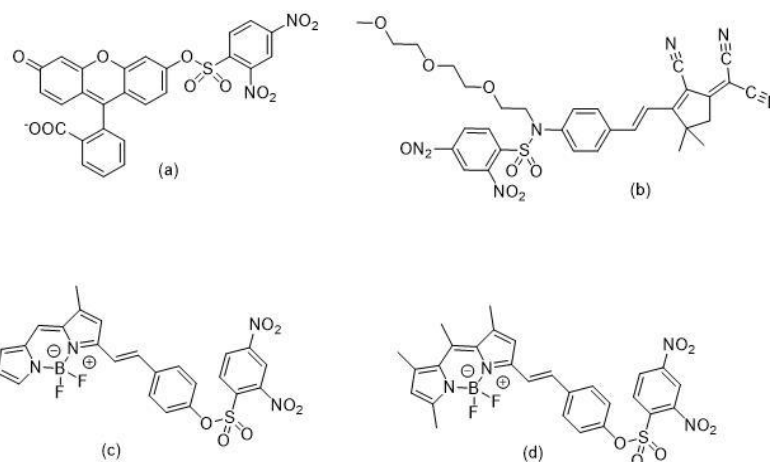


Figure 21: Fluorescent probes containing a DNBS moiety. Figures reproduced from references Hilderbrand et al.³⁹, Xu et al.⁴⁰, and Hue et al.⁴¹

1.4.2 Michael Addition for Thiol Labelling

Due to their excellent nucleophilicity, thiols readily react with Michael acceptors and it is only recently that Michael addition reactions have been used for thiol labelling.⁴² Several probes have been developed often using a maleimide moiety (**figure 22a**), quinone or an open chain Michael acceptor (**figure 22b**) to be used as a fluorescent sensor for thiols. Upon thiol addition, the conjugation in **figure 22b** is disrupted and the coumarin fluorescence is restored displaying a 200-fold increase in fluorescence through Michael addition processes as well as a low detection limit for Cys. The compound also shows a very low detection limit (1 μM) for Cys in a 25 mM phosphate buffer (pH 7.4).

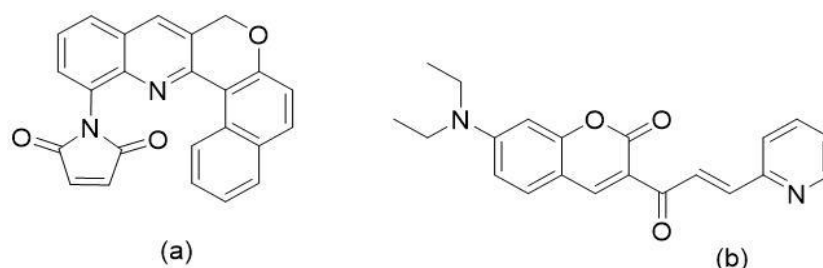


Figure 22: Michael addition used for maleimide (a) compounds and open chained Michael acceptors (b). Figures reproduced from references Talukdar et al.⁴³ and Long et al.⁴⁴

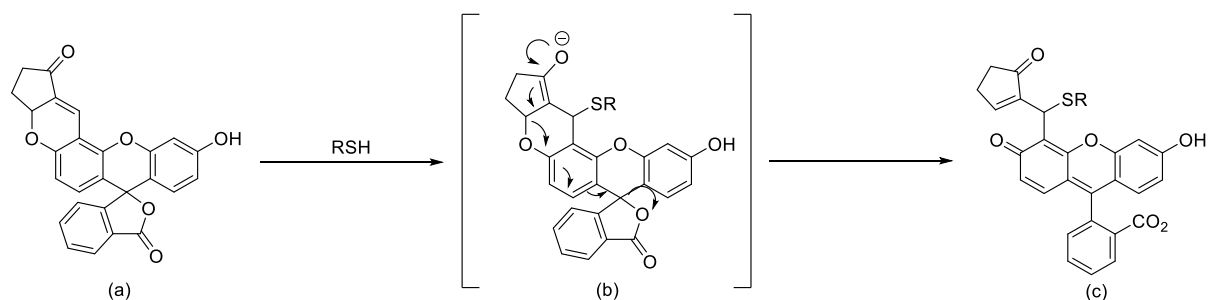
Modifications in Michael addition processes have also begun to study Michael addition triggered ring-opening reaction in the development of thiol probes as in **scheme 5**,



Scheme 5: Michael addition triggered ring-opening reactions to produce 4-nitrophenolate moiety, where -RSH is any thiol containing species. Scheme reproduced from reference Yin et al.⁴⁵

Upon ring opening to produce the 4-nitrophenolate moiety, a fast (10 s) and visual colour change was observed from colourless to yellow.⁴⁵ Further ring opening based Michael addition reactions have also been developed (**scheme 6**).

The probe produced in **scheme 6** responds selectively to Cys, Homocysteine (HCy) and GSH forming a fluorescent conjugate (c) with detection of thiols in the nM range. Analytes that do not contain thiols induced only small changes in fluorescence intensity. The probe was carried forward to show that thiol species existing within zebrafish were detected by the probe after 5 μ M 1-hour exposure.⁴⁶

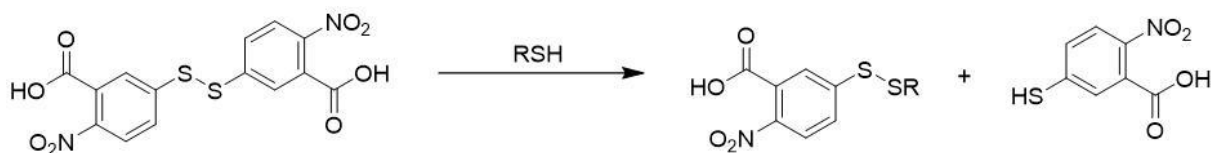


Scheme 6: Michael addition triggered ring-opening reactions to detect biothiols. Scheme reproduced from reference Yin et al.⁴⁵

1.4.3 Disulphide Cleavage for Thiol Labelling

One of the most important features of thiols is their reducing abilities which allows them to gain integral biological functions. The reduction of the disulphide bond in the probes by sulphur containing thiols results in production of a free chromophore which absorbs strongly in the UV-Vis range and therefore can be recorded on a UV-Vis spectrophotometer. A well-known example where disulphide cleavage is demonstrated is Ellman's reagent (5,5'-dithiobis-2-nitrobenzoic acid or DTNB).⁴⁷ The structure of DTNB lends itself to disulphide cleavage as a result of its two electron-deficient phenyl groups linked by a highly oxidising 'activated' disulphide bond which can be stoichiometrically reduced by free thiols in an exchange reaction. This process forms a mixed disulphide as well as forming one molecule of the highly chromogenic product (5-thio-2-nitrobenzoate, TNB) which has a high absorbance, **scheme 7**.

However, an issue with the Ellman's reagent is its low stability as under basic conditions it undergoes degradation leading to unwanted background absorption increase.⁴⁸ For optimal reaction rates slightly basic conditions are needed ($\text{pH} > 8$) and as a result other compounds containing disulphide linkages with higher stabilities have been developed.



Scheme 7: DTNB (Ellman's reagent) response to thiols which results in a disulphide bond cleavage. Scheme reproduced from reference Thorpe et al.⁴⁸

There are a variety of compounds in the literature which sought to eliminate instabilities associated with basic conditions (**figure 23**).

All the compounds listed react with thiols such as GSH and protein thiols, absorbing strongly when they are reduced. Furthermore, the reactivity of the disulphide bond towards thiols was found to be enhanced when the nitrogen on the pyridyl ring is protonated.

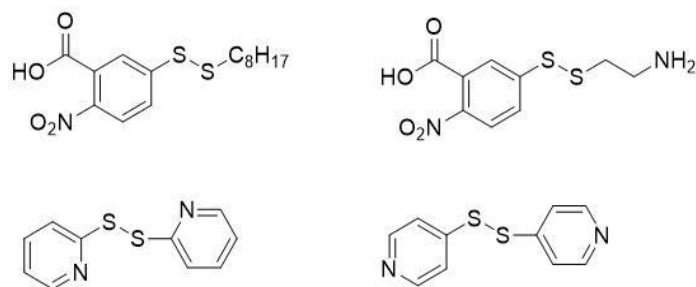
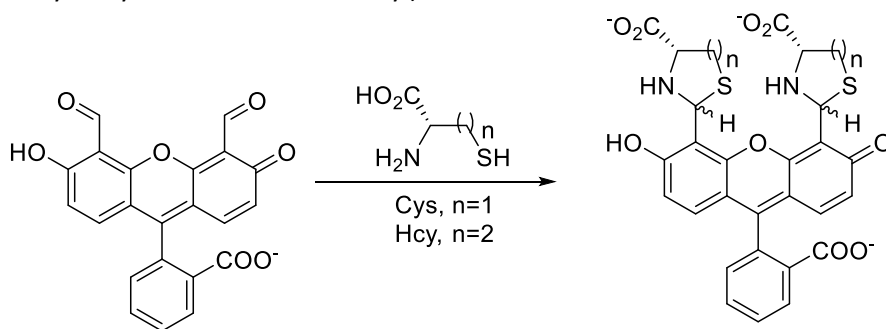


Figure 23: Thiol probes developed containing disulphide linkages for Michael addition. Figure reproduced from references Heintz et al.⁴⁹, Pei et al.⁵⁰, Means et al.⁵¹, and Murray et al.⁵²

1.4.4 Selectivity amongst thiols

To date, most indicators for thiol detection have been based on the strong nucleophilicity of the sulfhydryl group and due to its presence in a wide variety of thiol proteins, it's selectivity to react with many different compounds is not limited. Therefore, being able to develop a compound that can selectively react with certain thiols is highly desirable particularly ones that are related to many diseases.

Detection methods for specific thiols have been researched in the literature for quite some time however challenges arise when attempting to discriminate thiols such as Cys and Hcy from each other using a single probe due to their structural similarity which differ by a single methylene unit in their side chains. In 2004 this dilemma was explored through the pioneering work of the Strongin group that reported a colorimetric method for the selective detection of Cys by using an aldehyde, 2-(4,5-diformyl-6-hydroxy-3-oxo-3H-xanthen-9-yl) benzoate.⁵³



Scheme 8: The reaction of 2-(4,5-diformyl-6-hydroxy-3-oxo-3H-xanthen-9-yl)benzoate with Cys or Hcy. Scheme reproduced from reference Strongin et al.⁵³

Through this work, the reaction between the aldehyde (1.0×10^{-6} M, H₂O, pH 9.5) and *N*-terminal Cys and Hcy (1.0×10^{-3} M) (scheme 8) promotes a colorimetric response *via* formation of a thiazolidine between the aldehyde and Cys, which is observed visually by a colour change from a bright yellow to a brownish-orange, figure 24.



Figure 24: Colour changes of 3-(4-(dimethylamino) phenyl) acryl aldehyde with (L-R) no analyte, L-Cys, L-HCy, bovine serum albumin, L-glycine, and n-propylamine. Figure reproduced from reference Strongin et al.⁵³

There is a noticeable shift in the UV-Vis absorbance when the concentration is changed from 10^{-5} and 10^{-6} M via a 25 nm red shift (from 480 nm to 505 nm) which is selective for Cys and Hcy analytes (figure 25) as well as a decrease in the fluorescence intensity compared to when other common thiols, amino acids and amines are used instead. When other analytes are used, they exhibit relatively small absorbance and no shift in wavelength is observed.

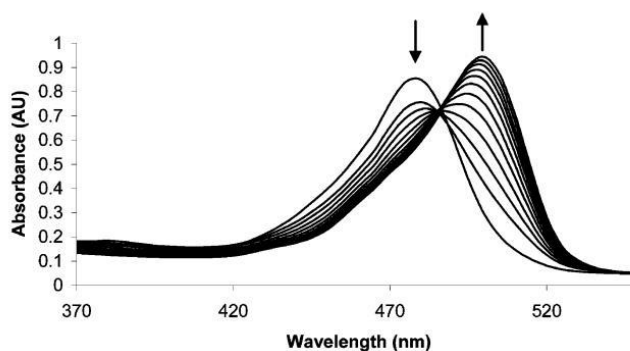
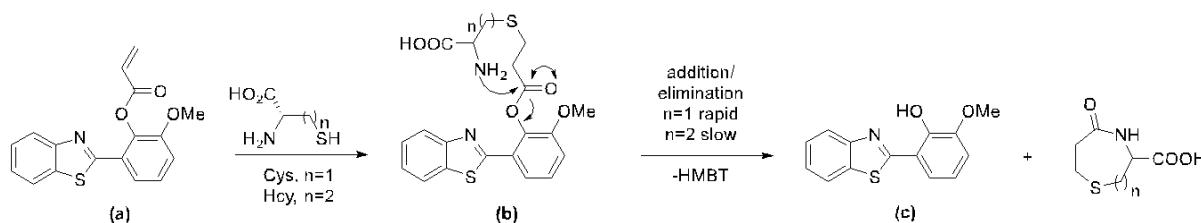


Figure 25: UV-Vis spectra of 2-(4,5-diformyl-6-hydroxy-3-oxo-3H-xanthen-9-yl)benzoate (4×10^{-6} M) and L-Cys (4.9×10^{-5} – 7.4×10^{-4} M) containing 1.0 mM GSH (pH 9.5). It is shown that as the concentration of L-Cys increases, a red shift from 480-500 nm is observed. Figure reproduced from reference Strongin et al.⁵³

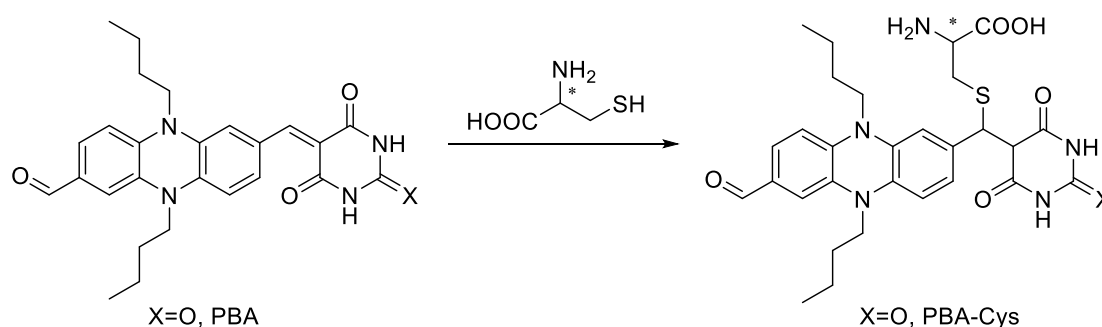
Following on from this, in 2012 the Strongin group looked into a probe that is designed from the fluorophore, 2-(2'-hydroxy-3'-methoxyphenyl)benzothiazole (HMBT). It was proposed that replacing the hydroxyl group of the fluorophore with an α,β -unsaturated carbonyl moiety could then be used to react with Cys and Hcy to produce a selective dual emission differentiation of the two thiols based on their different reaction rates, scheme 9.⁵⁴



Scheme 9: The reaction sequence for the sensing and differentiation of Cys and Hcy. Scheme reproduced from reference Strongin et al.⁵⁴

The HMBT fluorophore is used to facilitate this process via the measurable differences in the emission bands of the enol (b) ($\lambda = 377$ nm) and keto ($\lambda = 487$ nm) after conjugate addition of Cys and Hcy followed by intramolecular nucleophilic attack from the amino group to release a HMBT fluorophore producing a change in the fluorescence.

In 2017, Hua *et al.* were able to design a phenazine-barbituric acid (PBA) based colorimetric and ratiometric fluorescent probe which was used for the ultrasensitive and selective detection of biothiols particularly towards Cys.⁵⁵ The reduced phenazine was chosen based on its excellent optical properties and the electron-deficient barbituric moiety acted as the recognition group towards the biothiols and for attachment to surface platforms such as Titanium dioxide (TiO₂) useful for assembling such sensor devices for their detection in biological environments. In addition, the electron-withdrawing properties of the barbituric acid would lead to measurable bathochromic shifts in absorption and fluorescence emission, **scheme 10**.



Scheme 10: Sensing mechanism of probes PBA and PTA towards Cys. Scheme reproduced from reference Hua et al.⁵⁵

The conjugate addition reaction between the PBA and PTA with Cys produces an acceptor-donor-acceptor (A-D-A') structure with two different routes for intramolecular charge transfer (ICT).

The optical studies of PBA were measured using a concentration-dependant absorption spectrum (**figure 26**) where the high absorption wavelengths were due to the strong ICT process between phenazine and barbituric acid groups and the other two smaller absorption bands as a result of the absorption of the phenazine and aldehyde group.

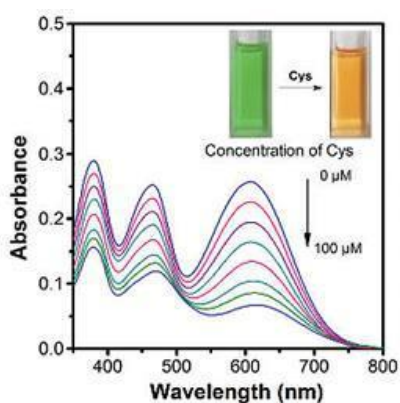
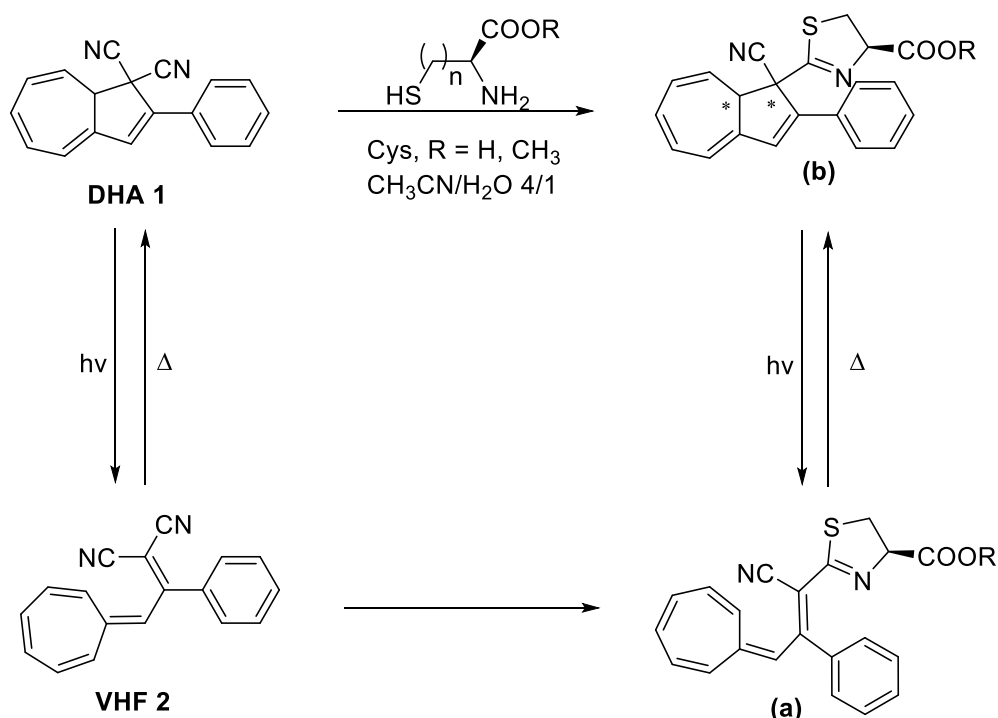


Figure 26: Concentration-dependant absorption spectra of PBA (10 μM) towards differing amounts of Cys (0-100 μM). Figure reproduced from reference Hua et al.⁵⁵

The selectivity of the probe towards Cys is especially prominent in the absorption and fluorescence spectra when compared to HCy and GSH where reaction rates and responses were much weaker by comparison.

More specifically although still in their infancy, thiol sensors are also starting to be explored in azulene based systems such as in dihydroazulene/vinylheptafulvene (DHA/VHF) systems⁵⁶ through a colorimetric response as naked-eye probes due to the difference in their strong colours as a result of their different electronic properties. The tuneable optical properties (and therefore colours) of such systems are starting to make azulene based compounds attractive for use as detection probes.



Scheme 11: Reaction scheme to show compounds that are formed in the presence of Cys or Cys methyl ester. Scheme reproduced from reference Nielsen et al.⁵⁶

Upon addition of Cys a colour change from orange to a slight yellow was observed only for the Cys however no obvious colour change was observed for the other amino acids tested (**figure 27**).

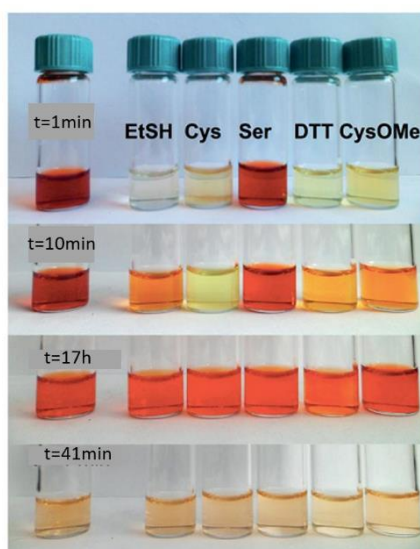


Figure 27: Colour changes of a 1.0 mM solution of DHA/VHF in CH₃CN/H₂O upon addition of 10 eq. of (L-R) EtSH, Cys, Serine (Ser), DTT and Cys-OMe. Figure reproduced from reference Nielsen et al.⁵⁶

The solution was further tested using mass spectrometric assays (MALDI-TOF) which supports the process occurring in **scheme 11** where there is a reaction between the thiol groups of the Cys with one of the cyano groups of the DHA. Measurements of the solution using UV-Vis absorption showed a small redshift after 24 hour and a decrease in the absorption band of DHA at 356 nm.

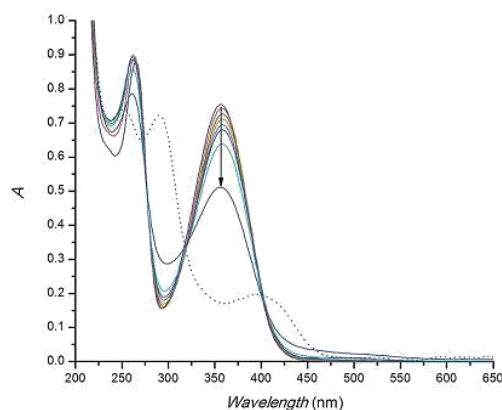


Figure 28: Absorption spectra of the reaction between DHA (5.5×10^{-2} mM) and Cys (50 eq.) in $\text{CH}_3\text{CN}/\text{H}_2\text{O}$ (4:1) at 25 °C for 2 d in the dark. Top to bottom, $t = 0, 4, 8, 12, 16, 20, 24$ and 48 h. Dotted line shows the final solution after 48 h which indicates possible precipitation due to Cys aggregates. Figure reproduced from reference Nielsen *et al.*⁵⁶

The characteristic absorption band at 402 nm which is blue shifted compared to VHF which has an absorption maximum at 478 nm suggests that an intermediate is formed (**figure 11a** above) and a further absorption maximum is observed at 293 nm is proposed to be the structure of (**figure 11b**).

In other studies, selective detection of GSH was found when two fluorescent probes which were developed by T. D. James and co-workers were used for detection.⁵⁷

These molecules are of particular interest as TCF-based fluorophores have an internal charge transfer (ICT) donor- π -acceptor (D- π -A) structure with long emission wavelengths and in previous studies such systems have been used for the detection of thiols previously when coupled with a PEG unit to provide good aqueous stability. However, the compounds developed by T. D. James *et al.* were able to detect biological thiols based on an analogous sulfonate ester in aqueous solutions without the need for an additional PEG unit.

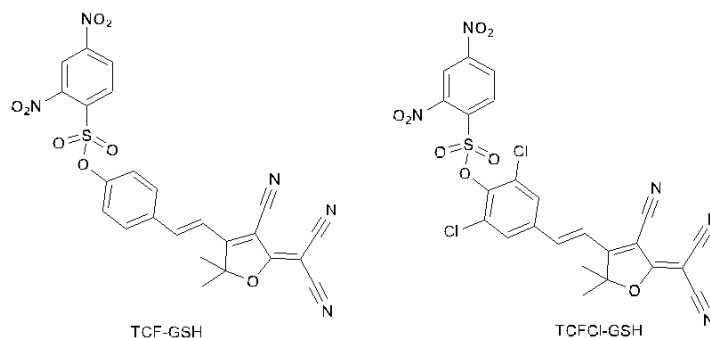


Figure 29: TCF containing fluorescent probes (TCF-GSH and TCFCl-GSH) developed by T. D. James *et al.* for the detection of biological thiols.⁵⁷

Of the molecules developed, it was found that TCF-GSH was particularly sensitive towards GSH however at higher concentrations of GSH the fluorescence intensity for the compound was reduced and toxicity became an issue. However, for the other compound that was synthesised, TCFCl-GSH, this was not found to be the case as the compound was non-toxic and the fluorescence was able to be 'turned on' for GSH, Cys and HCy. In addition, it was also found that upon addition of NAC, the GSH levels were increased and the fluorescence was enhanced.

Chapter 2: Results and Discussion

2.1. Sulfide Sensors

The goals of this project were to develop azulene/guaiazulene based sulfide sensors for the detection of thiols. To date, there have been no reports in the literature of azulene/guaiazulene colorimetric or fluorescent probes for thiols hence the work carried out in this area would be novel. Furthermore, research in this area would provide interesting information into the chemistry of such molecules and allow for greater understanding of sulphur detection and methods of validation.

Several reactions have been carried out using a wide range of synthesis methods and this has allowed for several novel compounds to be developed and subsequently tested with thiol analytes.

2.1.1 Guaiazulene and Azulene functionalised barbituric acid motifs (5-membered ring)

As the Lewis group has already extensive knowledge in the chemistry and applications of azulene and guaiazulene compounds,^{26,30,58} efforts were focused on using such compounds for thiol detection, initially starting on the development of azulene/guaiazulene containing barbituric acid motifs.

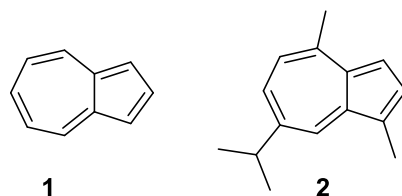
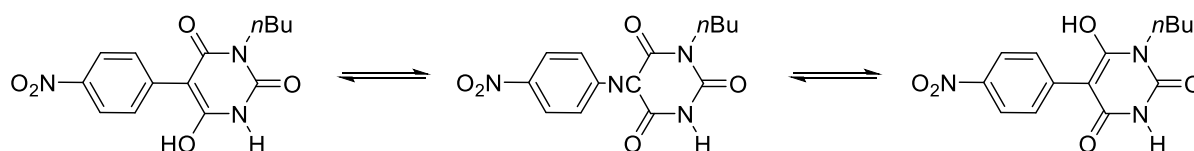


Figure 30: Structures of azulene (1) and guaiazulene (2)

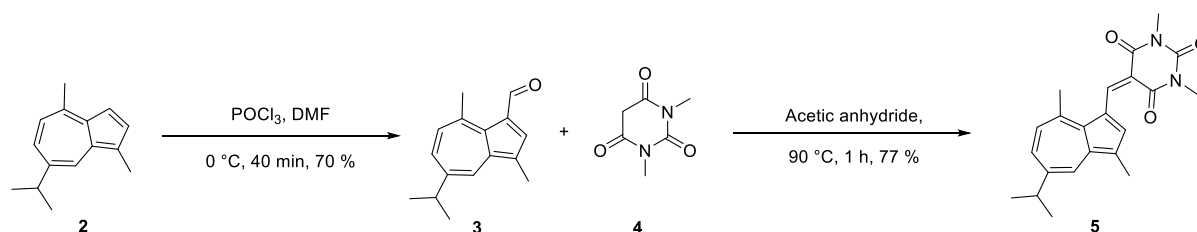
The barbituric acid motif was chosen following a paper by Bolz and Spange⁵⁹ who reported synthesising an enolisable barbiturate based on barbituric acid for the detection of nucleic acid bases and related compounds. The paper stated that certain merocyanine dyes containing the barbituric acid moiety as an electron withdrawing substituent has a molecular recognition sequence related to those of nucleic acid bases.



Scheme 12: Barbituric acid derivative, keto-enol equilibrium

Therefore by changing the conditions of the chromophore containing the barbituric acid, the acidity and basicity of the molecules can be varied ultimately leading to a bathochromic shift which can be detected by UV-Vis absorption spectroscopy. Using this barbituric acid as a motif was then explored further through the works of Hua *et al.* in which it was used as a recognition sensor for biothiols including Cys (scheme 10).

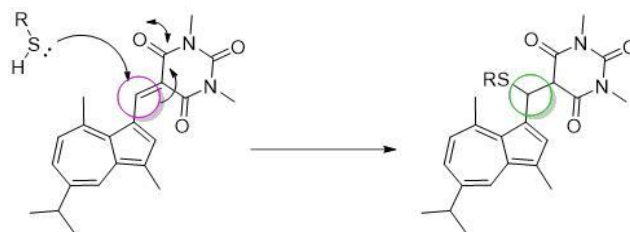
One of the initial compounds synthesised **5** via Knoevenagel condensation is shown below.⁶⁰



Scheme 13: Knoevenagel Condensation of 3 with 4

¹HNMR analysis showed the formation of the desired product formed in a 77 % yield. Once the product was synthesised, the next stage was to attach the thiol to the compound to initiate a 1,4-Michael addition thereby inducing a change in the electronic structure.

Theoretically, the thiol nucleophile would attack the compound though conjugate addition, resulting in enol formation from the movement of the double bonds which will then result in enol-keto tautomerism to produce the keto version on the 1,3-dimethylbarbituric acid.



Scheme 14: Upon thiol attack to 5, changes to the electronic structure cause a change from sp^2 (pink) to a sp^3 hybridization (green)

As the highlighted carbon of the compound changes from a sp^2 to a sp^3 hybridisation upon thiol attack, the conjugation from **2** and **4** is altered and the two moieties in effect act as two separate π -systems with their own conjugation. This means that the colour of the compound upon thiol attack will in theory revert to becoming blue (the same colour as standard guaiazulene). In this way, a visual colour observation can be used to deduce whether a reaction has taken place.

In order to carry out these tests DMSO and dimethylformamide (DMF) were the solvents of choice with NAC as the chosen analyte based on its ability to dissolve in both solvents.

Eq. Sensor: Analyte	Solvent	Colour change
1:1	DMSO	None
1:8	DMSO	None
1:1	DMF	None
1:8	DMF	None
1:10	CH ₃ CN	None

Table 2: Sensor and Analyte at varied equivalents in different solvents

In all conditions tested, no colour change was observed in any of the cases. To show this, pictures were taken and an example using MeCN solvent is shown where a series of analytes (each at 5 mM/H₂O) were tested at room temperature with compound **5** (0.5 mM).



Figure 31: Image taken of 5 with a range of different analytes

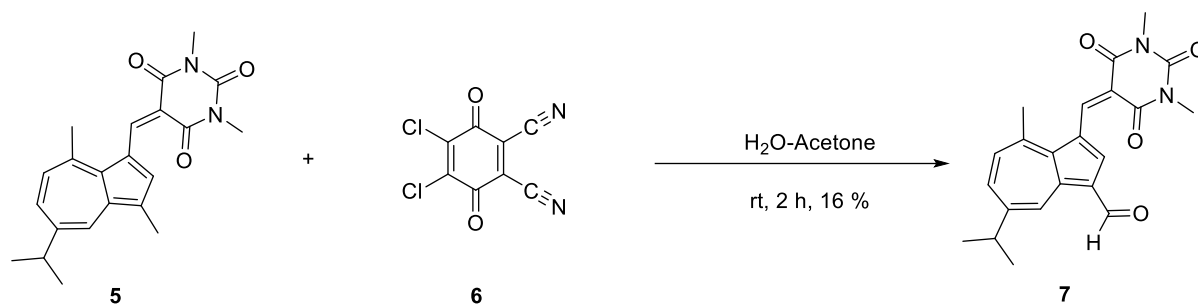
The analytes tested were, L-R: control, Cys, Na₂S, NAC, NaCl, NaBr, NaI, NaF, cysteamine and NaNO₃ in MeCN.

In addition to what is already shown, the samples were also stirred at rt. at room temperature for one week and heated at reflux at 10-100 eq. of NAC for 16 hours however no colour change was observed. The sample was even reacted with 5 % lithium chloride such that it would act as a source of nucleophilic chloride ions to see if any colour change ensues however the reaction mixture did not change colour.

It was initially thought that the high electron density inside the guaiazulene ring could be the issue and that the alkene position is not electrophilic enough for the nucleophilic thiol to attack.

Therefore, modifications were made on the side chains of the guaiazulene to reduce the electron density surrounding the alkene position attached to the guaiazulene.

The first approach taken was to introduce a carbonyl group to replace the methyl group on the 1 position of the guaiazulene 5-membered ring. This procedure has already been reported using a similar compound by Okajima and Kurokawa⁶¹ with yields > 99 % using **6** (DDQ) as a reagent. DDQ oxidation is a unique technique used for changing the unreactive 1-methyl group into a formyl group.



*Scheme 15: DDQ oxidation to convert the 1-methyl group into a formyl group converting **5** into **7***

Compounds **5** and **6** were added together as a 1:7 eq. to produce desired compound **7** in a good 71 % yield. However, this compound did not appear to change colour with any of the analytes tested.



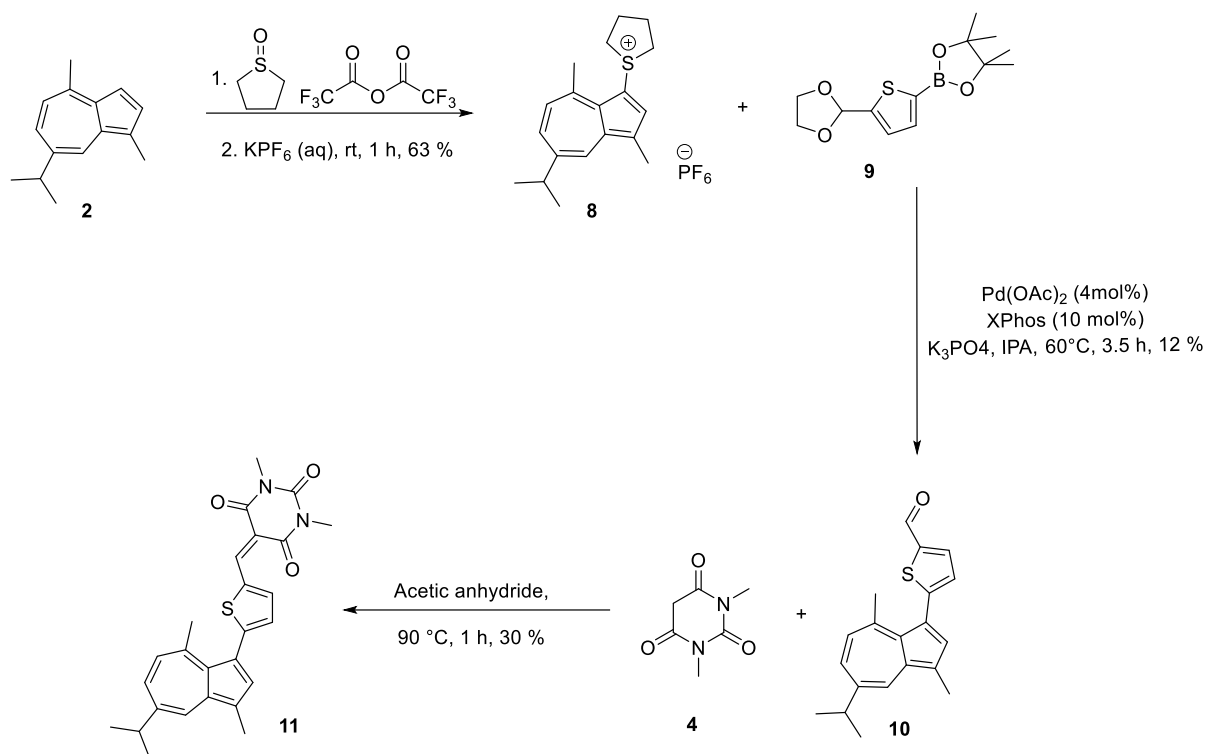
*Figure 32: Image taken of **7** with a range of different analytes*

The analytes tested were, L-R: control, Cys, Na₂S, NAC, NaCl, NaBr, NaI, NaF, cysteamine and NaNO₃ in MeCN.

Similarly, to previous samples the solution was stirred at rt. for one week and heated at reflux using 10-100 eq. of NAC for 16 hours however no colour change was observed. In addition, the compound was also reacted with 5 % LiCl such that nucleophilic chloride ions would be available however no colour change was observed.

Following on from this, research began to investigate the potential for attaching a linker compound such as thiophene in between the guaiazulene motif and the 1,3-dimethylbarbituric acid to reduce the electron donating effects from the guaiazulene ring and to make the desired site of thiol attack more electrophilic. The following series of reactions were carried out (**scheme 16**).

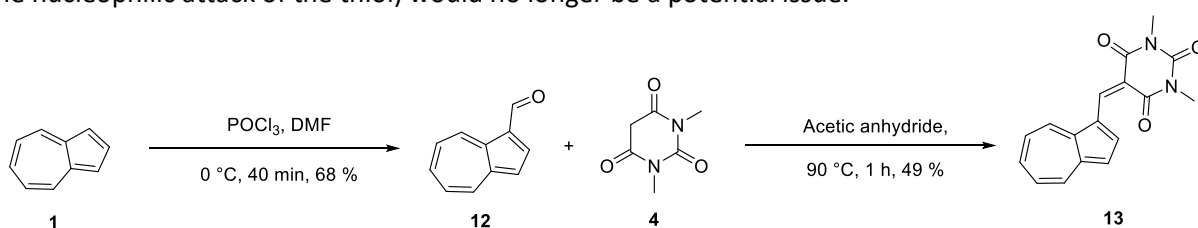
In the first stage of these reactions, an interrupted Pummerer reaction was carried out to produce **8** in a 63 % yield.⁶² This was then followed by a Suzuki-Miyaura coupling reaction of **8** with **9** to produce **10** which *via* a Knoevenagel condensation produced the desired compound **11** in a 30 % yield.



Scheme 16: Synthesis towards developing a thiophene linker to separate the guaiazulene and 1,3-dimethylbarbituric acid moieties.

The thiophene bridged compound **11** was then reacted with NAC in DMSO and heated at 90 °C for 16 hours however no desired product was obtained, and no colour change was observed. This reaction was also undertaken in CH₃CN at high temperatures (85 °C) and reacted with 5 % LiCl however, no colour change was observed.

In order to overcome some of the potential issues surrounding the compounds synthesised thus far and their lack of reactivity towards nucleophilic thiol attack, an azulene linked 1,3-dimethylbarbituric acid was synthesised. In this way, the C4-methyl group of the guaiazulene (which may be hindering the nucleophilic attack of the thiol) would no longer be a potential issue.



Scheme 17: Synthesis of substituted azulene with 1,3-dimethylbarbituric acid

Compound **1** was reacted *via* the Vilsmeier-Haack process to produce **12**, which was then reacted with **4** *via* a Knoevenagel condensation to produce **13**. This compound was then reacted with a series of nucleophiles (analytes) to determine whether it displayed any reactivity.

As the results in **table 3** show, a series of analytes were tested with **13** in MeCN at 85 °C for 16 hours however, no new product was indicated *via* a lack of visual colour change even when tested with 5 % LiCl.

This result led to the hypothesis that the methyl group on the guaiazulene is not the hindering factor in these reactions and that the lack of reactivity may come from the strong electron donating ability of the azulene ring.

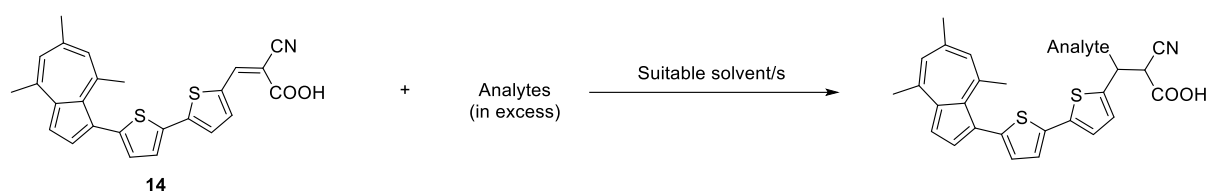
Eq. Sensor: Analyte in CH₃CN	Analyte	Colour change
1:10	NAC	None
1:10	Na ₂ S	None
1:10	NaCl	None

Table 3: Analytes tested with 13 in MeCN as a solvent

2.1.2 Guiazulene and Azulene functionalised cyanoacetic acid (5-membered ring)

Due to the unsuccessful reaction between 1,3-dimethylbarbituric acid connected with a series of guiazulene and azulene based compounds with different thiols under a variety of different conditions and solvents, our investigations focused towards studying the reaction between functionalised guiazulene and azulene motifs when attached to a cyanoacetic acid moiety. Such compounds have been studied before in the group and colour changes had been noticed before when brine was used during work up processes hence indicating potential 1,4-Michael addition reactions. Following on from this, investigation using a thiol anion which ultimately favours conjugate addition coupled with the strong electron withdrawing effects of the nitrile and carboxylic acid was studied.

In order to begin this investigation, a compound supplied by a previous member of the group, Dr. Paul Cowper was tested with a series of analytes under different conditions and in different solvents (scheme 18).



Scheme 18: Reaction between **14** and a variety of different analytes (in excess) in suitable solvents to produce the resulting product of conjugate addition reactions

In order to carry out these tests, a series of analytes (each at 5 mM/H₂O) were tested at room temperature with **14** (0.5 mM) in three different solvents; MeCN, THF and DMSO. It was observed that colour change was most noticeable with NAC in all the solvents tested.



Figure 33: Images taken of **14** with a range of different analytes. Top-bottom: In MeCN, THF, DMSO.

The analytes tested were, L-R: control, Cys, Na₂S, NAC, NaCl, NaBr, NaI, NaCN, NaF, cysteamine and NaNO₃ in solvents, from top to bottom: MeCN, THF and DMSO. Most noticeable colour change in all samples were observed for NAC from a yellow to an orange colour immediately upon addition of the NAC.

The UV-Vis absorption spectra were recorded for these test samples. In each solvent, there is a noticeable shift in the absorption maxima for NAC which correlates to the change in colour visually observed.

As shown by **figure 34**, the peak maxima for the other analytes excluding NAC remain at around 420 nm however the peak absorption maxima for NAC have shifted to 435 nm (15 nm difference).

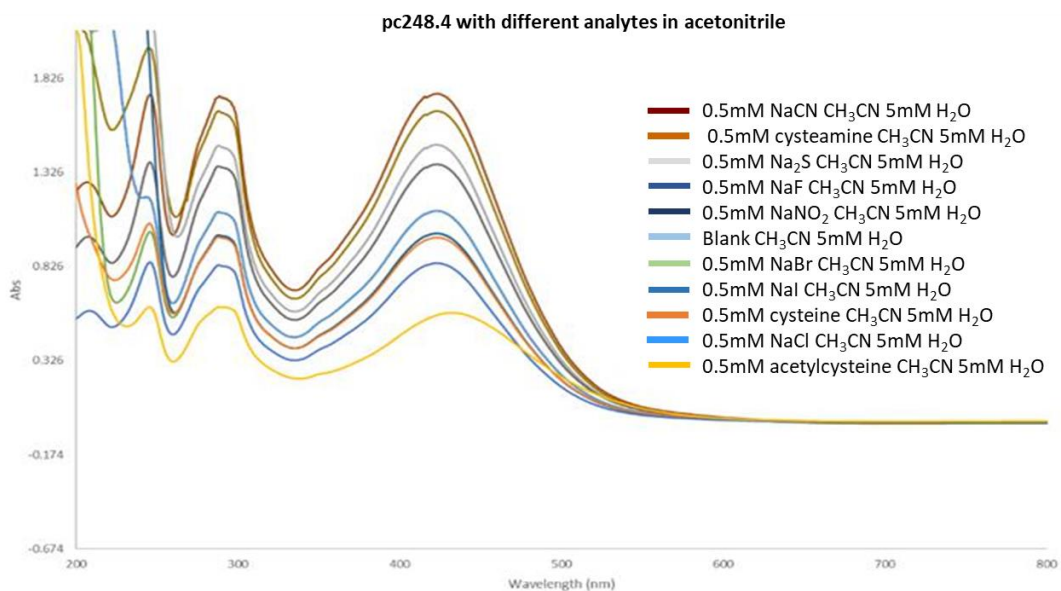


Figure 34: UV-Vis Absorption spectra for 14 (0.5 mM) in MeCN with analyte (5 mM).

Similarly, there is a noticeable shift in the absorption peak maxima in THF solvent which appears at 420 nm for all other analytes and 434 nm for NAC (14 nm difference).

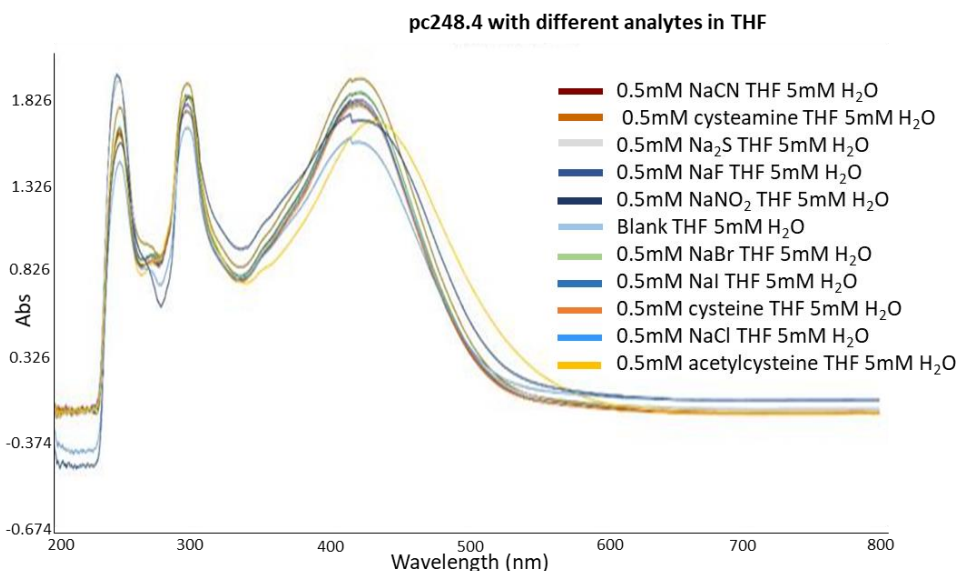


Figure 35: UV-Vis Absorption spectra for 14 (0.5 mM) in THF with analyte (5 mM).

Finally, the last solvent investigated was DMSO. Once again, there is a noticeable shift in the absorption maxima 426 nm for all the other analytes and 438 nm for NAC (12 nm difference). In addition to the standard concentrations used so far in the analysis (0.5 mM for the sensor and 5 mM for the analyte, a 1:10 eq. of sensor to analyte), concentrations of the analyte were increased to 10, 15, 25 and 50 mM to study what effect this would have on the absorption maxima for the compound.

As **figure 36** shows, generally as the concentration of the analyte is increased above 5 mM, the absorption bands decrease.

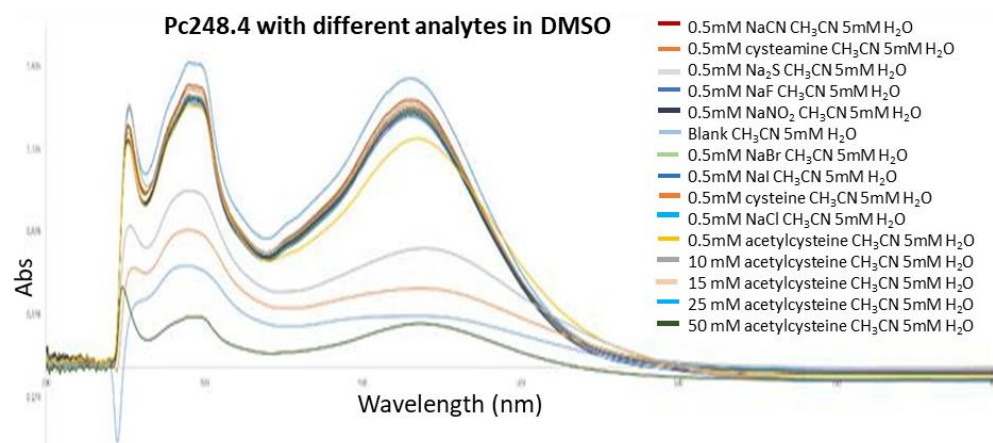
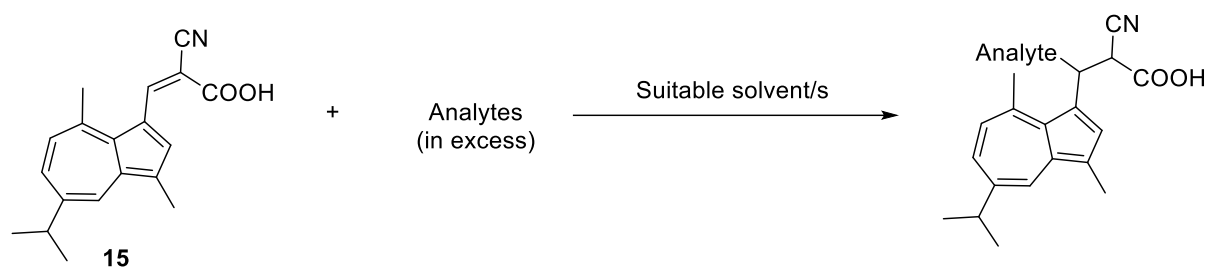


Figure 36: UV-Vis Absorption spectra for **14** (0.5 mM) in DMSO with analyte (5 mM).

In order to study what effect the thiophene linkers may have towards the absorption properties of the compound with different analytes, an alternative compound without the thiophene linkers was also investigated.



Scheme 19: Reaction between **15** and a variety of different analytes (in excess) in suitable solvents to produce the product of conjugate addition.

15 has been synthesised previously⁶³ and measurements of its absorbance characteristics were recorded, where it displayed a strong absorbance band within 375-550 nm and a very weak absorption tail extending beyond 650 nm. The guaiazulene compound was compared against its azulene counterpart and it was found that the absorption was very sensitive to ring substitution, whereby the addition of the alkyl substituents on the azulene ring for guaiazulene produced noticeable red shifts.

Similar to the experiments carried out previously, the same three solvents were used, and concentrations remained at 5 mM and 0.5 mM for the analyte and sensor respectively and that the compound produced a noticeable colour change from a yellow solution (no analyte present) to an orange colour upon addition specifically for NAC.

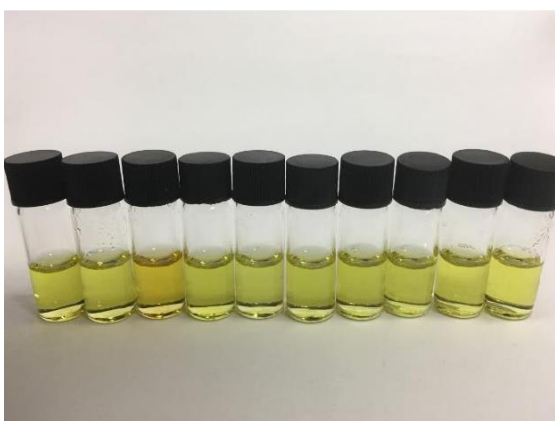
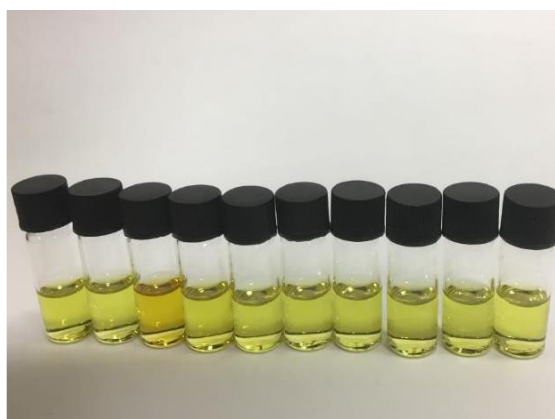
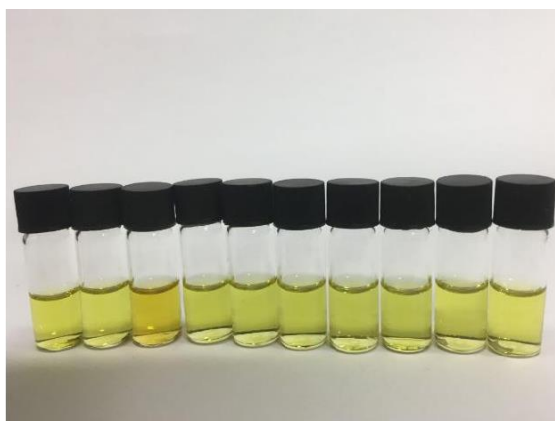


Figure 37: Images taken of 15 with a range of different analytes. Top-bottom: In MeCN, THF, DMSO.

The analytes tested were, L-R: control, Na_2S , NAC, Cys, NaCl, NaBr, NaI, NaF, NaNO_3 and cysteamine in solvents, from top to bottom, MeCN, THF and DMSO. Most noticeable colour change in all samples was observed for NAC from a yellow to an orange colour immediately upon addition of the NAC.

The UV-Vis absorption spectra were recorded for these test samples and is shown below.

In **figure 38**, the absorption peak maxima occurs around 439 nm for all analytes aside from NAC where the peak maxima has been shifted to 465.5 nm (26.5 nm shift).

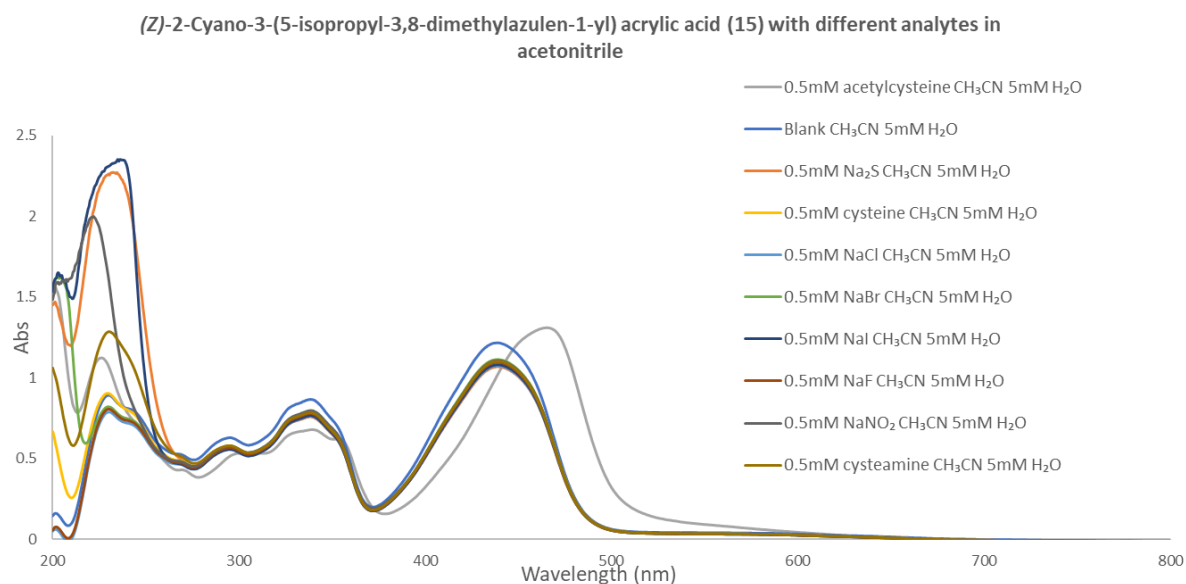


Figure 38: UV-Vis Absorption spectra for 15 (0.5 mM) in CH₃CN with analyte (5 mM).

In **figure 39**, there is also a peak maximum shift towards higher wavelengths in THF. The absorption maxima appears at 436 nm for all analytes aside from NAC where the peak maxima has shifted to 466 nm (30 nm shift).

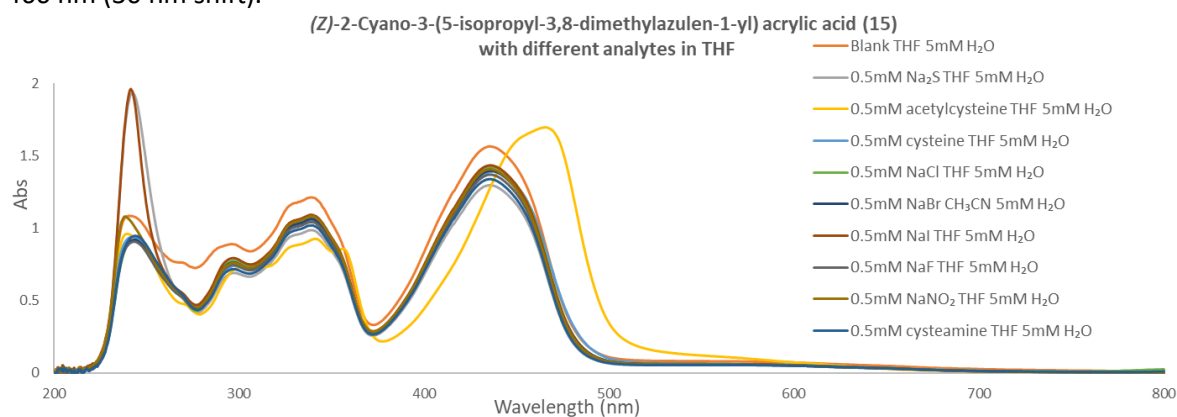
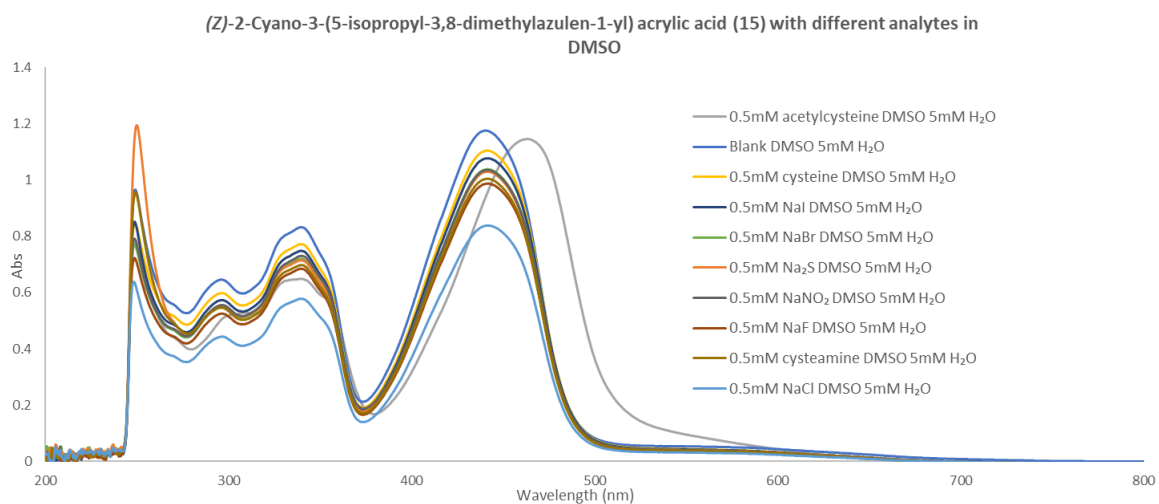


Figure 39: UV-Vis Absorption spectra for 15 (0.5 mM) in THF with analyte (5 mM).

In **figure 40**, the highest peak maxima absorbance is at 440.5 nm for all analytes apart from NAC which is at 463.5 nm (23 nm shift).



The results from all the UV-Vis measurements are summarised below.

Compound	Solvent	Longest wavelength peak maxima for analytes excl. NAC	Longest wavelength peak maxima for NAC	Shift (nm)
14	CH ₃ CN	420	435	15
	THF	420	434	14
	DMSO	426	438	12
15	CH ₃ CN	439	465.5	26.5
	THF	436	466	30
	DMSO	440.5	463.5	23

Table 4: List of solvents used for UV absorption experiments and their respective peak maxima values in different analytes compared to NAC

Due to the colour change observed for the NAC analyte, a change of species present was expected as the NAC becomes covalently attached to either compound through conjugate addition. However, when a thin layer chromatography (TLC) was taken of the sample, no new spot had appeared (phosphomolybdic acid (PMA) was used to help with visualisation) and ¹HNMR analysis also confirmed no new product formation as only the starting materials were apparent.

To study why a colour change might only be observed for this compound, a hypothesis was suggested that perhaps the reason for this might be due to potential hydrogen bonding which existed between the carboxylic acid functionality of the sensor molecule and the carboxylic acid functionality of the NAC molecule, an illustration is shown in **figure 41**.

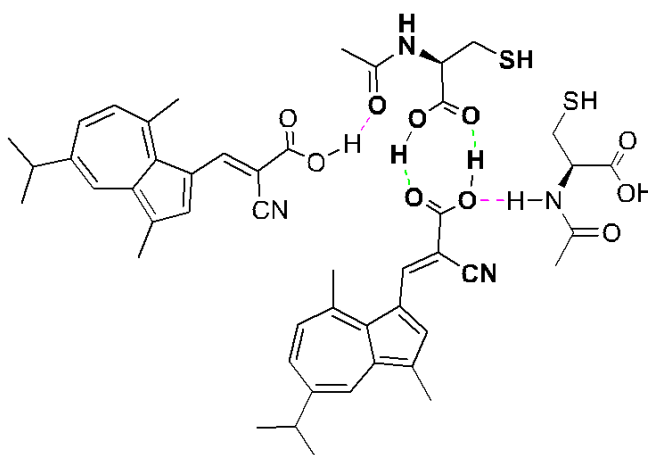


Figure 41: H-bonding interactions between the 15 with NAC. Primary H-bonding effects are shown by the green dotted line and secondary H-bonding effects are shown by the pink dotted line

Secondary hydrogen bonding can also exist between the -NH proton of the NAC and the oxygen atom from the compound in addition to the ketone oxygen from the NAC. Clearly neither of the other analytes would show this effect as they do not contain a carboxylic acid, NH functionality and carbonyl oxygen on one molecule. Cys exists as a zwitterion and as a result of this, the proton attached to the acidic functionality can transfer to the amine group. No attempt was made to calculate the entropic change such an interaction would cause; other forms of supramolecular interaction could also be proposed.

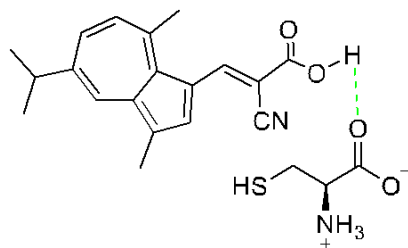


Figure 42: H-bonding interactions between the 15 with Cys.

As **figure 42** shows, only the carboxylic oxygen on the Cys can H-bond to the carboxylic acid functionality of the cyanoacetic acid compound and therefore due to the reduced H-bonding networks the colour change will be less noticeable.

In order to test the likelihood of this theory, tests were carried out using *N*-acetylglycine which does not contain an -SH group but still contains the carboxylic acid functionality, an -NH group and the carbonyl oxygen.

For comparison, this test was run using a blank, and four other analytes (Na_2S , NAC, NaI and cysteamine) which have known colour changes as measured previously. The colour changes are shown in **figure 43**.

This test confirms that the change in colour is as a result of the H-bonding effects that exist between 15 and NAC and not due to formation of a new compound.

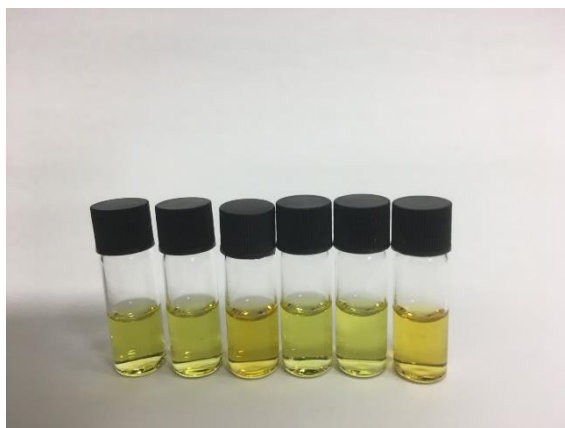
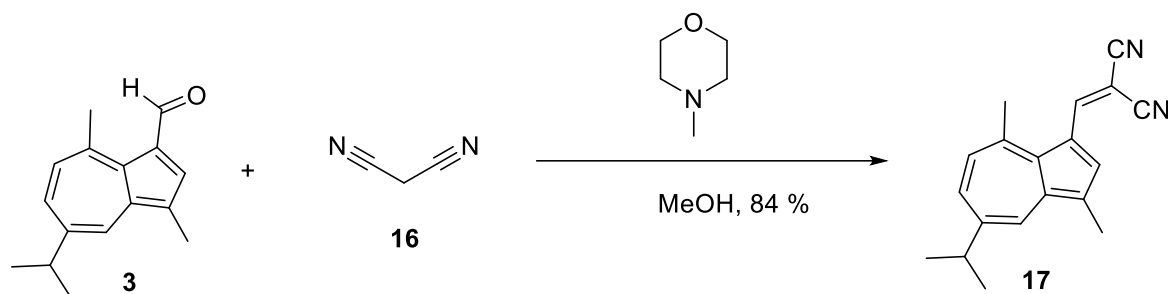


Figure 43: Images taken of 15 with a range of different analytes

The analytes tested were, L-R: control, Na_2S , NAC, NaI, cysteamine and *N*-acetylglycine in MeCN.

It was found that the compound does not produce any noticeable colour change with NAC under reflux overnight using a 10-100 eq. of the thiol as confirmed *via* ^1H NMR analysis.

In order to test whether there may be potential for conjugate addition to ensue with the addition of two highly electron withdrawing groups that do not contain any functional groups that could hydrogen bond with the NAC, **17** was synthesised from **3** using **16** and *N*-methyl-morpholine in methanol.⁶⁴



Scheme 20: Synthesis of 17

This synthesis would help to confirm whether the colour change observed for NAC seen previously was due to hydrogen bonding effects.

As before, the same analytes were tested with **17** (figure 44).

The colorimetric results concluded that no colour change was observed for any of the analytes. This further supports the conclusion that the colour changed observed previously was due to hydrogen bonding effects as in these set of tests the colour of the solution did not change with NAC. In addition, despite using two highly electron withdrawing groups (both nitrile functionalities) no conjugate addition reaction occurred.

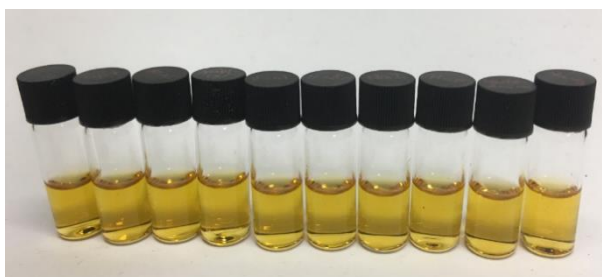


Figure 44: Images taken of 17 with a range of different analytes

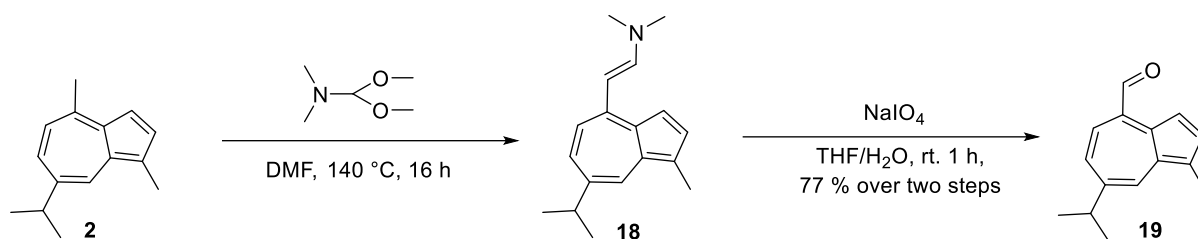
The analytes tested were, L-R: control, Na₂S, NAC, NaI, cysteamine and *N*-acetyl glycine in MeCN.

2.1.3 Guaiazulene as a thiol receptor motif on 7-membered ring

In order to study the electronic effects of the guaiazulene and azulene constructs, efforts were focused towards substituting the 7-membered ring of guaiazulene with electron withdrawing groups. It was anticipated that the electron poor characteristics of the tropylium cation of the 7-membered ring may help to encourage 1,4-Michael addition (conjugate addition) reactions to occur through the attack at the position adjacent to the 7-membered ring.

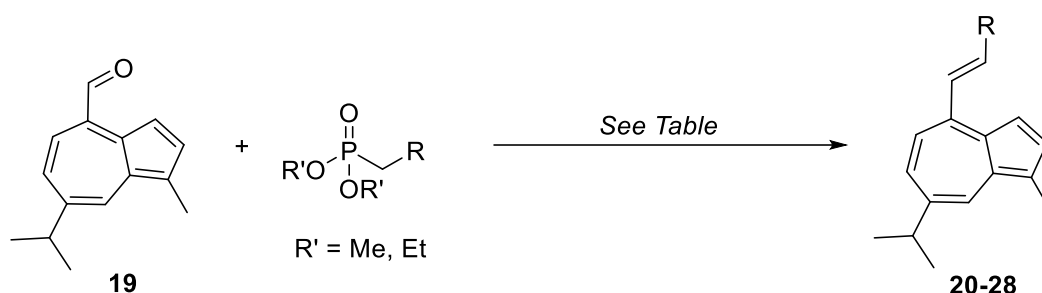
2.1.3.1 Michael Acceptors on 7-membered ring

Through literature research, a method of synthesis was found which involved functionalising methyl groups of azulene as enamine groups and then converting them into formylazulenes.^{65,66,67} It was proposed that a similar transformation may occur on the unusually acidic methyl group on the 7-membered ring of the guaiazulene. Through this scheme, the intermediate enamine product (**18**) was obtained by heating **2** and *N,N*-dimethylformamide dimethyl acetal in DMF at 140 °C. The crude enamine (**18**) was then reacted with sodium periodate at room temperature to furnish the novel formylazulene (**19**). The transformation between products was visually apparent starting from a deep blue (**2**) to green (**18**) and finally to a lighter blue solution (**19**).



Scheme 21: Functionalisation of the methyl group of an 8-Methyl Guaiazulene into 19

From **19**, a range of different products were synthesised through Horner–Wadsworth–Emmons reactions which include several electron withdrawing groups, in the expectation that these products could undergo conjugate additions with thiol analytes.



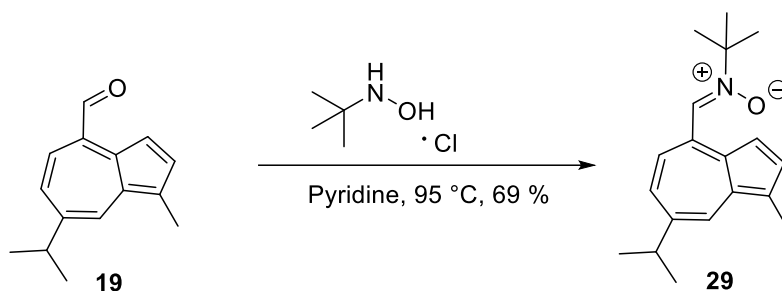
Scheme 22: Horner-Wadsworth-Emmons reactions using phosphonates to introduce conjugated EWGs

Entry	R	Product	R'	Method ^{a,b}	Yield (%)
1		20	Et	B	38
2		21	Et	B	46
3		22	Et	B	18
4		23	Et	B	56
5		24	Et	B	42
6		25	Et	B	44
7		26	Me	A	41
8		27	Et	A	33
9		28	Et	B	50

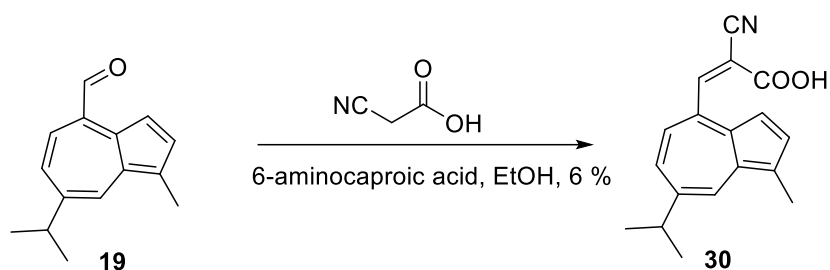
^a Method A: LiCl (3 eq.), DBU (3 eq.), THF, 0 °C, 3 h ^b Method B: 60 % NaH (2 eq.), THF, rt, 2 h

Table 5: List of Horner-Wadsworth-Emmons products including all experimental details and associated yields

Other products were synthesised, including introduction of a nitron and cyanoacetic acid functional groups.



Scheme 23: Synthesis of a nitron containing guaiazulene compound (29)



Scheme 24: Synthesis of a cyanoacetic acid-guaiazulene adduct (30)

All the synthesised products were novel and were either isolated as a blue or green gum.

Treatment of these analogues with a strong acid protonates at the 3-position on the 5-membered ring in all cases revealing a reversible halochromic behaviour. NMR studies were used to determine the protonation site of the analogues, such as the example for **25** (figure 45).

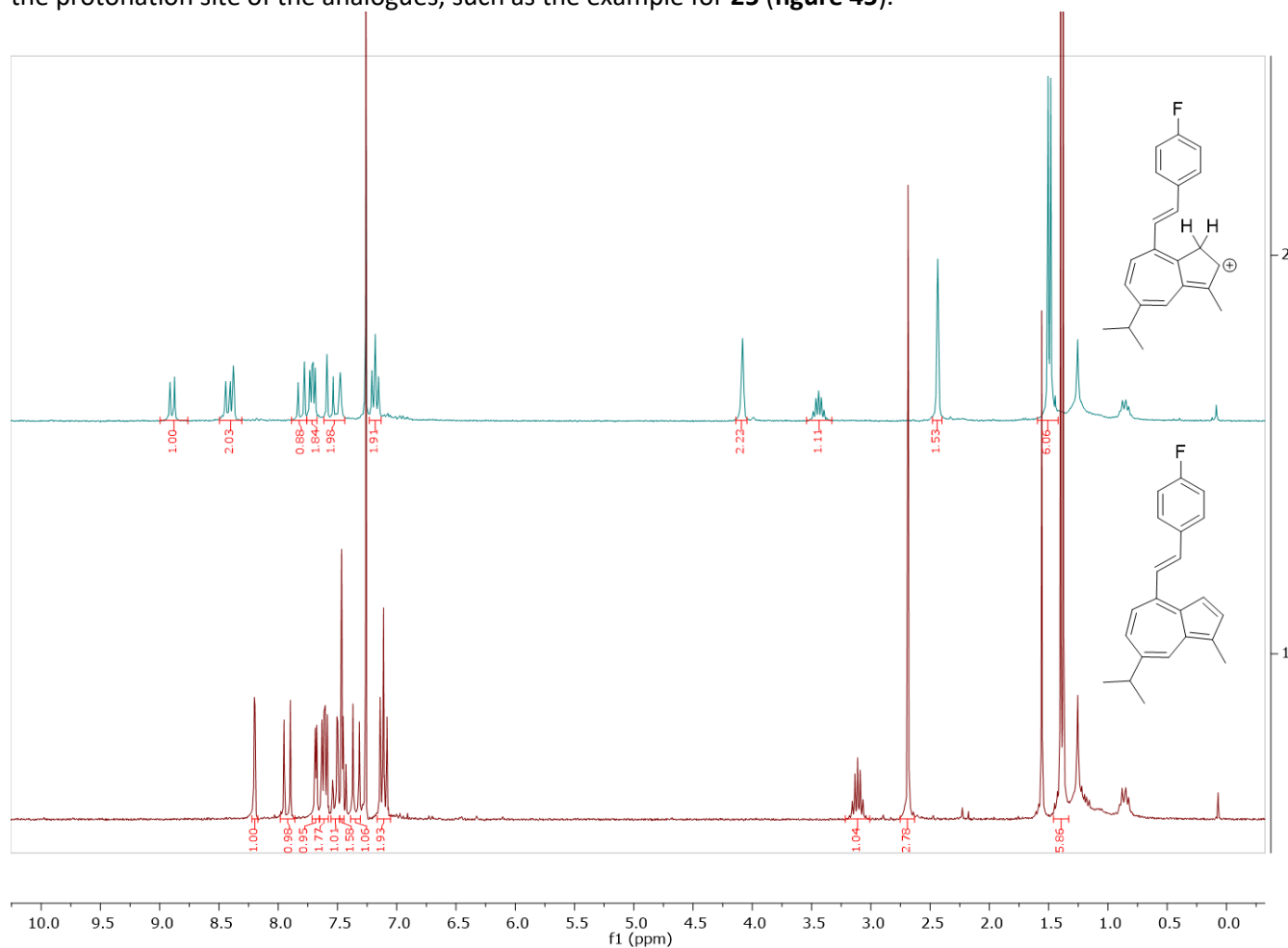


Figure 45: ¹H NMR spectra of 25 in CDCl₃: TFA (v:v, 9:1), with TFA (above) and in CDCl₃ only (below).

Examination of the UV-Vis spectra in the neutral state (in DCM) shows that all derivatives showed a broad profile with the onset of absorption at 448 nm for **25** particularly. The effect of acid on the absorption was investigated using a 10 % solution of TFA in DCM. In all cases, a bathochromic shift in the main absorption band signalled the dependence of conjugation on the relative absorbances of the analogues. The spectra for the other compounds are shown in the appendix.

Furthermore, increasing amounts of TFA signalled an increase in absorption maxima at higher wavelengths and a decreasing absorption maximum at lower wavelengths, as **figure 46** shows. This trend was consistent amongst all analogues that were tested.

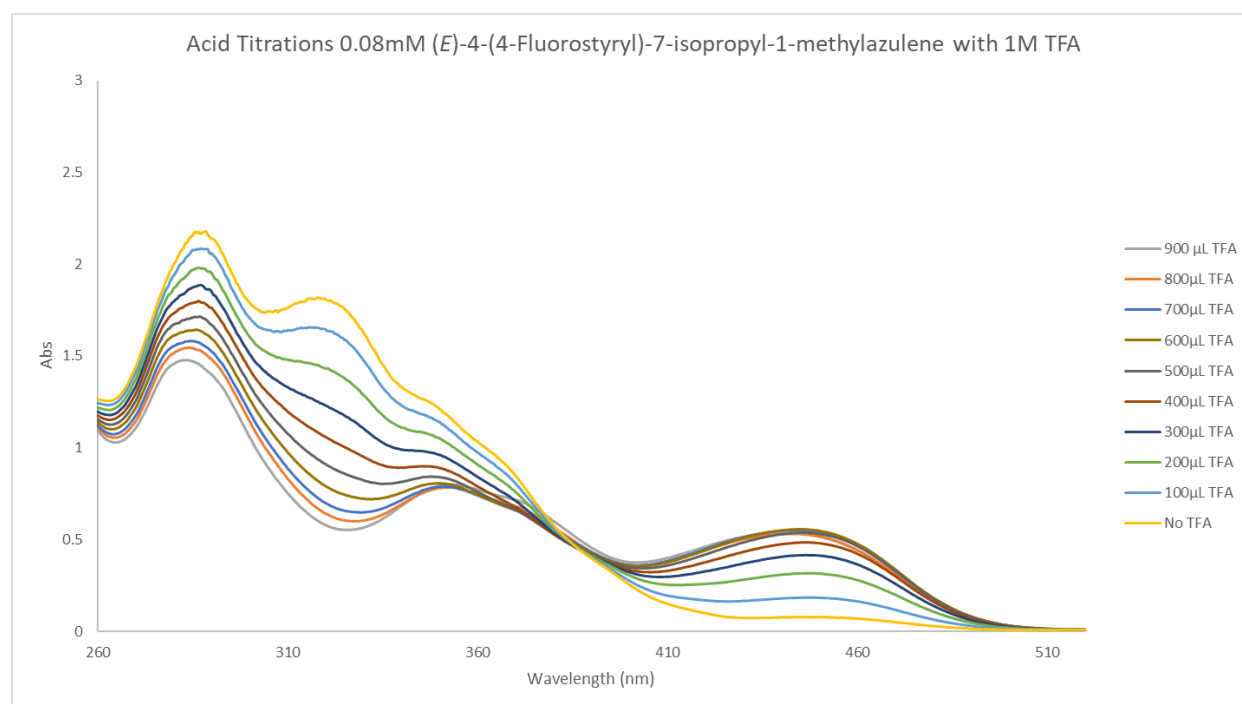


Figure 46: Absorption spectra of 25 at 0.08 mM upon titration with a solution of TFA in DCM

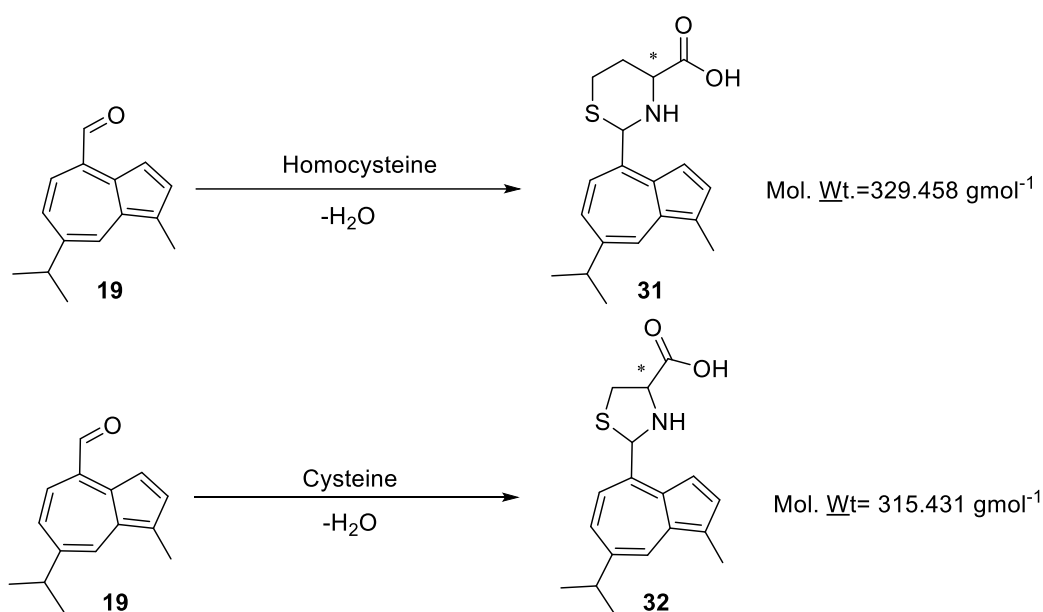
Following the acid titrations, attempts were then made to study these compounds through thiol testing.

The conditions used to test all these products with thiols followed the same conditions highlighted in chapter 2, 2.1.1 and 2.1.2. Unfortunately, however no reaction with the thiol analytes occurred when studied through NMR, MS, UV-Vis and naked eye testing. Furthermore, attempts to encourage a reaction were aided by the addition of a small catalytic amount of base (0.05 eq.) of triethylamine and caesium carbonate to the sensors and left to react for several hours however still no positive results were obtained.

2.1.3.2 Cyclic Adducts on 7-membered ring

In previous literature studies, there have been reports of several HCy/Cys probes which contain aldehyde groups that are used to target the reactivity of the thiol group of HCy and Cys, forming thiazolidine and thiazine ring systems respectively (e.g. see **Scheme 8**).^{68,69,70} Such changes induce shifts in the UV-Vis absorption spectra that can be used as indications of relative structural changes upon thiol addition.

In accordance with these literature studies, selectivity tests using the aldehyde **19** as a possible sensor were carried out. The selectivity of the sensor towards Cys and HCy was tested against a selection of amino acids. **19** reacted with both HCy and Cys as expected and formed the desired thiazolidine (**31**) and thiazine (**32**) ringed systems respectively *via* MS analysis.



Scheme 25: Subsequent ring cyclisation's that occur when **19** is attacked via HCy or Cys to produce **31** and **32** respectively and their molecular mass values

All tests were carried out in DMSO solvent in which the **19** product appeared as an ocean blue colour. Upon reaction with Cys and HCy the colour turned to a deeper blue although this change was difficult to observe visually through naked eye.

All test samples were analysed through UV-Vis absorption at a range of different concentrations and equivalents of analytes. In order to observe changes that may occur in the visible region of the UV-Vis spectrum i.e., at longer wavelengths, the starting formylazulene was prepared as a 3 mM sensor solution in DMSO and reacted with the desired thiols and other amino acids and allowed to react for 1 hour.

The following table is used to show the sensor concentrations and the different analytes that were tested and their associated concentrations,

Sensor Concentration	Analytes (HCy/Cys/Val/Ala/Pro/Glu/Arg/GSH/Leu/Threo/NAC-Gly/Methio/Lys/NAC/Ser/Ph-Al)
3 mM	5, 15, 25, 35, 50 mM (excl. Cys)
100 μ M	200 μ M, 600 μ M, 1 mM, 1.4 mM, 2 mM

Table 6: Sensor concentrations and the associated analytes and the concentrations used in each selectivity test

For simplicity, only the UV-Vis spectrum for HCy, Cys and Val are shown below however the trends are similar amongst all other analytes to Val i.e. there is a shift in the absorption maxima to lower

wavelengths upon the addition of HCy and Cys as indicated by the symbol (*). Unfortunately Cys was not able to be tested at a 3 mM concentration as a result of insolubility.

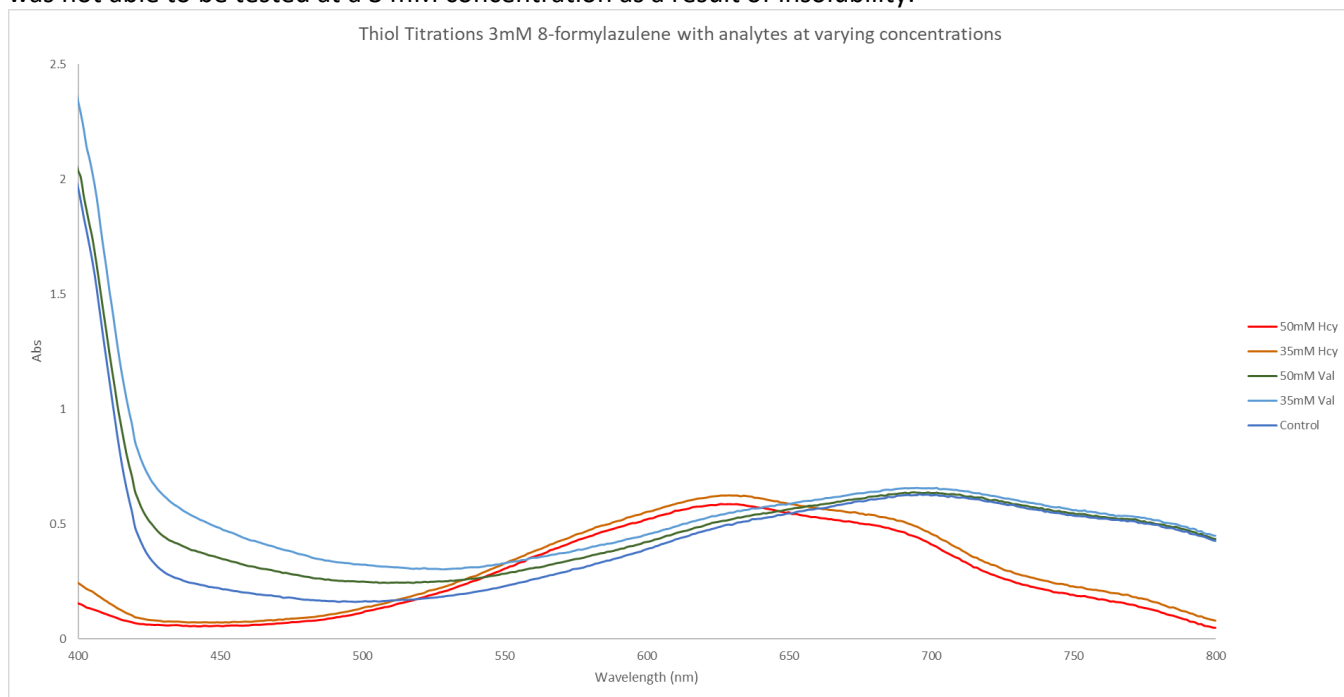


Figure 47: UV-Vis thiol titrations for 3 mM 19 with 35 mM and 50 mM HCy and Val

This shift to shorter wavelength maxima for Cys and HCy is also true in the UV region (when spectra are acquired at lower concentrations), whereby the peak maxima occur at shorter wavelengths as figure 48 shows,

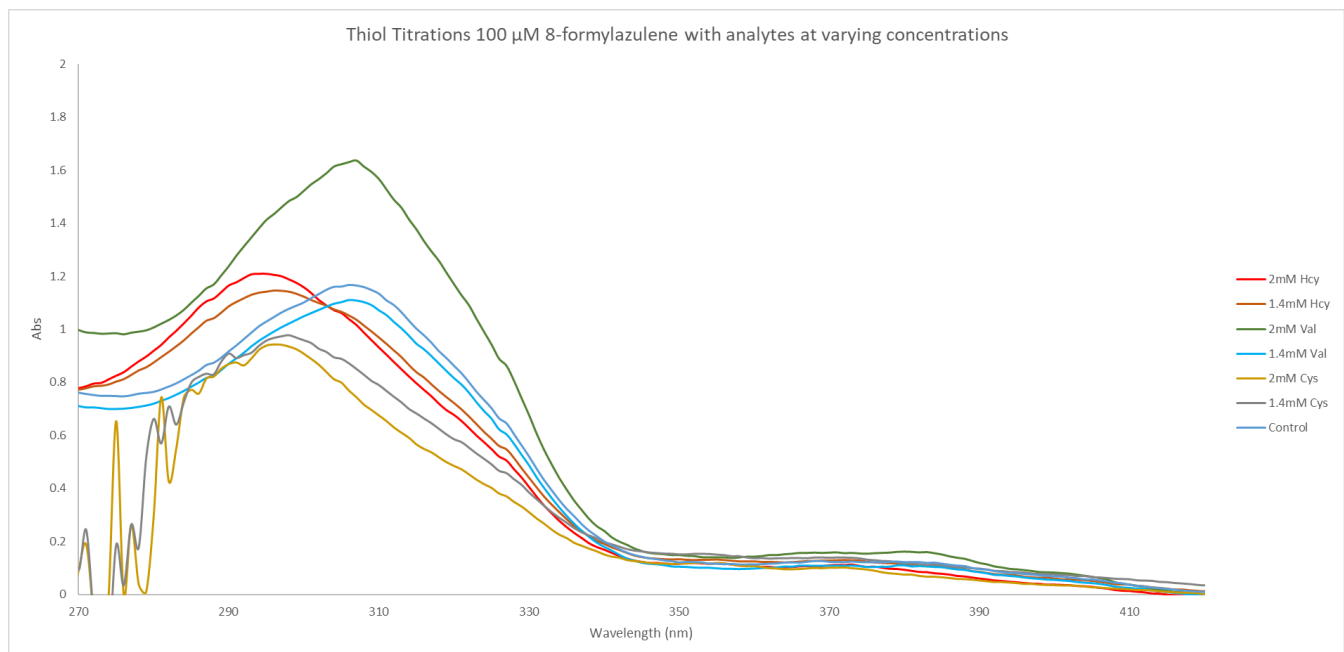


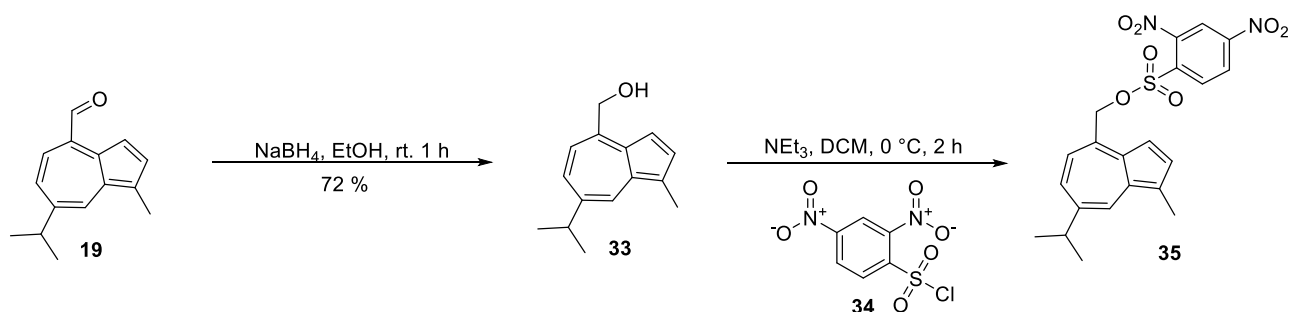
Figure 48: UV-Vis thiol titrations for 100 μM 19 with 1.4 mM and 2 mM HCy, Val and Cys

2.1.3.3 Nosyl Group on 7-membered ring

Literature studies have reported the use of several 2,4-dinitrobenzene sulfonyl groups as promising electron deficient groups that are able to be attacked by thiol groups *via* a nucleophilic aromatic substitution reaction.⁷¹

As such, attempts to functionalise the 8-position of the guaiazulene derivative with a 2,4-dinitrobenzene sulfonyl chloride group (**34**) (a highly electron deficient and therefore excellent leaving group) was investigated through the reduction of the **19** into (7-isopropyl-1-methylazulen-4-yl)methanol (**33**) followed by treatment with 2,4-dinitrobenzenesulfonyl chloride (**34**) in the presence of NEt₃ to produce the potential probe product (**35**).

The NMR of the resulting product provides strong evidence for the formation of the product (see spectrum in appendix) however success at purification could not be achieved to date.



Scheme 26: Synthesis of 35

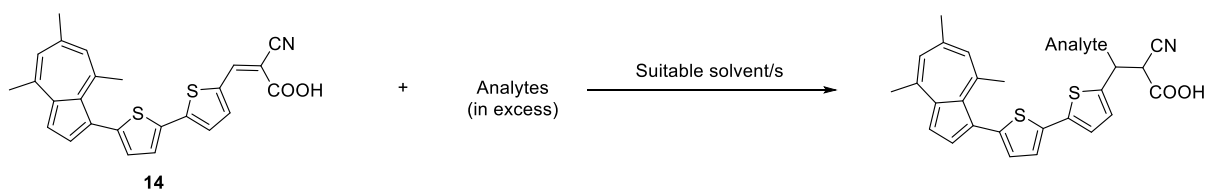
Chapter 3: Conclusions and future work

3.1. Conclusion

A series of novel compounds have been developed containing either guaiazulene or azulene motifs for evaluation as thiol-based sensors and are initially built upon the work of Cacciarini *et al.* It was concluded following these investigations that incorporating 1,3-dimethylbarbituric acid functionalities into the systems produced no noted conjugate addition reactions towards thiol analytes. This was thought to be as a result of insufficient electron withdrawing effects of the 1,3-dimethylbarbituric acid functionality and therefore attempts were made to modify the structure by adding greater electron withdrawing functionalities in order to attenuate the high electron density of the guaiazulene and azulene rings however similarly this also did not produce any anticipated conclusions.

Following on from this, investigation into cyanoacetic acid functionalities coupled to guaiazulene and azulene compounds were then explored to determine if these molecules would perhaps be more susceptible to conjugate addition with thiol analytes. This was based on the notion that a molecule consisting of two strongly electron withdrawing groups (nitrile and carboxylic acid derivatives) would lead to a very electrophilic alkenic site of attack for a thiol nucleophile and thus lead to an sp^2 to sp^3 change in hybridisation. Such compounds had already been investigated by a former student of the Lewis group (Dr Paul Cowper) who reportedly was able to visualise a colour change when such cyanoacetic acid functionalised azulene/guaiazulene compounds were washed with brine solutions.

Initial lab experiments confirmed that a noticeable colour change was observed when one example of a compound provided by Dr Paul Cowper was added to a series of analytes in three different solvents. In all solvents tested, a colour change from yellow to orange took place selectively only however when NAC was used as the analyte.



Scheme 27: Theoretical overview of a conjugate addition reaction which ensues when a nucleophilic thiol is used to attack a selected guaiazulene/azulene based molecule.

The reactivity associated with this molecule was studied by visual observations coupled with UV-Vis measurements which show that a noticeable shift of the absorption maxima to higher wavelengths with NAC is detected compared to the other analytes when a 1:10 eq. of the sensor and analyte is studied respectively. Interestingly, upon analysis of this compound with NAC, no product formation was identified other than the initial starting materials.

From this, further tests using *N*-acetylglycine (structure similar to NAC, but lacking the thiol functionality) was studied and it was found that an orange colour was produced for this compound as well which suggested potentially that the colour change was most likely attributed to the hydrogen bonding effects that existed between the cyanoacetic acid compound and the analyte (in this case NAC and *N*-acetylglycine).

Further investigation towards synthesising a malononitrile based compound was also explored. Despite replacing the carboxylic acid functionality with a much stronger electron withdrawing group,

no colour change was produced with any of the analytes neither with NAC which helped to confirm that the colour change seen earlier with previous cyanoacetic acid compounds was due to hydrogen bonding effects.

With knowledge gathered thus far, efforts to investigate other sites on the overall guaiazulene/azulene construct begun to be explored. As the greatest electron density of the molecule resides in the 5-membered ring, it was decided to turn efforts and focus on introducing electron withdrawing groups on the 7-membered ring on the molecule. In theory, the lower electron density on the 7-membered ring should be better suited for conjugate addition reactions as it enables the alkenic position to become more electron poor and thus more likely to react with thiol analytes. Such molecules that were developed were synthesised initially using an adapted procedure in the literature to produce 8-formylazulene. This starting product was then used to produce numerous other compounds that all consisted of electron withdrawing groups located at the 8-position of the molecule i.e., on the 7-membered ring. Thus, to explore and understand the properties of guaiazulene containing chromophores, treatment of these with a strong acid was carried out to protonate the molecules and determine the electron-rich position of these molecules.

Following the pioneering work of Strongin *et al.* and subsequent works by researchers at the University of Bath (Dr Jordan Gardiner)⁷², it was proposed that the initial 8-formylazulene may be responsive towards thiol analytes through the formation of thiazolidine and thiazine rings from HCy and Cys analytes respectively. The molecule was tested with several thiols and amino acids and despite not an obvious visual colour change, this binding and cyclisation caused changes to the UV-Vis absorption which were apparent as a blue shift (50 nm).

These changes represent a significant step forward in developing a thiol sensor using azulene/guaiazulene based systems. Initial tests confirm that the 8-formylazulene developed reacts selectively with HCy and Cys molecules to produce thiazolidine and thiazine rings respectively and thus producing corresponding changes in UV-Vis absorbance.

3.2. Future Work

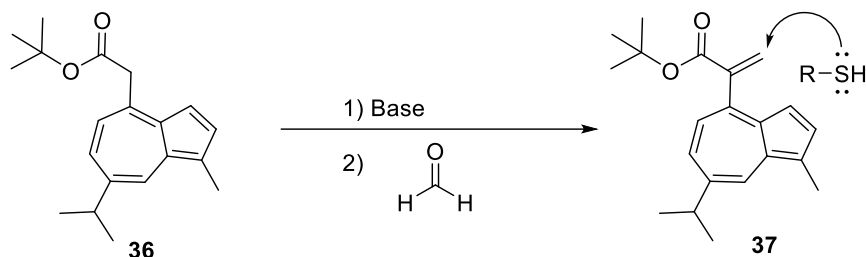
Due to the importance of biological thiols, there has been an increasing interest to develop new detection methods for these compounds. Thus far, the focus of this work has investigated developing thiol-based sensors for this purpose based around azulene/guaiazulene motifs.

When studying the chemistry involved in creating a better probe for Michael addition reactions, the 7-membered ring of azulene/guaiazulene is significantly more electron poor than the 5-membered ring hence it is more likely that such Michael addition will be favourable with electron-withdrawing groups located on the 7-membered ring.

As such, a potential thiol-based sensor (8-formylazulene) has been developed that responds to thiols through a change in the absorption maxima in the UV-Vis spectra through a blue shift (50 nm). Future work could focus on collecting further analysis data for this compound i.e., fluorescence spectra etc. to understand more about its properties with regards to becoming a feasible thiol-based sensor. In addition, the other electron withdrawing based compounds developed from the initial 8-formylazulene could also be studied to determine whether they have reactivity towards thiol analytes as well.

Further work could also be focused on attempting to purify the 2,4-dinitrobenzene sulfonyl chloride product (**35**) as this molecule may also be used as a potential thiol-based sensor. Based on initial observations, it is anticipated that such a molecule will be able to show a significant colour change from a potential orange/yellow coloured solution to a blue colour upon the addition of thiol analytes. This would allow for a visually colour changing thiol probe to be developed which would also be able to provide analytical information associated with the changes that occur through thiol addition like that for 8-formylazulene.

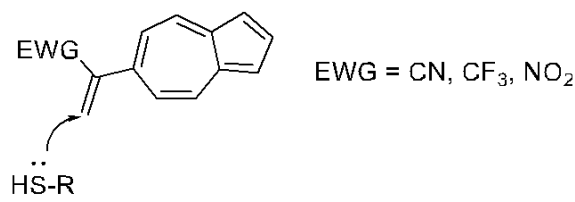
In keeping with other possible substitutions on the 8-position of the guaiazulene ring, further functionalisation on the guaiazulene ring could also be undertaken on the acidic proton of the methyl group situated on the 8 position of the guaiazulene ring (**scheme 28**).



Scheme 28: Substitution reactions on the acidic methyl group of the guaiazulene (8 position) to produce an alkene using formaldehyde for further reactions with nucleophilic thiols.

Incorporating both electron-withdrawing groups (azulene/guaiazulene motif and electron-withdrawing group) on the same side of the double bond would seek to further enhance the rate at which the thiol nucleophile attacks the alkene double bond hence increasing the possibility of a Michael addition reaction. The compounds developed for this would also be novel and would allow for a plethora of different compounds to be made for uses as sensor designs. It would be useful if compounds containing hydroxy or carboxylic groups could be incorporated into these systems for potential water solubility which would then allow for the compounds to be analysed through cell analysis.

Further reactions based on azulene backbones could be envisaged due to the versatility of this compound in electronic characteristics for uses in sensor applications. In the first instance, reactions could focus on substituting the 7-membered ring of the azulene construct, particularly the 6-position to be used for further conjugate additions reactions using nucleophilic thiols. In order to favour conditions suited to conjugate additions, desired compounds could contain constructs which have one or more electron-withdrawing groups attached to an alkene to favour attack by a thiol (**scheme 28**). As such, the 1,3-dimethylbarbituric acid compound used previously could be incorporated into these reactions along with the possibility of attaching nitrile, nitro and trifluoromethyl groups from a starting aldehyde as performed previously. These types of compounds which incorporate an EWG on the side chain would be novel as most of the previous literature performed on these compounds in this position has only incorporated methyl groups.



Scheme 29: Theoretical structure of desired compounds to be synthesised based on the azulene construct followed by attack from nucleophilic thiols.

Chapter 4: Experimental

Reactions which required the use of anhydrous, inert atmosphere techniques were carried out under an atmosphere of argon. In most cases, solvents were obtained by passing through anhydrous alumina columns using an Innovative Technology Inc. PS-400-7 solvent purification system. In most cases, solvents were purchased as “anhydrous” grade from Fisher Scientific. “Petrol” refers to petroleum spirit b.pt. 40-60 °C.

TLC unless otherwise stated was performed using aluminium backed plates pre-coated with Alugram®SIL G/UV 254 nm. Where needed, visualisation was accomplished by UV light and/or KMnO₄ or using phosphomolybdic acid (PMA) dip followed by gentle warming. Following work up, the organic layers were routinely dried using anhydrous MgSO₄ and evaporated using a Büchi rotary evaporator. When necessary, further drying was facilitated by high vacuum. During purification, flash column chromatography was carried out using 60 angstroms (Å) silica gel (40-75 micron) purchased from Sigma Aldrich.

NMR Spectroscopy: ¹H and ¹³C NMR spectra (unless otherwise specified) on Agilent ProPulse 500 MHz or Bruker Advanced 250, 300, 400 or 500 megahertz (MHz) instruments at 298 K. All spectra were referenced to residual solvent peaks; chemical shifts are reported in parts per million (ppm) relative to residual chloroform ($\delta = 7.26$ ppm, ¹H; 77.16 ppm, ¹³C). All ¹³C {¹H} resonances are assumed to be singlets, unless stated otherwise. Coupling constants, *J*, reported in Hz, were calculated using *Mestrenova* 9.0 to the nearest 0.1 Hz. The following abbreviations are used to label the multiplicities: s, singlet; d, doublet; t, triplet; q, quartet; quin, quintet; sex, sextet; sep, septet; dd, doublet of doublets; dq, doublet of quartets; td, triplet of doublets; m, multiplet and br, broad. ¹H and ¹³C{¹H} assignments for novel compounds are corroborated through 2D (COSY, HSQC, HMBC).

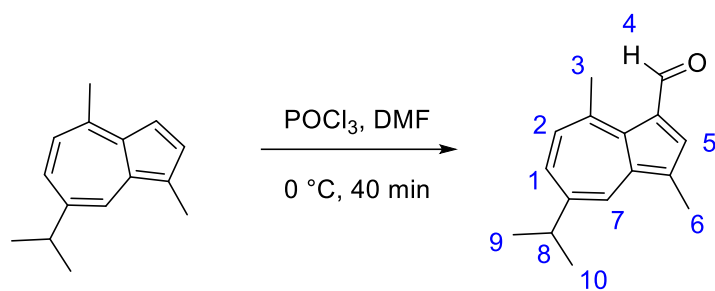
Infrared Spectroscopy: Infrared (IR) spectra were recorded on a Perkin-Elmer PerkinElmer Spectrum 100 ATR-FTIR spectrometer with only selected absorbances quoted as ν in cm⁻¹.

Mass Spectrometry: A microTOF electrospray time-of-flight (ESI-TOF) mass spectrometer (Bruker Daltonik GmbH, Bremen, Germany) was used. Data are reported in the form of *m/z* (intensity relative to the base peak = 100). The observed mass and isotope pattern matched the corresponding theoretical values as calculated from the expected elemental formula.

Melting Points: Melting points (mp) were determined on a Stanford Research Systems OptiMelt automated capillary melting point apparatus in open capillary tubes and are uncorrected.

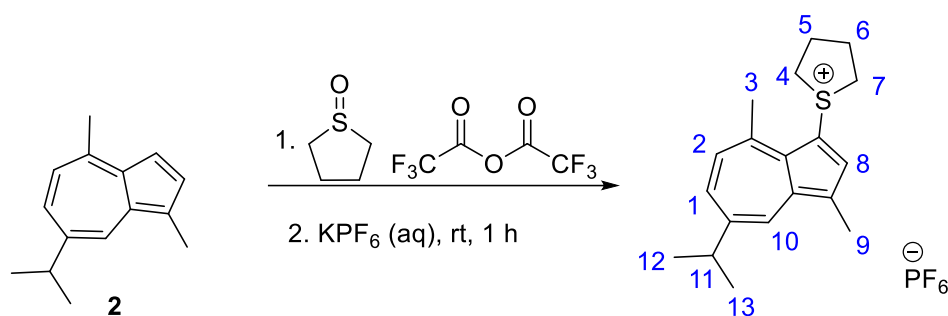
X-Ray Crystallography: X-Ray crystallography was recorded on a Nonius Kappa CCD diffractometer with Mo- $K\alpha$ radiation ($\lambda=0.71074$ Å). All structures were solved by direct methods and refined on all F₂ data using SHELX-97 suite of programs.

5-Isopropyl-3,8-dimethylazulene-1-carbaldehyde (3)



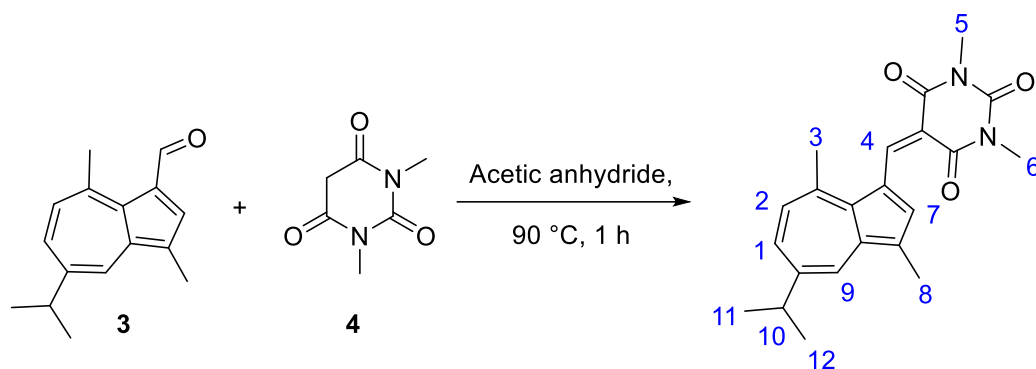
Via cannula at $0\text{ }^\circ\text{C}$, phosphorus(V) oxychloride (POCl_3) (0.54 mL, 5.8 mmol) in DMF (10 mL) was transferred slowly to a cold solution of **2** (0.5 g, 2.5 mmol) in DMF (5 mL) at $0\text{ }^\circ\text{C}$. The reaction turned from blue to green then red in colour. Upon complete addition, the ice bath was removed and the stirred for 40 minutes or until no more starting material remained. Ice cold water (45 mL) was added and then the dark red/brown suspension is basified from pH 1 to pH 14 with 2 M KOH (25 mL). The new purple coloured solution was then extracted with dichloromethane ($4 \times 25\text{ mL}$). The combined organic phases were then washed with 5 % LiCl solution ($3 \times 30\text{ mL}$), dried over MgSO_4 and dried *in vacuo*. The crude was purified by silica column chromatography (Petrol : EtOAc, 80:20 R_f 0.70) to afford green crystals (0.40 g, 1.7 mmol, 70 %). ^1H NMR (300 MHz, CDCl_3) δ 1.39 (d, $J = 6.9\text{ Hz}$, 6H, $\text{H}^{9,10}$), 2.59 (d, $J = 0.8\text{ Hz}$, 3H, H^3 or H^6), 3.23-3.09 (m, 4H, H^8 and H^3 or H^6), 7.44 (d, $J = 10.9\text{ Hz}$, 1H, H^2), 7.60 (dd, $J = 10.8, 2.2\text{ Hz}$, 1H, H^1), 8.24 (s, 1H, H^5), 8.30 (d, $J = 2.2\text{ Hz}$, 1H, H^7), 10.65 (s, 1H, H^4), in agreement with literature data.⁸⁹

**1-(5-Isopropyl-3,8-dimethylazulen-1-yl) tetrahydro-1H-thiophen-1-ium hexafluorophosphate(V)
(8)**



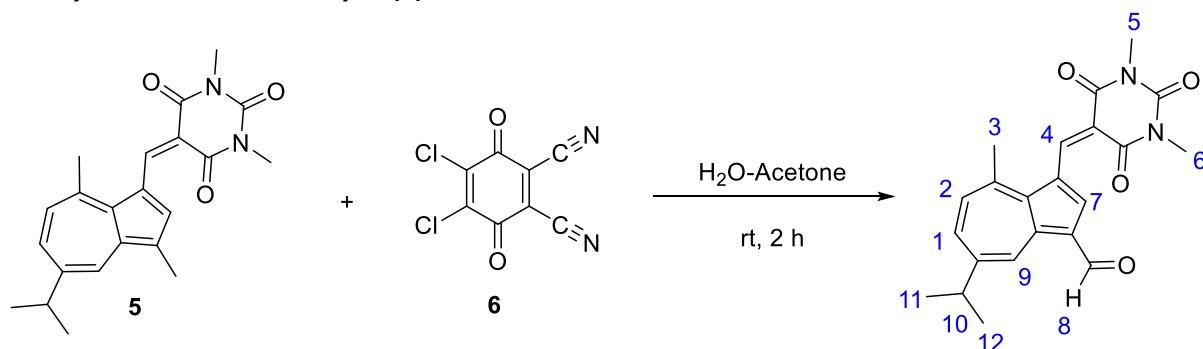
Tetramethylene sulfoxide (5.86 mg, 56.3 mmol) was added to a stirred solution of **2** (2.8 g, 14.1 mmol) in dichloromethane (45 mL). A solution of trifluoroacetic anhydride (2.97 mL, 21.1 mmol) and dichloromethane (5 mL) was added dropwise *via* cannula causing an immediate colour change to purple. The reaction mixture was stirred for 1 hour at room temperature followed by dilution with dichloromethane (50 mL) and water (3×200 mL). The combined aqueous layers were washed with KPF_6 and extracted with diethyl ether (3×200 mL). The organic phase was dried with MgSO_4 . This was filtered under gravity and the solvent was removed *in vacuo*. Diethylether was then added to the solid to triturate the sample to yield a purple/black solid (3.8 g, 8.8 mmol, 63 %). ^1H NMR (500 MHz, CDCl_3) δ 1.39 (d, $J = 6.8$ Hz, 6H, $\text{H}^{12,13}$), 2.59-2.44 (m, 2H, $\text{H}^{5\text{ax},6\text{ax}}$), 2.65 (s, 3H, H^9), 2.80-2.65 (m, 2H, $\text{H}^{5\text{eq},6\text{eq}}$), 3.24-3.13 (m, 1H, H^{11}), 3.25 (s, 3H, H^3), 3.55-3.38 (m, 2H, $\text{H}^{4\text{ax},7\text{ax}}$), 4.15 (dt, $J = 13.0, 6.6$ Hz, 2H, $\text{H}^{4\text{eq},7\text{eq}}$), 7.52 (d, $J = 10.8$ Hz, 1H, H^2), 7.72 (s, 1H, H^8), 7.77 (dd, $J = 10.8, 2.2$ Hz, 1H, H^1), 8.39 (d, $J = 1.9$, 1H, H^{10}), in agreement with literature data.⁹⁰

5-((5-Isopropyl-3,8-dimethylazulen-1-yl)methylene)-1,3-dimethylpyrimidine-2,4,6(1H,3H,5H)-trione (5)



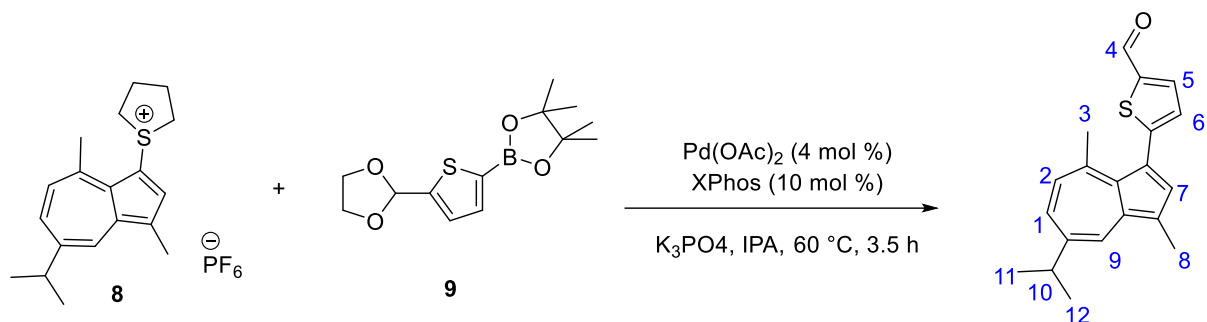
Acetic anhydride (0.66 mL, 7.0 mmol) was added to a combination of **3** (100 mg, 0.4 mmol) and **4** (69 mg, 0.4 mmol). The mixture was stirred and heated to 90 °C for 1 hour after which a purple to red colour change was observed. The resulting mixture was diluted with dichloromethane (30 mL) and washed with water (3 × 10 mL). The organic phase was then dried with MgSO₄, filtered under gravity and then concentrated *in vacuo*. The crude was purified by silica column chromatography (Petrol : EtOAc 15:85 R_f 0.46) to yield a black solid (123.4 mg, 0.3 mmol, 77 %). ¹H NMR (500 MHz, CDCl₃) δ 1.40 (d, *J* = 6.9 Hz, 6H, H^{11,12}), 2.58 (s, 3H, H⁸), 3.22 (s, 1H, H³), 3.21-3.11 (m, 1H, H¹⁰), 3.43 (s, 1H, H^{5,6}), 7.53 (d, *J* = 11.1 Hz, 1H, H²), 7.62 (dd, *J* = 11.1, 2.1 Hz, 1H, H¹), 8.21 (d, *J* = 2.1 Hz, 1H, H⁹), 9.46 (s, 1H, H⁴), 8.95 (s, 1H, H⁷). ¹³C NMR (125 MHz, CDCl₃) δ 13.21, 24.33, 28.24, 28.60, 29.84, 38.23, 106.15, 123.81, 129.20, 134.54, 135.86, 136.92, 143.86, 145.65, 147.21, 148.23, 150.44, 150.66, 152.15, in agreement with literature data.⁹²

3-((1,3-Dimethyl-2,4,6-trioxotetrahydropyrimidin-5(2H)-ylidene) methyl)-7-isopropyl-4-methylazulene-1-carbaldehyde (7)



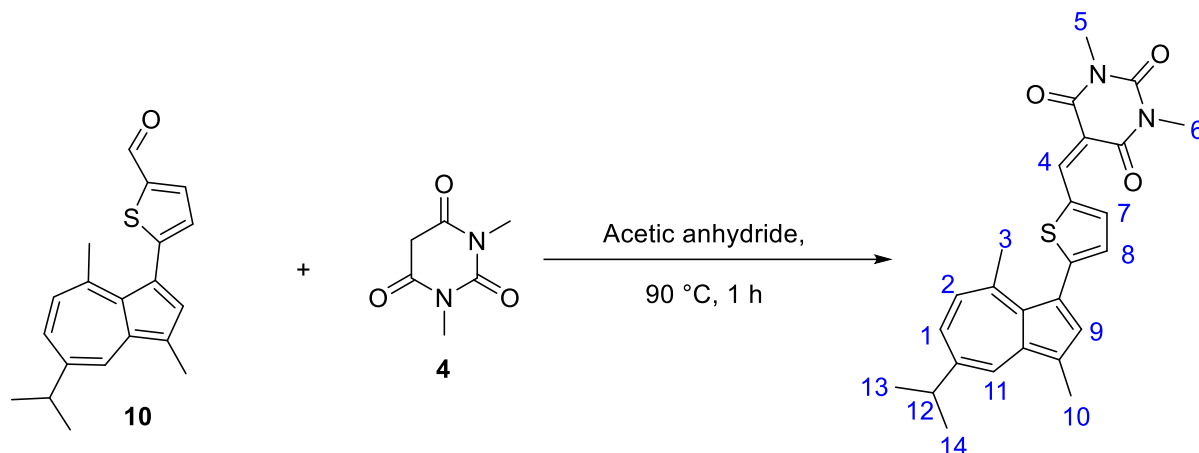
5 (10 mg, 0.03 mmol), **6** (44 mg, 0.2 mmol) were added to acetone: water (1:1) (5 mL total) in a round bottomed flask and stirred. After 15 minutes, the colour changed from a pink to a brick red. The reaction mixture was then stirred for a further 10 minutes and then diluted with dichloromethane (50 mL). The aqueous extracts were washed with dichloromethane (3 × 50 mL). The organic fractions were then combined, dried with MgSO₄ and concentrated *in vacuo* to afford a black/red solid. The crude was purified by silica column chromatography (Petrol: EtOAc 8:2 R_f 0.34) to yield a dark reddish solid (7.2 mg, 0.002 mmol, 16 %). ¹H NMR (500 MHz, CDCl₃) δ 1.43 (d, *J* = 6.9 Hz, 6H, H^{11,12}), 3.21 (s, 3H, H³), 3.34-3.25 (m, 1H, H¹⁰), 3.44 (d, *J* = 6.3 Hz, 6H, H^{5,6}), 7.77 (d, *J* = 10.9 Hz, 1H, H²), 7.83 (dd, *J* = 10.8, 2.1 Hz, 1H, H¹), 9.37 (d, *J* = 5.6 Hz, 2H, H⁹), 9.97 (d, *J* = 2.2 Hz, 1H, H⁴), 10.30 (s, 1H, H⁸). ¹³C NMR (75 MHz, CDCl₃) δ 24.28, 28.31, 28.89, 29.75, 38.43, 110.24, 123.30, 126.22, 137.71, 139.21, 139.29, 144.89, 145.66, 150.84, 150.93, 151.20, 151.23, 152.94, 156.01, 161.26, 163.64, 188.14. IR ν_{max} (cm⁻¹) 750.79, 1375.43, 1645.86. HMS (ESI⁺): calc. for C₂₂H₂₂N₂O₄ [M+H]⁺ 378.1580, found 379.1682.

5-(5-Isopropyl-3,8-dimethylazulen-1-yl)thiophene-2-carbaldehyde (10)



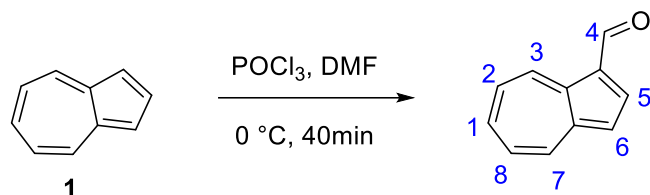
8 (500 mg, 1.2 mmol), **9** (492 mg, 1.7 mmol), palladium acetate (Pd(OAc)₂) (4 mol %, 0.05 mmol), 2-dicyclohexylphosphino-2',4',6'-triisopropylbiphenyl (XPhos) (10 mol %, 0.1 mmol) and tripotassium phosphate (K₃PO₄) (316 mg, 2.3 mmol) were added together. The flask was evacuated and filled with argon followed by degassed 2-propanol (5 mL). The reaction mixture was then heated to 60 °C under argon and stirred for 1 hour after which the solution had turned black/green and it was then allowed to cool back to room temperature. The solvent was concentrated and the residue was extracted with diethylether (30 mL). The combined organic extracts were then concentrated to give a green solid. The green solid was then re-dissolved in acetone (20 mL) and water (10 mL) and a catalytic quantity of *p*-toluenesulfonic acid monohydrate. The solution was then stirred at 30 °C until complete conversion of the starting material to the product (approx. 1 hour). The reaction mixture was concentrated under reduced pressure, the residue was partitioned between diethylether and water. The organic extract was then removed, dried over MgSO₄ and the solvent was concentrated *in vacuo*. The crude was purified by silica column chromatography (Petrol: EtOAc 97:3 R_f0.4) to yield a dark green solid (44 mg, 0.1 mmol, 12 %). ¹H NMR (500 MHz, CDCl₃) δ 1.37 (s, 3H, H³ or H⁸), 1.39 (s, 3H, H³ or H⁸), 2.70-2.61 (m, 6H, H^{11,12}), 3.11 (p, *J* = 6.9 Hz, 1H, H¹⁰), 7.0 (d, *J* = 3.8 Hz, 1H, H^{5,6}), 7.07 (d, *J* = 10.8 Hz, 1H, H²), 7.47 (dd, *J* = 10.8, 2.1 Hz, 1H, H¹), 7.62 (s, 1H, H⁷), 7.72 (d, *J* = 3.8 Hz, 1H, H^{5,6}), 8.24 (d, *J* = 2.2 Hz, 1H, H⁹), 9.89 (s, 1H, H⁴). ¹³C NMR (125 MHz, CDCl₃) δ 12.92, 24.76, 24.89, 27.41, 38.08, 118.82, 124.95, 128.75, 129.44, 133.50, 134.51, 135.83, 136.45, 139.30, 140.72, 142.01, 142.77, 146.46, 154.22, 182.95. HMS (ESI⁺): calc. for C₂₀H₂₀OS [M+H]⁺ 308.1236, found 309.1254, in agreement with literature data.⁹³

5-((5-(5-Isopropyl-3,8-dimethylazulen-1-yl)thiophen-2-yl)methylene)-1,3-dimethylpyrimidine-2,4,6(1H,3H,5H)-trione (11)



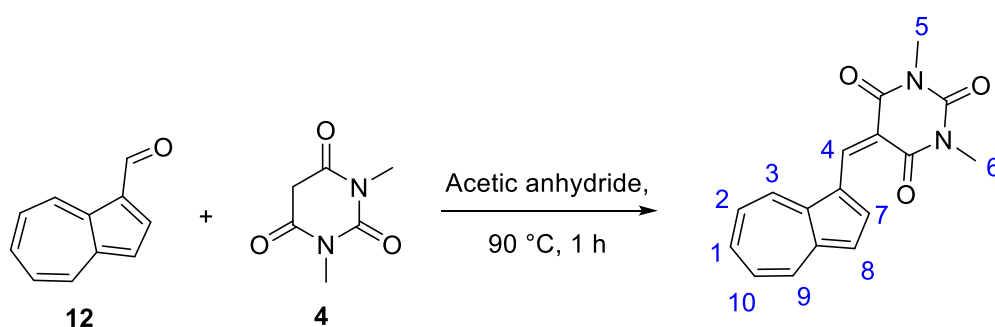
Acetic anhydride (0.30 mL, 3.2 mmol) was added to a combination of **10** (32.7 mg, 0.1 mmol) and **4** (50 mg, 0.3 mmol). The mixture was stirred and heated to 90 °C for 3 hours where a colour change from green to red/pink was observed. The resulting mixture was then diluted with dichloromethane (30 mL), washed with water (5 × 10 mL) and aqueous sodium carbonate (5 × 20 mL). The organic extracts were then dried over MgSO₄, filtered under gravity and concentrated *in vacuo* to yield a dark black/pink solid (14 mg, 0.03 mmol, 30 %). ¹H NMR (500 MHz, CDCl₃) δ 1.38 (d, *J* = 6.8 Hz, 6H, H^{13,14}), 2.63 (d, *J* = 0.7 Hz, 3H, H³ or H¹⁰), 2.68 (s, 3H, H³ or H¹⁰), 3.13 (hept, *J* = 13.7, 7.2, 6.7 Hz, 1H, H¹²), 3.43 (d, *J* = 2.3 Hz, 6H, H^{5,6}), 7.08 (d, *J* = 4.0 Hz, 1H, H⁷ or H⁸), 7.11 (d, *J* = 10.9 Hz, 1H, H²), 7.49 (dd, *J* = 10.7, 2.1 Hz, 1H, H¹), 7.76 (s, 1H, H⁹), 7.85 (d, *J* = 4.1 Hz, 1H, H⁷ or H⁸), 8.22 (d, *J* = 2.1 Hz, 1H, H¹¹), 8.68 (s, 1H, H⁴). ¹³C NMR (125 MHz, CDCl₃) δ 1.18, 12.93, 24.74, 27.83, 28.22, 29.00, 38.14, 108.23, 119.74, 125.62, 129.37, 130.11, 133.97, 134.39, 135.91, 136.10, 140.29, 141.10, 142.87, 146.24, 146.69, 148.94, 161.69, 163.25. IR ν_{\max} (cm⁻¹) 786.17, 1075.13, 1348.72, 1375.12, 1651.48. HMS (ESI⁺): calc. for C₂₆H₂₆N₂O₃S₁ [M+H]⁺ 446.1664, found 447.1659. Melting point 207-211 °C.

1-formylazulene (12)



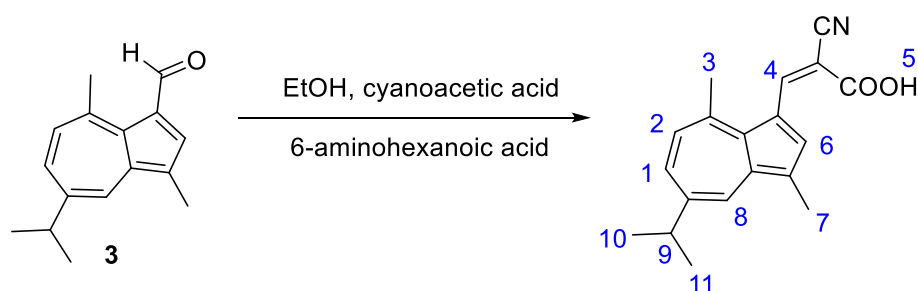
Via cannula at 0 °C, phosphorus(V) oxychloride (0.65 mL, 7.0 mmol) in DMF (3 mL) was transferred slowly to a cold solution of **1** (300 mg, 2.3 mmol) in DMF (20 mL) at 0 °C at which the point the colour turned red. Upon complete addition, the solution was cooled to room temperature and stirring was continued for a further 30 minutes. The reaction mixture was then quenched with water (40 mL) followed by the addition of aqueous NaOH (1 M, 18 mL). The reaction mixture extracted with chloroform (3 × 50 mL). The combined organic extracts were then concentrated, and the residue was re-dissolved in diethyl ether. The solution was washed with water (5 × 10 mL) and saturated LiCl solution (5 × 20 mL). The organic extracts were then washed with water and saturated NaCl solution, dried over MgSO₄, filtered under gravity and concentrated *in vacuo* to yield a pink/red oily solid (248.3 mg, 1.6 mmol, 68 %). ¹H NMR (125 MHz, CDCl₃) δ 7.34 (d, *J* = 4.1 Hz, 1H, H³), 7.53 (t, *J* = 9.7 Hz, 0.9 Hz, 1H, H² or H⁸), 7.63 (t, *J* = 9.9 Hz, 0.9 Hz, 1H, H² or H⁸), 7.86 (tt, *J* = 9.9 Hz, 1.2 Hz, 1H, H¹), 8.27 (d, *J* = 4.2 Hz, 1H, H⁷), 8.50 (dd, *J* = 9.7, 1.1 Hz, 1H, H⁶), 9.59 (d, *J* = 9.7 Hz, 1H, H⁵), 10.36 (s, 1H, H⁴), in agreement with literature data.⁹⁴

5-(Azulen-1-ylmethylene)-1,3-dimethylpyrimidine-2,4,6(1H,3H,5H)-trione (13)



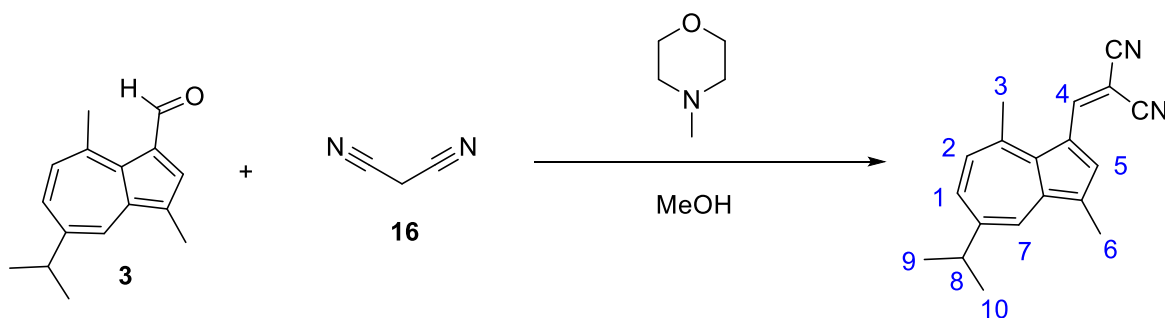
Acetic anhydride (1.5 mL, 10.6 mmol) was added to a combination of **12** (137.6 mg, 0.8 mmol) and **4** (412.7 mg, 2.6 mmol). The mixture was stirred and heated to 90 °C for 1 hour. The resulting mixture was then diluted with dichloromethane (50 mL), washed with water (5 × 20 mL) and aqueous sodium carbonate (3 × 100 mL). The organic extracts were then dried over MgSO₄, filtered under gravity and concentrated *in vacuo*. The crude was purified by recrystallization from ethanol to yield black crystals (128 mg, 0.4 mmol, 49 %). ¹H NMR (400 MHz, CDCl₃) δ 3.46 (t, *J* = 1.5 Hz, 6H, H^{5,6}), 7.57 (d, *J* = 4.6 Hz, 1H, H⁷ or H⁸), 7.66 (td, *J* = 9.7, 1.0 Hz, 1H, H^{2,10}), 7.80-7.70 (m, 1H, H¹), 7.94 (t, *J* = 9.8 Hz, 1H, H⁹), 8.51 (d, *J* = 9.6 Hz, 1H, H^{2,10}), 8.98 (d, *J* = 9.9 Hz, 1H, H³), 9.28 (s, 1H, H⁴), 9.66 (d, *J* = 4.5 Hz, 1H, H⁷ or H⁸). ¹³C NMR (125 MHz, CDCl₃) δ 28.37, 29.05, 108.95, 123.07, 123.86, 129.64, 130.68, 134.67, 138.44, 140.03, 144.86, 145.49, 147.62, 148.47, 152.10, 161.93, 164.61. IR ν_{max} (cm⁻¹) 749.43, 1057.16, 1280.37, 1347.23, 1637.70. HMS (ES⁺): calc. for C₁₇H₁₄N₂O₃ [M+H]⁺ 294.1004, found 295.1008.

(Z)-2-Cyano-3-(5-isopropyl-3,8-dimethylazulen-1-yl) acrylic acid (15)



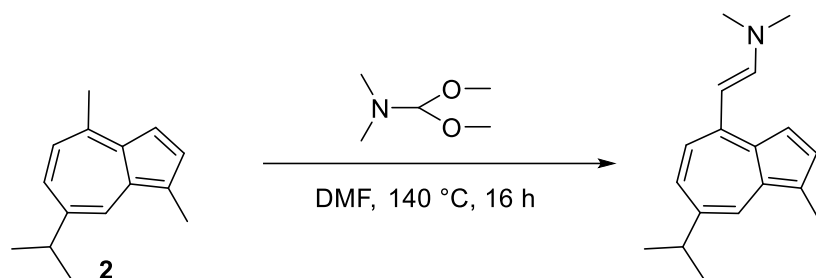
3 (200 mg, 0.8 mmol) and 6-aminohexanoic acid were mixed with ethanol (4.1 mL) and heated to 50 °C for 3.5 hours. After cooling to room temperature, aqueous 1 M sulfuric acid (8 mL) was added to precipitate the product which was removed by vacuum filtration, washed with water and ice-cold ethanol and dried. The crude was purified by neutral aluminium oxide column chromatography (Petrol: CH₂Cl₂ 7:3 R_f 0.5) to yield a brown solid of pure (Z)-2-cyano-3-(5-isopropyl-3,8-dimethylazulen-1-yl) acrylic acid (182 mg, 0.6 mmol, 70 %). ¹H NMR (400 MHz, DMSO-d₆) δ 1.34 (d, *J* = 6.8 Hz, 6H, H^{10,11}), 2.58 (s, 3H, H³ or H⁷), 3.08 (d, *J* = 1.56, 3H, H³ or H⁷), 3.28-3.17 (m, 1H, H⁹), 7.57 (d, *J* = 10.9, Hz, 1H, H¹ or H²), 7.82 (dd, *J* = 10.9, 2.1 Hz, 1H, H¹ or H²), 8.36 (d, *J* = 2.0 Hz, 1H, H⁸), 8.55 (s, 1H, H⁶), 9.06 (d, *J* = 1.7, 1H, H⁴), 13.10 (s, 1H, H⁵). ¹³C NMR (100 MHz, DMSO-d₆) δ 12.89, 24.07, 28.52, 37.08, 92.42, 118.97, 119.67, 128.90, 134.54, 135.80, 136.29, 137.78, 140.14, 143.46, 147.82, 148.05, 148.44, 165.52.

2-((5-Isopropyl-3,8-dimethylazulen-1-yl)methylene)malononitrile (17)



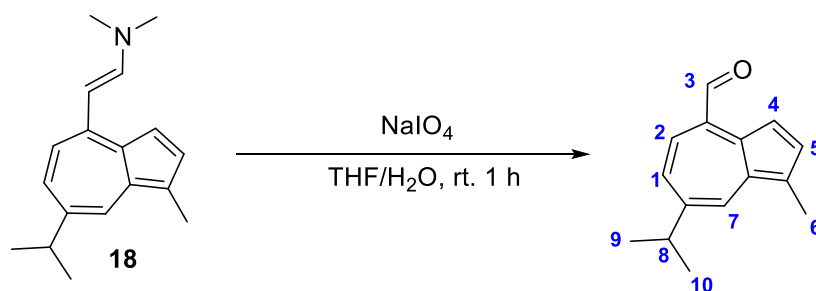
3 (92.7 mg, 0.4 mmol) was added to a solution of **16** (32.5 mg, 0.4 mmol) and *N*-methyl-morpholine (103.6 mg, 1.0 mmol) in methanol (5 mL). After heating the resulting solution at 50 °C for 1 hour, the volatile materials were evaporated under reduced pressure and the crude solid was purified by silica column chromatography (Petrol: EtOAc 85:15 R_f 0.4) to yield a dark yellow solid (94 mg, 84 %). ¹H NMR (75 MHz, CDCl₃) δ 1.40 (d, *J* = 6.8 Hz, 6H, H^{10,11}), 2.59 (s, 3H, H³ or H⁷), 3.10 (s, 3H, H³ or H⁷), 3.28-3.10 (m, 1H, H⁸), 7.48 (d, *J* = 11.0 Hz, 1H, H²), 7.66 (dd, *J* = 10.9, 2.2 Hz, 1H, H¹), 8.27 (d, *J* = 2.2 Hz, 1H, H⁷), 8.47 (s, 1H, H⁵), 8.63 (s, 1H, H⁴), in agreement with literature data.

(E)-2-(7-isopropyl-1-methylazulen-4-yl)-N,N-dimethylethen-1-amine (18)



To a stirred solution of **2** (323 mg, 1.6 mmol, 1.0 eq.) in anhydrous DMF (5 mL) was added dropwise N,N-dimethylformamide dimethyl acetal (0.41 mL, 3.3 mmol, 2.0 eq.) and heated to 140 °C under nitrogen. The mixture was heated until most of the starting material was consumed (approx. 16 h). The mixture was cooled to room temperature and extracted with EtOAc (2 x 50 mL), dilute water (2 x 25 mL) and 5 % LiCl (aq) (4 x 25 mL). The combined organic fractions were dried over MgSO₄ and filtered, then the filtrate was evaporated under reduced pressure. The crude product was used immediately without purification.

7-isopropyl-1-methylazulene-4-carbaldehyde (19)

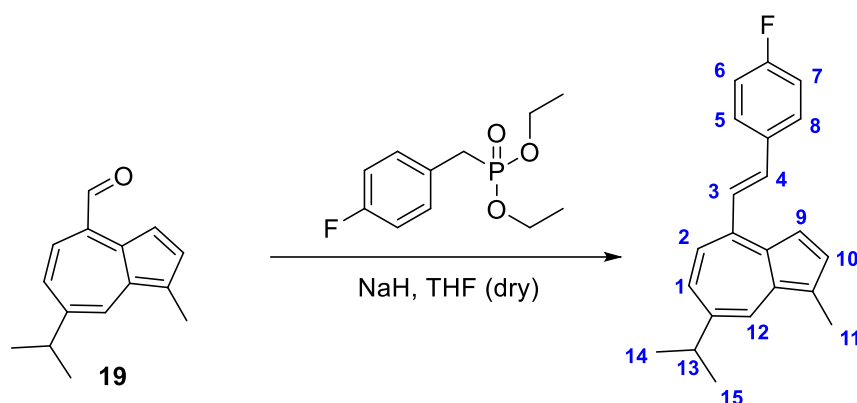


To a stirred solution of **18** (40 mg, 0.2 mmol, 1.0 eq.) in a mixture of THF/H₂O (14 mL) was added NaIO₄ (102 mg, 0.5 mmol, 3.0 eq.) and stirred for approx. 1 h. The mixture was extracted with EtOAc (2 x 25 mL) and sat. NaHCO₃ (3 x 20 mL). The combined organic fractions were dried over MgSO₄ and filtered, then the filtrate was evaporated under reduced pressure. The crude solid was purified by column chromatography (Petrol: EtOAc 95:5 R_f 0.5) to yield a dark black solid (26 mg, 77 %). ¹H NMR (500 MHz, CDCl₃) δ 1.40 (d, *J* = 6.9 Hz, 6H, H^{9,10}), 2.71 (s, 3H, H⁶), 3.15 (hept, *J* = 6.9 Hz, 1H, H⁸), 7.56 (d, *J* = 10.4 Hz, 1H, H²), 7.63 (dd, *J* = 10.5, 1.9 Hz, 1H, H¹), 7.92 (d, *J* = 3.6 Hz, 1H, H⁴), 8.08 (d, *J* = 3.7 Hz, 1H, H⁵), 8.25 (d, *J* = 1.3 Hz, 1H, H⁷), 10.77 (s, 1H, H³) ppm. ¹³C NMR (125 MHz, CDCl₃) δ 13.0, 24.6, 39.0, 112.4, 123.8, 126.2, 133.9, 134.1, 134.1, 134.7, 136.1, 141.4, 141.6, 145.1, 195.1 ppm. IR ν_{max} 701.22, 761.60, 1682.52, 2861.56, 2924.05, 2955.40 cm⁻¹. Melting point 81-84 °C. HMS (ESI): calc. for C₁₅H₁₆O found 213.1274, calc 213.1278.

General Procedure A: Horner-Wadsworth-Emmons reaction

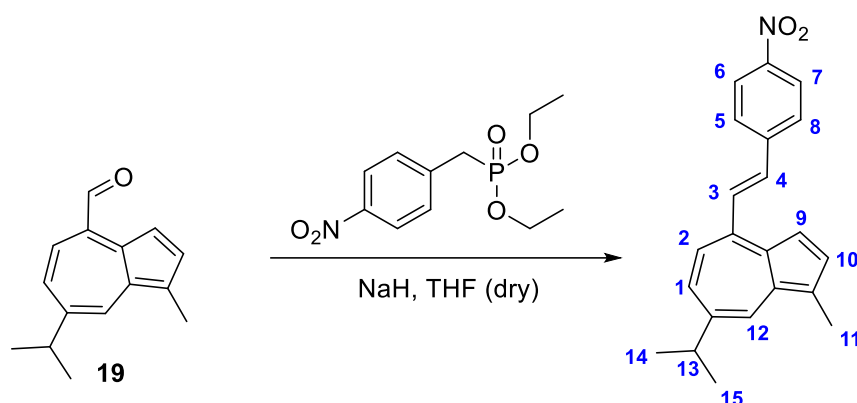
To a stirred solution of 60 % NaH (11 mg, 0.3 mmol, 2.0 eq.) in anhydrous THF (3 mL) was added dropwise a solution of the required phosphonate (0.3 mmol, 2.0 eq.) in anhydrous THF (4 mL) under nitrogen. The mixture was stirred for 10 min after which a solution of **11** (30 mg, 0.1 mmol, 1.0 eq.) in anhydrous THF (3 mL) was added dropwise. The mixture was stirred at rt until the starting material was consumed as shown by TLC (approx. 2 h). The reaction mixture was diluted with water (10 mL) and extracted with CH₂Cl₂ (3 × 30 mL). The combined organic fractions were dried over MgSO₄ and filtered, then the filtrate was evaporated under reduced pressure. Purification was achieved by silica column chromatography to give the desired alkenylazulene.

(E)-4-(4-Fluorostyryl)-7-isopropyl-1-methylazulene (**25**)



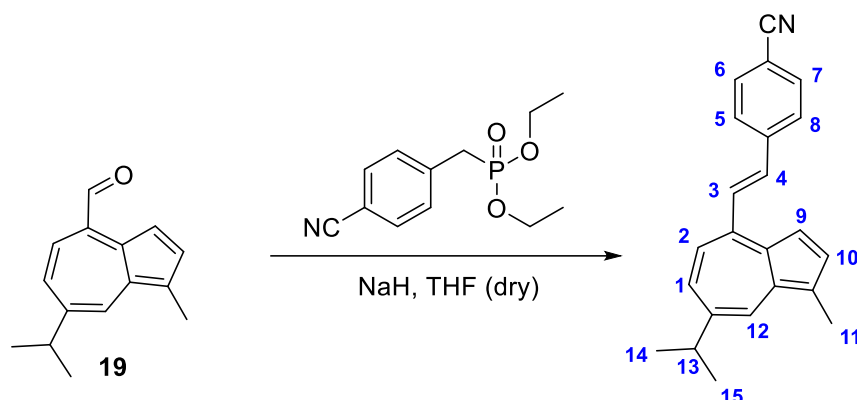
To a stirred solution of 60 % NaH (11 mg, 0.3 mmol, 2.0 eq.) in anhydrous THF (3 mL) was added dropwise a solution of diethyl (3-fluorobenzyl) phosphonate (70 mg, 0.3 mmol, 2.0 eq.) in anhydrous THF (4 mL) under nitrogen. The mixture was stirred for 10 mins after which a solution of the **19** (30 mg, 0.1 mmol, 1.0 eq.) in anhydrous THF (3 mL) was added dropwise. The mixture was stirred at rt until most of the starting material was consumed (approx. 2 h). The mixture was then quenched with dilute water (10 mL) and the THF was evaporated under reduced pressure. The mixture was extracted with DCM (3 x 30 mL) and the combined organic fractions were dried over MgSO₄ and filtered, then the filtrate was evaporated under reduced pressure. Purification was achieved by silica column chromatography using petrol (100 % R_f 0.3) to yield a green waxy gum (19 mg, 44 %). ¹H NMR (500 MHz, (CD₃)₂CO) δ 1.38 (d, *J* = 6.9 Hz, 6H, H^{14,15}), 2.66 (s, 3H, H¹¹), 3.15 (hept, *J* = 6.9 Hz, 1H, H¹³), 7.21 (dd, ³*J*_{HH} = 8.8 Hz, ³*J*_{HF} = 8.8 Hz, 2H, H^{6,7}), 7.54 (d, *J* = 16.2 Hz, 1H, H⁴), 7.59 (br s, 2H, H^{1,2}), 7.60 (d, *J* = 4.0 Hz, 1H, H⁹), 7.66 (d, *J* = 4.0 Hz, 1H, H¹⁰), 7.85 (dd, ³*J*_{HH} = 8.6 Hz, ⁴*J*_{HF} = 5.5 Hz, 2H, H^{5,8}), 8.12 (d, *J* = 16.2 Hz, 1H, H³), 8.26 (s, 1H, H¹²) ppm. ¹³C NMR (125 MHz, (CD₃)₂CO) δ 13.1, 25.0, 38.9, 113.1, 116.5 (d, ²*J*_{CF} = 21.8 Hz), 120.8, 126.6, 129.9 (d, ⁵*J*_{CF} = 2.4 Hz), 130.0 (d, ³*J*_{CF} = 8.1 Hz), 133.6, 133.7, 134.8 (d, ⁴*J*_{CF} = 3.3 Hz), 135.7, 137.4, 137.7, 138.0, 140.9, 142.4, 164.7 (d, ¹*J*_{CF} = 246.5 Hz) ppm. IR ν_{max} 771.07, 1215.47, 1504.95, 2954.54 cm⁻¹. HMS (ES⁺): calc. for C₂₂H₂₁F [M+H]⁺ 305.1700, found 305.1706.

(E)-7-Isopropyl-1-methyl-4-(4-nitrostyryl)azulene (22)



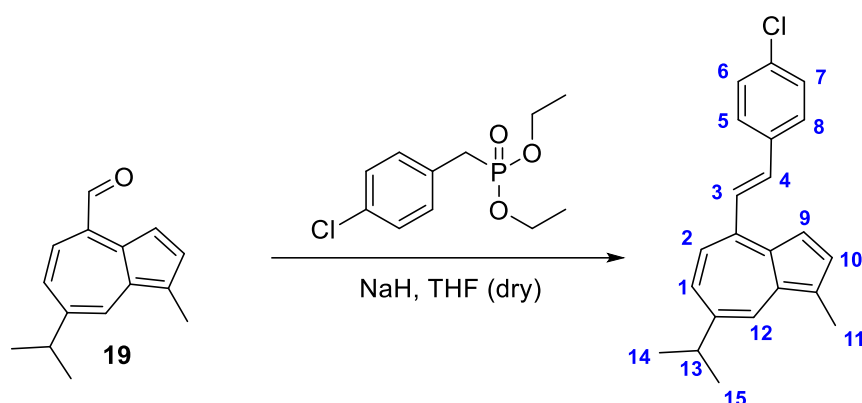
The general procedure A was used with diethyl (4-nitrobenzyl)phosphonate (77 mg, 0.3 mmol, 2.0 eq.) to yield a dark green waxy gum (8.6 mg, 18 %) following purification via silica column chromatography using petrol (100 % R_f 0.4). ^1H NMR (500 MHz, $(\text{CD}_3)_2\text{CO}$) δ 1.39 (d, $J = 6.9$ Hz, 6H, $\text{H}^{14,15}$), 2.67 (s, 3H, H^{11}), 3.17 (hept, $J = 6.9$ Hz, 1H, H^{13}), 7.63 (s, 2H, $\text{H}^{1,2}$), 7.64 (d, $J = 4.0$ Hz, 1H, H^9), 7.67 (d, $J = 16.6$ Hz, 1H, H^4), 7.72 (d, $J = 4.0$ Hz, 1H, H^{10}), 8.07 (d, $J = 8.6$ Hz, 2H, $\text{H}^{5,8}$), 8.30 (d, $J = 8.3$ Hz, 2H, $\text{H}^{6,7}$), 8.41 (d, $J = 16.1$ Hz, 1H, H^3) ppm. ^{13}C NMR (125 MHz, $(\text{CD}_3)_2\text{CO}$) δ 13.0, 25.0, 39.0, 113.2, 120.9, 124.8, 126.9, 128.9, 132.6, 133.9, 134.6, 135.7, 137.7, 138.2, 138.2, 138.3, 141.4, 141.6, 144.8, 148.2 ppm. IR ν_{max} 744.72, 1335.98, 1511.76, 1592.73, 2924.14, 2957.87 cm^{-1} . HMS (ES^+): calc. for $\text{C}_{22}\text{H}_{21}\text{NO}_2$ $[\text{M}+\text{H}]^+$ 332.1645, found 332.1653.

(E)-4-(2-(7-Isopropyl-1-methylazulen-4-yl)vinyl)benzonitrile (21)



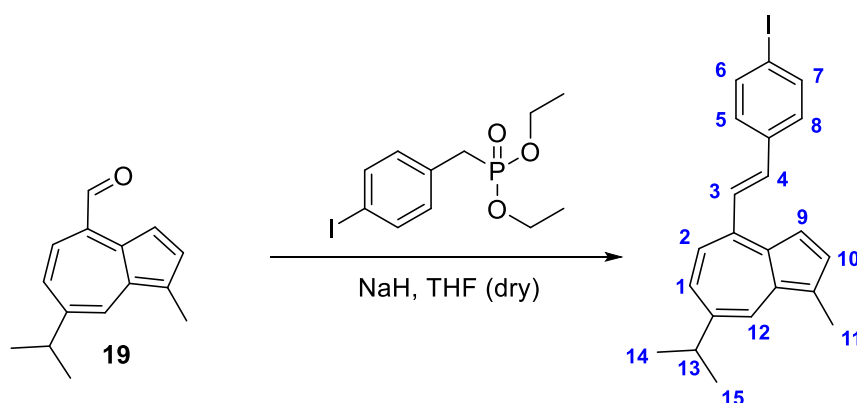
The general procedure A was used with diethyl (4-cyanobenzyl)phosphonate (72 mg, 0.3 mmol, 2.0 eq) to yield a green crystalline solid (20 mg, 46 %) following purification via silica column chromatography using petrol (100 % R_f 0.4). ^1H NMR (500 MHz, $(\text{CD}_3)_2\text{CO}$) δ 1.38 (d, $J = 6.9$ Hz, 6H, $\text{H}^{14,15}$), 2.66 (s, 3H, H^{11}), 3.16 (hept, $J = 6.9$ Hz, 1H, H^{13}), 7.59 (d, $J = 15.9$ Hz, 1H, H^4), 7.59-7.60 (m, 2H, $\text{H}^{1,2}$), 7.63 (d, $J = 3.9$ Hz, 1H, H^9), 7.70 (d, $J = 3.9$ Hz, 1H, H^{10}), 7.81 (d, $J = 8.4$ Hz, 2H, $\text{H}^{5,8}$), 7.98 (d, $J = 8.3$ Hz, 2H, $\text{H}^{6,7}$), 8.28 (s, 1H, H^{12}), 8.33 (d, $J = 16.3$ Hz, 1H, H^3) ppm. ^{13}C NMR (125 MHz, $(\text{CD}_3)_2\text{CO}$) δ 13.0, 24.9, 38.9, 112.1, 113.2, 119.4, 120.8, 126.8, 128.7, 133.0, 133.4, 133.7, 133.9, 135.7, 137.7, 138.1, 138.2, 141.4, 141.6, 142.7 ppm. IR ν_{max} 738.14, 787.20, 1262.88, 2222.06, 2849.21, 2917.04, 2959.59 cm^{-1} . HMS (ES^+): calc. for $\text{C}_{23}\text{H}_{21}\text{N}$ $[\text{M}+\text{H}]^+$ 312.1747, found 312.1753.

(E)-4-(4-Chlorostyryl)-7-isopropyl-1-methylazulene (24)



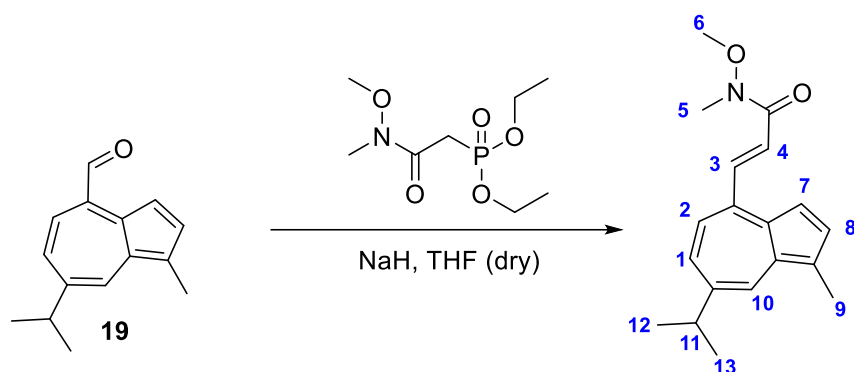
The general procedure A was used with diethyl (4-chlorobenzyl)phosphonate (74 mg, 0.3 mmol, 2.0 eq.) to yield a green waxy gum (19 mg, 42 %) following purification via silica column chromatography using petrol (100 % R_f 0.4). ^1H NMR (500 MHz, $(\text{CD}_3)_2\text{CO}$) δ 1.38 (d, $J = 7.0$ Hz, 6H, $\text{H}^{14,15}$), 2.65 (s, 3H, H^{11}), 3.15 (hept, $J = 6.8$ Hz, 1H, H^{13}), 7.46 (d, $J = 8.5$ Hz, 2H, $\text{H}^{5,8}$), 7.54 (d, $J = 16.2$ Hz, 1H, H^4), 7.59-7.60 (m, 2H, $\text{H}^{1,2}$), 7.61 (d, $J = 4.3$ Hz, 1H, H^9), 7.68 (d, $J = 4.0$ Hz, 1H, H^{10}), 7.82 (d, $J = 8.6$ Hz, 2H, $\text{H}^{6,7}$), 8.19 (d, $J = 16.4$ Hz, 1H, H^3), 8.26 (s, 1H, H^{12}) ppm. ^{13}C NMR (125 MHz, $(\text{CD}_3)_2\text{CO}$) δ 13.0, 24.9, 38.9, 113.1, 120.7, 126.6, 129.6, 129.7, 130.8, 133.5, 133.7, 134.3, 135.6, 137.1, 137.4, 137.7, 137.8, 141.0, 142.1 ppm. IR ν_{max} 772.69, 817.72, 1011.72, 1090.82, 1489.62, 2922.73 cm^{-1} . HMS (ES^+): calc. for $\text{C}_{22}\text{H}_{21}\text{Cl}$ $[\text{M}+\text{H}]^+$ 321.1405, found 321.1412.

(E)-4-(4-iodostyryl)-7-isopropyl-1-methylazulene (20)



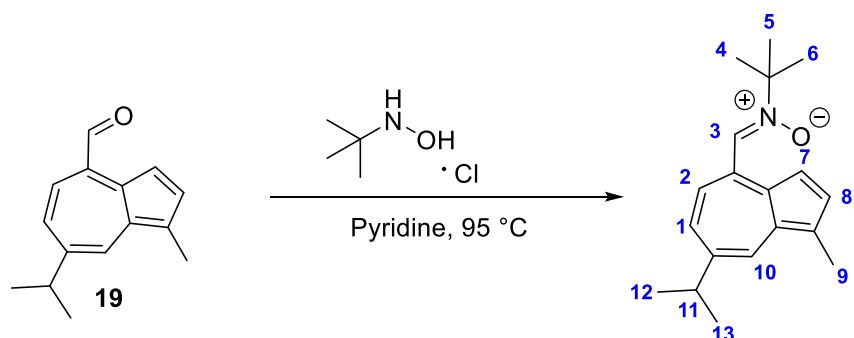
The general procedure A was used with diethyl (4-iodobenzyl)phosphonate (100 mg, 0.3 mmol, 2.0 eq.) to yield a green waxy gum (22 mg, 38 %) following purification via silica column chromatography using petrol (100 % R_f 0.5). ^1H NMR (500 MHz, $(\text{CD}_3)_2\text{CO}$) δ 1.38 (d, $J = 6.9$ Hz, 6H, $\text{H}^{14,15}$), 2.66 (s, 3H, H^{11}), 3.15 (hept, $J = 6.9$ Hz, 1H, H^{13}), 7.48 (d, $J = 16.2$ Hz, 1H, H^4), 7.58-7.61 (m, 5H, $\text{H}^{1,2,5,8,9}$), 7.67 (d, $J = 3.9$ Hz, 1H, H^{10}), 7.80 (d, $J = 8.4$ Hz, 2H, $\text{H}^{6,7}$), 8.20 (d, $J = 16.2$ Hz, 1H, H^3), 8.25 (s, 1H, H^{12}) ppm. ^{13}C NMR (125 MHz, $(\text{CD}_3)_2\text{CO}$) δ 13.1, 24.9, 38.9, 94.2, 113.1, 120.8, 126.8, 130.0, 130.9, 133.7, 133.7, 135.6, 137.5, 137.7, 137.8, 138.0, 138.8, 141.0, 142.1 ppm. IR ν_{max} 763.39, 950.11, 2958.07 cm^{-1} . HMS (ES^+): calc. for $\text{C}_{22}\text{H}_{21}\text{I}$ $[\text{M}+\text{H}]^+$ 413.0761, found 413.0771.

(E)-3-(7-isopropyl-1-methylazulen-4-yl)-N-methoxy-N-methylacrylamide (28)



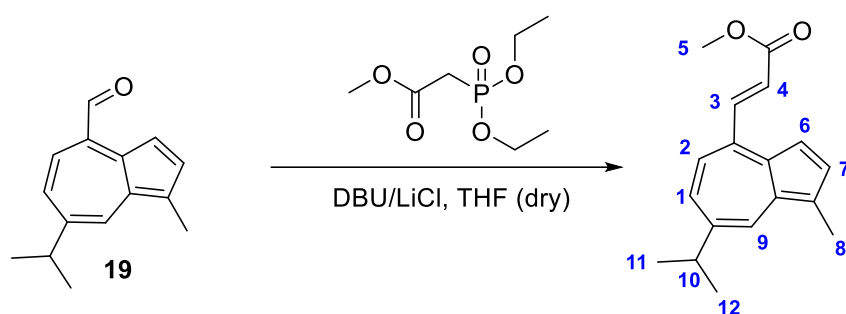
The general procedure A was used with diethyl (2-(methoxy(methyl)amino)-2-oxoethyl)phosphonate (68 mg, 0.3 mmol, 2.0 eq.) to yield a light blue waxy gum (28 mg, 50 %) following purification via silica column chromatography using petrol (100 % R_f 0.3). ^1H NMR (500 MHz, $(\text{CD}_3)_2\text{CO}$) δ 1.38 (d, J = 6.9 Hz, 6H, $\text{H}^{12,13}$), 2.67 (s, 3H, H^9), 3.16 (hept, J = 6.9 Hz, 1H, H^{11}), 3.30 (s, 3H, H^5), 3.84 (s, 3H, H^6), 7.36 (d, J = 15.7 Hz, 1H, H^4), 7.46 (d, J = 3.9 Hz, 1H, H^7), 7.50 (d, J = 10.9 Hz, 1H, H^2), 7.61 (dd, J = 10.9, 1.9 Hz, 1H, H^1), 7.74 (d, J = 3.9 Hz, 1H, H^8), 8.30 (d, J = 1.9 Hz, 1H, H^{10}), 8.51 (d, J = 15.7 Hz, 1H, H^3) ppm. ^{13}C NMR (125 MHz, $(\text{CD}_3)_2\text{CO}$) δ 13.0, 13.0, 24.9, 39.0, 62.4, 113.0, 121.2, 122.5, 127.1, 134.2, 135.7, 138.0, 138.4, 138.8, 140.1, 142.2, 143.6, 143.7 ppm. IR ν_{max} 977.19, 1000.56, 1377.78, 1414.11, 1651.76, 2957.96 cm^{-1} . HMS (ES^+): calc. for $\text{C}_{19}\text{H}_{23}\text{NO}_2$ $[\text{M}+\text{H}]^+$ 297.1729, found 297.1737.

(Z)-N-tert-butyl-1-(7-isopropyl-1-methylazulen-4-yl)methanimine oxide (29)



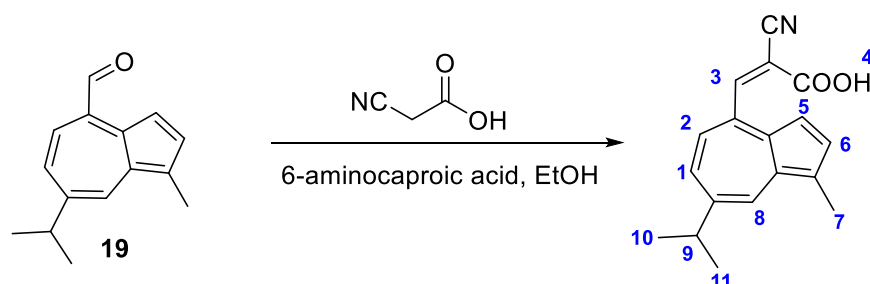
To **19** (70 mg, 0.3 mmol, 1.0 eq.) was added *N*-tert-butylhydroxylamine hydrochloride (62 mg, 0.5 mmol, 1.5 eq.) and pyridine (5 mL) under nitrogen. The solution was heated to 95 °C and stirred for 3 h. The mixture was stirred at 95 °C until all the starting material was consumed (approx. 3 h). After cooling to rt, the mixture was then quenched with dilute water (10 mL) and the pyridine was evaporated under reduced pressure. The mixture was extracted with EtOAc (3 x 30 mL) and the combined organic fractions were washed with brine and dried over MgSO_4 and filtered, then the filtrate was evaporated under reduced pressure to yield a turquoise/green waxy gum (64 mg, 69 %). ^1H NMR (500 MHz, CDCl_3) δ 1.38 (d, J = 6.9 Hz, 6H, $\text{H}^{12,13}$), 1.71 (s, 9H, $\text{H}^{4,5,6}$), 2.68 (s, 3H, H^9), 3.12 (hept, J = 6.9 Hz, 1H, H^{11}), 7.18 (d, J = 3.7 Hz, 1H, H^7), 7.57 (dd, J = 11.1, 2.0 Hz, 1H, H^2), 7.67 (d, J = 3.7 Hz, 1H, H^8), 8.21 (d, J = 1.8 Hz, 1H, H^1), 8.37 (s, 1H, H^{10}), 8.85 (d, J = 11.0 Hz, H^3) ppm. ^{13}C NMR (125 MHz, CDCl_3) δ 13.1, 24.7, 28.6, 38.7, 72.6, 109.7, 121.5, 125.4, 129.4, 133.5, 134.0, 135.3, 137.1, 137.4, 138.4, 143.3 ppm. IR ν_{max} 765.54, 1130.76, 1360.59, 1536.76, 2958.74 cm^{-1} . HMS (ES^+): calc. for $\text{C}_{19}\text{H}_{25}\text{NO}$ $[\text{M}+\text{H}]^+$ 283.1936, found 284.2019.

Methyl (*E*)-3-(7-isopropyl-1-methylazulen-4-yl)acrylate (**26**)



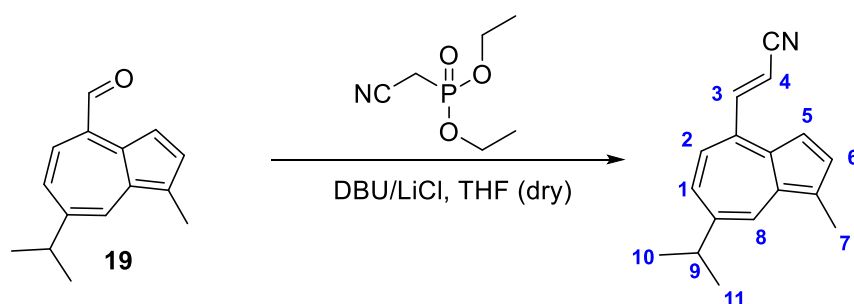
To methyl 2-(diethoxyphosphoryl)acetate (26 mg, 0.1 mmol, 1.0 eq.) in anhydrous THF (5 mL) was added 1,8-diazabicyclo[5.4.0]undec-7-ene (60 μ L, 0.4 mmol, 3.0 eq.) and Lithium Chloride (18 mg, 0.4 mmol, 3.0 eq.) under nitrogen. The mixture was stirred for 5 mins after which a solution of **19** (30 mg, 0.1 mmol, 1.0 eq.) in anhydrous THF (5 mL) was added dropwise. The mixture was stirred at rt until most of the starting material was consumed (approx. 3 h). The mixture was then quenched with dilute water (2 mL) and sat. NH_4Cl . The mixture was then extracted with EtOAc (3 x 20 mL) and the combined organic fractions were washed with distilled water (30 mL) and brine (30 mL), dried over MgSO_4 and filtered, then the filtrate was evaporated under reduced pressure. Purification was achieved by column chromatography using (Petrol: EtOAc 95:5 R_f 0.5) to yield a green wax gum (15 mg, 41 %). ^1H NMR (500 MHz, CDCl_3) δ 1.35 (d, J = 6.9 Hz, 6H, $\text{H}^{11,12}$), 2.65 (s, 3H, H^8), 3.07 (hept, J = 6.8 Hz, 1H, H^{13}), 3.83 (s, 3H, H^5), 6.61 (d, J = 15.9 Hz, 1H, H^4), 7.23 (d, J = 4.8 Hz, 1H, H^9), 7.42 (d, J = 3.9 Hz, 1H, H^6), 7.46 (dd, J = 10.8, 1.9 Hz, 1H, H^1), 7.71 (d, J = 3.3 Hz, 1H, H^7), 8.17 (d, J = 1.9 Hz, 1H, H^2), 8.53 (d, J = 15.9 Hz, 1H, H^3) ppm. ^{13}C NMR (125 MHz, CDCl_3) δ 13.1, 24.8, 38.6, 52.0, 112.6, 120.4, 122.8, 126.6, 133.6, 134.9, 137.3, 137.4, 138.4, 138.5, 141.7, 145.9, 167.3 ppm. IR ν_{max} 1018.14, 1169.33, 1272.75, 1717.94, 2958.16 cm^{-1} . HMS (ES^+): calc. for $\text{C}_{18}\text{H}_{20}\text{O}_2$ [$\text{M}+\text{H}$] $^+$ 268.1463, found 269.1535.

(*Z*)-2-cyano-3-(7-isopropyl-1-methylazulen-4-yl)acrylic acid (**30**)



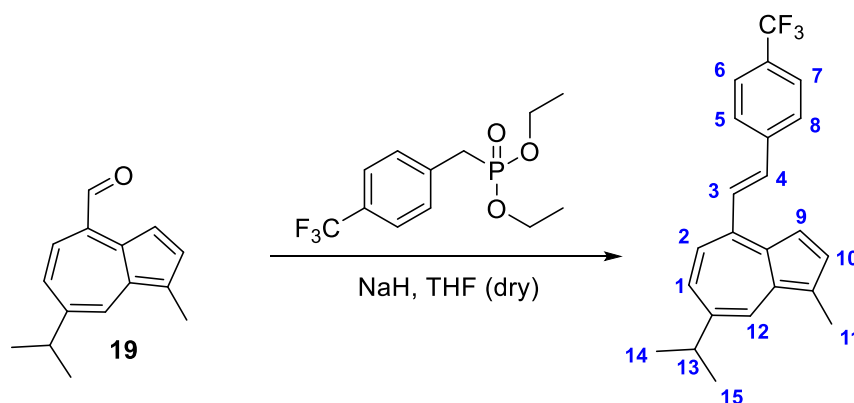
To **19** (77 mg, 0.4 mmol, 1.0 eq.) was added cyanoacetic acid (170 mg, 2.0 mmol, 5.5 eq.) and 6-aminocaproic acid (48 mg, 0.4 mmol, 1.0 eq.) and ethanol (3 mL). The solution was heated to 50 $^\circ\text{C}$ and stirred for 1 h until most of the starting material was consumed (approx. 1 h). After cooling to rt, the mixture was then quenched with 1M sulfuric acid (3 mL) and the product was collected via vacuum filtration, washed with water and dried. The product was recrystallised from EtOH to yield a black solid (1.9 mg, 6 %). ^1H NMR (500 MHz, $(\text{CD}_3)_2\text{CO}$) δ 1.41 (d, J = 6.9 Hz, 6H, $\text{H}^{10,11}$), 2.69 (s, 3H, H^7), 3.24 (hept, J = 6.9 Hz, 1H, H^9), 7.29 (d, J = 3.7 Hz, 1H, H^5), 7.48 (d, J = 10.5 Hz, 1H, H^2), 7.73 (dd, J = 10.6, 1.9 Hz, 1H, H^1), 7.80 (d, J = 3.7 Hz, 1H, H^6), 8.40 (d, J = 1.9 Hz, 1H, H^8), 9.08 (s, 1H, H^4) ppm. ^{13}C NMR (125 MHz, $(\text{CD}_3)_2\text{CO}$) δ 11.9, 23.8, 38.4, 109.8, 114.2, 121.5, 126.8, 134.2, 134.4, 135.2, 135.9, 138.7, 138.7, 143.8, 156.8, 162.0 ppm. IR ν_{max} 708.10, 755.88, 1267.00, 1677.09, 2217.93, 2515.06, 2640.21, 2962.32 cm^{-1} . HMS (ES^-): calc. for $\text{C}_{18}\text{H}_{17}\text{NO}_2$ [$\text{M}-\text{H}$] 279.1259, found 278.1186.

(E)-3-(7-isopropyl-1-methylazulen-4-yl)acrylonitrile (**27**)



To diethyl (cyanomethyl)phosphonate (25 mg, 0.1 mmol, 1.0 eq.) in anhydrous THF (5 mL) was added 1,8-diazabicyclo[5.4.0]undec-7-ene (60 μ L, 0.4 mmol, 3.0 eq.) and Lithium Chloride (18 mg, 0.4 mmol, 3.0 eq.) under nitrogen. The mixture was stirred for 5 mins after which a solution of **19** (30 mg, 0.1 mmol, 1.0 eq.) in anhydrous THF (5 mL) was added dropwise. The mixture was stirred at rt until most of the starting material was consumed (approx. 3 h). The mixture was then quenched with dilute water (2 mL) and sat. NH_4Cl . The mixture was then extracted with EtOAc (3 x 20 mL) and the combined organic fractions were washed with distilled water (30 mL) and brine (30 mL), dried over MgSO_4 and filtered, then the filtrate was evaporated under reduced pressure. Purification was achieved by column chromatography using (Petrol: EtOAc 20:80 R_f 0.6) to yield a dark green wax gum (10.2 mg, 33 %). ^1H NMR (500 MHz, CDCl_3) δ 1.38 (d, J = 6.9 Hz, 6H, $\text{H}^{10,11}$), 2.69 (s, 3H, H^7), 3.12 (hept, J = 6.8 Hz, 1H, H^9), 6.13 (d, J = 16.5 Hz, 1H, H^4), 7.15 (d, J = 10.7 Hz, 1H, H^1), 7.34 (d, J = 3.8 Hz, 1H, H^5), 7.50 (dd, J = 10.7, 2.0 Hz, 1H, H^2), 7.78 (d, J = 3.7 Hz, 1H, H^6), 8.22 (d, J = 1.9 Hz, 1H, H^8), 8.28 (d, J = 16.6 Hz, 1H, H^3) ppm. ^{13}C NMR (125 MHz, CDCl_3) δ 13.1, 24.7, 38.6, 101.3, 112.4, 118.0, 119.4, 127.2, 134.0, 134.8, 136.4, 136.9, 137.9, 139.1, 142.5, 151.9 ppm. IR ν_{max} 721.36, 786.65, 917.81, 976.45, 1421.82, 2215.28, 2959.22 cm^{-1} . HMS (ES $^-$): calc. for $\text{C}_{17}\text{H}_{17}\text{N}$ [$\text{M}-\text{H}$] $^-$ 235.1361, found 234.1290.

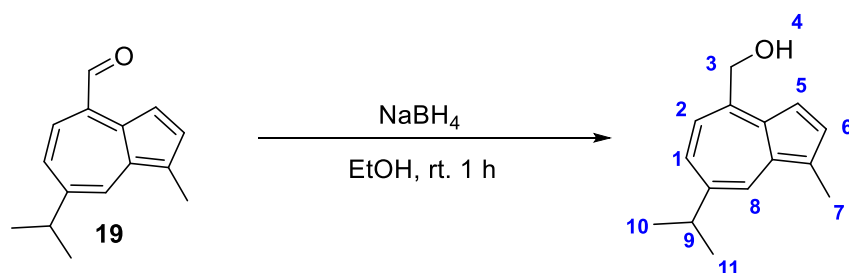
(E)-7-isopropyl-1-methyl-4-(4-(trifluoromethyl)styryl)azulene (**23**)



To a stirred solution of 60% NaH (10 mg, 0.3 mmol, 2.0 eq.) in anhyd. THF (3 mL) was added dropwise a solution of diethyl (4-(trifluoromethyl)benzyl)phosphonate (74 mg, 0.3 mmol, 2.0 eq) in anhyd. THF (4 mL) under nitrogen. The mixture was stirred for 10 mins after which a solution of **19** (27 mg, 0.1 mmol, 1.0 eq.) in anhyd. THF (3 mL) was added dropwise. The mixture was stirred at rt until most of the starting material was consumed (approx. 2 h). The mixture was then quenched with dilute water (10 mL) and the THF was evaporated under reduced pressure. The mixture was extracted with DCM (3 x 30 mL) and the combined organic fractions were dried over MgSO_4 and filtered, then the filtrate was evaporated under reduced pressure. Purification was achieved by column chromatography using Petrol (100 % R_f 0.6) to yield a green waxy gum (25 mg, 56 %). ^1H NMR (500 MHz, $(\text{CD}_3)_2\text{CO}$) δ 1.38 (d, J = 6.9 Hz, 6H, $\text{H}^{14,15}$), 2.66 (s, 3H, H^{11}), 3.15 (hept, J = 7.0 Hz, 1H, H^{13}), 7.59 (d, J = 16.2 Hz, 1H, H^4), 7.60 (m, 2H, $\text{H}^{1,2}$), 7.62 (d, J = 3.9 Hz, H^9), 7.69 (d, J = 3.8 Hz, 1H, H^{10}), 7.76 (d, J = 8.1 Hz, 2H, $\text{H}^{5,8}$), 7.99 (d, J = 7.8 Hz, 2H, $\text{H}^{6,7}$), 8.27 (s, 1H, H^{12}), 8.30 (d, J = 16.2 Hz, 1H, H^3). ^{13}C NMR (125 MHz, $(\text{CD}_3)_2\text{CO}$) δ 142.15 (q, $^4J_{\text{CF}}$ = 1.5 Hz), 141.76, 141.30, 138.10, 138.06, 137.62, 135.68, 133.84, 133.16, 132.88, 130.99 (q, $^2J_{\text{CF}}$ = 32.0 Hz), 128.54, 126.78, 126.50 (q, $^3J_{\text{CF}}$ = 3.9 Hz), 125.40 (q, $^1J_{\text{CF}}$ = 270.9 Hz), 120.87, 113.17, 38.92, 24.93, 13.04 ppm.

IR V_{\max} 825.58, 1065.15, 1106.63, 1320.29, 1413.16, 2960.15 cm^{-1} . HMS (ES⁺): calc. for $\text{C}_{23}\text{H}_{21}\text{F}_3$ $[\text{M}+\text{H}]^+$ 354.1595, found 355.1655.

(7-isopropyl-1-methylazulen-4-yl)methanol (33)



To a solution of **19** (75 mg, 0.3 mmol, 1.0 eq.) in EtOH was added NaBH_4 (27 mg, 0.7 mmol, 2.0 eq.) and an immediate greenish-blue to green colour was observed. The solution was stirred for 1 h at rt and the mixture was then quenched with dilute water (10 mL) and extracted with DCM (3 x 10 mL), dried over MgSO_4 and filtered, then the filtrate was evaporated under reduced pressure to yield the product as a turquoise gum (54.2 mg, 72 %). ^1H NMR (500 MHz, $(\text{CD}_3)_2\text{CO}$) δ 1.37 (d, $J = 6.9$ Hz, 6H, $\text{H}^{10,11}$), 2.65 (s, 3H, H^7), 3.14 (hept, $J = 6.9$ Hz, 1H, H^9), 4.57 (t, $J = 5.8$ Hz, 1H, H^4), 5.18 (d, $J = 5.3$ Hz, 2H, H^3), 7.25 (d, $J = 3.7$ Hz, 1H, H^5), 7.52 (d, $J = 10.7$ Hz, 1H, H^2), 7.62-7.59 (m, 2H, $\text{H}^{1,6}$), 8.27 (d, $J = 2.0$ Hz, 1H, H^8) ppm. ^{13}C NMR (125 MHz, $(\text{CD}_3)_2\text{CO}$) δ 12.9, 25.0, 39.0, 64.5, 111.3, 121.3, 125.4, 133.9, 135.7, 135.7, 137.2, 138.6, 141.4, 147.4 ppm. IR V_{\max} 1008.36, 1386.43, 2924.15, 2956.56, 3316.20 cm^{-1} . HMS (ES⁺): calc. for $\text{C}_{15}\text{H}_{18}\text{O}$ $[\text{M}+\text{H}]^+$ 214.1358, found 214.1365.

Chapter 5: References

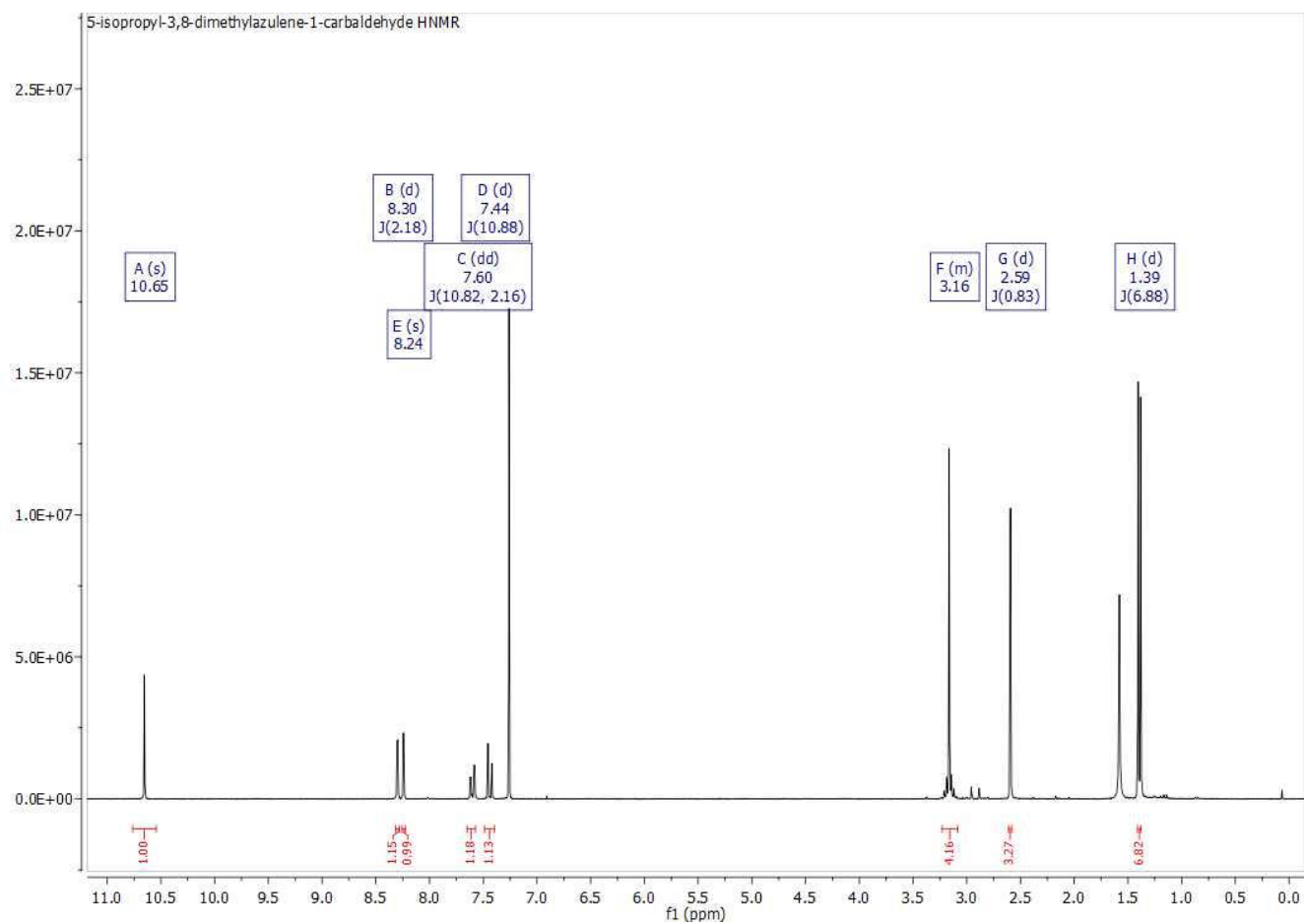
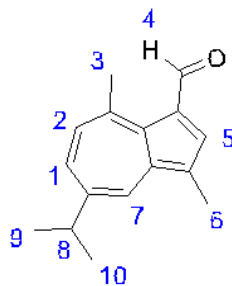
- 1 M. Trivedi, J. Laurence and T. Siahaan, *Curr Protein Pept. Sci*, 2009, **10**, 614–625.
- 2 H. Zhao, M. Chen and C. Ma, *Sensors (Switzerland)*, 2019, **19**, 2–10.
- 3 S. Lu, *Biochim Biophys Acta*, 2014, **1830**, 3143–3153.
- 4 F. Tietze, *Anal. Biochem.*, 1969, **27**, 502–522.
- 5 S. Shahrokhian, *Anal. Chem.*, 2001, **73**, 5972–5978.
- 6 R. Bavarsad Shahripour, M. R. Harrigan and A. V. Alexandrov, *Brain Behav.*, 2014, **4**, 108–122.
- 7 C. Kerksick and D. Willoughby, *J. Int. Soc. Sports Nutr.*, 2005, **2**, 38–44.
- 8 B. Poljsak, *Oxid. Med. Cell. Longev.*, 2011, **2011**, 1–15.
- 9 G. Pizzino, N. Irrera, M. Cucinotta, G. Pallio, F. Mannino, V. Arcoraci, F. Squadrito, D. Altavilla and A. Bitto, *Oxid. Med. Cell. Longev.*, 2017, **2017**, 1–13.
- 10 O. Nekrassova, N. S. Lawrence and R. G. Compton, *Talanta*, 2003, **60**, 1085–1095.
- 11 J. Bergquist and C. Turner, *Anal. Bioanal. Chem.*, 2018, **410**, 3235–3237.
- 12 D. R. Thévenot, K. Toth, R. A. Durst and G. S. Wilson, *Biosens. Bioelectron.*, 2001, **16**, 121–131.
- 13 P. Mehrotra, *J. Oral Biol. Craniofacial Res.*, 2016, **6**, 153–159.
- 14 Research Nester, <https://www.researchnester.com/reports/chemical-sensors-market-global-demand-analysis-opportunity-o>, 2019.
- 15 E. Cabane, X. Zhang, K. Langowska, C. G. Palivan and W. Meier, *Biointerphases*, 2012, **7**, 1–27.
- 16 G. Chang, C. Li, W. Lu and J. Ding, *Macromol. Biosci.*, 2010, **10**, 1248–1256.
- 17 F. Q. Schafer and G. R. Buettner, *Free Radic. Biol. Med.*, 2001, **30**, 1191–1212.
- 18 T. Y. Liu, S. H. Hu, D. M. Liu, S. Y. Chen and I. W. Chen, *Nano Today*, 2009, **4**, 52–65.
- 19 G. Saravanakumar, J. Kim and W. J. Kim, *Adv. Sci.*, 2017, **4**, 1–19.
- 20 S. Son, N. V. Rao, H. Ko, S. Shin, J. Jeon, H. S. Han, V. Q. Nguyen, T. Thambi, Y. D. Suh and J. H. Park, *Int. J. Biol. Macromol.*, 2018, **110**, 399–405.
- 21 G. Butcher, in *Tour of the Electromagnetic Spectrum*, 2016, pp. 1–29.
- 22 J. Fiori, R. Gotti, A. Albini and V. Cavrini, *Rapid Commun. Mass Spectrom*, 2008, **22**, 2698–2706.
- 23 C. M. López-Alled, A. Sanchez-Fernandez, K. J. Edler, A. C. Sedgwick, S. D. Bull, C. L. McMullin, G. Kociok-Köhn, T. D. James, J. Wenk and S. E. Lewis, *Chem. Commun.*, 2017, **53**, 12580–12583.
- 24 R. S. H. Liu and A. E. Asato, *J. Photochem. Photobiol. C Photochem. Rev.*, 2003, **4**, 179–194.
- 25 S. Wakabayashi, Y. Kato, K. Mochizuki, R. Suzuki, M. Matsumoto, Y. Sugihara and M. Shimizu, *J. Org. Chem.*, 2007, **72**, 744–749.
- 26 S. J. Webster, C. M. López-Alled, X. Liang, C. L. McMullin, G. Kociok-Köhn, C. L. Lyall, T. D. James, J. Wenk, P. J. Cameron and S. E. Lewis, *New J. Chem.*, 2019, **43**, 992–1000.
- 27 A. Oprisanu, I. G. Lazar, M. D. Pop, E. M. Ungureanu, R. Isopescu and L. Birzan, *Rev. Chim.*, 2017, **68**, 2215–2218.
- 28 Y. Son, S. Gwon and S. Kim, *Mol. Cryst. Liq. Cryst*, 2014, **600**, 189–195.
- 29 L. C. Murfin, K. Chiang, G. T. Williams, C. L. Lyall, A. T. A. Jenkins, J. Wenk, T. D. James and S. E. Lewis, *Front. Chem.*, 2020, **8**, 1–7.
- 30 L. C. Murfin, C. M. López-Alled, A. C. Sedgwick, J. Wenk, T. D. James and S. E. Lewis, *Front. Chem. Sci. Eng.*, 2020, **14**, 90–96.
- 31 D. Lichosyt, P. Dydio and J. Jurczak, *Chem. - A Eur. J.*, 2016, **22**, 17673–17680.
- 32 C. M. Lopez-Alled, PhD Thesis, University of Bath, 2020.
- 33 C. M. López-Alled, L. Murfin, G. Kociok-Kohn, T. D. James, J. Wenk and S. Lewis, *Analyst*, 2020, **145**, 6262–6269.
- 34 S. Wakabayashi, M. Uchida, R. Tanaka, Y. Habata and M. Shimizu, *Asian J. Org. Chem*, 2013, **2**, 786–791.
- 35 M. Prakash, N. Anwar, P. Tilak, M. S. Shetty, L. S. Prabhu, V. Kedage, M. S. Muttigi, V. Devaramane and P. V. Bhandary, *Online J. Heal. Allied Sci.*, 2009, **8**.
- 36 G. Petsko and D. Ringe, in *New Science Press*, 2004, pp. 30–40.
- 37 N. Sakai, K. Moritaka and T. Konakahara, *European J. Org. Chem.*, 2009, 4123–4127.
- 38 H. Peng, W. Chen, Y. Cheng, L. Hakuna, R. Strongin and B. Wang, *Sensors (Switzerland)*, 2012, **12**, 15907–15946.
- 39 J. Bouffard, Y. Kim, T. M. Swager, R. Weissleder and S. A. Hilderbrand, *Org. Lett.*, 2008, **10**, 37–40.
- 40 S. P. Wang, W. J. Deng, D. Sun, M. Yan, H. Zheng and J. G. Xu, *Org. Biomol. Chem.*, 2009, **7**, 4017–4020.
- 41 X. Li, S. Qian, Q. He, B. Yang, J. Li and Y. Hu, *Org. Biomol. Chem.*, 2010, **8**, 3627–3630.
- 42 D. P. Nair, M. Podgórski, S. Chatani, T. Gong, W. Xi, C. R. Fenoli and C. N. Bowman, *Chem. Mater.*, 2014, **26**, 724–744.
- 43 D. Kand, A. M. Kalle, S. J. Varma and P. Talukdar, *Chem. Commun.*, 2012, **48**, 2722–2724.

- 44 W. Lin, L. Yuan, Z. Cao, Y. Feng and L. Long, *Chem. - A Eur. J.*, 2009, **15**, 5096–5103.
- 45 F. J. Huo, Y. Q. Sun, J. Su, J. Bin Chao, H. J. Zhi and C. X. Yin, *Org. Lett.*, 2009, **11**, 4918–4921.
- 46 X. Chen, S. K. Ko, M. J. Kim, I. Shin and J. Yoon, *Chem. Commun.*, 2010, **46**, 2751–2753.
- 47 G. L. Ellman, *Arch. Biochem. Biophys.*, 1959, **82**, 70–77.
- 48 J. R. Winther and C. Thorpe, *Biochim. Biophys. Acta - Gen. Subj.*, 2014, **1840**, 838–846.
- 49 H. Faulstich, P. Tews and D. Heintz, *Anal. Biochem.*, 1993, **208**, 357–362.
- 50 J. Zhu, I. Dhimitruka and D. Pei, *Biochemistry*, 2004, **6**, 5–8.
- 51 M. Le and G. E. Means, *Anal. Biochem.*, 1995, **229**, 264–271.
- 52 D. R. Grassetti and J. F. Murray, *Arch. Biochem. Biophys.*, 1967, **119**, 41–49.
- 53 O. Rusin, N. N. S. Luce, R. A. Agbaria, J. O. Escobedo, S. Jiang, I. M. Warner, F. B. Dawan, K. Lian and R. M. Strongin, *J. Am. Chem. Soc.*, 2004, **126**, 438–439.
- 54 Y. Xiaofeng, Y. Guo and R. M. Strongin, *Angew Chem Int Ed Engl*, 2012, **50**, 10690–10693.
- 55 X. Zhang, Y. Yan, Y. Hang, J. Wang, J. Hua and H. Tian, *Chem. Commun*, 2017, **53**, 5760–5763.
- 56 M. Cacciarini, E. A. Della Pia and M. B. Nielsen, *European J. Org. Chem.*, 2012, **30**, 6064–6069.
- 57 A. C. Sedgwick, J. E. Gardiner, G. Kim, M. Yevglevskis, M. D. Lloyd, A. T. A. Jenkins, S. D. Bull, J. Yoon and T. D. James, *Chem. Commun.*, 2018, **54**, 4786–4789.
- 58 P. Cowper, A. Pockett, G. Kociok-Köhn, P. J. Cameron and S. E. Lewis, *Tetrahedron*, 2018, **74**, 2775–2786.
- 59 I. Bolz and S. Spange, *Chem. - A Eur. J.*, 2008, **14**, 9338–9346.
- 60 C. Heichert and H. Hartmann, *Zeitschrift für Naturforsch. - Sect. B J. Chem. Sci.*, 2016, **71**, 651–658.
- 61 O. Toshiya and K. Shinji, *Chem. Lett*, 1997, **26**, 1–50.
- 62 C. Wu, Masters Thesis, University of Bath, 2016.
- 63 X. H. Zhang, C. Li, W. B. Wang, X. X. Cheng, X. S. Wang and B. W. Zhang, *J. Mater. Chem.*, 2007, **17**, 642–649.
- 64 E. H. Ghazvini Zadeh, A. W. Woodward, D. Richardson, M. V. Bondar and K. D. Belfield, *European J. Org. Chem.*, 2015, **2015**, 2271–2276.
- 65 T. O. Leino, M. Baumann, J. Yli-Kauhaluoma, I. R. Baxendale and E. A. A. Wallén, *J. Org. Chem.*, 2015, **80**, 11513–11520.
- 66 K. Kurotobi, K. S. Kim, S. B. Noh, D. Kim and A. Osuka, *Angew. Chemie - Int. Ed.*, 2006, **45**, 3944–3947.
- 67 M. G. Vetelino and J. W. Coe, *Tetrahedron Lett.*, 1994, **35**, 219–222.
- 68 W. Lin, L. Long, L. Yuan, Z. Cao, B. Chen and W. Tan, *Org. Lett.*, 2008, **10**, 5577–5580.
- 69 H. Y. Lee, Y. P. Choi, S. Kim, T. Yoon, Z. Guo, S. Lee, K. M. K. Swamy, G. Kim, J. Y. Lee, I. Shin and J. Yoon, *Chem. Commun.*, 2014, **50**, 6967–6969.
- 70 K. S. Lee, T. K. Kim, J. H. Lee, H. J. Kim and J. I. Hong, *Chem. Commun.*, 2008, 6173–6175.
- 71 H. Maeda, H. Matsuno, M. Ushida, K. Katayama, K. Saeki and N. Itoh, *Angew. Chemie - Int. Ed.*, 2005, **44**, 2922–2925.
- 72 J. E. Gardiner, PhD Thesis, University of Bath, 2020.

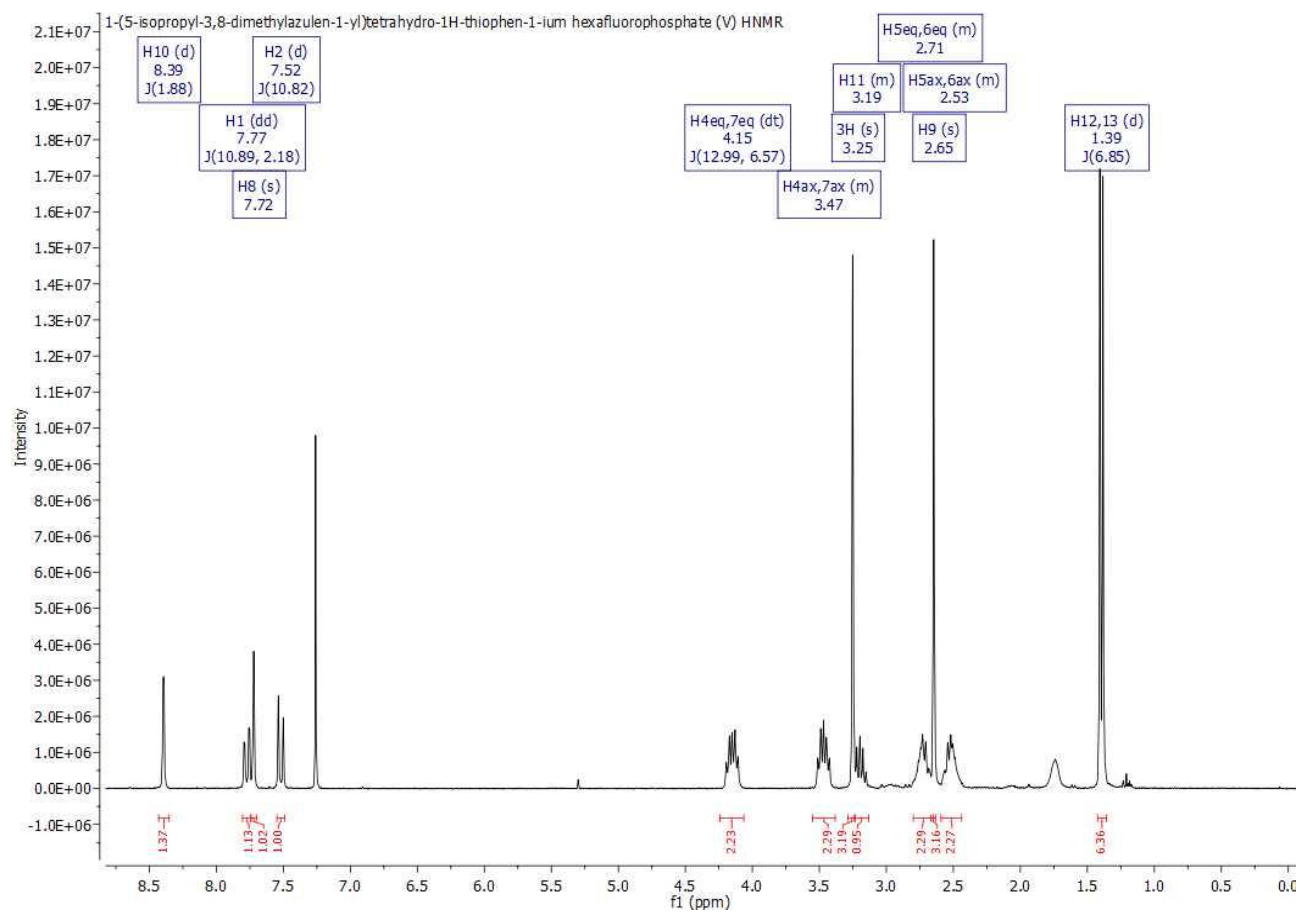
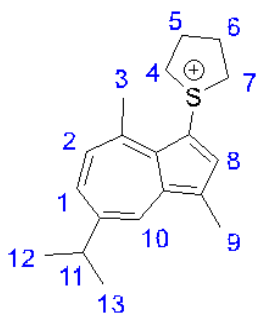
Chapter 6: Appendix 1 – Spectra and Charts

The following pages contain spectra and charts of collected data.

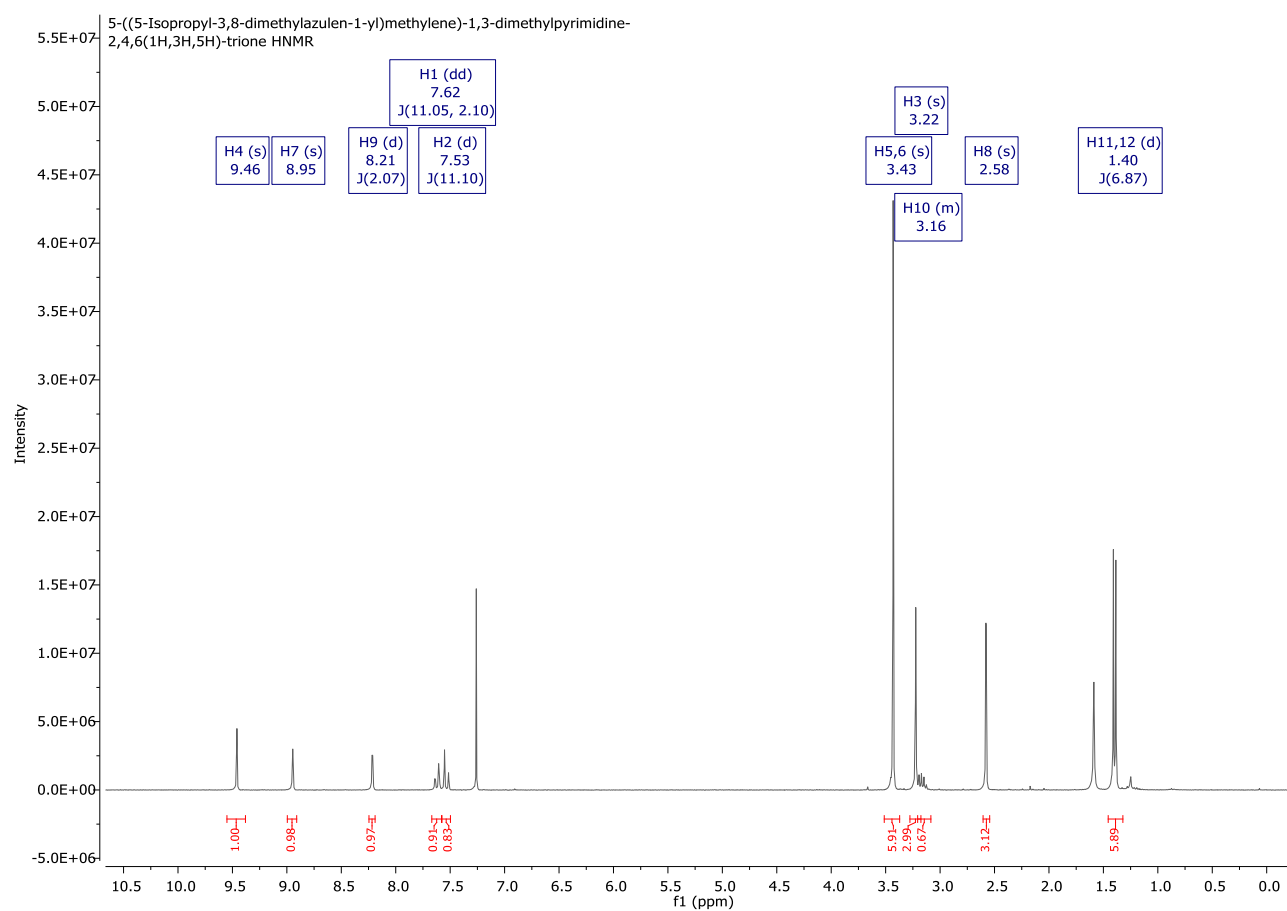
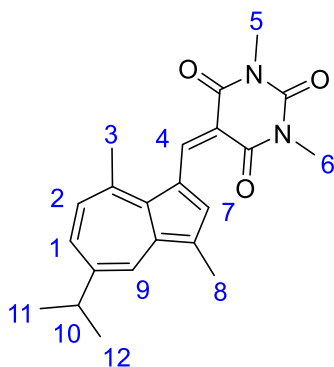
5-Isopropyl-3,8-dimethylazulene-1-carbaldehyde (3)

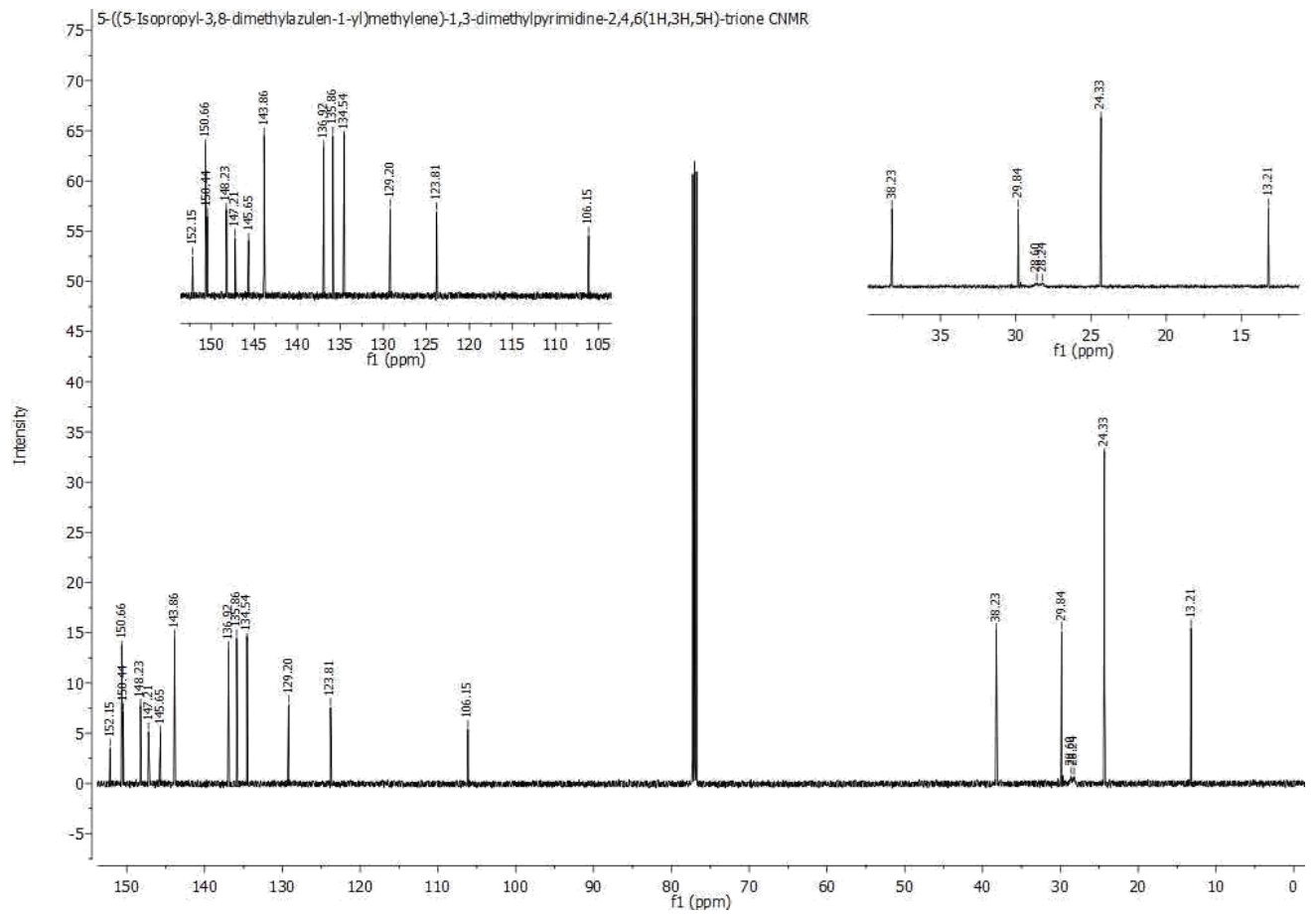


**1-(5-Isopropyl-3,8-dimethylazulen-1-yl) tetrahydro-1H-thiophen-1-ium hexafluorophosphate (V)
(8)**

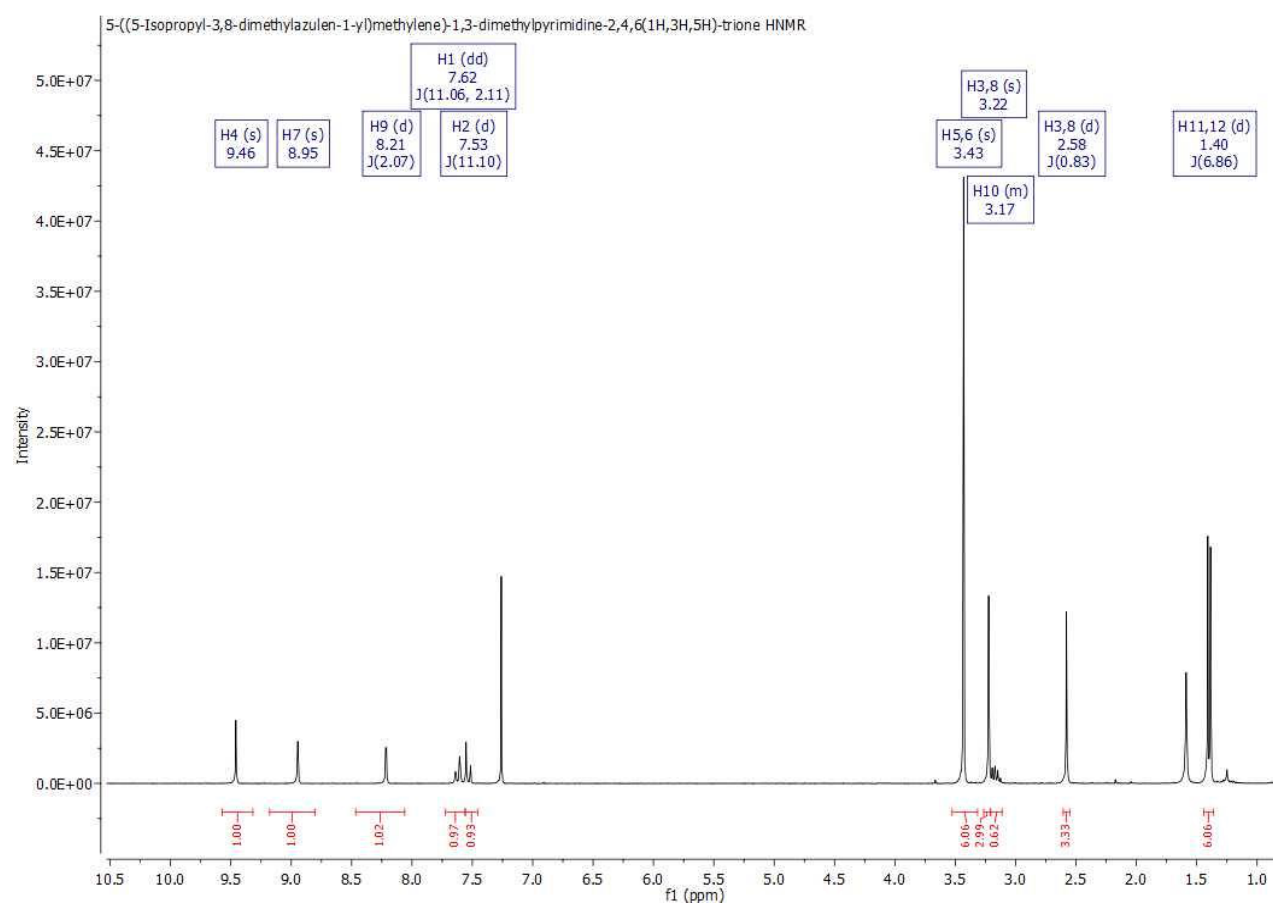
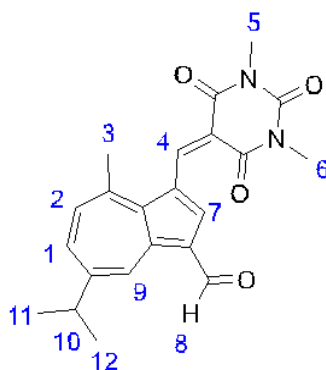


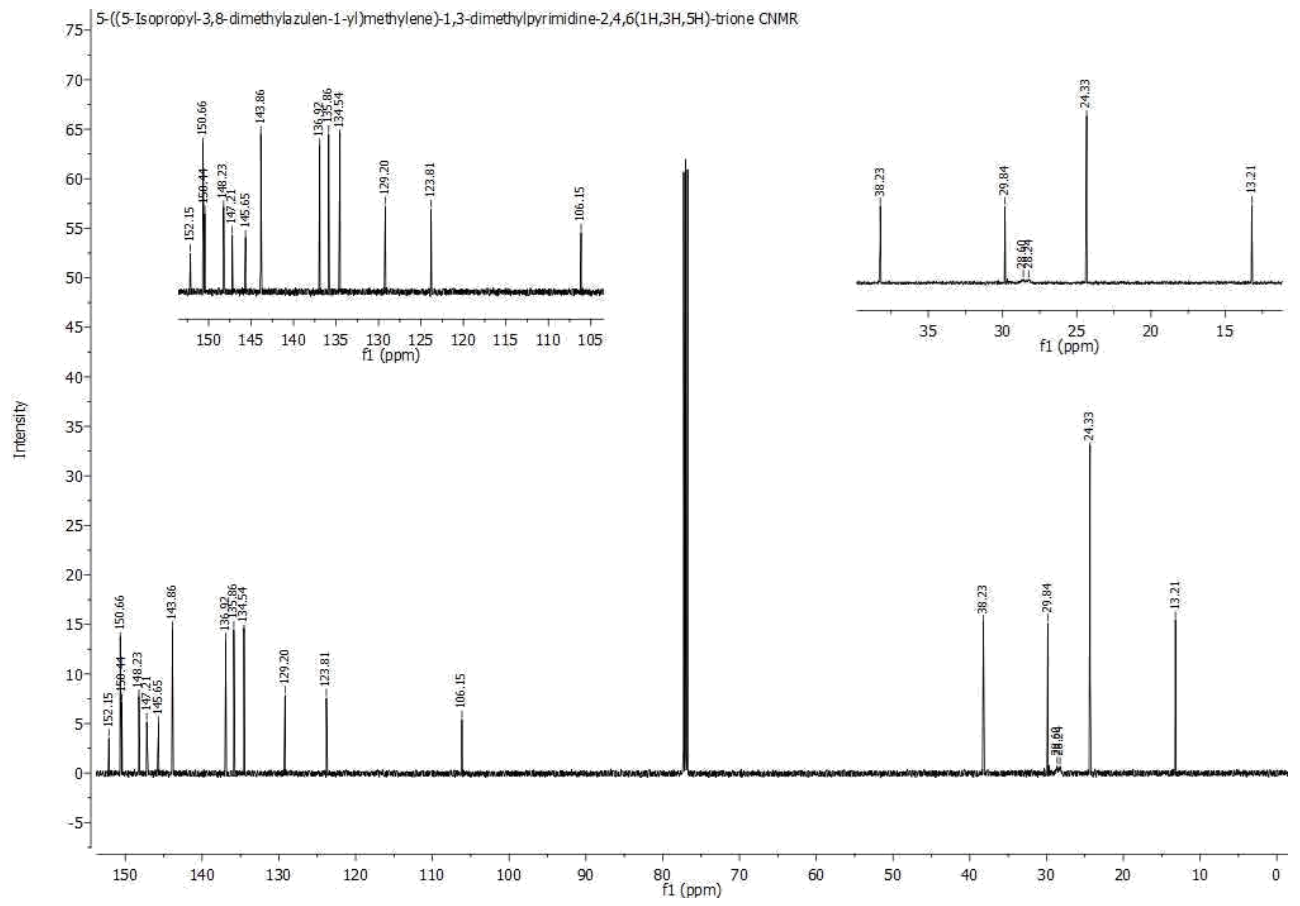
5-((5-Isopropyl-3,8-dimethylazulen-1-yl)methylene)-1,3-dimethylpyrimidine-2,4,6(1H,3H,5H)-trione (5)



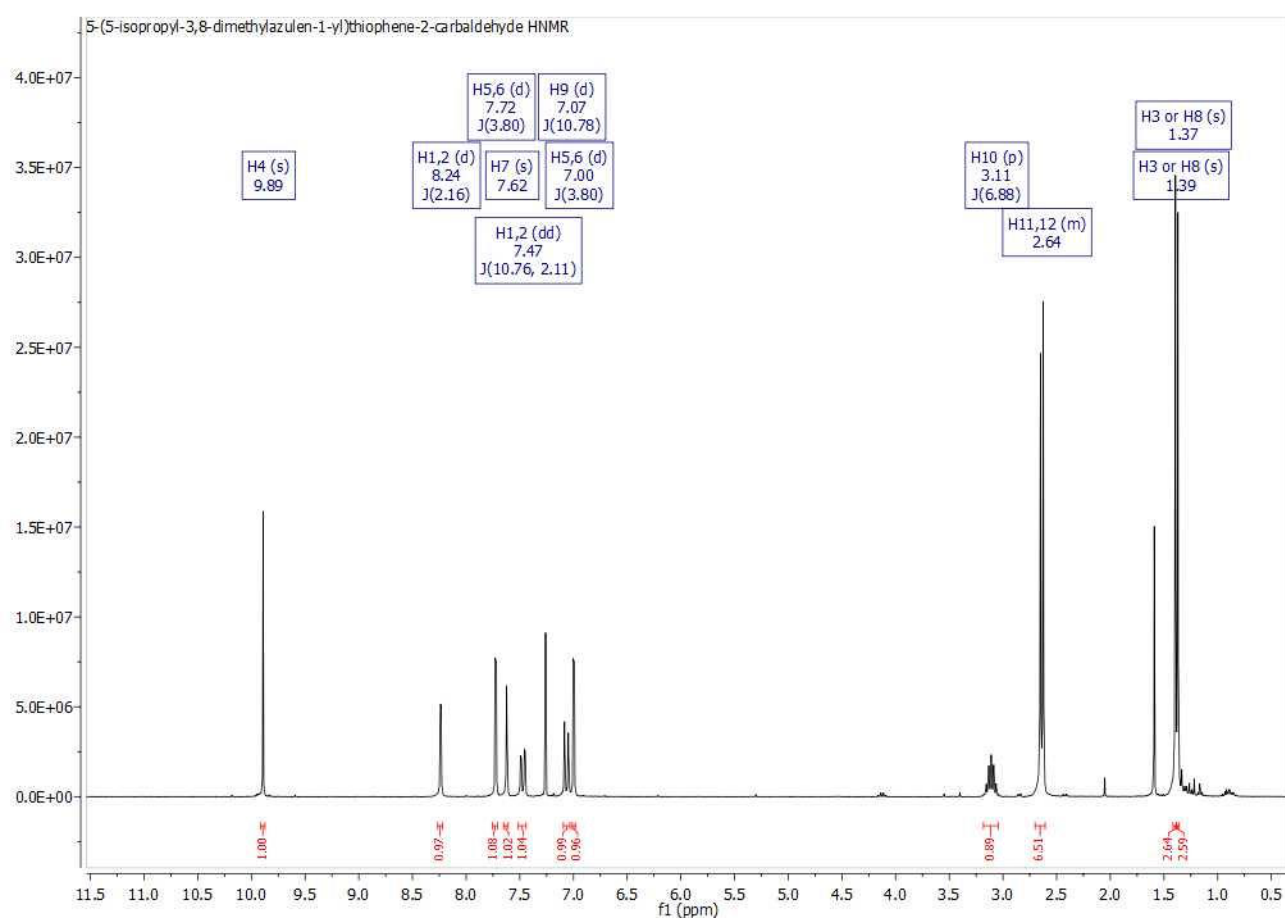
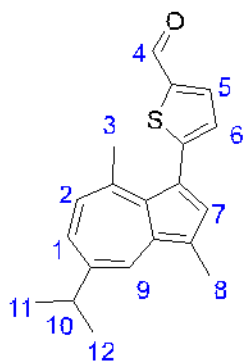


3-((1,3-Dimethyl-2,4,6-trioxotetrahydropyrimidin-5(2H)-ylidene) methyl)-7-isopropyl-4-methylazulene-1-carbaldehyde (7)

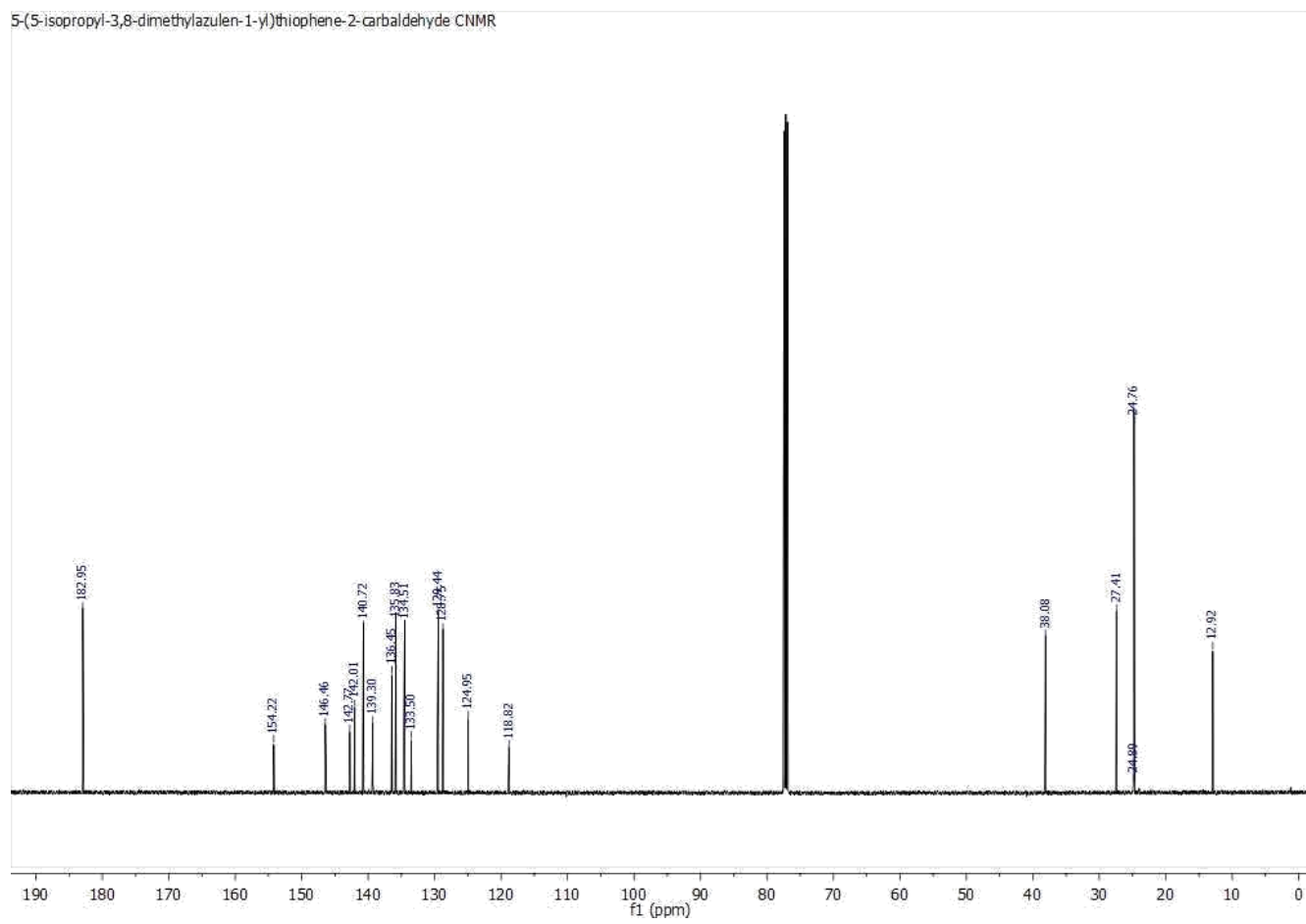




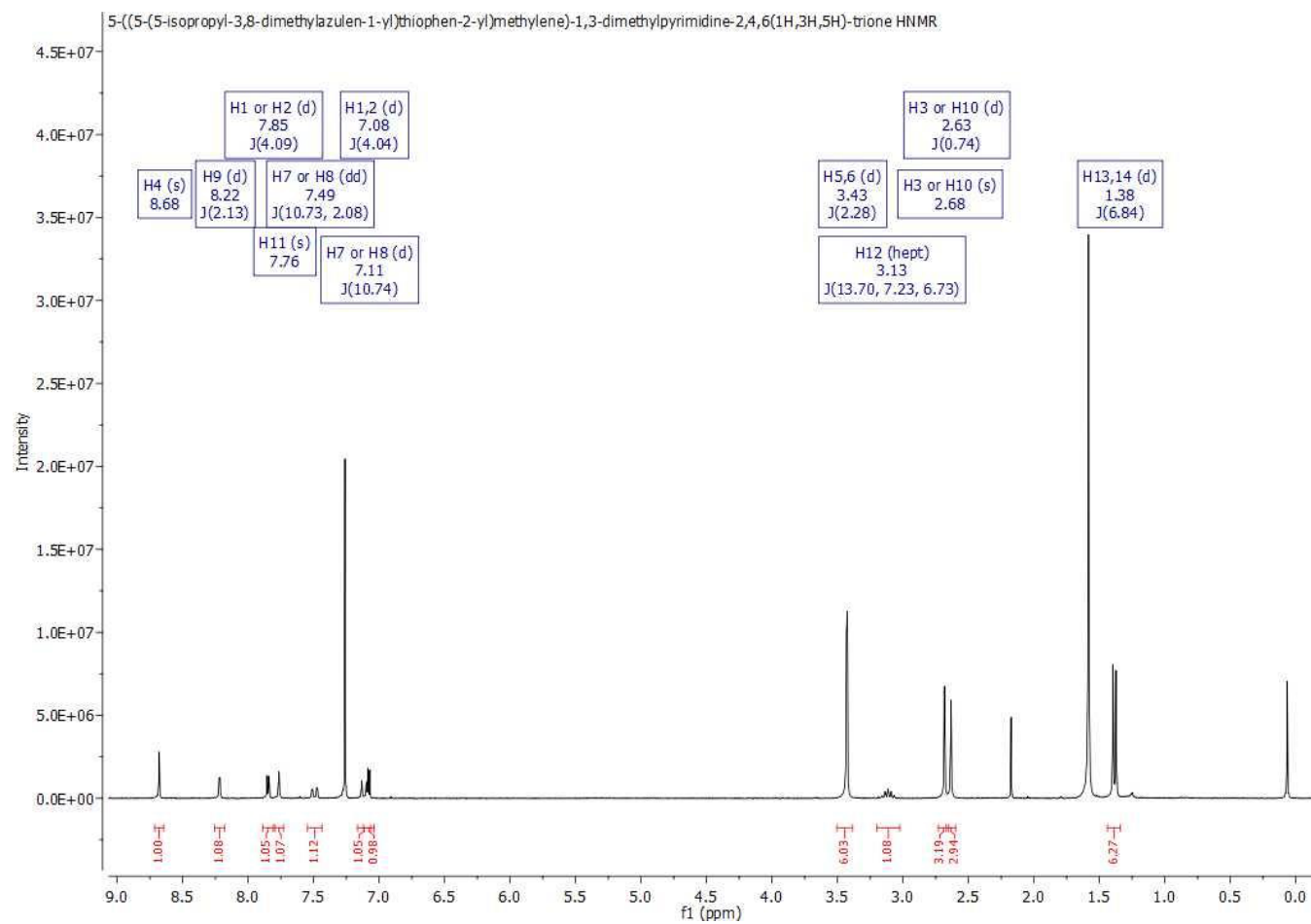
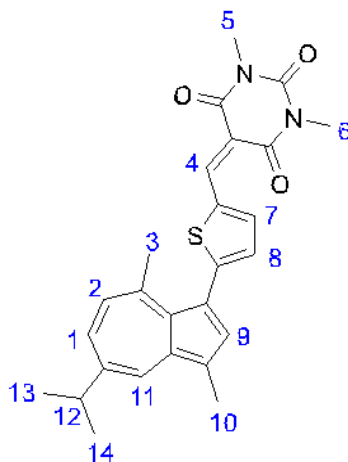
5-(5-isopropyl-3,8-dimethylazulen-1-yl)thiophene-2-carbaldehyde (10)



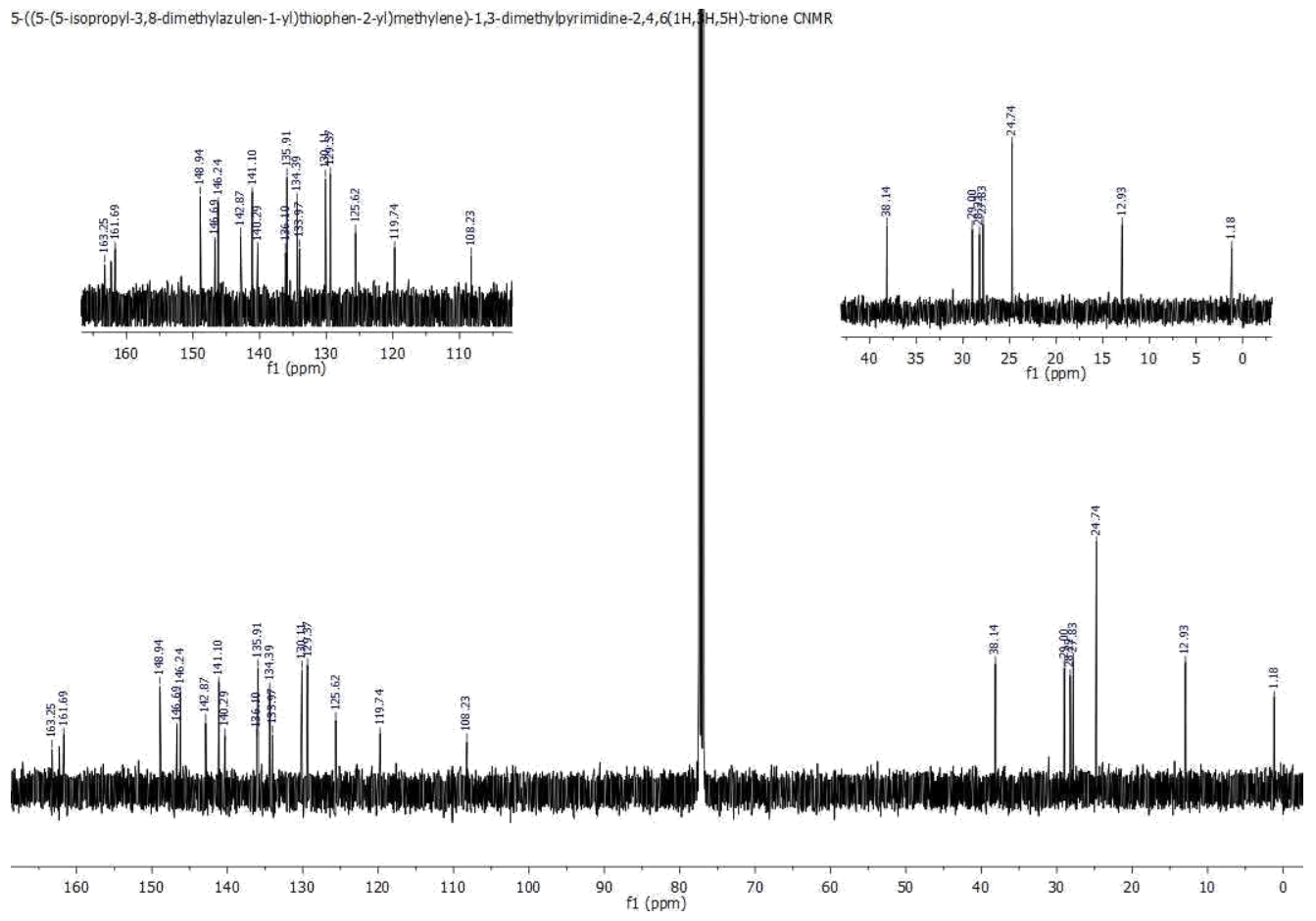
5-(5-isopropyl-3,8-dimethylazulen-1-yl)thiophene-2-carbaldehyde CNMR



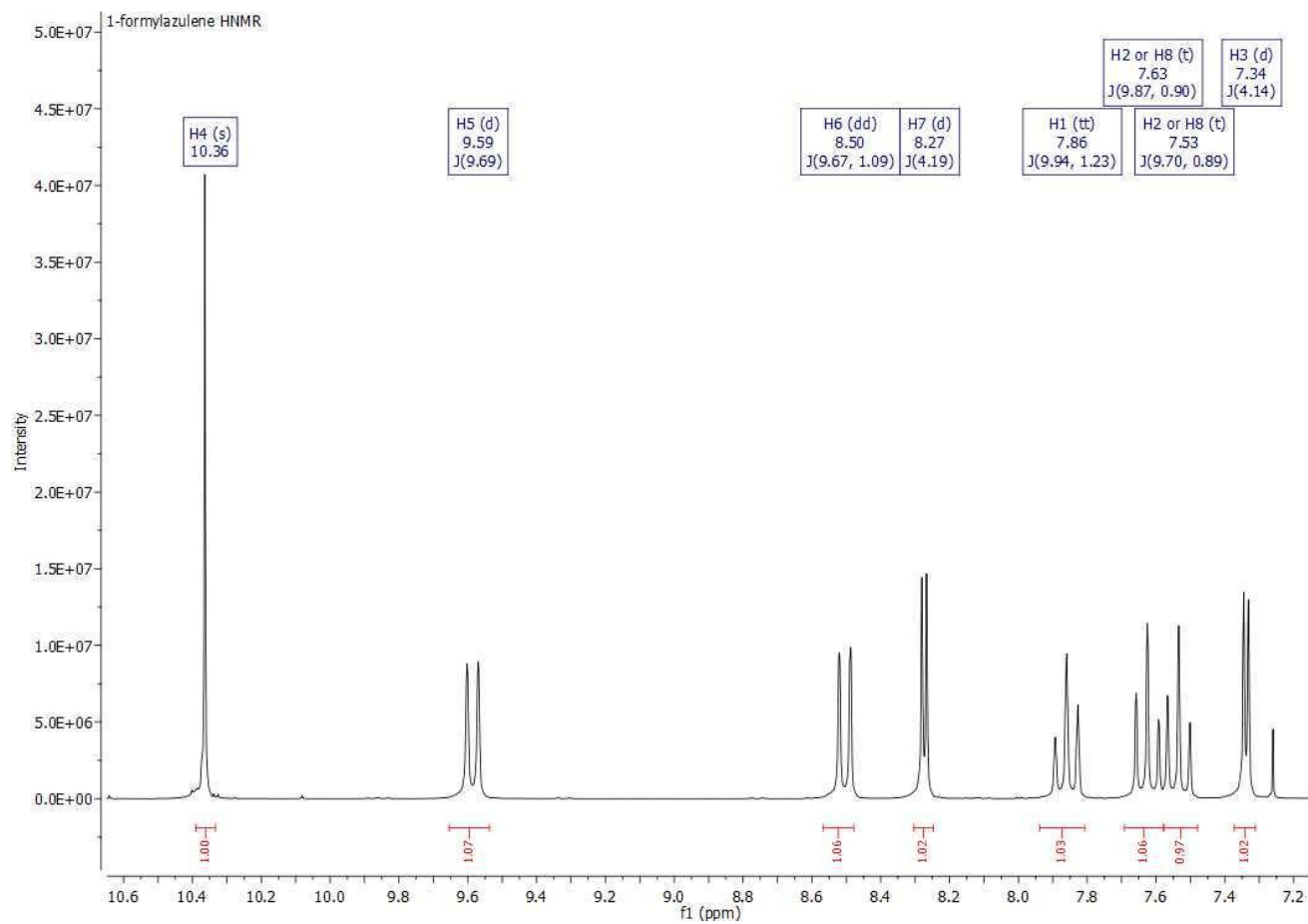
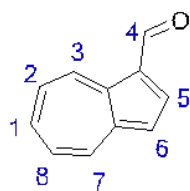
5-((5-(5-Isopropyl-3,8-dimethylazulen-1-yl)thiophen-2-yl)methylene)-1,3-dimethylpyrimidine-2,4,6(1H,3H,5H)-trione (11)



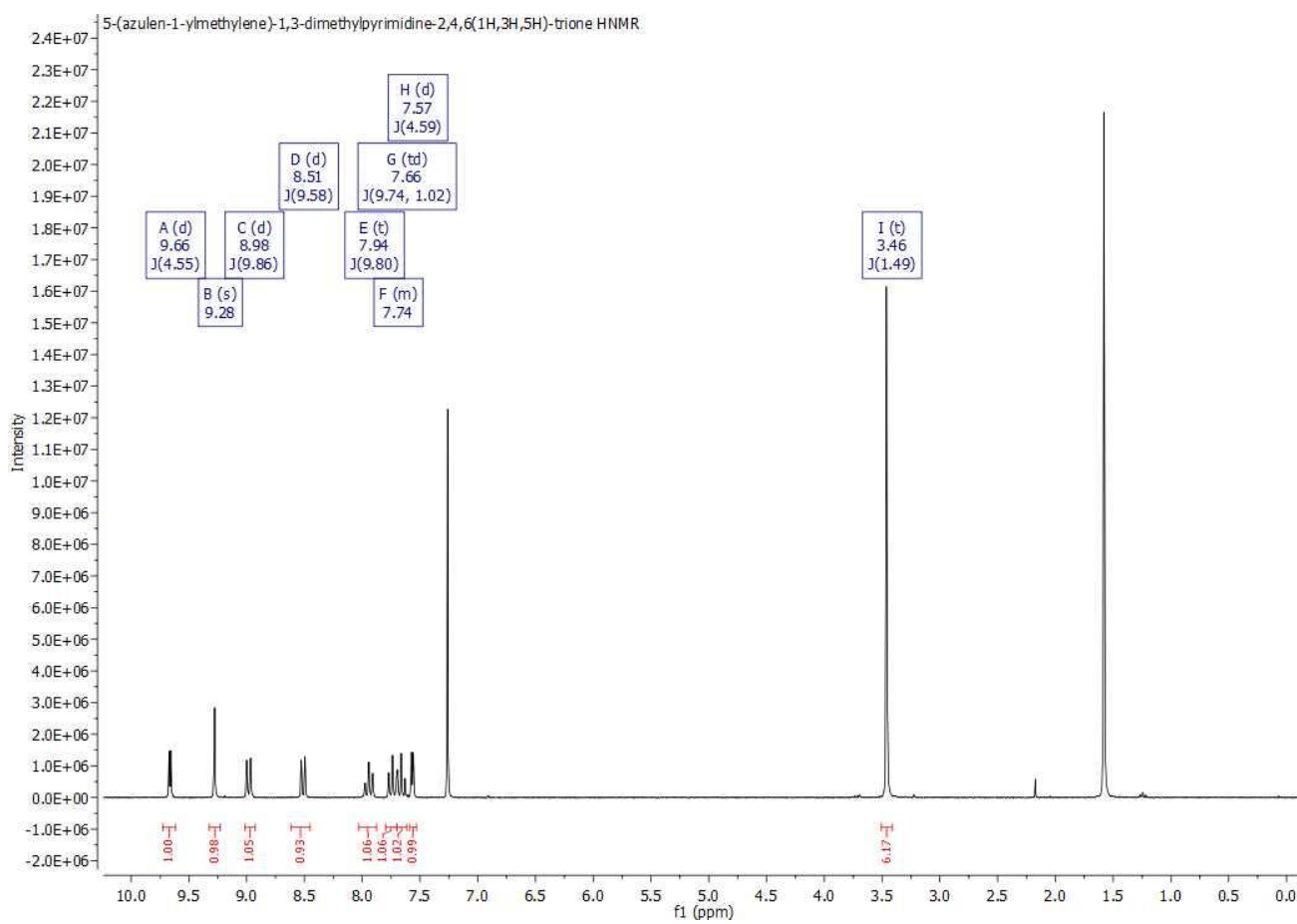
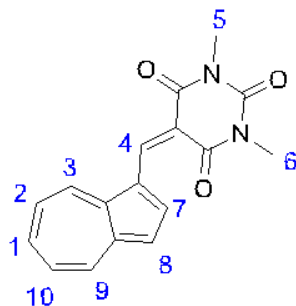
5-((5-(5-isopropyl-3,8-dimethylazulen-1-yl)thiophen-2-yl)methylene)-1,3-dimethylpyrimidine-2,4,6(1H,3H,5H)-trione CNMR

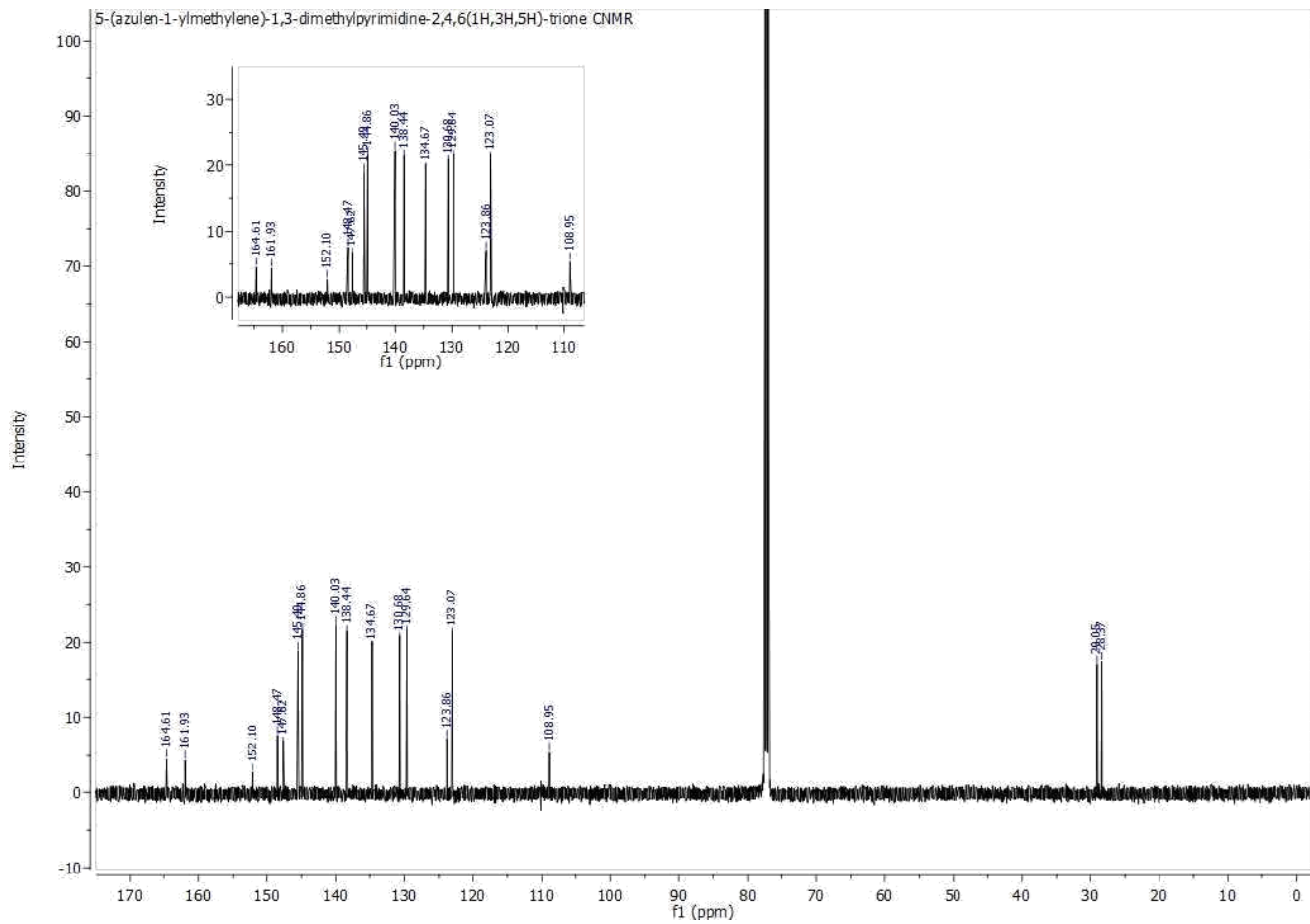


1-Formylazulene (12)

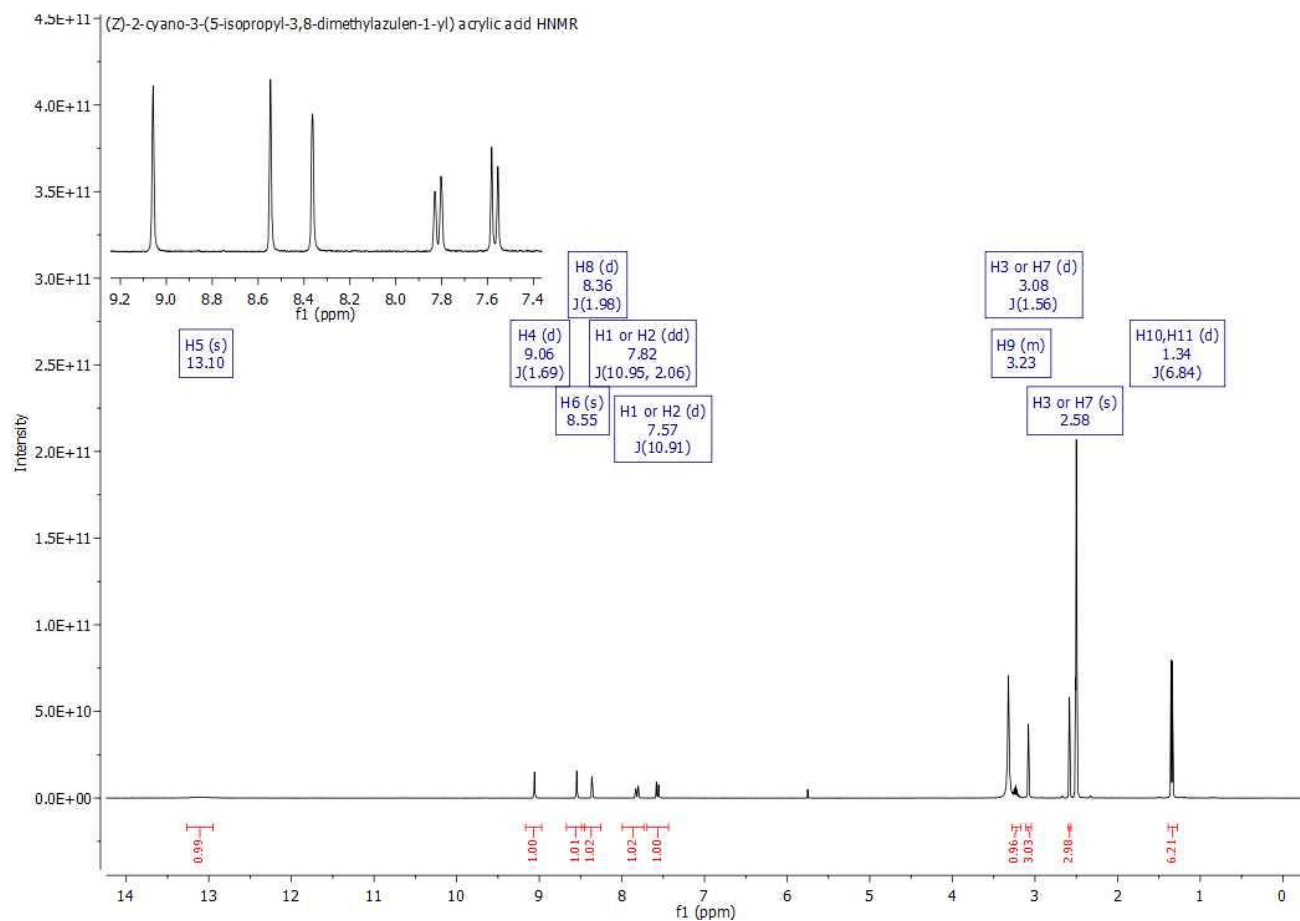
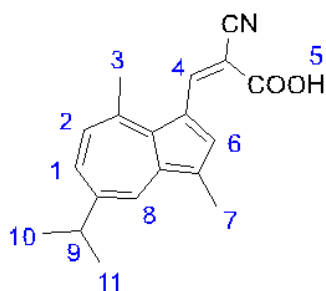


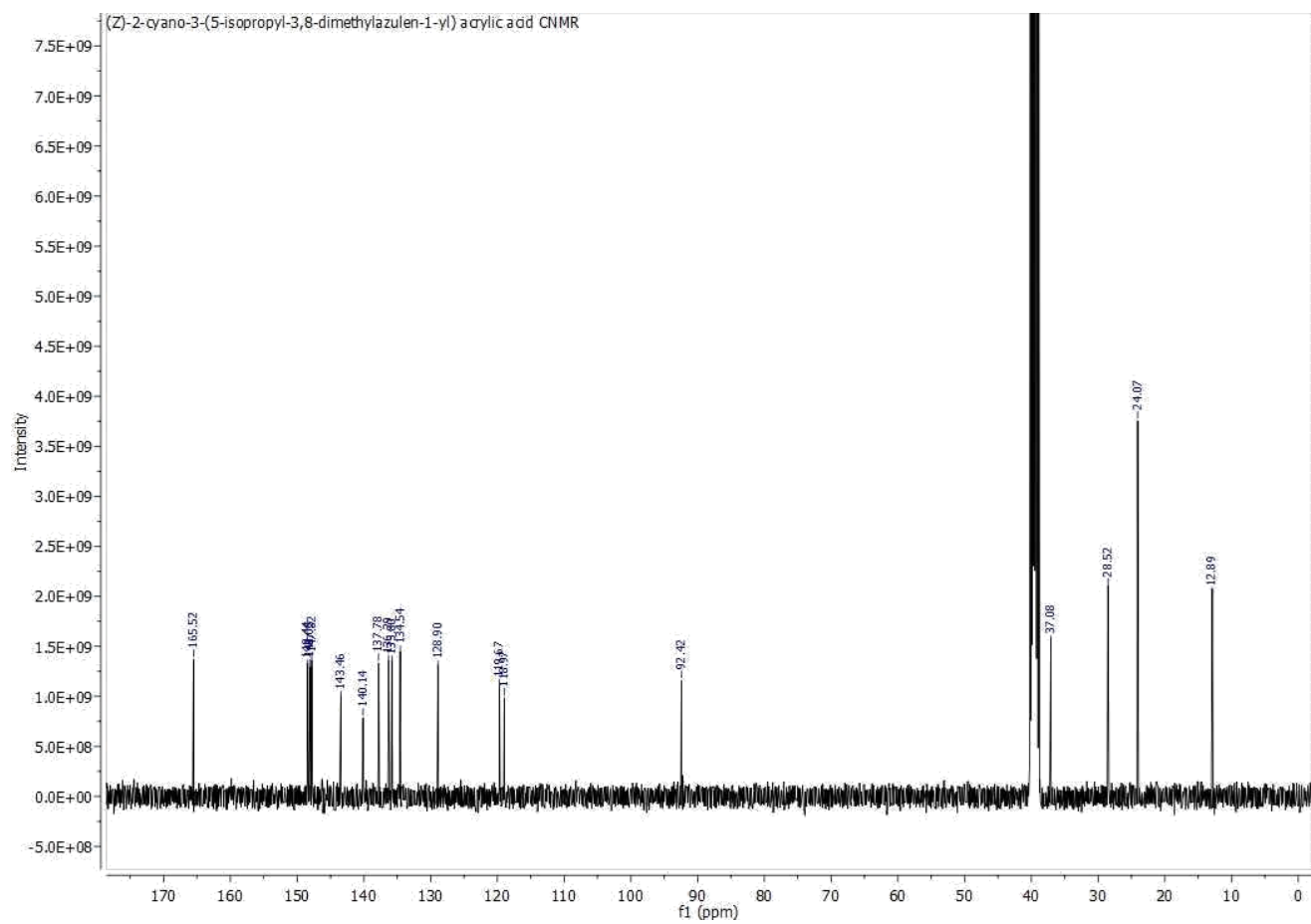
5-(Azulen-1-ylmethylene)-1,3-dimethylpyrimidine-2,4,6(1H,3H,5H)-trione (13)



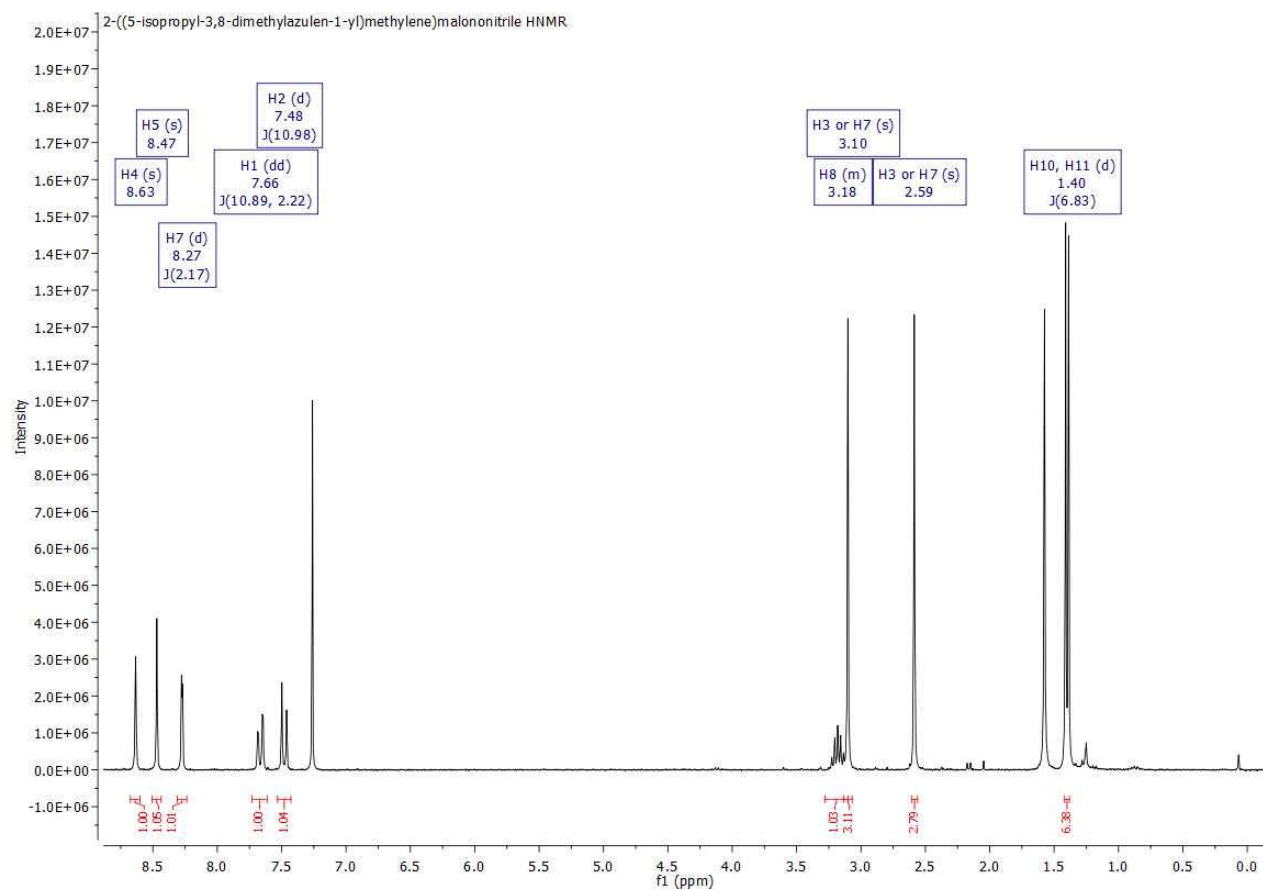
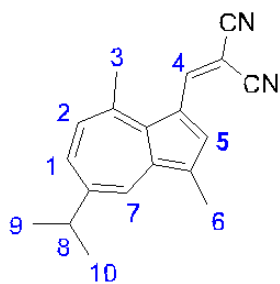


(Z)-2-Cyano-3-(5-isopropyl-3,8-dimethylazulen-1-yl) acrylic acid (15)

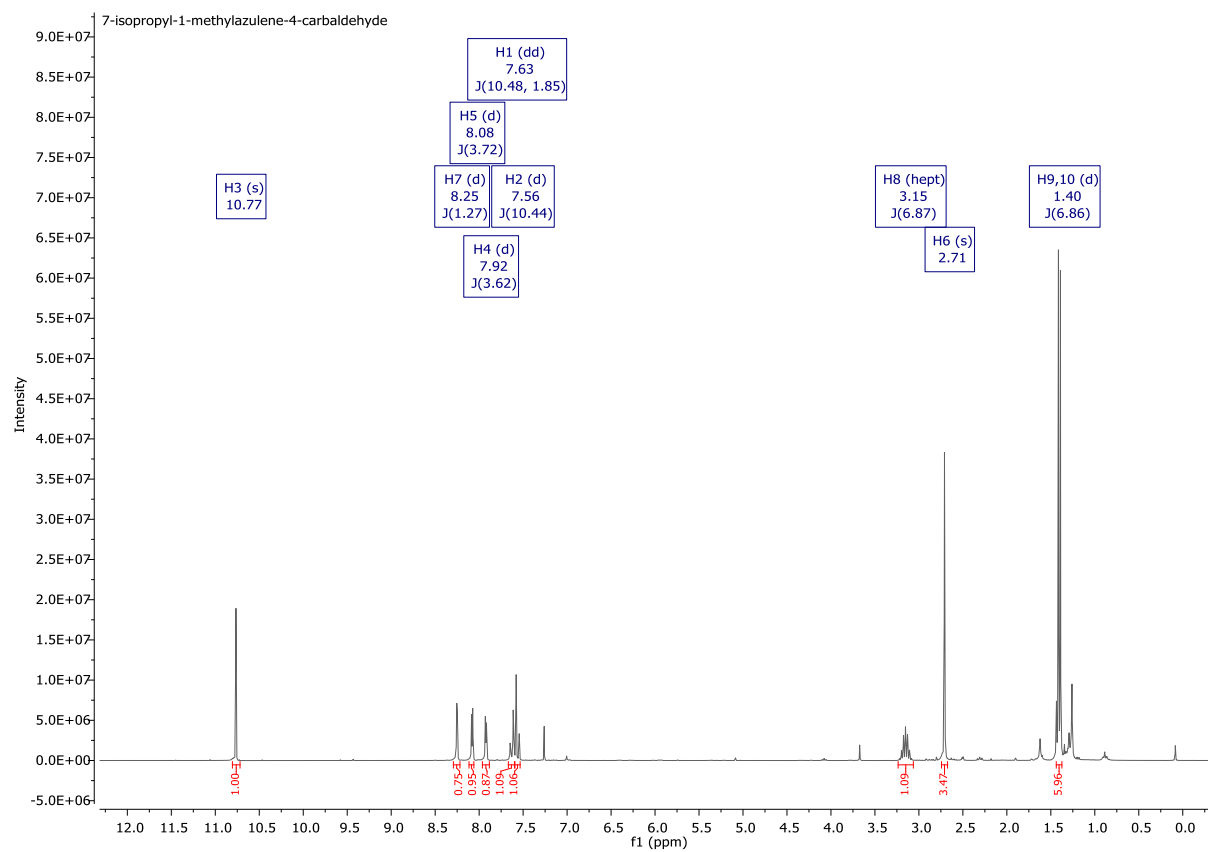
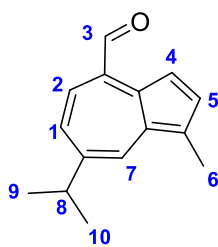




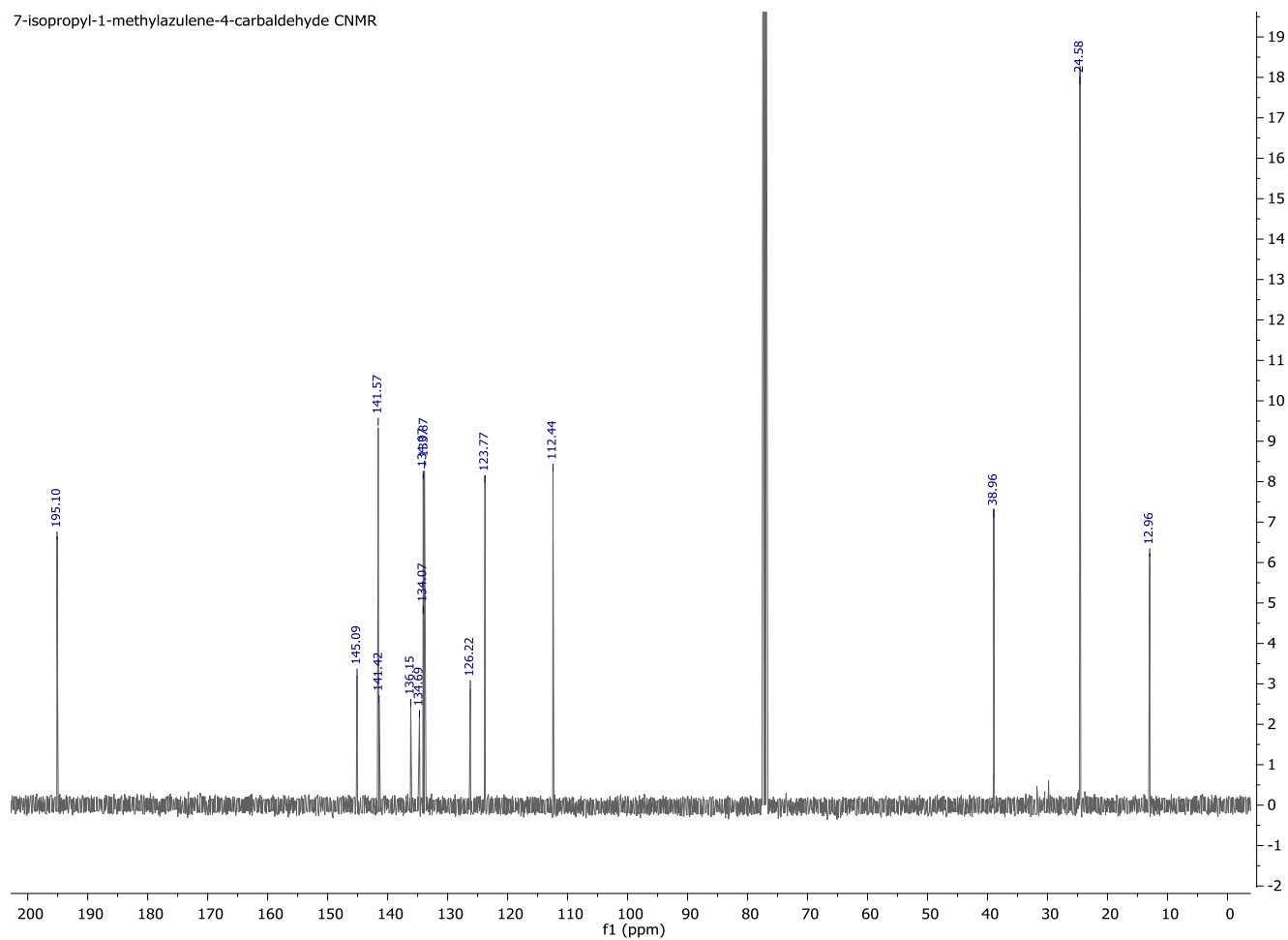
2-((5-Isopropyl-3,8-dimethylazulen-1-yl)methylene)malononitrile (17)



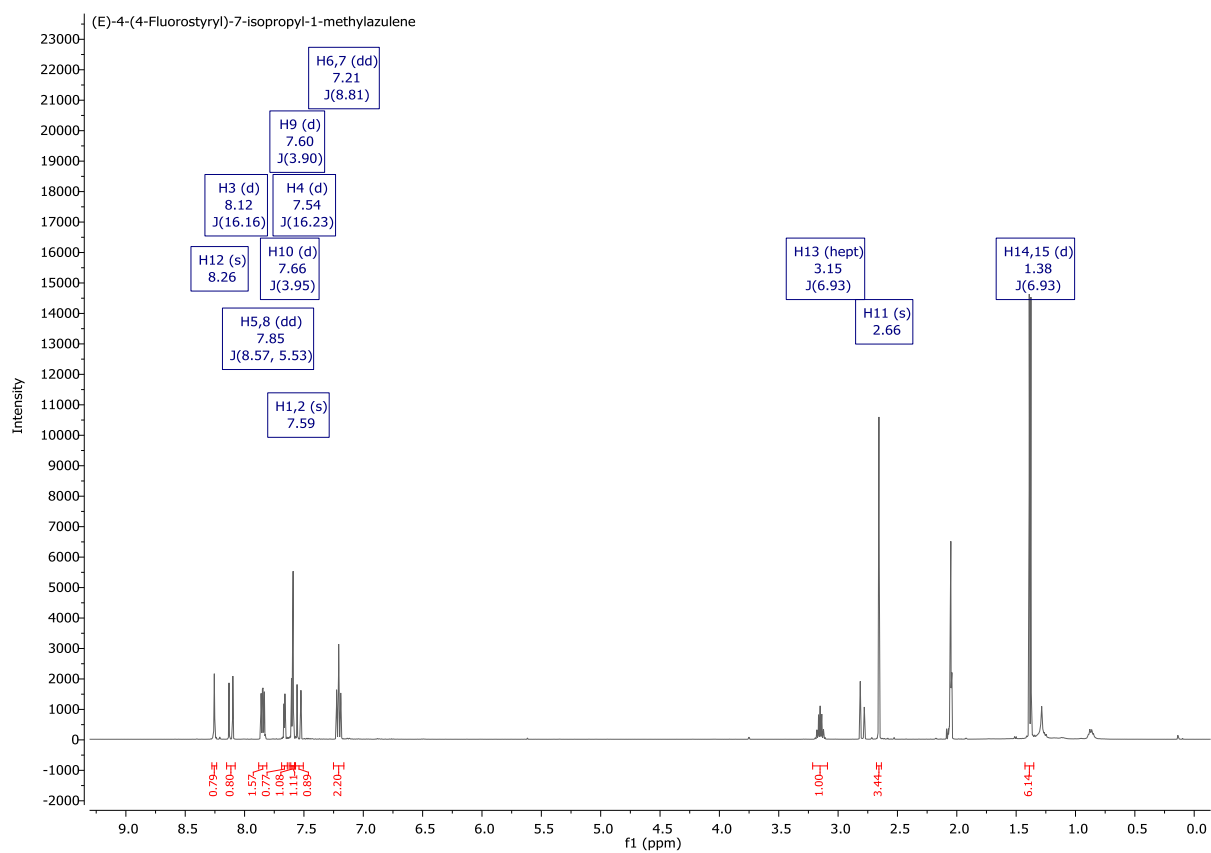
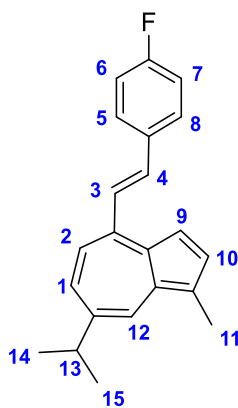
7-isopropyl-1-methylazulene-4-carbaldehyde (19)

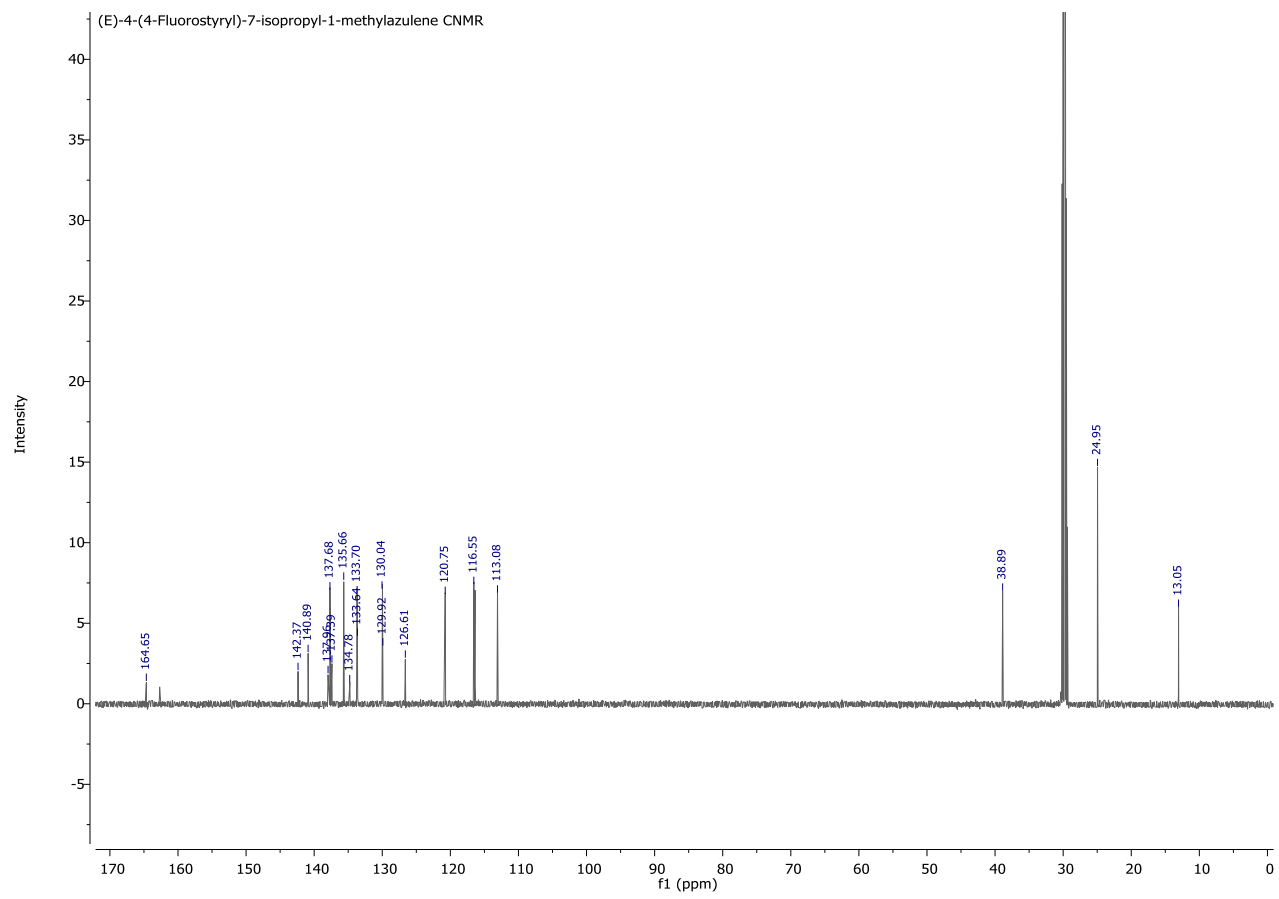


7-isopropyl-1-methylazulene-4-carbaldehyde CNMR

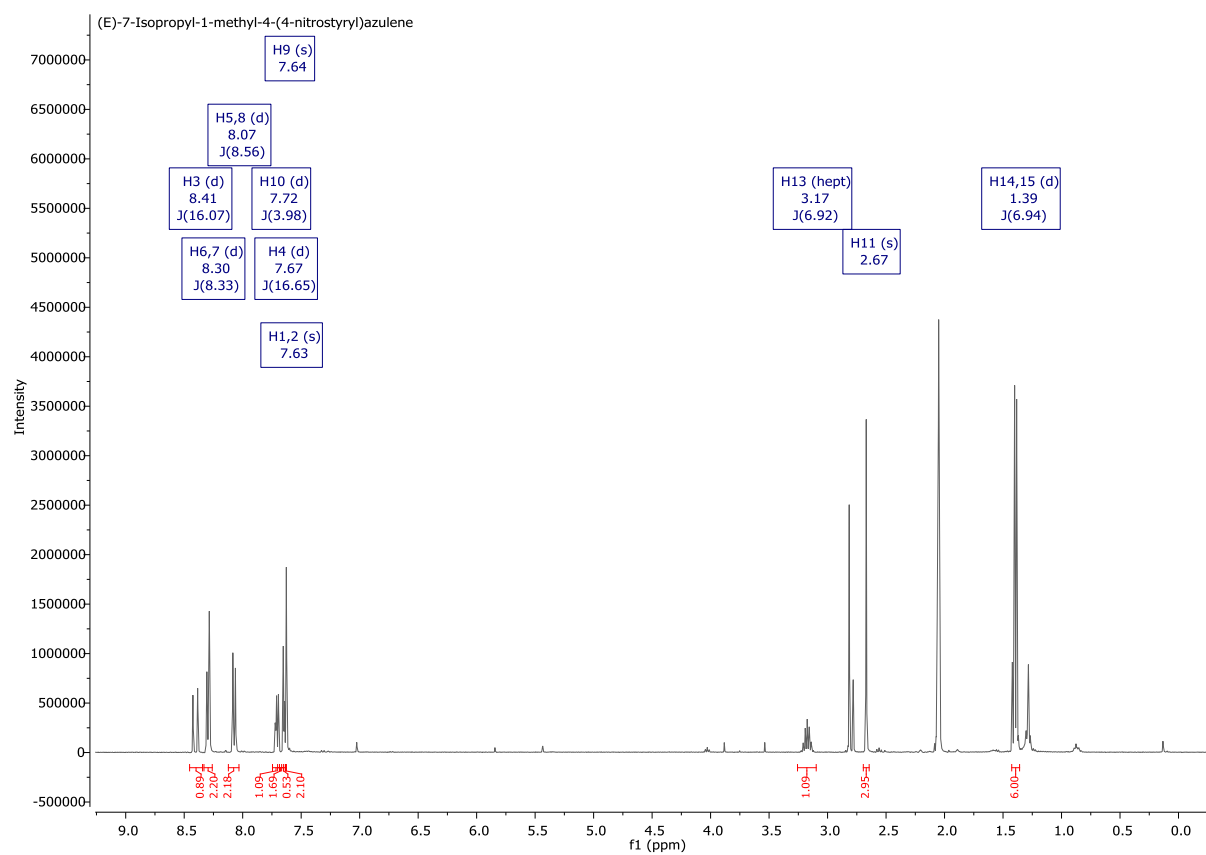
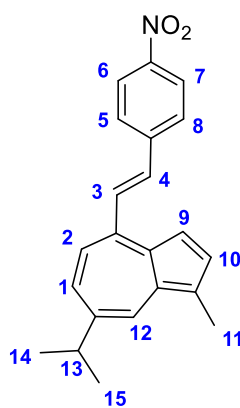


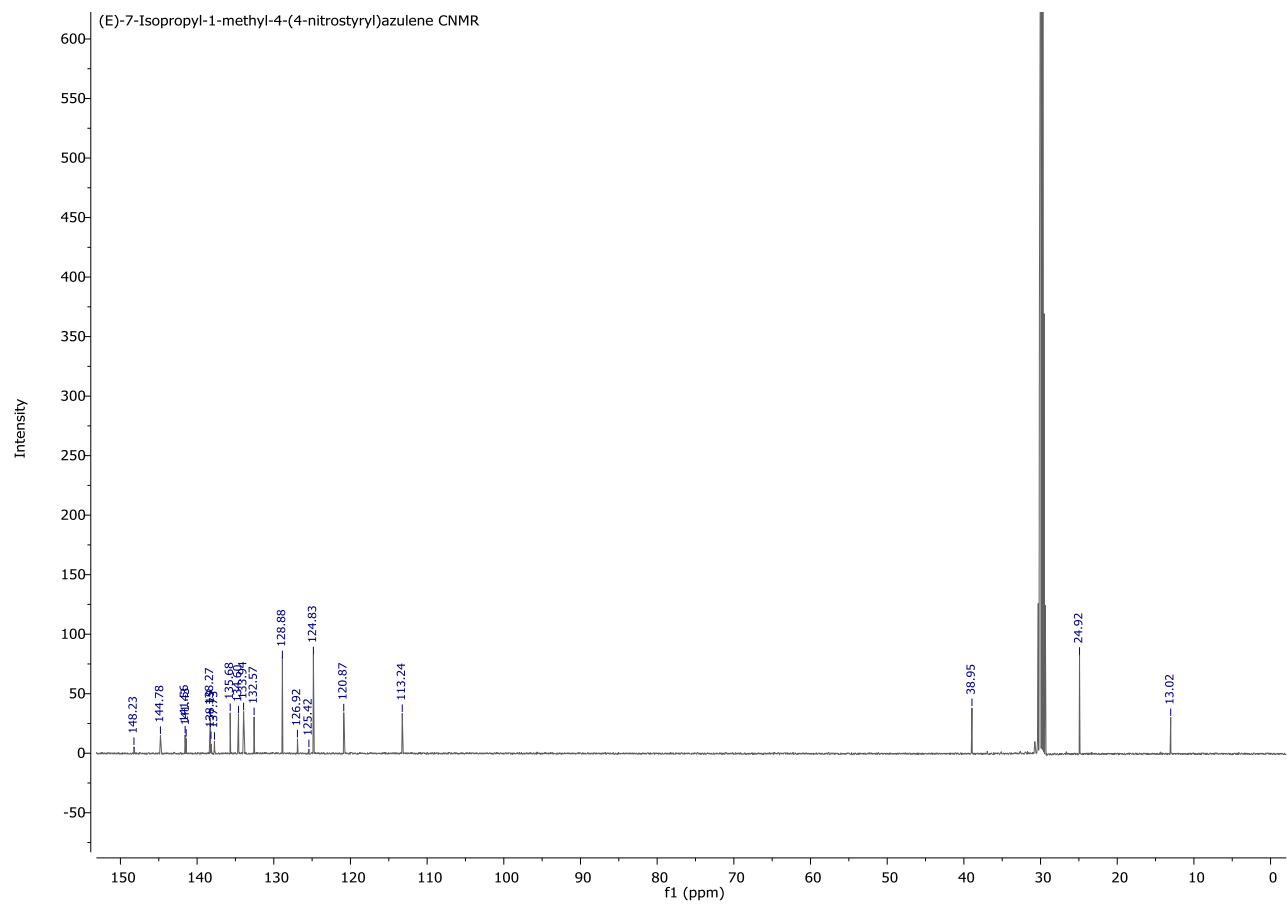
(E)-4-(4-Fluorostyryl)-7-isopropyl-1-methylazulene (25)



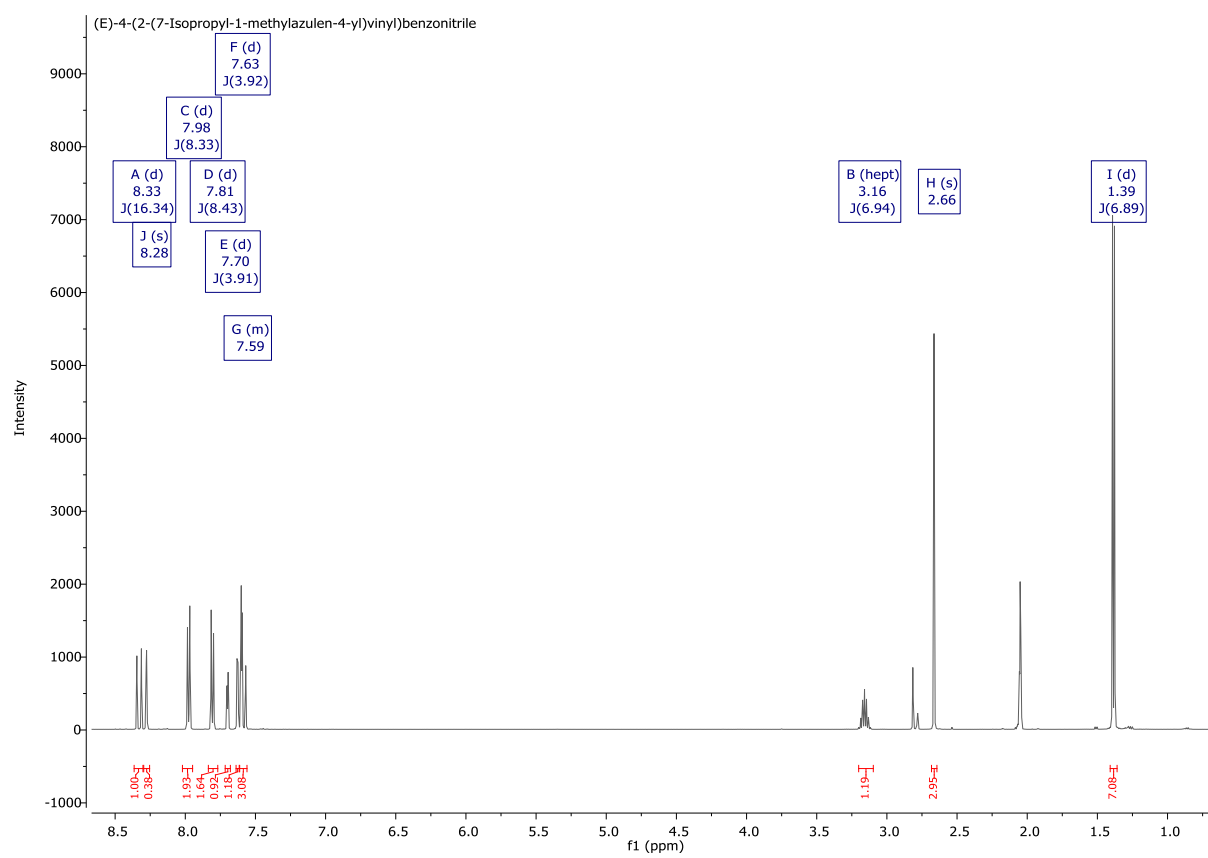
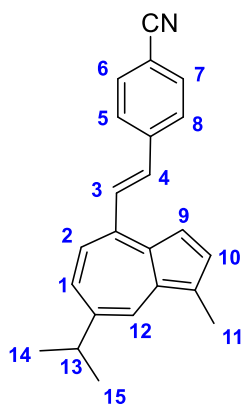


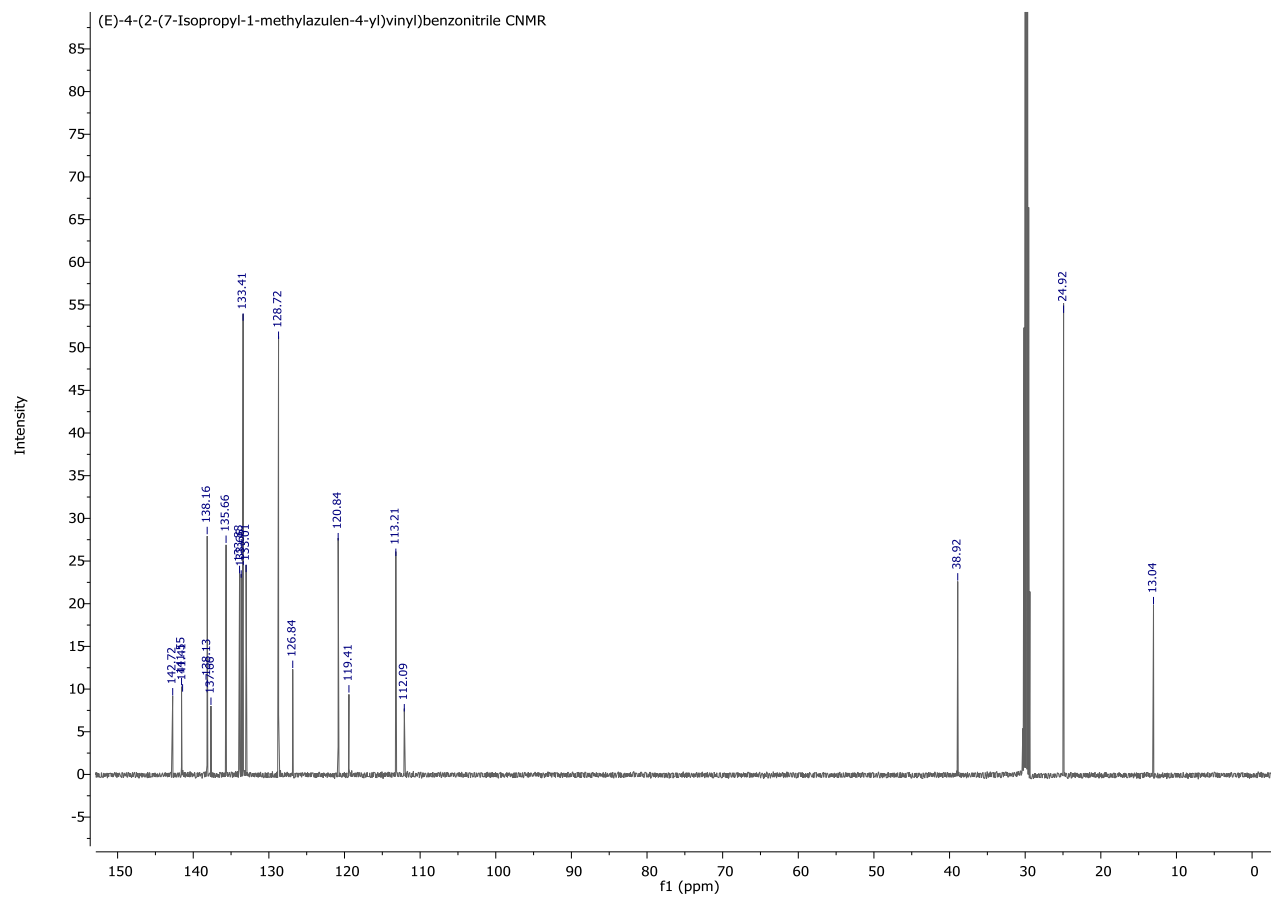
(E)-7-Isopropyl-1-methyl-4-(4-nitrostyryl)azulene (22)



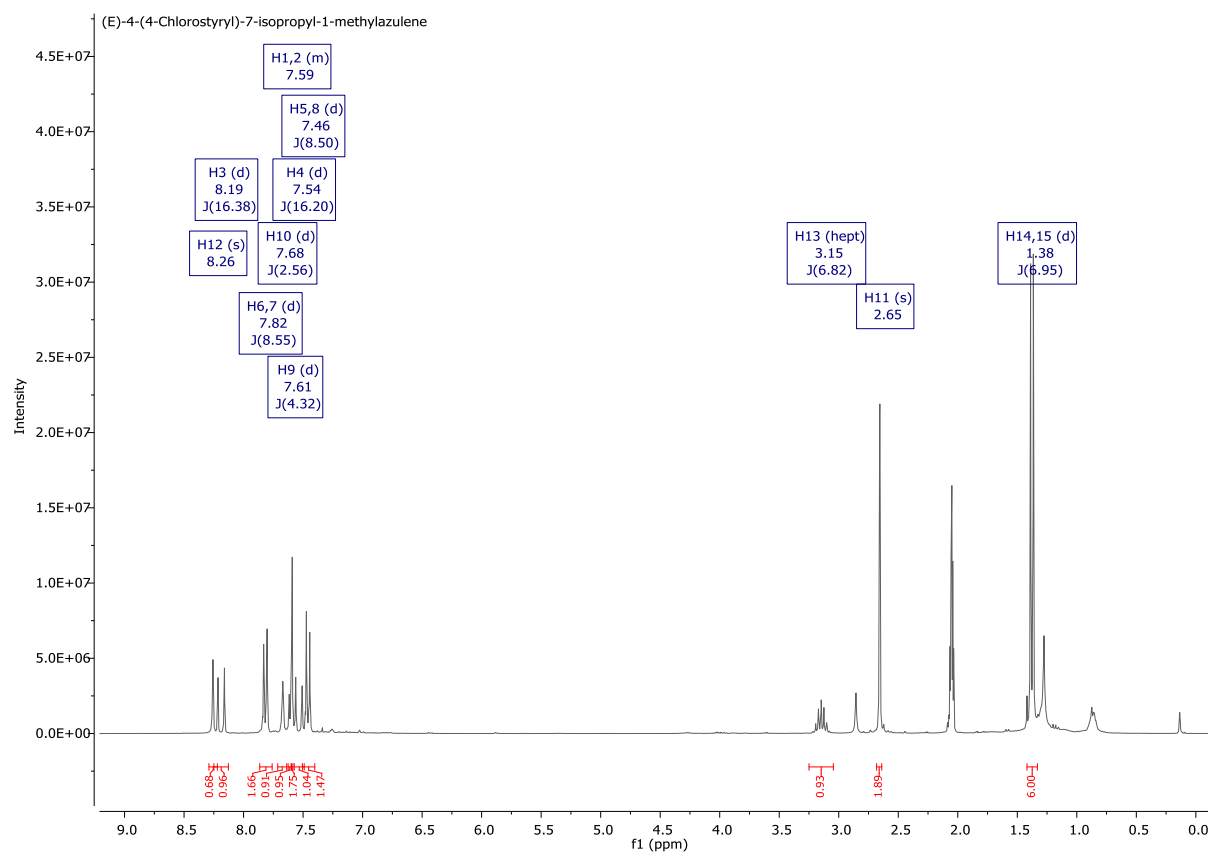
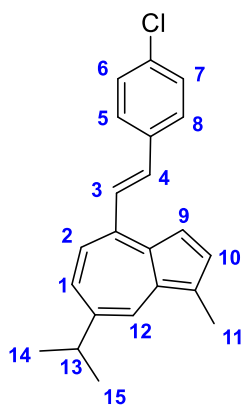


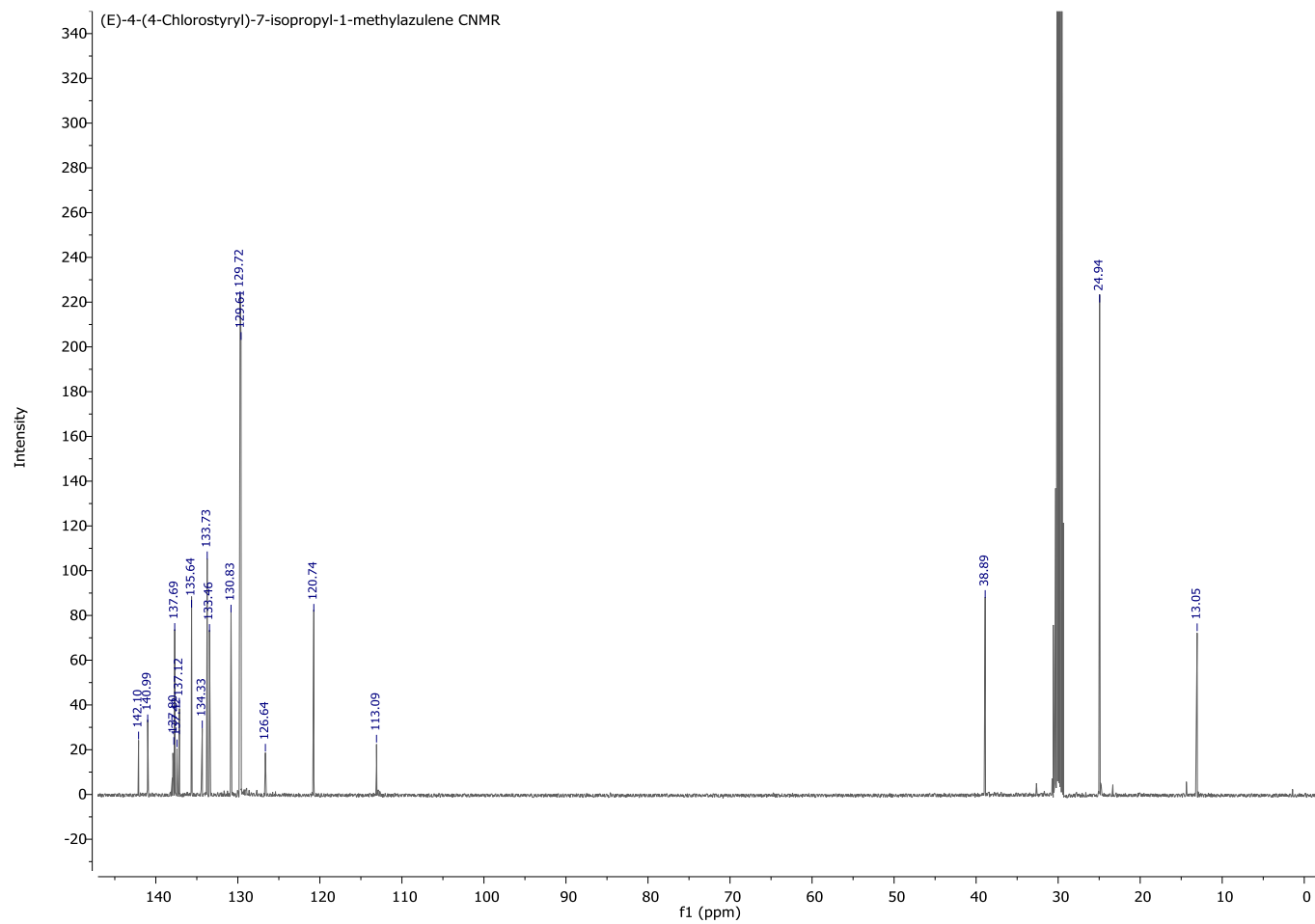
(E)-4-(2-(7-Isopropyl-1-methylazulen-4-yl)vinyl)benzonitrile (21)



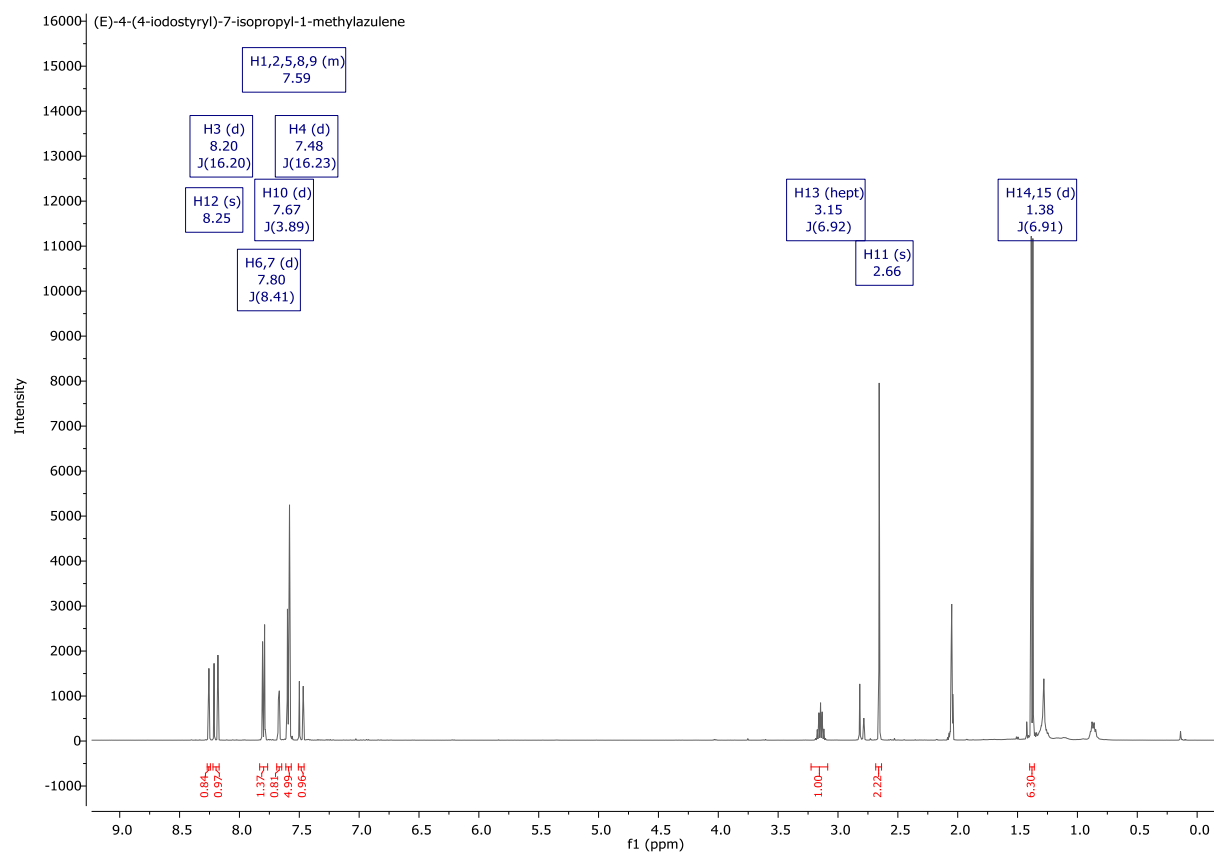
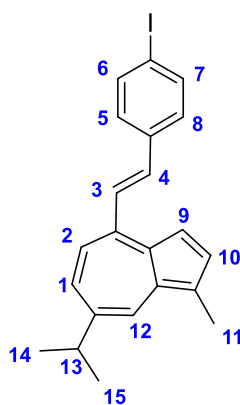


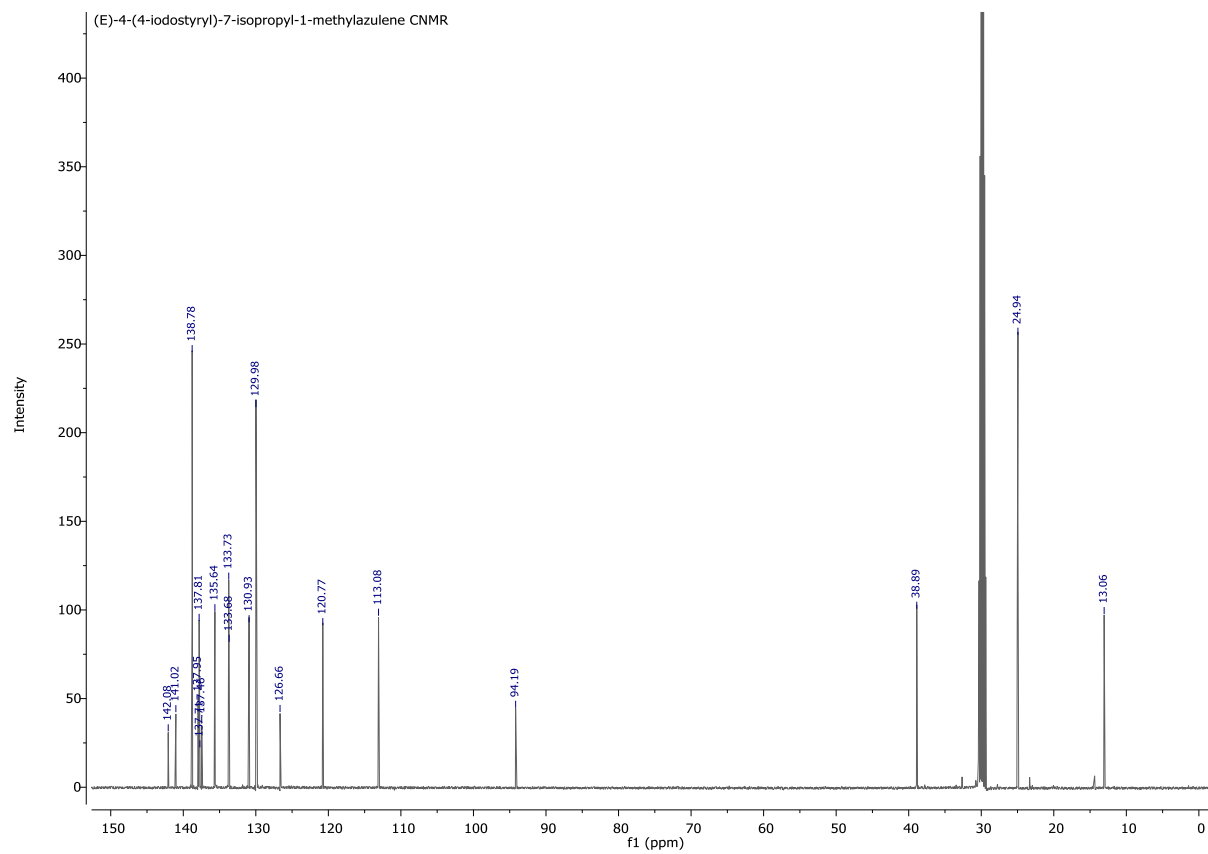
(E)-4-(4-Chlorostyryl)-7-isopropyl-1-methylazulene (24)



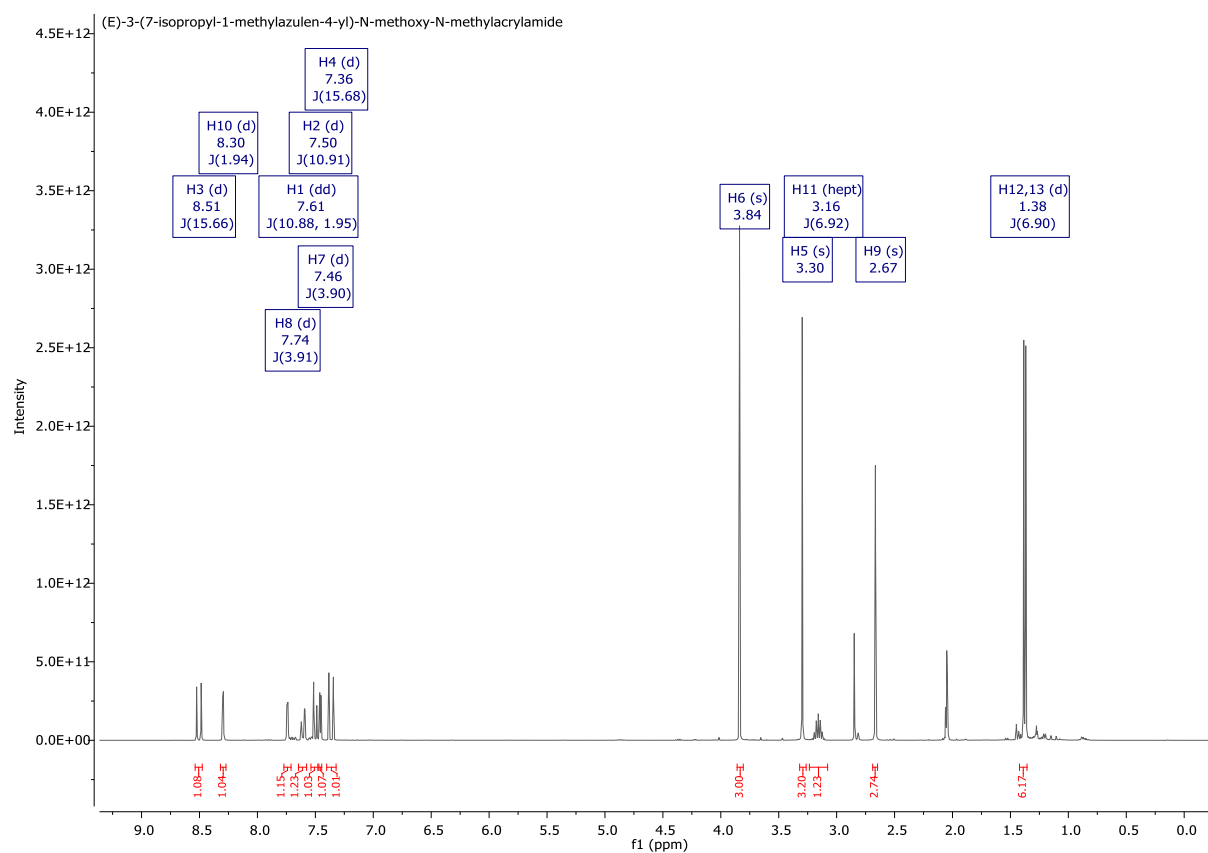
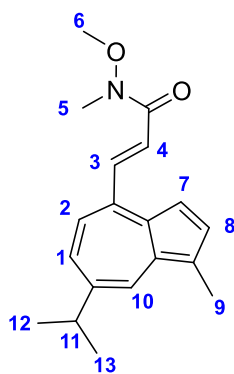


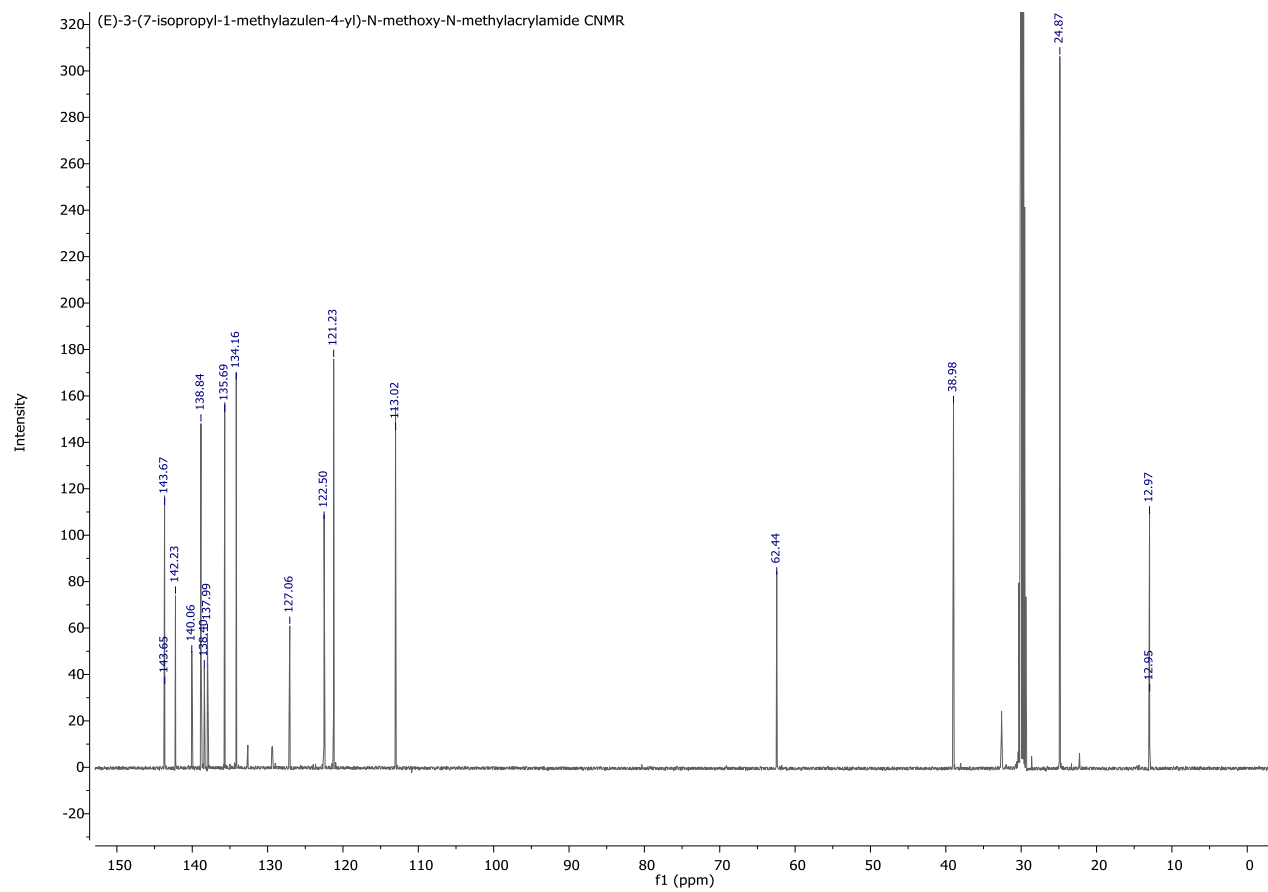
(E)-4-(4-iodostyryl)-7-isopropyl-1-methylazulene (20)



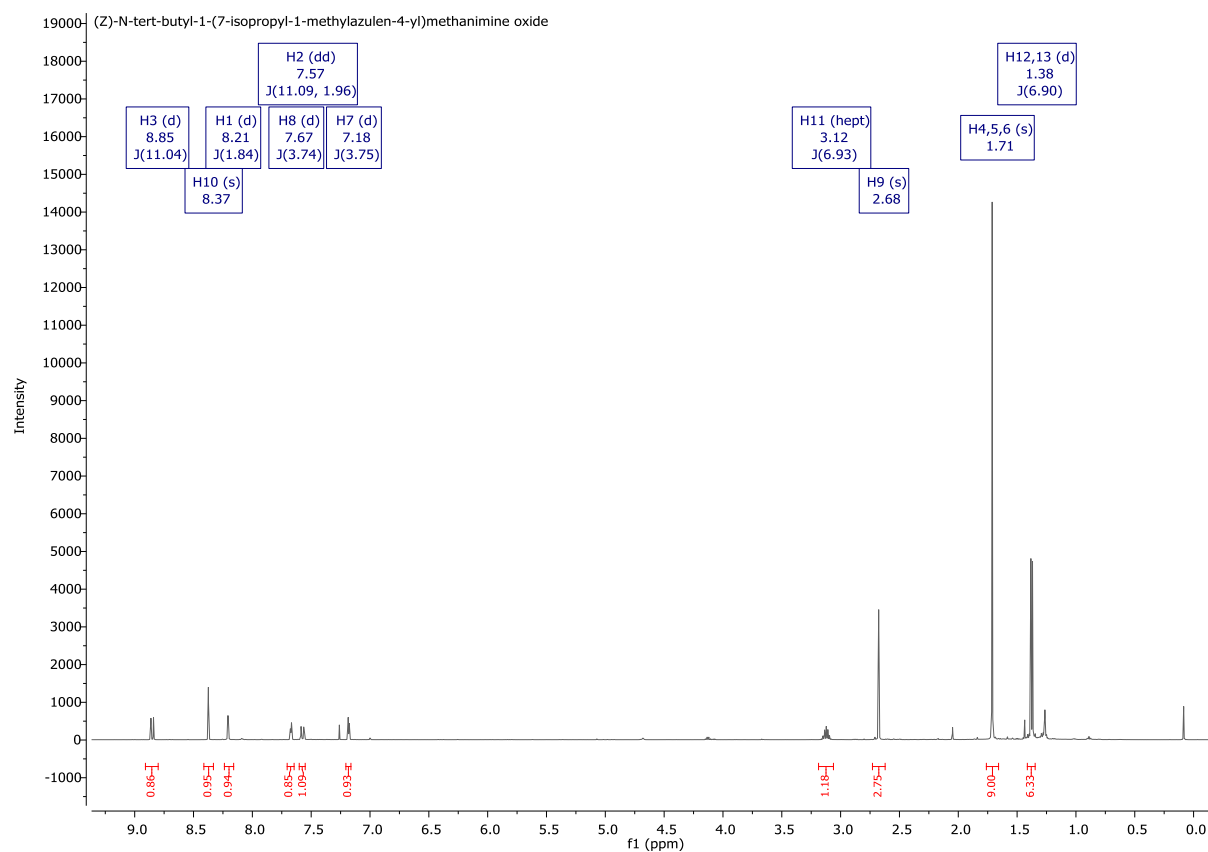
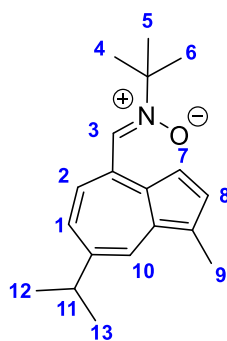


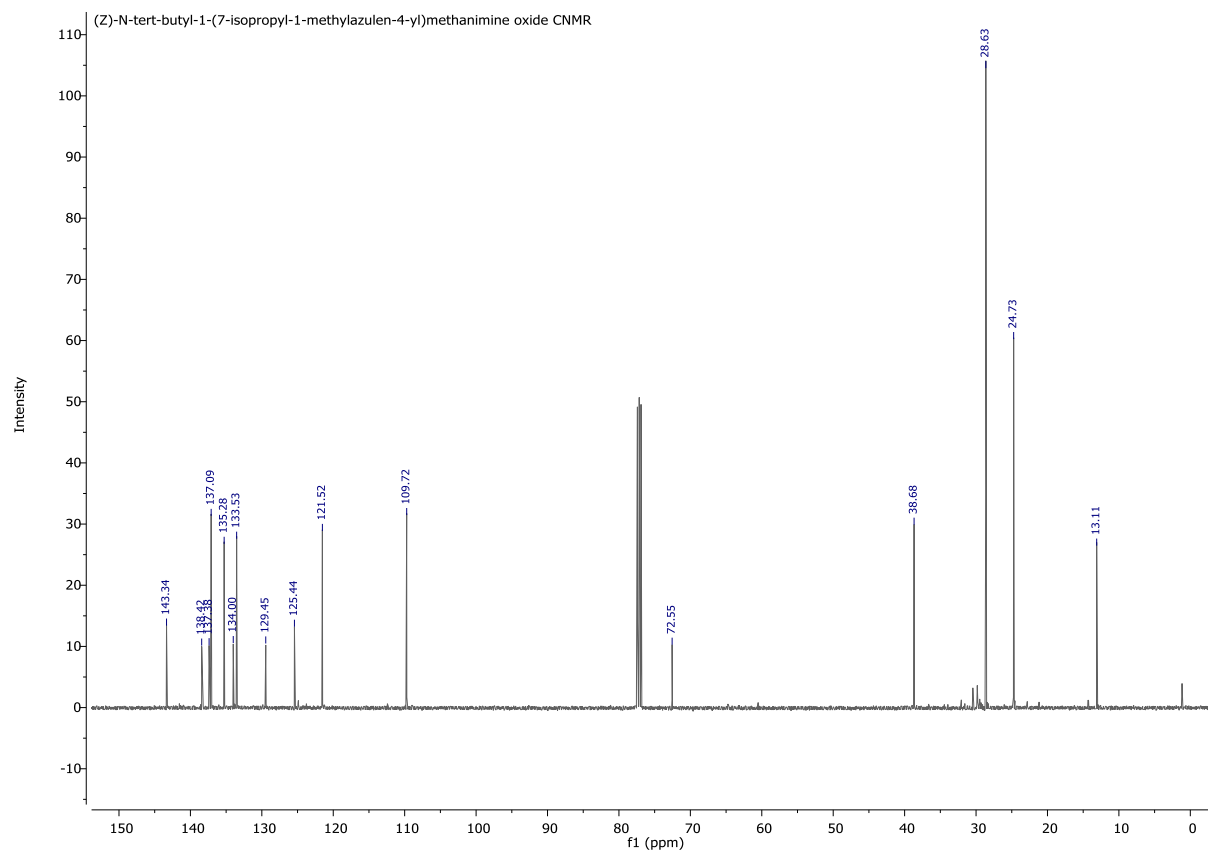
(E)-3-(7-isopropyl-1-methylazulen-4-yl)-N-methoxy-N-methylacrylamide (28)



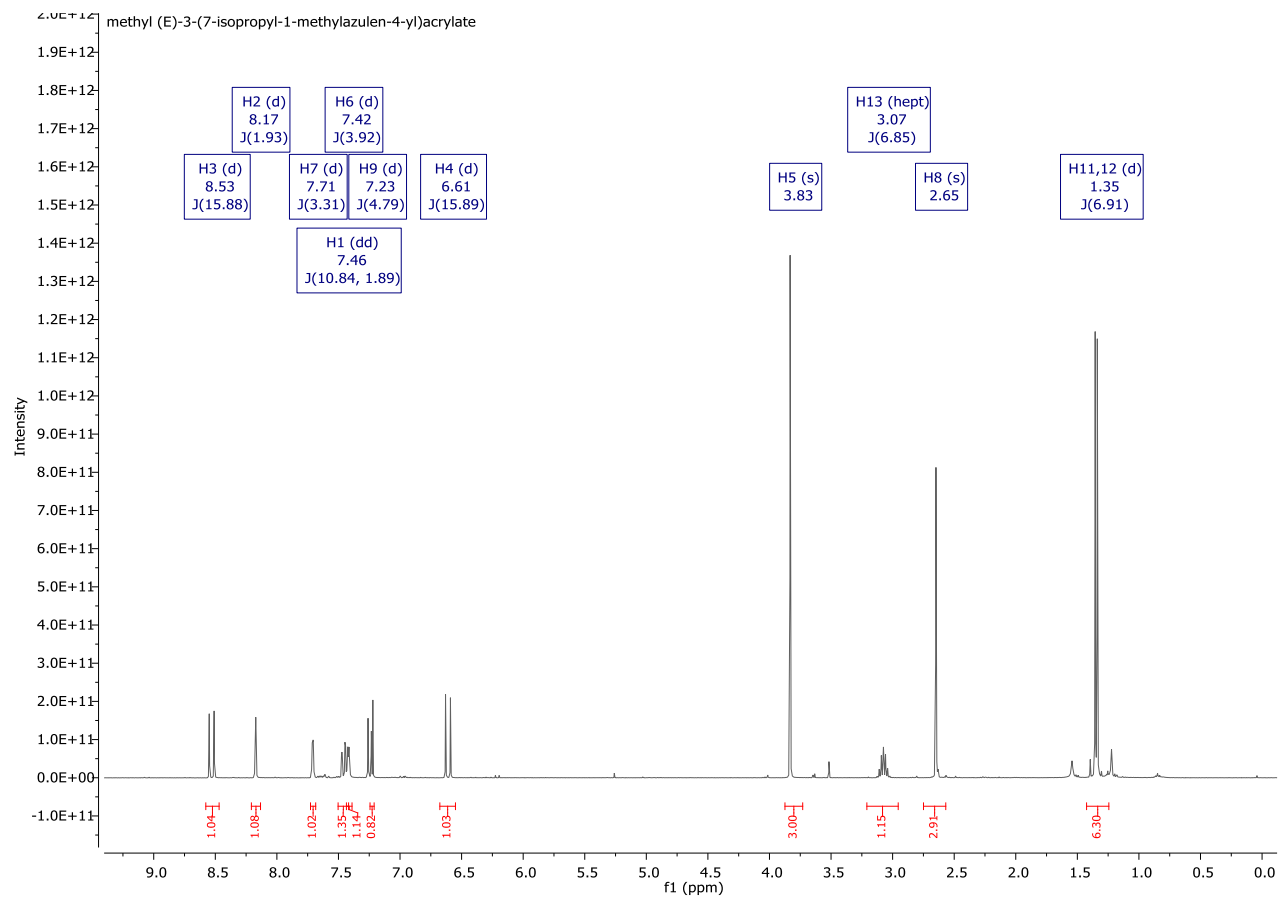
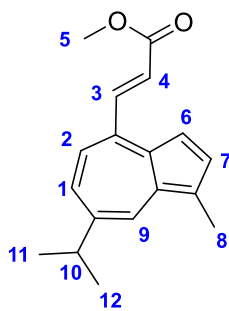


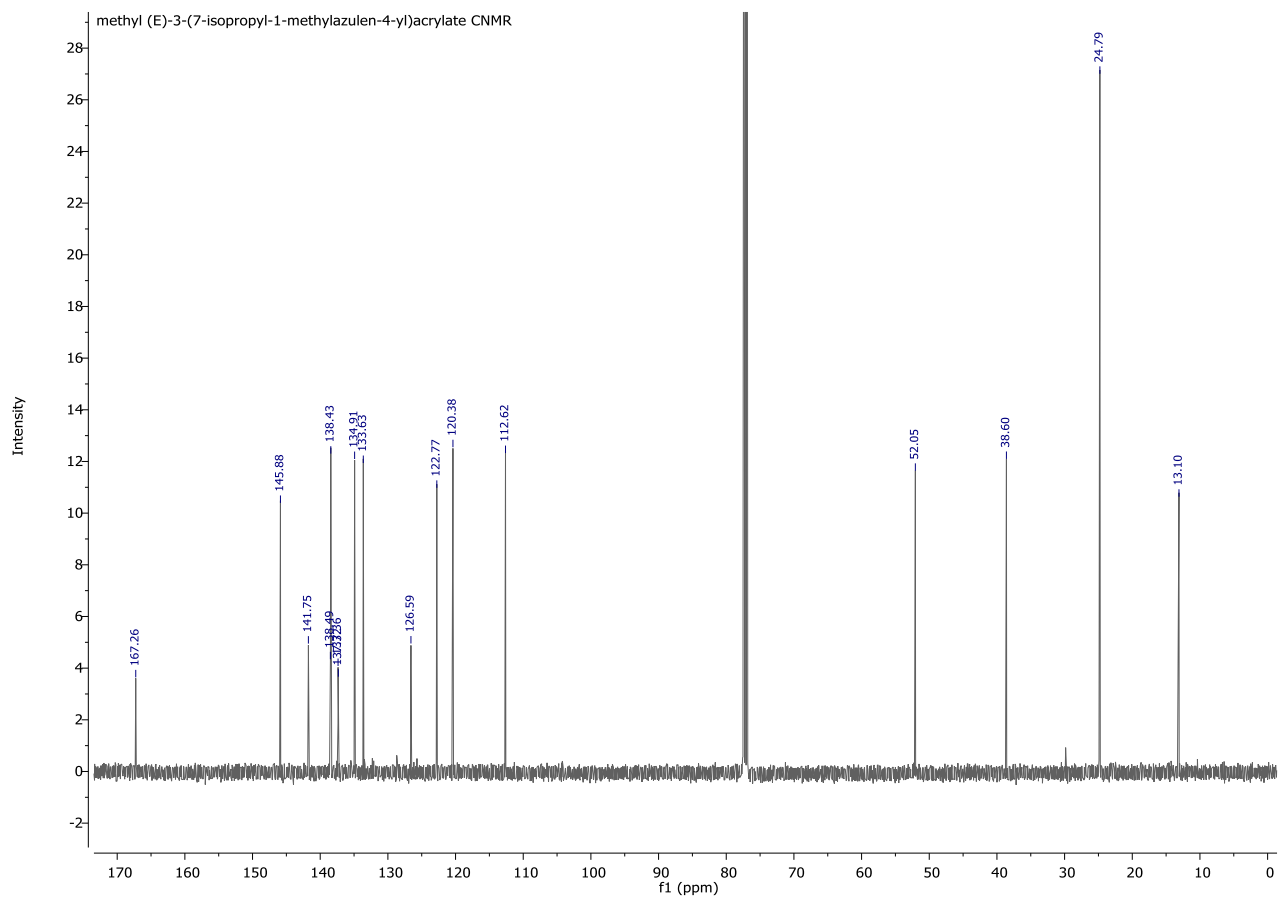
(Z)-N-tert-butyl-1-(7-isopropyl-1-methylazulen-4-yl)methanimine oxide (29)



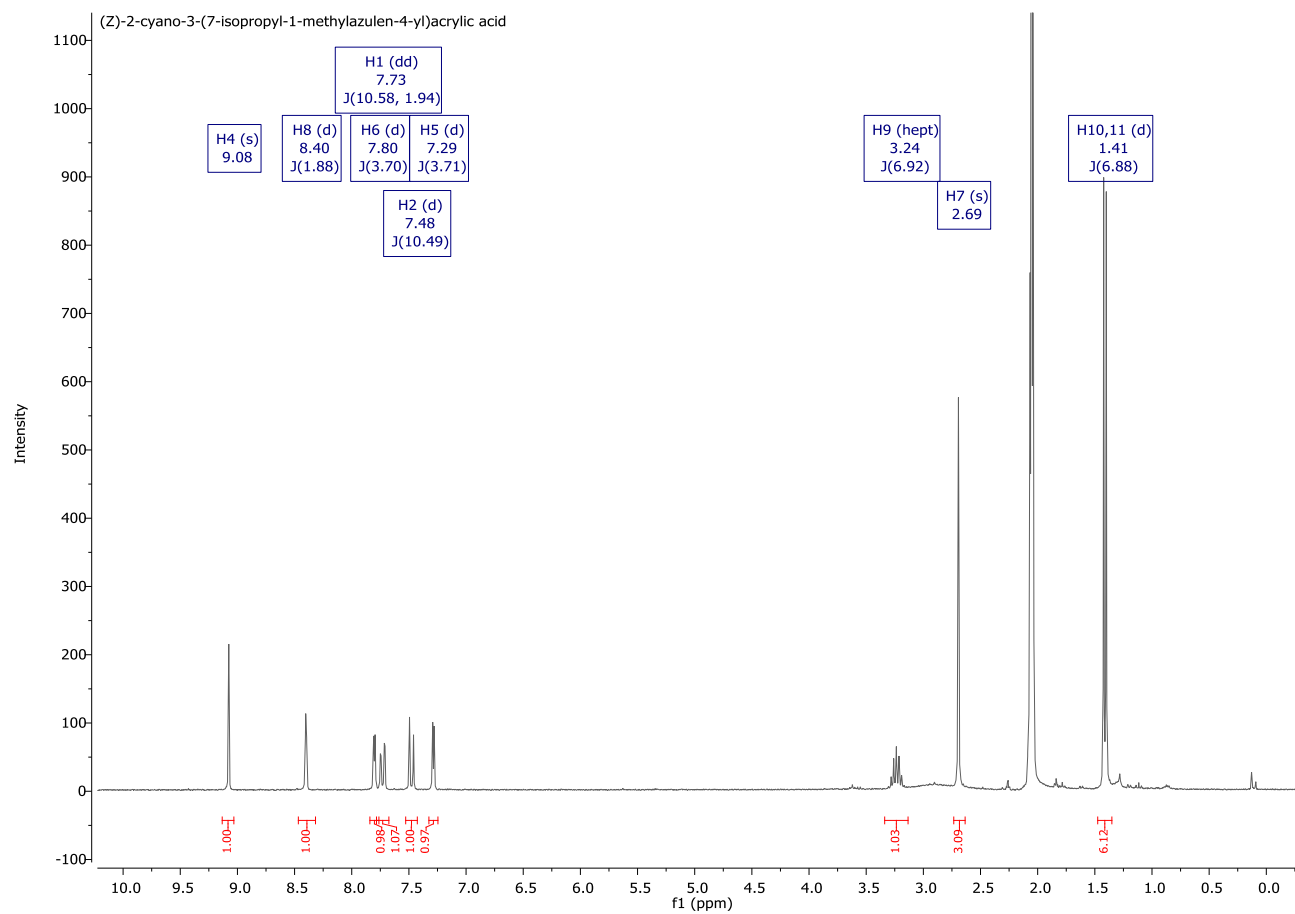
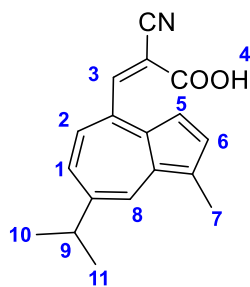


Methyl (E)-3-(7-isopropyl-1-methylazulen-4-yl)acrylate (26)

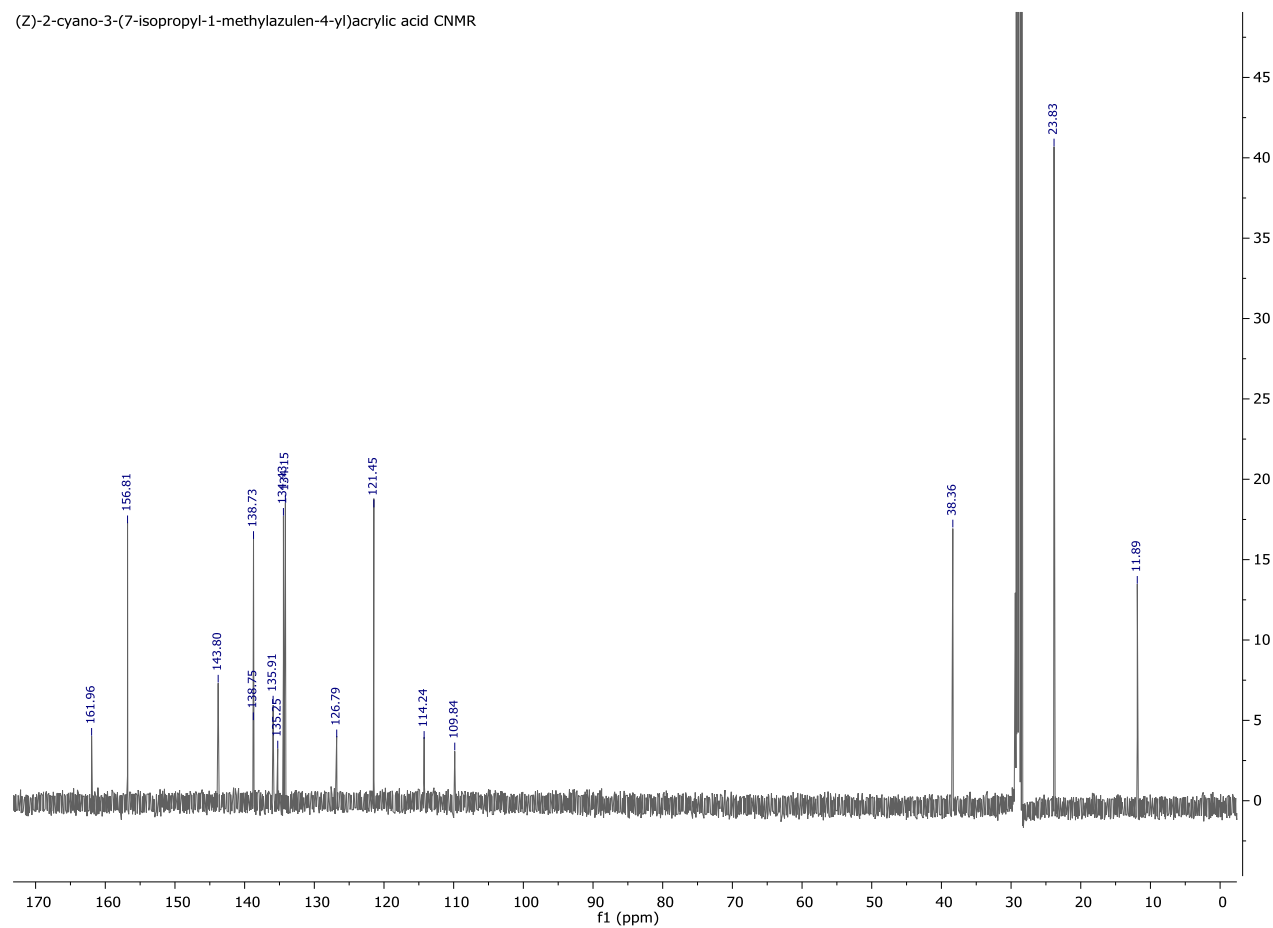




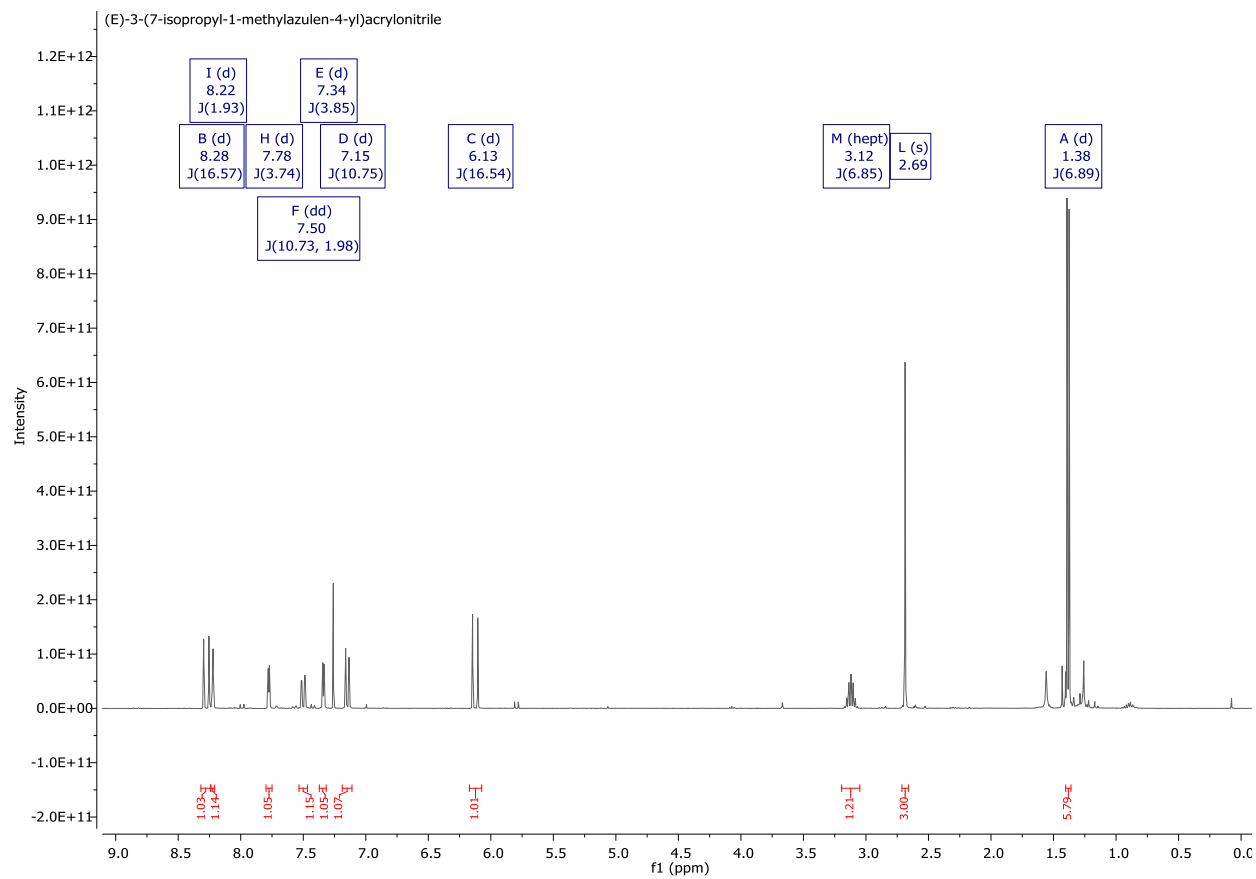
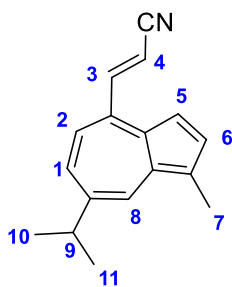
(Z)-2-cyano-3-(7-isopropyl-1-methylazulen-4-yl)acrylic acid (30)

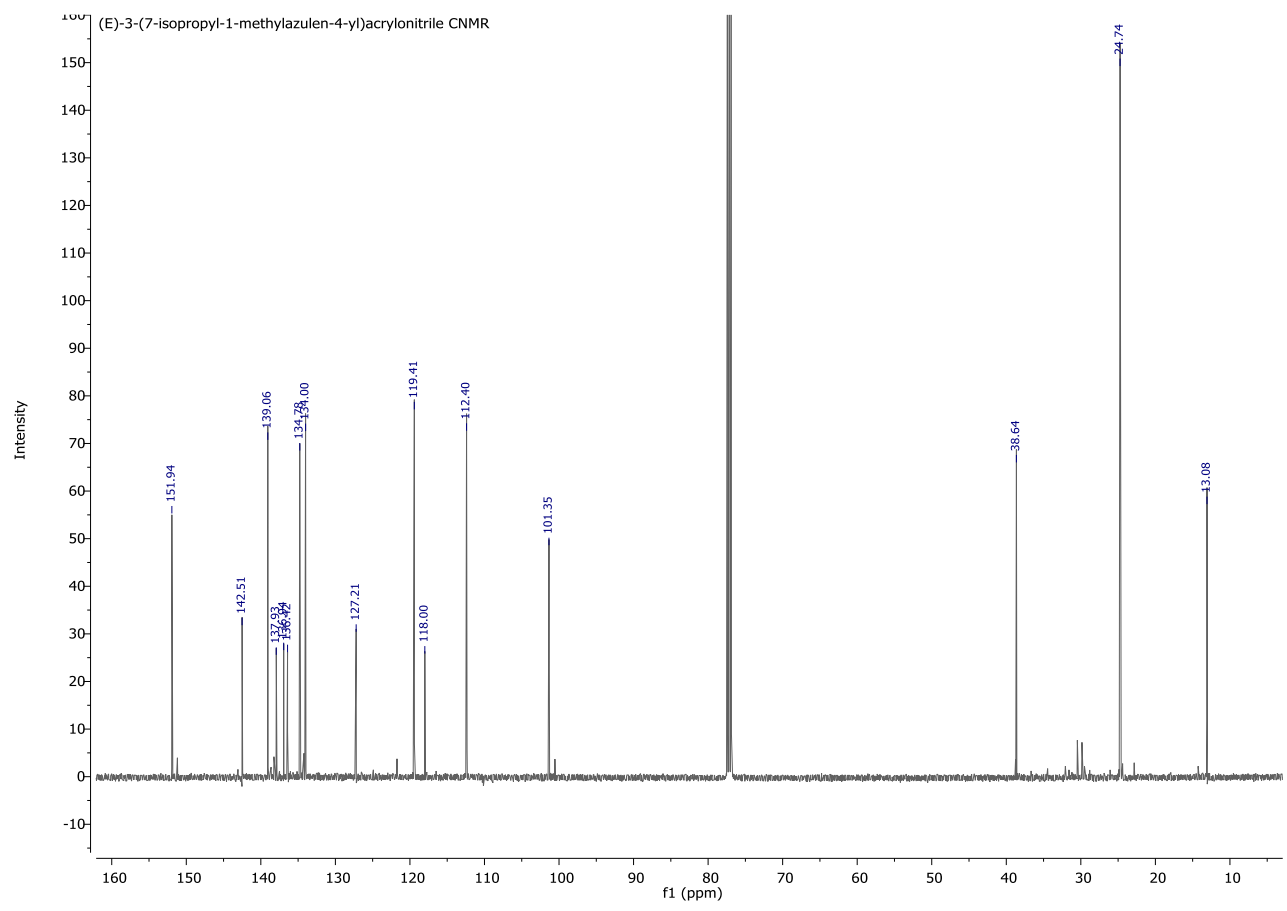


(Z)-2-cyano-3-(7-isopropyl-1-methylazulen-4-yl)acrylic acid CNMR

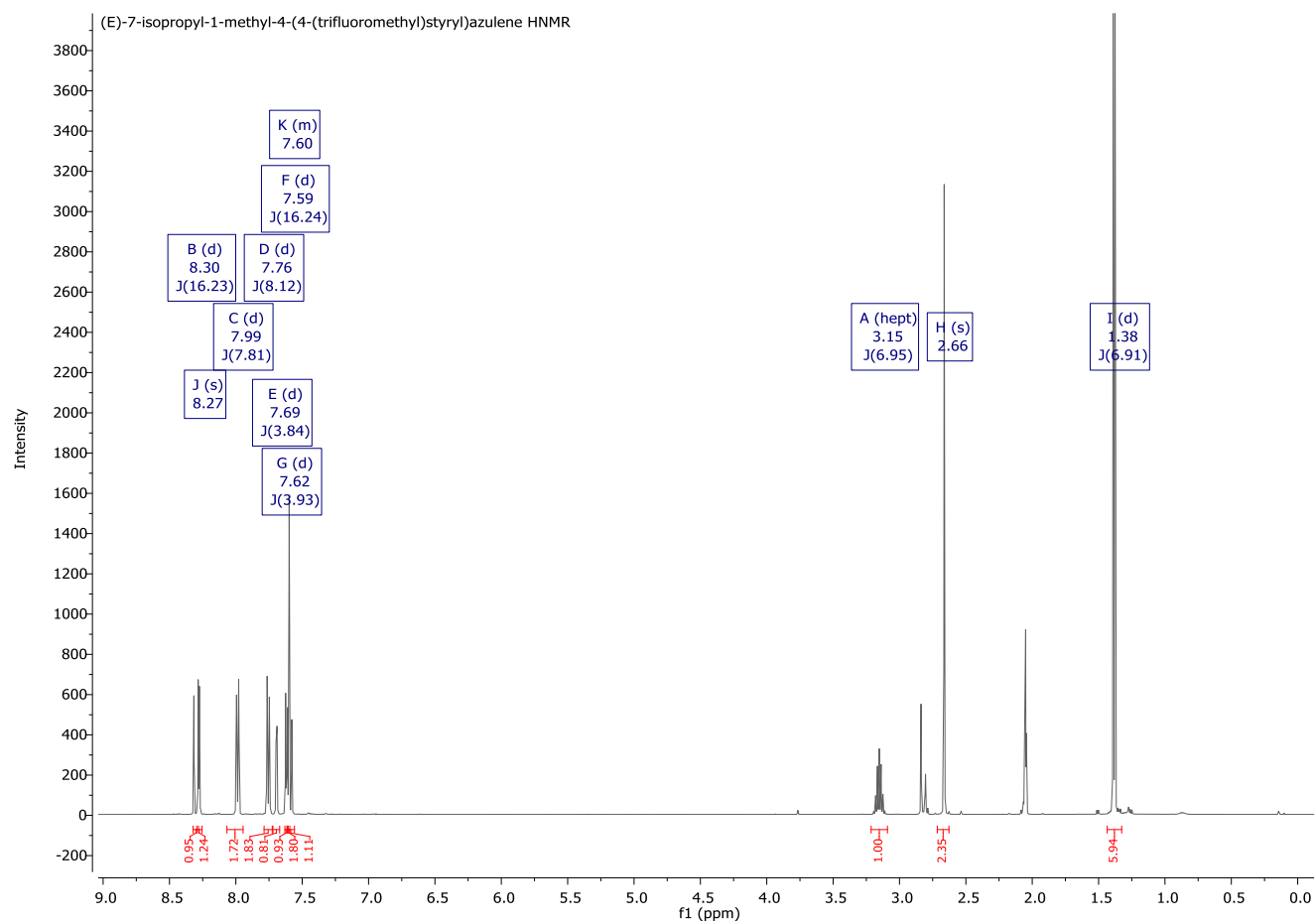
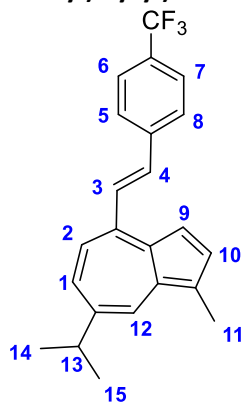


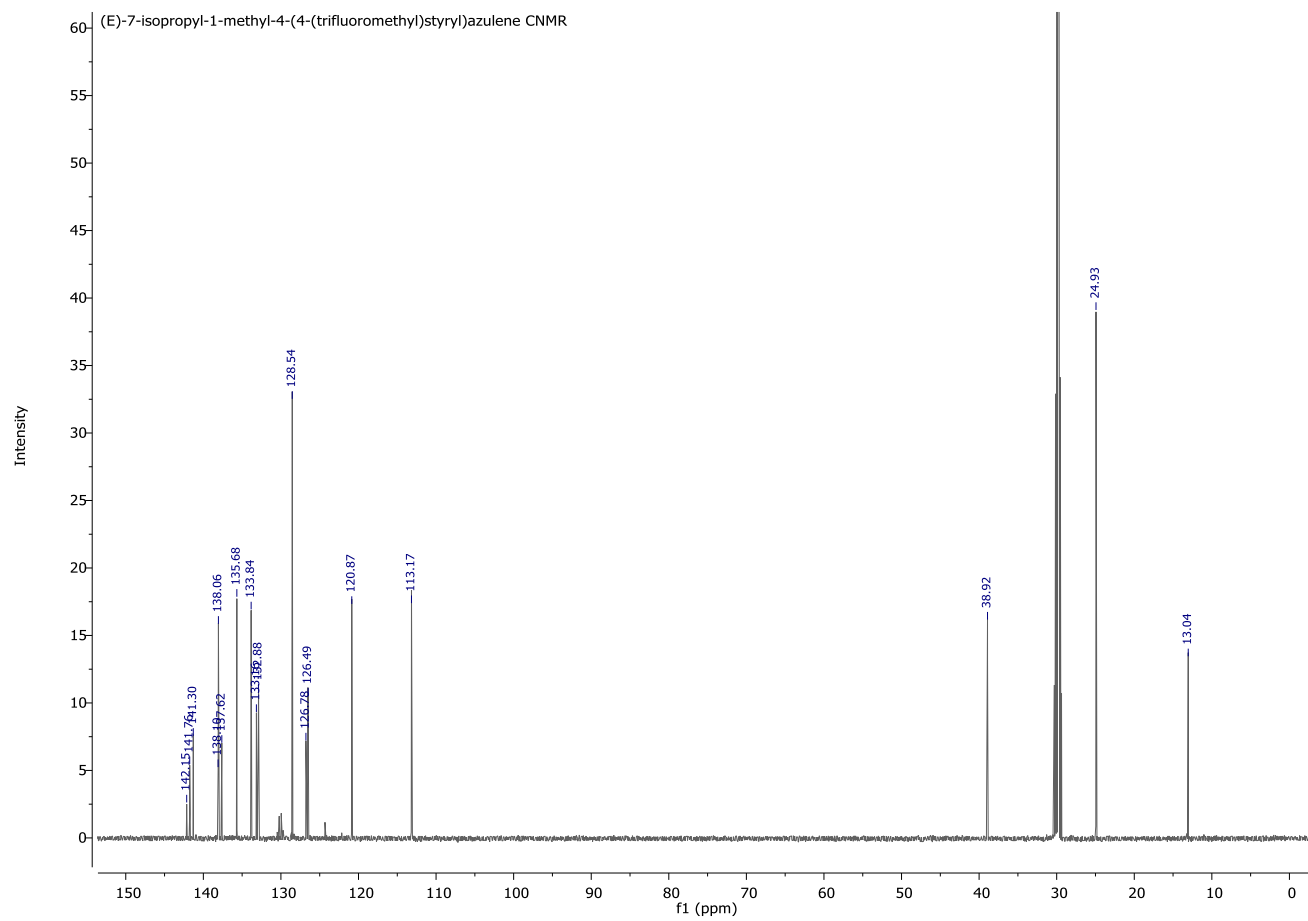
(E)-3-(7-isopropyl-1-methylazulen-4-yl)acrylonitrile (27)



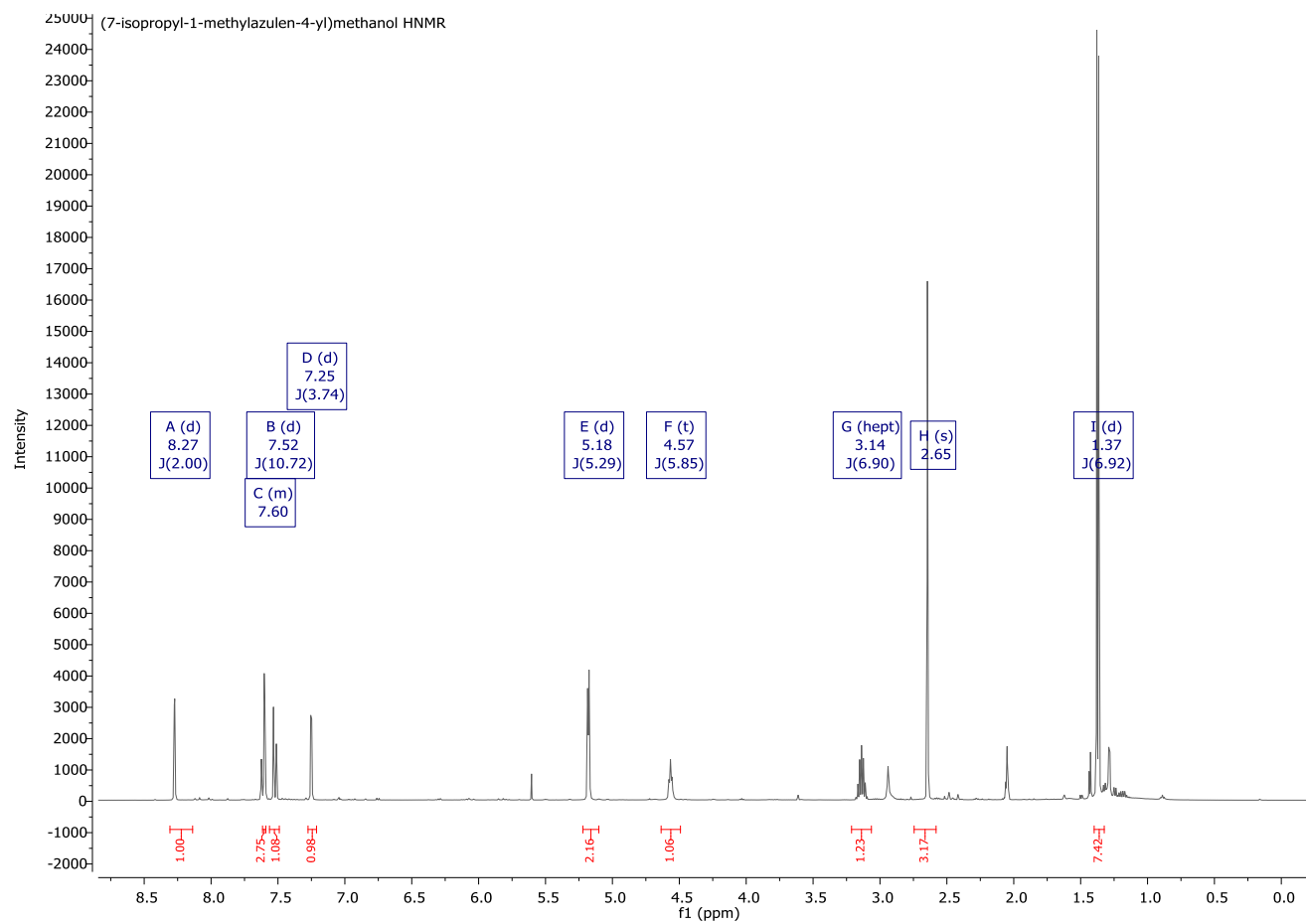
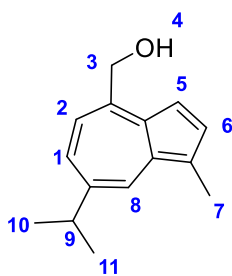


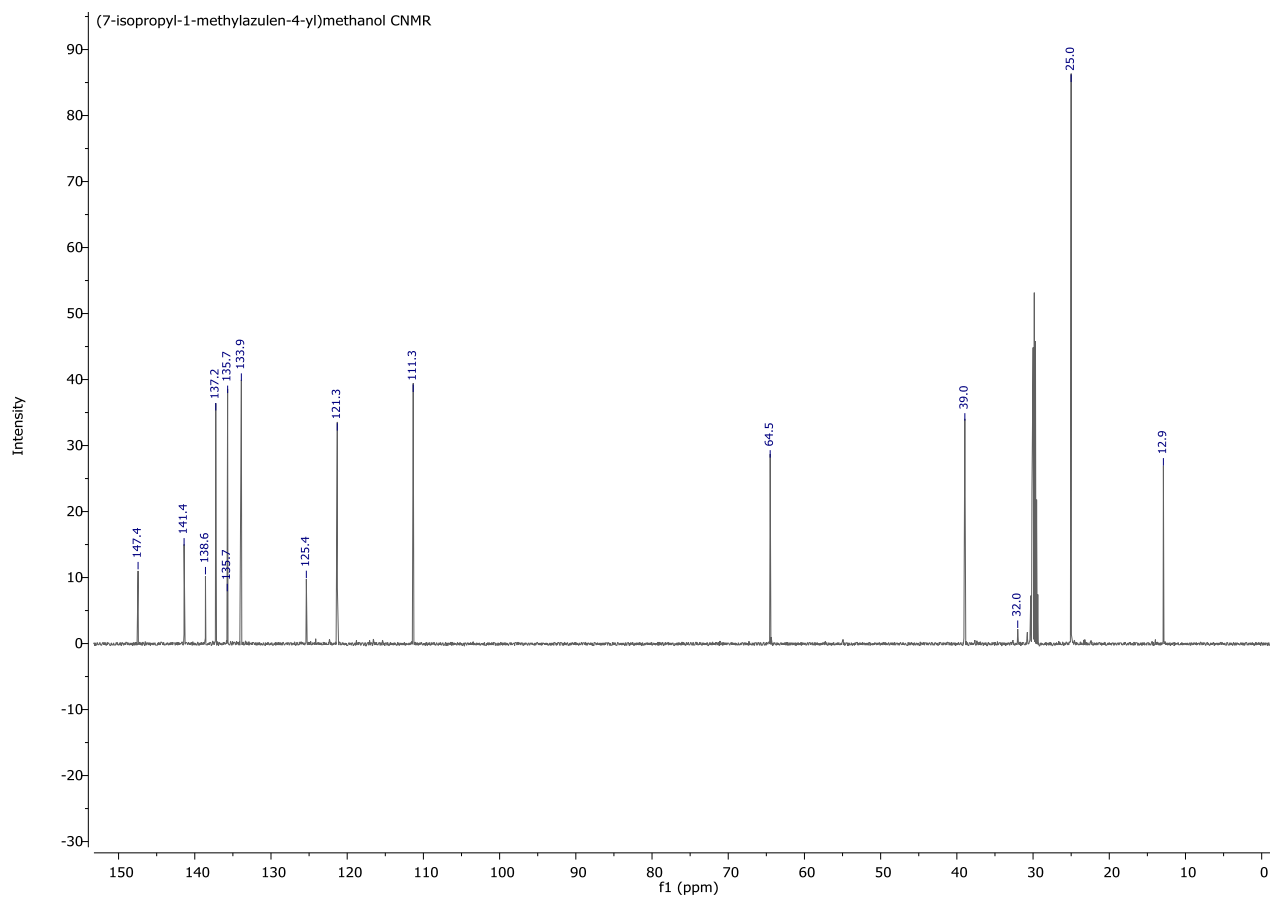
(E)-7-isopropyl-1-methyl-4-(4-(trifluoromethyl)styryl)azulene (23)





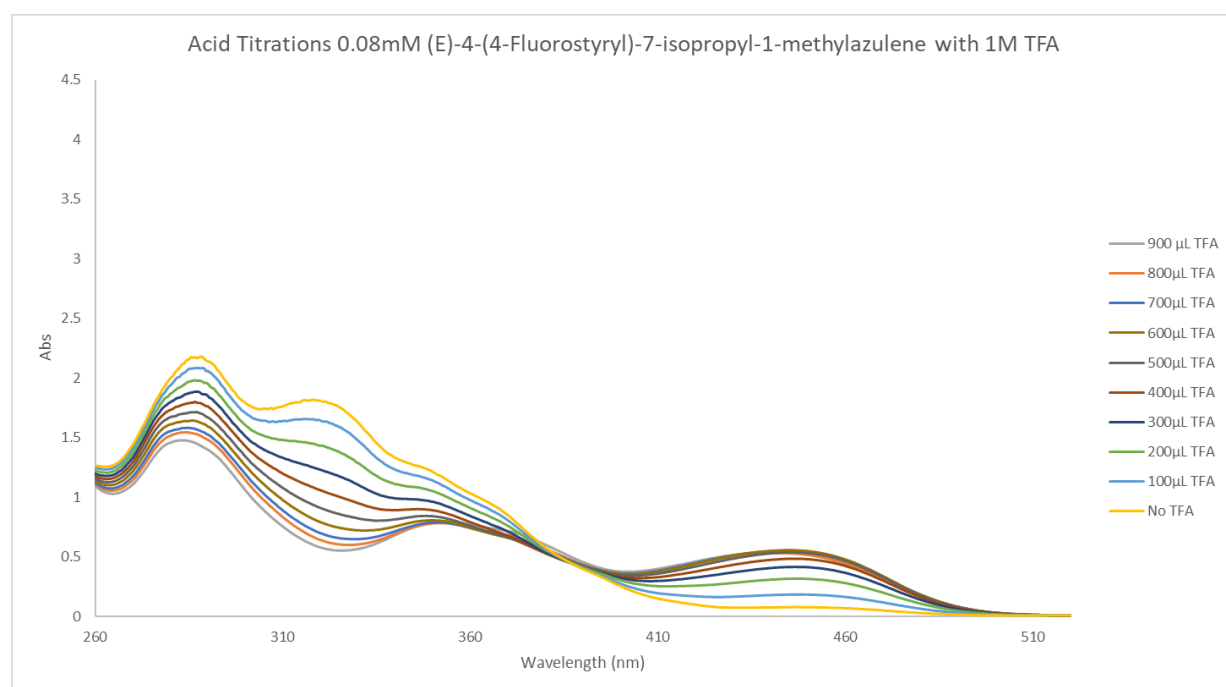
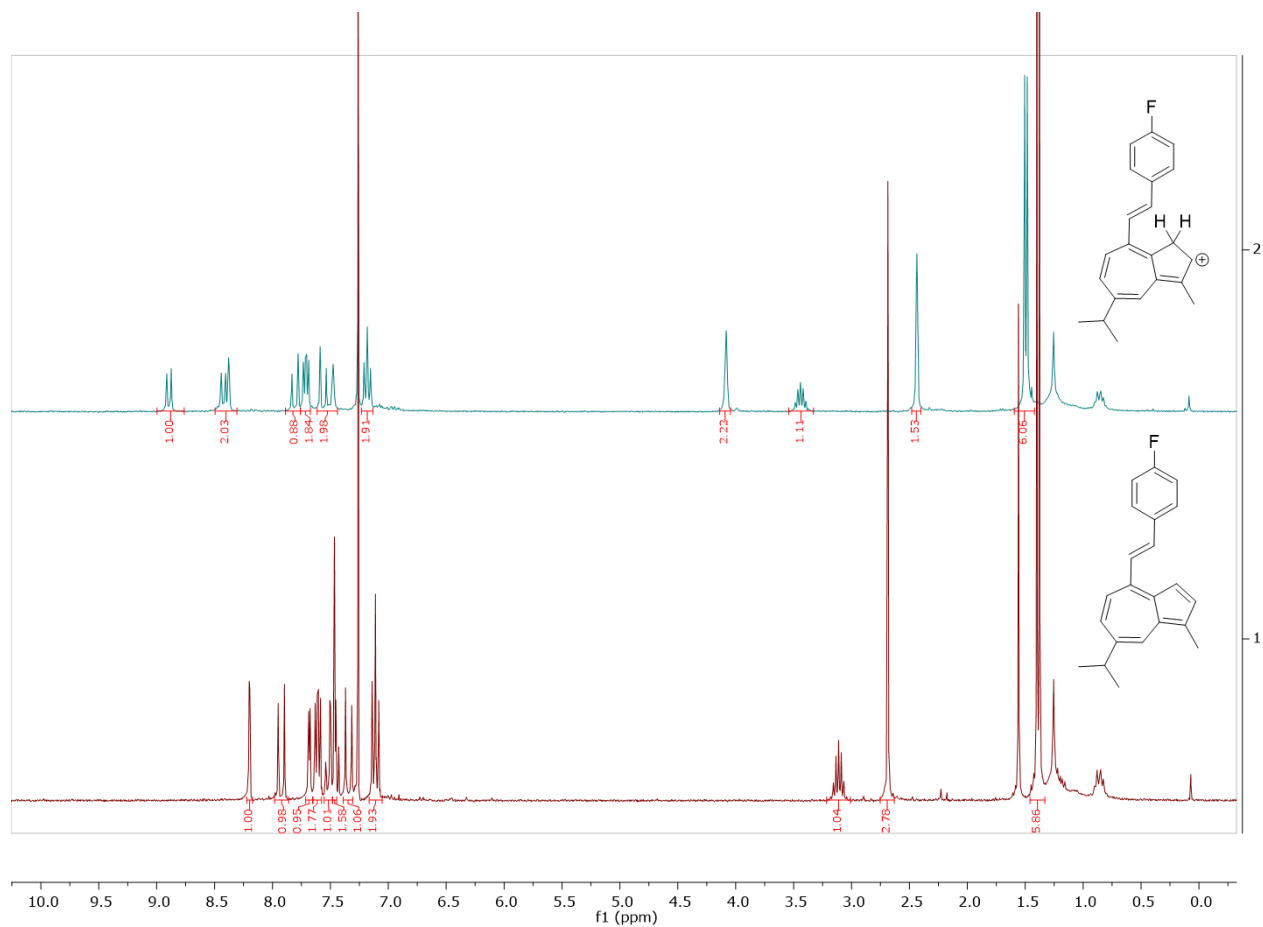
(7-isopropyl-1-methylazulen-4-yl)methanol (33)



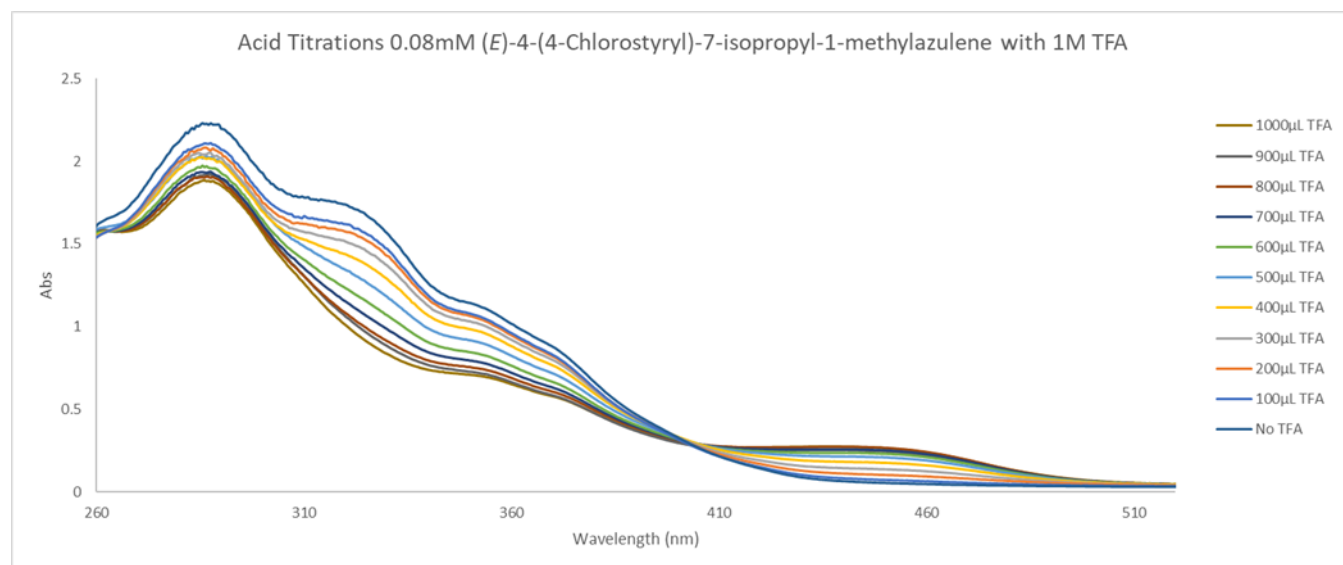
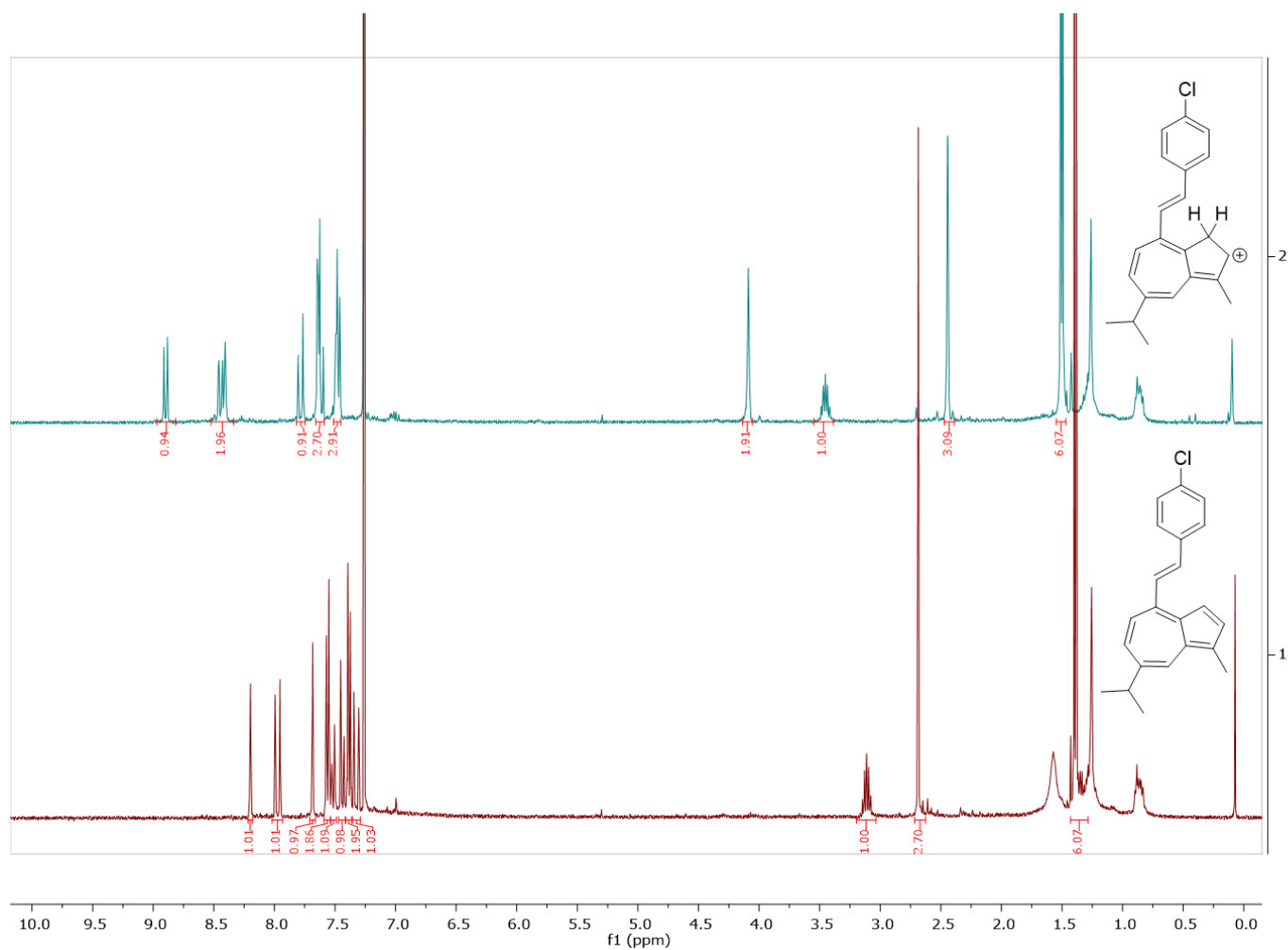


NMR Data and UV-Vis Spectra – Acid Titration

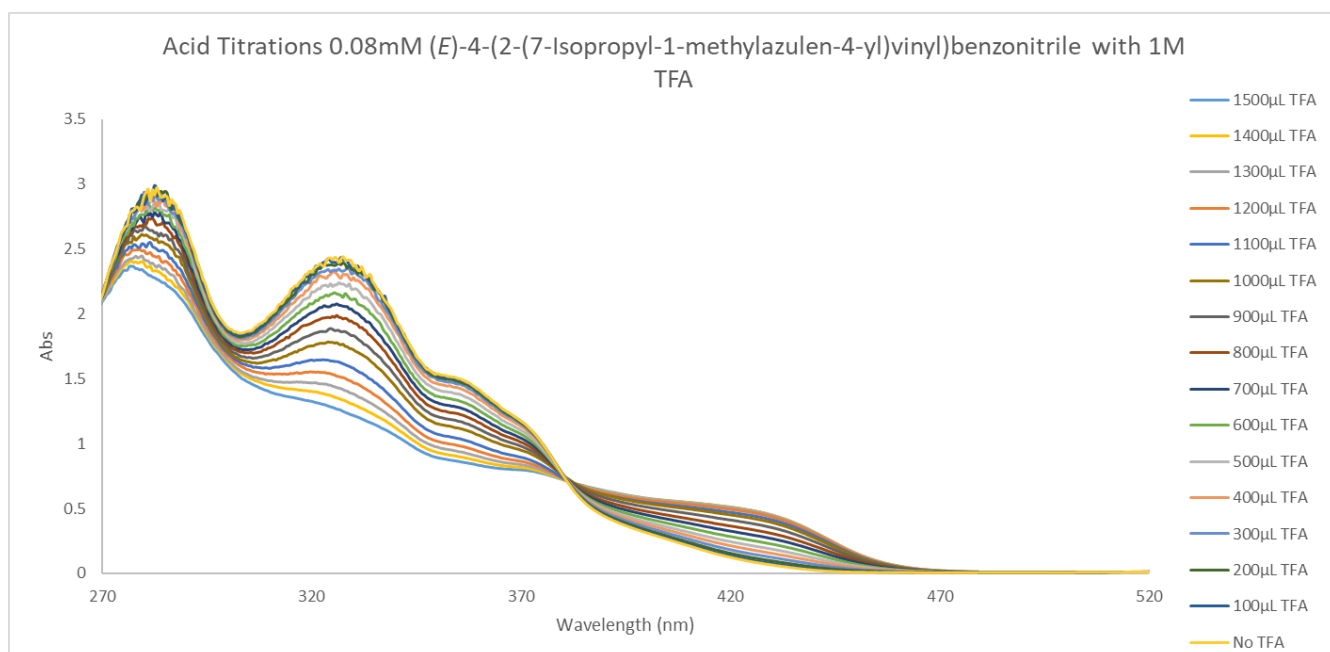
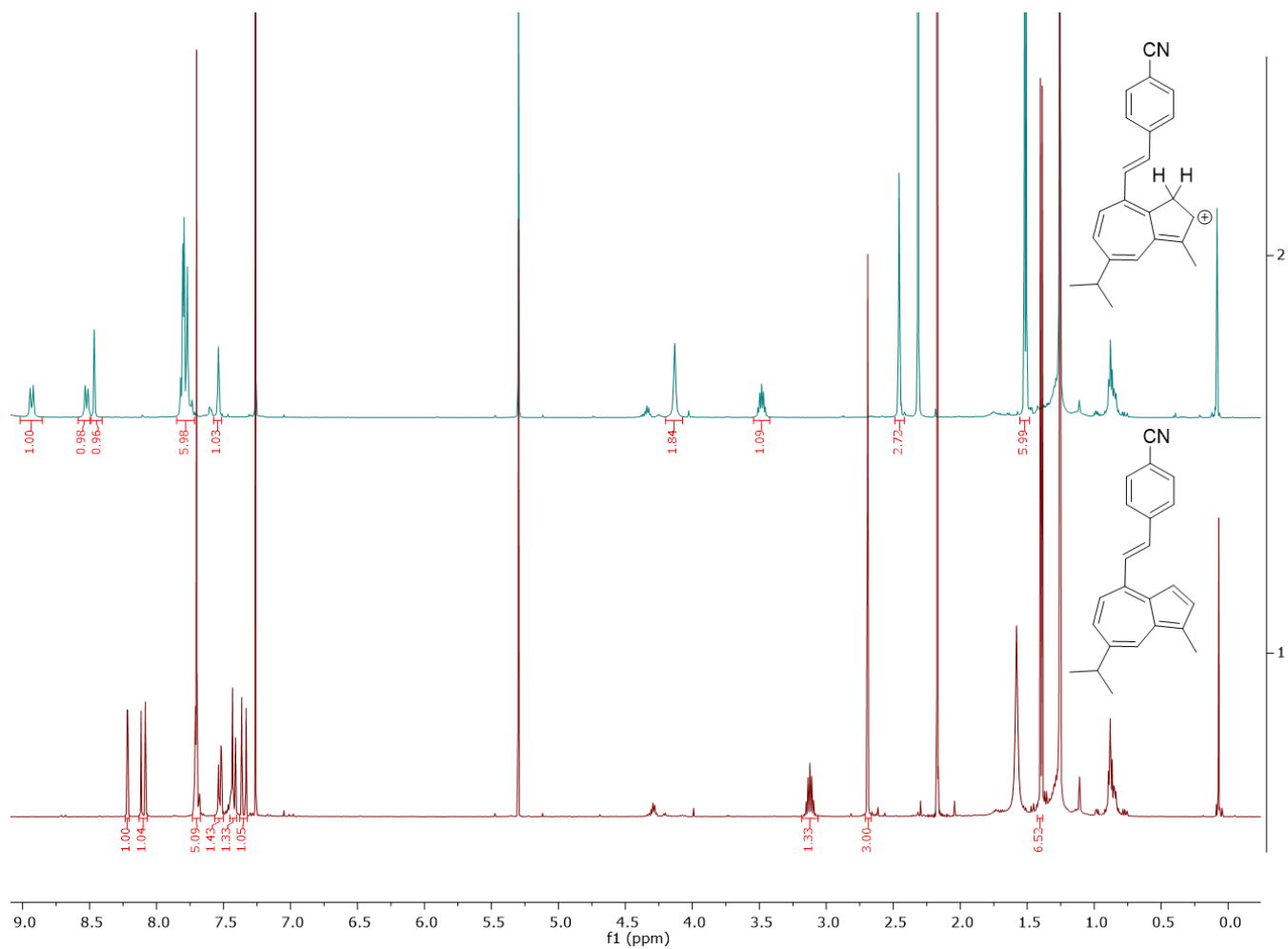
(E)-4-(4-Fluorostyryl)-7-isopropyl-1-methylazulene (25)



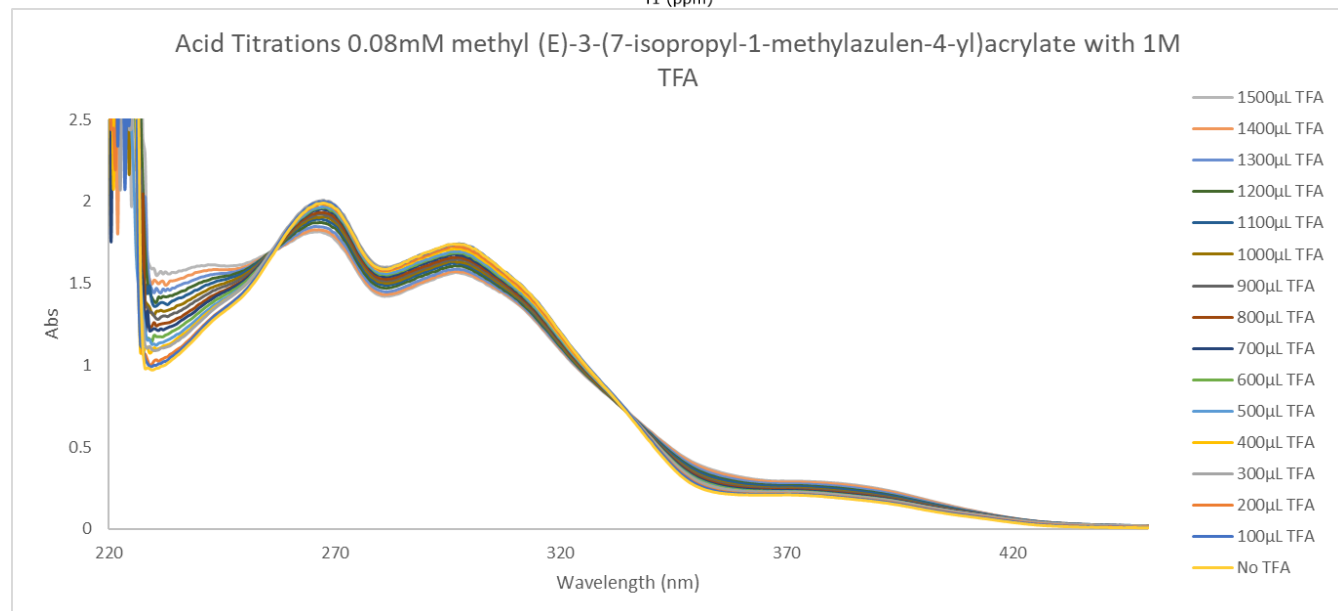
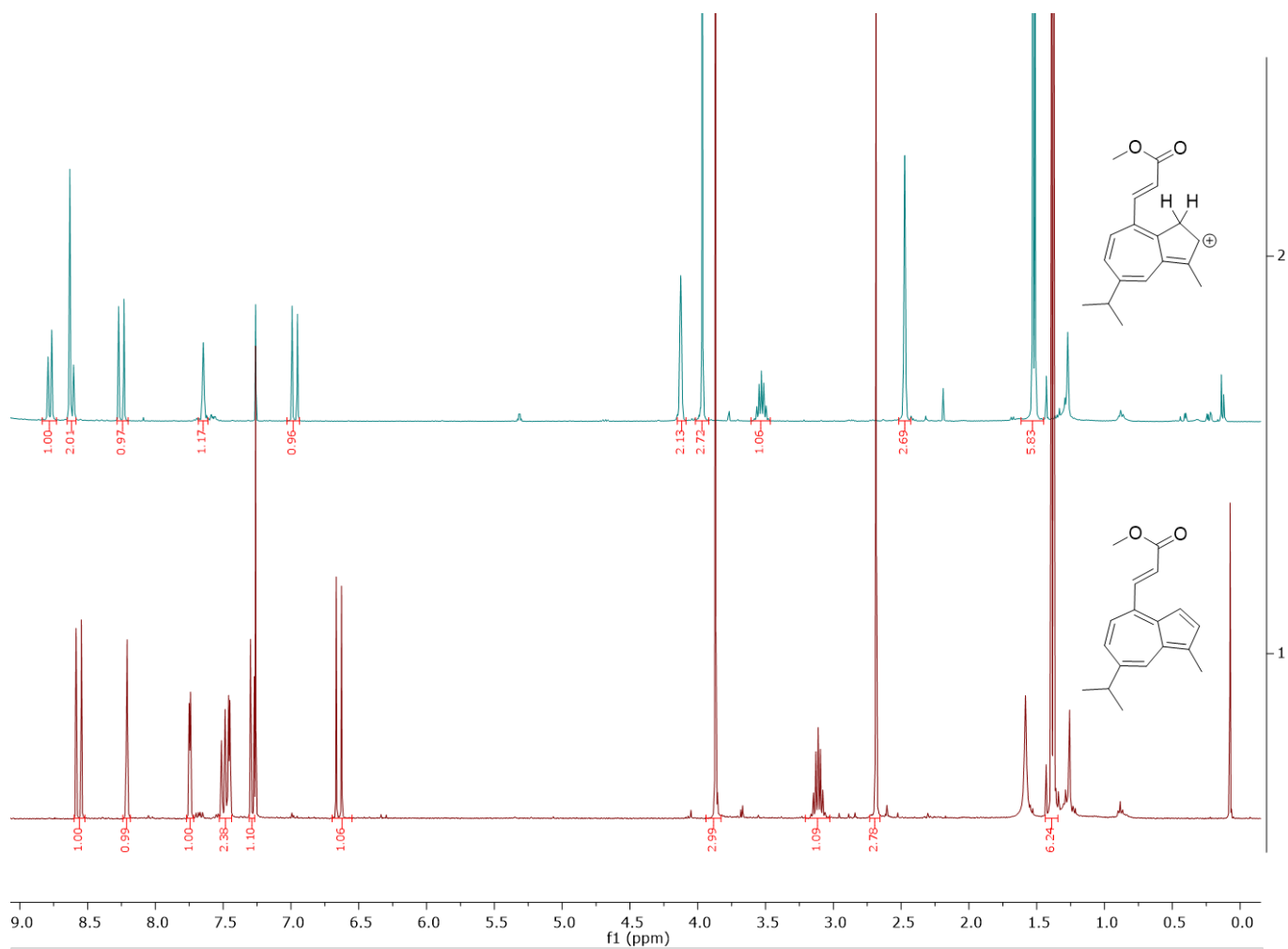
(E)-4-(4-Chlorostyryl)-7-isopropyl-1-methylazulene (24)



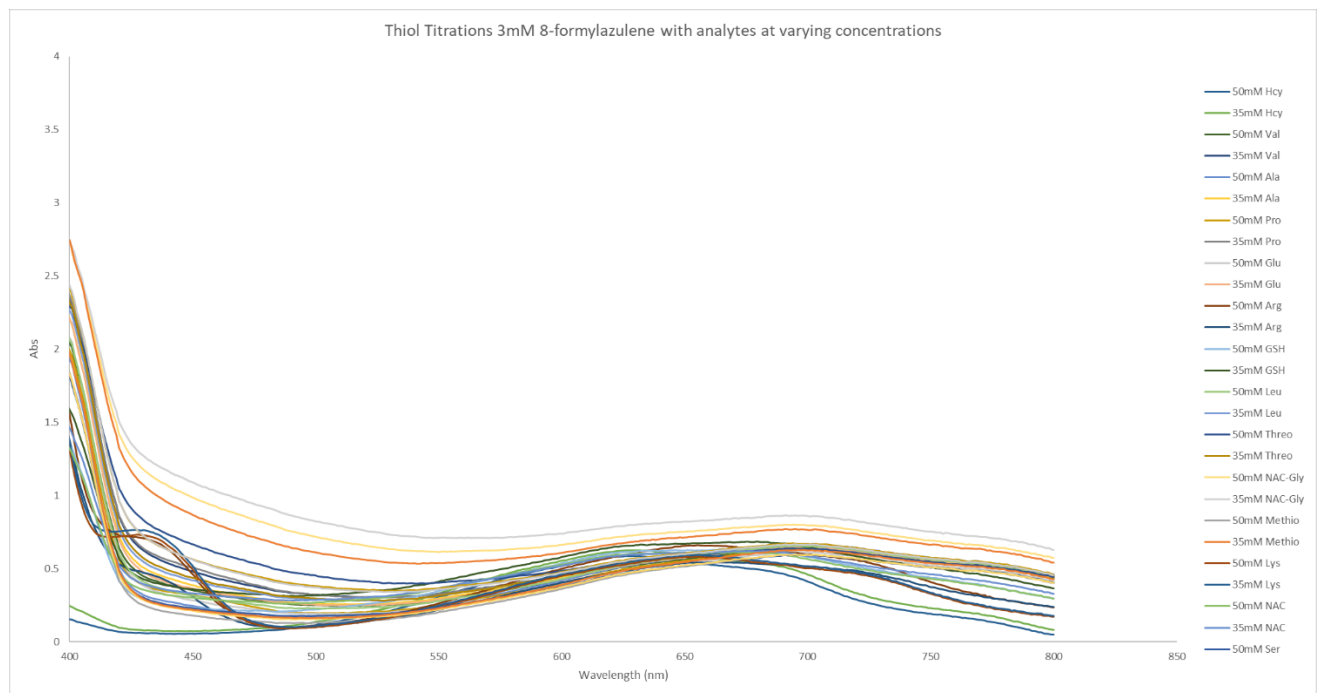
(E)-4-(2-(7-Isopropyl-1-methylazulen-4-yl)vinyl)benzonitrile (21)



Methyl (E)-3-(7-isopropyl-1-methylazulen-4-yl)acrylate (26)



UV-Vis Spectra – Selectivity Tests



(7-isopropyl-1-methylazulen-4-yl)methyl 2,4-dinitrobenzenesulfonate (Impure) (35)

